Katholieke Universiteit Leuven
Faculteit Landbouwkundige en Toegepaste
Biologische Wetenschappen

DISSERTATIONES DE AGRICULTURA

Doctoraatsproefschrift Nr. 597 aan de Faculteit Landbouwkundige
en Toegepaste Biologische Wetenschappen van de K.U.Leuven

A CONTINUOUS/DISCRETE EVENT MODELING METHODOLOGY FOR SIMULATING CONTROLLED ATMOSPHERE COOL STORAGE SYSTEMS

Promotor:
Prof. B. Nicolaï, K.U.Leuven
Prof. J. Van Impe, Faculteit Toegepaste
Wetenschappen, K.U.Leuven.

Leden van de jury:

Prof. J. Feyen K.U.Leuven, Voorzitter.
Dr. G. Alvarez, CEMAGREF, Paris France
Prof. D. Berchmans, K.U.Leuven.
Prof. J. De Baerdemaeker, K.U.Leuven
Prof. M. Hendrickx, K.U.Leuven.
Prof. H. Ramon, K.U.Leuven.
Dr. N. Scheerlinck, K.U.Leuven

Proefschrift voorgedragen tot
het behalen van de graad van
Doctor in de Toegepaste
Biologische Wetenschappen

door

Nahor Haddish Berhane

March 2004

To my wife and children

Eternity is not endless time or the opposite of time. It is the essence of time. If you spin a pinwheel fast enough, then all its colours blend into a single colour-white-which is the essence of all the colours of the spectrum combined. If you spin time fast enough, then time-past, time-present and time-to-come all blend into a single timelessness or eternity, which is the essence of all times combined.

Frederick Buechner

The Eternal may meet us in what is, by our present measurements, a day, or a minute or a second; but we have touched what is not in any way commeasurable with lengths of time, whether long or short. … for we are so little reconciled to time we are even astonished at it. "How he has grown!" we exclaim, "How time flies!" as though the universal form of our experience were again and again a novelty. It is as strange as a fish were repeatedly surprised at the wetness of the water. And that would be strange in deed; unless of course the fish were destined to become, one day, a land animal.

C.S. Lewis

And the end of all our exploring will be to arrive where we started; and know the place for the first time.

T. S Elliot

Acknowledgements

As the years go by, the physical body deteriorates and I believe it is somehow bartered with the experience, knowledge and hopefully wisdom acquired as the years slip away. Looking back to the moments I passed through, I dare say that this 'exchange rate' was the highest in the last 6 or so years of my life. To that end, I would like to acknowledge the people who shared this time of my life with me in particular, and to all the people who played a role, in some way or another, in shaping me to the man I am now.

I am grateful to my promoters Prof. Bart Nicolaï and Prof. Jan Van Impe for their guidance and support throughout this research work. I would like to express my deep and humble gratitude to Prof. Bart Nicolaï for providing me the opportunity to work under his supervision and initiating my interest in the subject. Bart, I am thankful and proud to be your student. I am always impressed by your academic ability and unique personality. I hope you have imparted some of both on me.

I would like to thank the Doctoral Examination Committee members for their willingness to participate as jury in my Ph.D. Their critical review and constructive suggestions were vital to make the scattered manuscript into the kind of book it is now.

My profound gratitude goes to Dr. Nico Scheerlinck. Nico, you were wonderful to me from the beginning till the end. Thank you for your unreserved support, not only

on the academics but also in the day-to-day life. You were a constant source of grand ideas and thoughts. I will miss those late night discussions we used to have. I hope we will have the opportunity to work together in the future to realise the visions we shared. I am indebted to Dr. Pieter Verboven, for his patience, support and resourceful ideas he shared with me. Moreover, for his unrelenting support during the difficult and demanding experiments in the VCBT as well as in the industry. Thank you Pieter.

I had the opportunity to work and interact with many enthusiastic and hard working colleagues in the Laboratory of Postharvest Technology and the Vlaams Centrum voor Bewaring van Tuinbouwproducten. My thanks go to all members and ex-members of these laboratories. Especially, I would like to acknowledge Jeroen Tirry for his dexterity during the experiments in the ULO's of the VCBT and all the computer and network related problems that he always solved for me. I would like to thank Dr. My Lan Hoang, and Dr. Ann Peirs for their simple and fine friendship. Moreover, my thanks go to Dr. Wendy Schotsmans, Dr. Els Veravverbeke, Dr. Jeroen Lammertyn and Christine Franck for creating conducive and friendly environment throughout, and especially, during the early days of my work. My sincere thanks go to Dr. Bert Verlinden for being always there whenever his ingenious ideas are needed. I have enjoyed the discussions I had with you.

I would like to express my thanks to the following people, who in some way or another assisted me in conducting my experiments. Ivo Lamerts and André Michielis of the TME division, Mechanical Engineering Department, Josef Vogeleer of the workshop of the faculty of Agriculture and Applied Biological Sciences, Luc Machiels, Jan Nijs and Geert Veugelen of the 'Belgische Fruitveiling', thank you all.

Many other individuals were munificent with material, moral and psychological support during the ebbs and flows of this thesis. Dr. Asfered & Netsanet, Dr. Seifu and Martha, Girma & Seble, Hibru & Seble, and the rest of the Ethiopian community in Leuven are appreciated for their friendship and concern. And the family of Russom and Askalu, Filipos & Senait, Daniel and the rest of the Eritrean Community in Belgium for easing the burden of living far from home. I thank the ICEL church community for providing a home church away from home. I also thank Dr. and Mrs. Agu for the magnificent friendship we shared. I am grateful to my brother-like friends Mussie, Laine, Efrem, Kibreab and Mequanint and their families, and all others I didn't list their names, for the warmth, support and encouragement I always got wherever you are; you guys are just great! I will always preserve a place in my heart for Negga S. for initiating my interest to continue my education. Negga, your faith, selflessness and patience will always be my source of inspiration.

I would like to express my deepest gratitude to my father Haddish Berhane and my mother Bizen Mesfun for their wonderful parenthood and encouragement. You sacrificed so much that I might get the best education. I am simply grateful and proud to be yours. And also to my brother Adonai and his family. I will always remember your sound counsel and your generosity, always preserving the best for

your little brother. I would like to thank my brother Yobio and his family for the support and love you have shown me all through the years. You were a constant source of encouragement. I express my sincere gratitude to my extended family, especially, Babba Kibreab & Mamma Haria, and my brothers and sisters, Henok and his family, Helen and her family, Muzit, Tsehay and Seye for shaping my childhood and adolescence days with compassionate love. And my mother in law Ethiopia for her support and encouragement especially during those difficult times. My sisters-in-law, Haregu, Ruth, Veronica, and Yodit were especially supportive. I also thank my cousins Tsehay Y. and Adiam B. for being there at the lowest point of my life. I extended my thanks to all parent-like and brother-like family members.

Lastly and fervently, I am indebted to my darling wife Fanna and my wonderful children Dan and Leah who shared with me the happiness and sorrows, for their patience, understanding and unfailing love. I would like to express with all respect and love my appreciation and thanks. You always bring inspiration, meaning and purpose to my life. You are a reason to go on, I love you.

The financial support from the Interfacultaire Raad voor Ontwinkkelingssamenwerking (IRO), the Research Council of the K. U. Leuven, Vlaamse Leergangen and Academiche Stichting and were instrumental in the successful completion of this work.

Above all, I thank and glorify my Lord Jesus Christ in whom I have eternal life and to God almighty on whom lies the glory of all mortal achievements.

Abstract

This dissertation contributes towards the *(i)* development of a methodology to model and simulate industrial controlled atmosphere storage systems by using the combined continuous and discrete event simulation paradigm, for sizing of the facility as a whole, design of a robust control strategy, model based product quality control and optimisation of operational conditions for increased productivity and profitability; and *(ii)* the development of a methodology for simultaneous and unique estimation of thermophysical properties of biological materials by using the optimal experimental design technique using the hot wire probe set up.

The CA cool storage system model was developed by dividing the system into the three interacting units, namely: *(i)* the cooled space, *(ii)* the refrigeration unit and *(iii)* the gas-handling unit. The dynamics of the heat and mass transfer of the components in the cooled space and the refrigeration unit was formulated by an overall energy and mass balance by considering the zoning approach, which resulted in a description of the components by a set of ordinary differential equations. The product respiration and quality deterioration processes were represented by Michaelis-Menten type models. A two-phase isothermal plug flow model was used to represent the gas-handling unit where the solid phase mass transfer was described

by a linear driving force model. The CA cool storage model was implemented using a general-purpose simulation environment EcosimPro (EA International, Madrid, Spain) that can handle combined continuous/discrete processes. The model was validated using pilot plant and industrial CA cool storage facilities by considering some selected variables (temperature, relative humidity, concentration of respiratory gas, product weight loss and firmness loss, respiration heat generation), which characterize the cool room, refrigerant and evaporator and the gas-handling unit. The selected variables were compared to experimental data in an empty, partially loaded and fully loaded conditions.

The adequacy of the proposed model was justified by its ability to represent the most important discrete and continuous process events with an accuracy less than the observed variability of the different variables (2 °C for room air, 1.5 °C for cooler surface temperature, 1.5°C for product temperature and 5% for RH) or at best with the accuracy level as set by the measurement instruments (0.5 °C for temperature and 5% for RH). Sensitivity analysis showed that the transient cooling phase was influenced by the accuracy of the heat transfer coefficients. Moreover, the initial product temperature influenced the product cooling rate and moisture loss substantially with practical implication on cooling strategy such that fast cooling of the product should always be accompanied by very high (near saturation) relative humidity of the cooling medium.

It was demonstrated that appraisal of the implication of practical industrial operational procedures directly on the product quality and plant performance/design issues was possible. The novelty of the present simulation model is that actual practical operation conditions and scheduling such as the stepwise loading of the product and the involved transients are simulated, providing a picture of the actual reality. Moreover, prediction of quality deterioration is incorporated. The global CA cool storage model demonstrated to be a pragmatic working tool for simulation of CA cool storage facility.

The application of optimal experimental design for the estimation of thermal properties of biological materials fosters the uniqueness and accuracy of the estimates by finding optimal experimental modus operandi. Careful choice of practically '*implementable*' heat generation, out of the theoretically found optimal profiles, as well as optimal measurement position are needed to achieve unique and accurate estimates.

Table of contents

Acknowledgement **i**

Abstract **v**

Table of contents **vii**

Chapter 1 General introduction **1**

1.1. Introduction 1
1.2. CA cool storage systems 3
1.2.1. Definitions 3
1.2.2. History 3
1.2.3. CA cool storage facilities: state-of-the-art 4
1.2.4. Optimal storage conditions 4
1.3. Simulation of cool storage systems 6
1.4. Objectives and outline 8
References 13

I. A CONTINUOUS DISCRETE EVENT SIMULATION FOR CA COOL STORAGE FACILITY 17

Chapter 2 Assessment and validation of existing gas exchange models for bulk storage of respiring produce 19

2.1. Introduction 19
2.2. Literature review 21
2.3. Materials and method 24
2.3.1. Gas exchange models assessment 24
2.3.2. Experimental set up 27
2.3.3. The gas exchange model 28
2.4. Results 30
2.4.1. Estimation of leakage/diffusion parameters 30
2.4.2. Validation of respiration models 31
2.5. Discussion 37
2.6. Conclusion 38
References 39

Chapter 3 A continuous-discrete event simulation model for a CA cool store facility: model development 41

3.1. Introduction 41
3.2. Literature review 43
3.2.1. Complete refrigeration system models 43
3.2.2. Product models 44
3.2.3. Implementation of complete refrigeration systems model 45
3.2.4. Discussion 47
3.3. Model formulation 48
3.3.1. Cool room and accessories 49
3.3.1.1 Room air model 50
3.3.1.2 Heat exchanger (cooling battery) model 52
3.3.1.3 Surface model 55
3.3.1.4 Door model 57
3.3.1.5 Product model 58
3.3.1.6 Accessories 61
3.3.2. Refrigeration unit 61
3.3.2.1 Evaporator 62
3.3.2.2 Condenser 63
3.3.2.3 Compressor 64
3.3.2.4 Holding tank 64

3.3.3. Gas handling unit 66
3.4. Implementation aspects 69
3.5. Discussion 74
3.6. Conclusion 76
References 77

Chapter 4 A continuous-discrete event simulation model for a CA cool store facility: model validation 81

4.1. Introduction 81
4.2. Literature review 82
4.3. Materials and methods 84
4.3.1. Cool room and accessories 84
4.3.1.1 The cool room 84
4.3.1.2 Model parameters 85
4.3.1.3 Measurements and validation method 89
4.3.2. Refrigeration unit model 92
4.3.2.1 The experimental refrigerator 92
4.3.2.2 Model parameters 93
4.3.2.3 Measurements and validation method 94
4.3.3. Gas handling unit model 95
4.3.3.1 Model parameters 95
4.3.3.2 Measurements 96
4.3.4. Global CA cool storage model: measurement and validation method 97
4.3.5. Sensitivity analysis 99
4.4. Results 100
4.4.1. Cool room and accessories: model assessment 100
4.4.2. Refrigeration unit model validation 109
4.4.2.1 Validation results 109
4.4.2.2 Sensitivity analysis 111
4.4.3. Global CA storage model validation 116
4.4.3.1 Validation results 116
4.4.3.2 Sensitivity analysis 128
4.5. Discussion 144
4.6. Conclusion 148
References 150

Chapter 5 Validation using industrial CA cool storage facility 153

5.1. Introduction 153
5.2. Materials and methods 154

5.2.1. The CA cool storage facility 154
5.2.2. Model formulation 155
5.2.2.1 Evaporator 156
5.2.2.2 Product model 157
5.2.2.3 Gas handling unit 158
5.2.3. Measurements 158
5.3. Results 162
5.3.1. Room Air 162
5.3.2. Evaporator and refrigerant 167
5.3.3. Product 169
5.4. Discussion 172
5.5. Conclusion 173
References 175

Chapter 6 Application: plant performance/design and product quality 177

6.1. Introduction 177
6.2. Materials and methods 178
6.3. Results 180
6.3.1. Effect of loading strategy on product quality 180
6.3.1.1 Product cooling rate 180
6.3.1.2 Product weight loss 181
6.3.1.3 Product firmness loss 182
6.3.2. Effect of loading strategy on mechanical plants' performance/design 184
6.3.2.1 Refrigeration unit 184
6.3.2.2 Gas handling unit 187
6.4. Discussion 190
6.4. Conclusion 191
References 192

II. OPTIMAL EXPERIMENTAL DESIGN FOR ESTIMATING THERMAL PROPERTIES OF BIOLOGICAL MATERIALS 193

Chapter 7 Optimal experimental design for estimating thermal properties of biological materials 195

7.1. Introduction 195
7.2. Literature review 197
7.3. Materials and methods 200
7.3.1. Experimental set up 201

7.3.2. Conduction heat transfer model 202
7.3.3. Finite element model 203
7.3.4. Model validation method 204
7.3.5. Optimal experimental design for parameter estimation: Theoretical framework 206
7.3.5.1 Parameter estimation 206
7.3.5.2 Optimal experimental design 207
7.3.5.3 Optimal design criteria 213
7.4.Results 213
7.4.1. Model Validation 213
7.4.2. Optimal experimental design for parameter estimation: Optimal heating profile. 215
7.4.3. Optimal experimental design for parameter estimation: Optimal sensor position. 219
7.4.3.1 Computational results 219
7.4.3.2 Implementation 223
7.4.4. Optimisation of parameterised input heating profile 224
7.4.3.1 Computational results 224
7.4.4.2 Implementation 225
7.5. Discussion 228
7.6. Conclusion 230
References 233

Chapter 8 General conclusions and future research 237

8.1 General conclusions 237
8.1.1 CA cool storage system simulation 238
8.1.2 Optimal experimental design for parameter estimation 242
8.2 Future research 243
8.2.1 CA cool storage system 243
8.2.2 Optimal experimental design for parameter estimation 244

Appendix A Cool room accessory models 247

A.1 Control strategies and controllers 247
A.2 Control valve model 249
References 251

Appendix B CA cool storage model parameters **253**

B.1. Global parameters 254
B.2. The cool room model parameters 254
B.3. Refrigeration unit model parameters 259
B.4. Gas handling unit model parameters 260
References 262

Appendix C Simulation results of the refrigeration and gas handling units **265**

C.1. Refrigeration unit 265
C.2. Gas handling unit 267
References 272

Symbols and abbreviations **273**

List of publications **283**

Nederlandse samenvatting **287**

Chapter 1

General introduction

1.1. Introduction

'*Of every tree* of the garden thou mayest freely eat ... ' (Genesis 1, 16). This was the first commandment given to man regarding the diet from his Creator, according to the Bible. Nowadays, people are getting increasingly conscious about what they eat. A healthy diet is regarded as one including raw fruits and vegetables and a great deal of freshly squeezed fruit juices. As a result, there is growing interest in fruit and vegetables, in general, on top of the rising number of people who classify themselves as vegetarians (no meat but other animal products), vegans (no animal products at all) and fruitarians (only fruit). This growing interest is the driving force behind the development and advancement of long-term storage as well as long-distance transport for increased marketable life of the fruit and vegetables. Thompson (1998) states two reasons in particular: *(i)* consumer expectation in supply of all types of fresh fruit and vegetables throughout the year is increasingly taken for granted and *(ii)* the free market situation brought about a competition among suppliers, who put stringent quality specifications to maintain and increase their market share.

In its 2001 review of refrigerated warehouses based on the USDA's 42nd biennial survey, the International Association of Refrigerated Warehouses (IARW) has reported that 5.78 million m^3 storage capacity for apples and pears exists in the USA alone, amounting to 24% of the total refrigerated ware house capacity (www 1, 2001). Of this 28% is CA cool storage facility. In Belgium, the total capacity of CA storage rooms is estimated about 400,000 tons with 90% adopted for Ultra Low Oxygen (ULO) storage (Anonymous, 2001). This shows that long-term storage facilities are heavily employed to increase storage and shelf life of fruit and vegetables. Moreover, in relation to long distance transport, in 2000 the EU's fresh fruit and vegetable imports amounted to 9.5 million tons worth 8.3 billion Euros from as far as South Africa, the Americas and New Zealand (www 2, 2001). The long distance journey stipulates storage facilities during transport, again for increased marketable life of the produce.

Given that most of the produce is harvested during a specific season and area, the challenge is to improve postharvest losses and provide the consumer with best quality produce using improved storage methods. This includes enhanced design and construction of storage rooms and improved control of the micro-environment. Any strategy to improve the quality maintenance of the stored produce or optimal operation of the storage facilities requires to be assisted by techniques which allow quantitative assessment of alternative cool storage designs. In this regard, predictive modelling and computer simulation play an important role. The present work will focus on these issues.

This introduction provides further information on the history and recent developments of the postharvest storage technology of fruits. Accordingly, Section 1.2 offers an overall view on the controlled atmosphere storage in general, comprising the history, state-of-the-art of the facility and a summary of optimal storage conditions of some pome fruit cultivars. In Section 1.3, the paradigms employed in modelling and simulation of systems, in general, and available software and their applicability to CA storage systems will be cited. Finally, to conclude this chapter, the objectives and outline of the present work will be delineated in Section 1.4.

1.2. CA cool storage systems

1.2.1. Definitions

To clear the confusion in the use of different terms referring to the manipulation of atmosphere during storage, Bishop, 1997 defined commonly employed terms such as Controlled Atmosphere (CA), Modified Atmosphere (MA) and Ultra Low Oxygen (ULO) and some others such as gas storage and controlled ventilation. Controlled Atmosphere is the creation of a high or low oxygen and/or carbon dioxide atmosphere by natural respiration or artificial means and controlled by a sequence of measurements and corrections throughout the storage period. In contrast, Modified Atmosphere is the creation of an atmosphere by respiration or by flushing with premixed gas and the desired composition is maintained over the storage life through the equilibrium established by the permeation of the packaging and respiration of the produce (mostly in retail packing). Thus, no measurements and corrections take place. The term Ultra-Low Oxygen is commonly used for storage of produce in oxygen concentrations of 3% and below. In this thesis, the use of the terms will be in the bounds of the above given definitions.

1.2.2. History

In general, controlled atmosphere storage involves the manipulation and control of the temperature, humidity and atmosphere to create the optimal condition necessary to extend the life of any respiring product. This means it is used together with refrigeration. Before low temperature was known to preserve fruit for longer period after harvest, the Swiss plumes and apples were plastered with wax and were dipped in honey during the Roman Empire. Though the evidence is sketchy, the first use of low temperature to store fruit (in caves or holes in the ground and in barns or cellars packed with ice or snow) is also attributed to this period (Mack, www3, 2003). Later, the preservative properties of ice were common knowledge for a long time where fruit were stored in an insulated icebox and transported over long distances by rail and ships. It was not until the mid-nineteenth century that development in mechanical refrigeration started by James Prescott Joule and William Thompson where fresh produce were directly stored for up to 5-6 months (Pitt, 1997). Pitt (1997) argues that of all the food preservation mechanisms available today, refrigeration is the only one that is expected to provide *as fresh* results.

Concerning storage of produce in conditions other than normal air, Bishop (1997), indicated that there was some evidence that Egyptians and Samarians used sealed limestone crypts to store their crops in the second century BC. He also speculates that this technology might have been used by Joseph in the Old Testament Egypt during preparation for the seven years of draught (Genesis 41). The first recorded experiments to control fruit ripening by changing the surrounding atmosphere were carried out by the French scientist Jacquet Bernard in 1821. He observed that harvested fruit respire during storage and the absence of oxygen slowed down ripening of fruit (Thomson, 1998). The idea failed to inspire commercial application up until 1929, where the first commercial store was built in the UK. This was mainly the result of the work of Kidd and West who studied the effect of atmospheric composition on the metabolism of harvested fruit and vegetables. Later in 1934, after studying with Kidd and West, Eaves introduced CA storage to North America, where he discovered the use of hydrated lime in place of caustic soda for removal of CO_2 (Bishop, 1997). Kidd and West are considered the pioneers of the research field in postharvest storage technology (Fidler, 1965).

1.2.3. CA cool storage facilities: state-of-the-art

Nowadays, CA cool storage facilities are widely used for long-term storage of pome fruit. They are constructed in relatively smaller compartments with 'complete' air tightness. Almost all CA storages now being built in Europe are from metal faceted insulation panels inter-locked together in some manner. In order to avoid pressure build up in the rooms, air bags equipped with relief valves are provided. Several methods exist to achieve fast removal of O_2 and excess CO_2. The most modern and being widely in use is the Pressure Swing Adsorption (PSA) technology for both N_2 generation and CO_2 removal. Moreover, ethylene removal mechanisms are in place though not a common commercial practice for fruits (except kiwi) (Bishop, 1997). In automated CA cool storage systems, control of the respiratory gases is achieved by injecting O_2 from the atmosphere and removing CO_2 by scrubber. In case where O_2 concentration is higher due to some excessive leakage, N_2 is injected.

1.2.4. Optimal storage conditions

With the advances of the CA storage techniques arrived new sorts of disorders such as 'core flush', 'internal breakdown', 'soft scald' and 'core breakdown'. These disorders are caused when extreme modified or controlled atmosphere are applied

causing oxygen deficit and excess carbon dioxide in the fruit. As a result, an imbalance in energy metabolism yields to an inability of the fruit to repair membrane damage (Kader, 1988). Optimisation of CA storage conditions are based on traditional experiments to determine optimal O_2 and CO_2 conditions for long-term storage and rely on practical experience of different horticultural institutes. The experiments are carried out by testing a number of commercial storage conditions until satisfactory condition is obtained. Often, they focus on the relationship of external O_2 partial pressure and respiration to identify the lower O_2 limit of the fruit. Some typical storage conditions advised for the season 2001-2002 by the Flanders Centre of Postharvest Technology (Belgium) are listed in Table 1.1 (Schenk, 2002). More often, it is attempted to maintain these 'optimal' *a priori* known conditions to avoid the possible disorders that might occur due to too low O_2 or too high CO_2.

Table 1.1 Recommended storage conditions for some commercial culivars of pome fruit in Belgium (Schenk, 2002)

Apple cultivars	**CA conditions**			**ULO conditions**		
	°C	CO_2%	O_2%	°C	CO_2%	O_2%
Golden, Gloster, Mutsu, Gala	0.5	2-3	2-3	0.5	2-2.5	1-2
Elstar, Idared	1	1-2	2-3	1	< 1	2-2.5
Jonagold Jonagold-mutants Jonagored, Pinova	0.8	2-3	1-2	0.8	2.5	1
Cox Orange Pippin Boskoop	3-3.5	< 1	2-3	3-3.5	< 0.8	2-2.5
Granny Smith		--		0.5	1	1
Pear cultivars	**CA conditions**			**ULO conditions**		
Conference				-1/-0.5	< 0.7	2.5-3
Doyenné du Comice				-0.5/0	< 0.7	2-2.5

1.3. Simulation of cool storage systems

As stated earlier, any improvement in the overall design and operation of CA cool storage systems requires quantitative assessment of the processes involved. This is carried out by the use of appropriate modelling methodology and implementation of the methodology in the most natural manner towards obtaining a realistic representation of the processes and physical systems.

In general, systems behave in both continuous and discrete manner. In industrially relevant models the continuous behaviour is described by mass, energy and momentum balances, which describe how a simulated component responds when subjected to different situations, usually represented by differential equations. This is realised by slicing the time into smaller arbitrary steps where rates of change can be represented by difference (quasi-continuous) instead of differential equations. New states and/or rates are then calculated based on the changes during the last time interval causing smooth changes in the state variables. On the other hand, discrete events occur during the continuous operation due to several activities such as controller action, operator intervention, cell loading, door opening and start-up and shutdown operations. These events cause a sudden change from one state to another.

Even though the combined nature of systems has been recognised for many years, Sierenburg (1997) states that modellers have abstracted real systems' behaviour until it conforms to one of the categories, classifying themselves as continuous or discrete modellers, being prisoners of their own field. The simulation of systems that belong to either of these categories has a considerable history dating back to 1950's (Kreutzer, 1986). Barton (1992) asserts that Fahrland (1970) was the first to promote the development of combined continuous discrete simulation languages. He demonstrated how this class of problems could be solved. The simulation paradigm was first justified from representational point of view in that it enables representation of physical system in its natural form. Latter, the inclusion of the discrete events to the continuous models was advocated by Cellier (1979) from efficiency and accuracy point of view.

By 1977 at least 18 combined continuous and discrete simulation languages were reported (Oren, 1977). However, since the languages were developed based on existing discrete simulation languages to encompass continuous capabilities or vice versa, this resulted in the inadequate continuous or discrete simulation capabilities

for many applications. In late 80's and early 90's, the second generation combined continuous and discrete simulation languages emerged. Though they addressed most of the problems of the first generation languages, they were mainly application oriented and were still not meeting many of the demands of potential industrial users. The history and development of combined continuous simulation languages can be found in Kreutzer (1986).

Substantial work on plant simulation has been done in the field of Chemical Engineering. As a result, recently, general-purpose combined and continuous process simulation packages suitable for entire range of industrial processing and physical system operations have emerged. Of these, Extend (Imagine that Inc., USA), gPROMS (Process System Enterprise Ltd., UK), EcosimPro (EA International, Spain) and PROSIM (Prosim BV, Zoetermeer, The Netherlands) can be mentioned. The choice of an appropriate simulation tool and simulation language is of vital importance for successful implementation of a given model. Depending on the application area, the major evaluation criteria of a combined continuous and discrete simulation software could be classified as: *(i)* time management and event handling, *(ii)* modelling flexibility which includes mathematical capabilities and ability to create new modelling constructs, *(iii)* ease of use during developing, compiling and running of models, *(iv)* architectural aspects such as openness.

Regarding refrigerated cool storage systems simulation, up to now only custom-built environments, tailored to fit the specific application are in use where discrete event is entirely not dealt with or at best, addressed to some extent (RADS by Cleland, 1985; FME by James, 1988; STANSAN-PC SOFTWARE SYSTEMS by Glökner et al., 1990; RefSim by Lovatt, 1992). The use of discrete and continuous simulation paradigm in the simulation of cool storage systems enables *(i)* to accurately represent step response transients such as defrosting action, door opening and control actions and *(ii)* to model various operation conditions that require scheduling, for instance, different product loading strategies, which have significant influence on the optimal operation of the facility as a whole. This class of problems is impossible to deal with using only continuous simulation softwares. In view of the availability of the general purpose combined continuous and discrete simulation environments, one can argue that CA cool storage systems can best be implemented in such environments for flexibility and reduced complexity. This enables the engineer to dedicate more time to develop the modelling methodology, rather than focusing on implementation aspects.

In the present work, the general-purpose combined continuous and discrete simulation environment EcosimPro (EA International, Madrid, Spain) will be employed. Some of the features of this software are as follows. Based on object-oriented architecture, it features modular and hierarchical implementation of models. The environment uses a dedicated modelling language called EL, which can call FORTRAN, C, and C++ routines. The modules can be nested to form hierarchy to any depth. The resulting models can be run efficiently as compiled C++ programs, and delivered to others as stand-alone models. It has also a graphical user interface, and supports graphical creation of models, which facilitates the modelling task. An interesting feature is the support of "simulation experiments" for a given model. This allows isolating of the modules from the bigger system and analysing them independently. It is also equipped with robust automatic differential equation (DA) solvers. However, in dealing with partial differential equations one has to write his own code to reduce them into ODE's, thus the software is not equipped with space discretisation (meshing) tools. Besides the above-mentioned features, which satisfy the requirements for successful implementation of a CA cool storage system model, the price of the software was in the affordable range. Thus, given these advantages, the software was selected for implementation of the CA cool storage model.

1.4. Objectives and outline

The implementation of a cool storage system is an iterative process of analysis, selection, construction and optimisation. First, the selection of the equipment is carried out based on steady state analysis by considering mean rates of heat, moisture and gas requirements. Then assembly of the equipment and construction takes place. Before the plant is set into operation optimisation and tuning of the controllers is carried out on the actual system. During this stage, however, it might require changing and/or customisation of some of the equipment. This does not only prove to be expensive, tedious and time consuming but also, even after these efforts and resources are put in, the facilities often operate in sub-optimal conditions. This is because of bottlenecks and large safety factors considered in order to compensate for the unaccounted dynamic situations.

Here, the missing link is the 'design validation' prior to assembly and construction, preferably using a virtual facility. Hence, the development of a simulation tool, which takes into account, *(i)* the dynamic processes of the interacting units and components, *(ii)* different operational conditions and scheduling, *(iii)* the characterisation of the quality of the stored produce, is indispensable. As a result,

not only a robust design at less cost is achieved, but also optimisation of the facility and its operation with respect to plant performance and product quality is possible. Needless to say, the simulation tool essentially stipulates for combined discrete and continuous simulation paradigm.

Recently, attempts have been made to characterise the dynamics of the conventional (excluding CA) cool/cold[1] storage systems. However, these attempts, pioneering as they are, portray the following shortcoming.

- Discrete events were partially or not at all addressed, leading to unnatural representation of the involved processes especially in relation to the step response transients. As a result, different operational situations, which stipulate rigorous discrete event simulation, could not be dealt with.

- Since the models were developed for conventional cool/cold storage systems, gas exchange and quality of the stored product and the dynamics of the corresponding gas-handling unit was not considered. This means that little focus was rendered on the modelling of the stored product with respect to gas exchange and quality deterioration.

The stored produce being the centre of focus, the challenge nowadays concerning CA cool storage systems is the control of the micro-environment in which the produce are stored based on the dynamic behaviour and response of the fruit rather than trying to maintain the *a priori* known optimal storage conditions. This challenge can be met by the use of predictive models, which characterise not only the involved processes, but also the dynamics of the stored produce. This means that the responses of the produce need to be represented using models that describe the interaction with the micro-environment and the changes that take place within the product in response to that.

Successful modelling and simulation of CA cool room installations, on the other hand, highly depends on the accuracy of the involved different input parameters. These parameters can be classified in to those that are related to the cooling installation as a whole (thermophysical properties of the involved hardware, cooling media, and any relevant heat transfer coefficients) and those that are related to the

[1] The distinction between cold and cool stores is that the former generally operates at air temperatures below –2°C (typically –15°C - –30°C) and thus the stored product contains ice; whereas in the latter, the air temperature is above –2°C (typically –2°C - +10°C) and ice is not involved (Cleland, 1990).

stored product. For the former class of parameters there exist well-established methods for their calculation and determination and readily available databases in the literature (e.g. Touloukian et al., 1970; Touloukian et al., 1978a; Touloukian et al., 1978b; ASHRAE, 1993). However, for biological materials in general, owing to their diversity and variability, there exists no well-defined procedure to determine them and hence no well established database. Different methods of determination of thermal properties of foods and agricultural products are outlined in Mohsenin (1980). Moreover, several investigators have attempted to estimate the thermophysical properties of various foods using different methods (Reidy and Rippen, 1971; Rahman and Potluri, 1991; Tagawa et al., 1996). However, the reproducibility of the estimates is highly dependent on the method and set up employed.

The main objectives of the thesis are:

1. To develop a methodology for modelling and simulation of controlled atmosphere cool storage systems considering *(i)* the heat, moisture, and gas exchange in the cooled space, *(ii)* the quality evolution of the stored produce and *(iii)* the dynamics of the involved mechanical plants. A hierarchical and modular implementation approach using a combined continuous and discrete simulation environment will be pursued.

2. To develop a methodology for parameter estimation of thermophysical properties of biological materials based on the application of optimal experimental design techniques for the unique and accurate simultaneous estimation of the parameters. Here, the simultaneous estimation of thermal conductivity k and the volumetric heat capacity ρc are selected.

Accordingly, the thesis is organised in two parts to address these main objectives. With respect to the first objective, the CA cool storage facility will be divided into three sub-units, namely: *(i)* the cooled space, *(ii)* the refrigeration unit and *(iii)* the gas-handling unit. In the first step, it is attempted to model and validate each unit separately. In the second step, the units will be interconnected to formulate the global CA storage model and will be validated. Finally, application of the global CA cool storage facility will be carried out. This Part includes Chapters 2 to 6.

In Part two (Chapter 7), which deals with the second objective, a hot wire probe set up will be developed and the probe and its environment will be modelled using the finite element method. The model will then be validated using several static and

dynamic heat generation profiles. The model will further be employed to design informative experiments with respect to optimal heating strategy and optimal sensor position towards unique and accurate simultaneous estimation of the involved parameters.

The diagram in Figure 1.1 shows the flow of the thesis and depicts the sub-objectives in each Chapter.

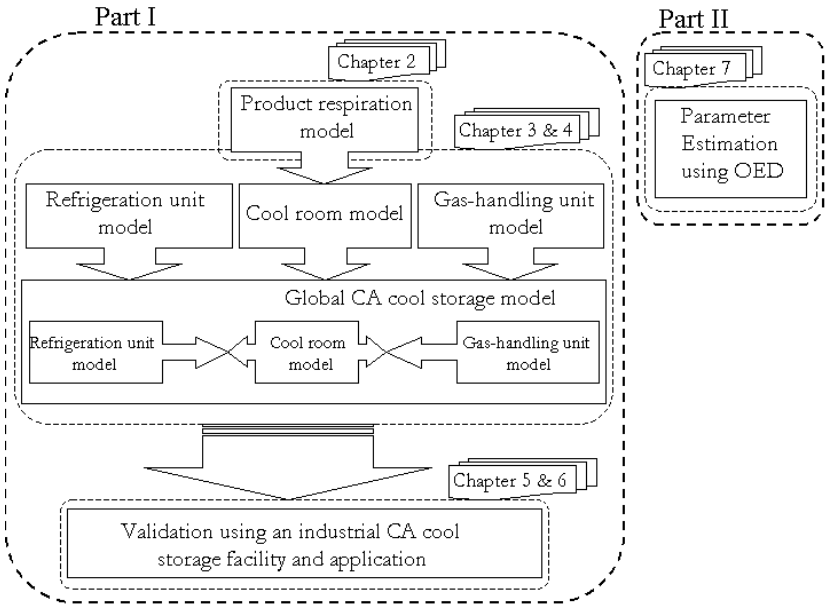

Figure 1.1 Schematic diagram of the relationships of the different chapters towards the development of the global CA cool storage model.

In Chapter 2, assessment and validation of existing product respiration models for their applicability to bulk storage of produce is presented. Here, existing empirical and semi-mechanistic models will be assessed. The feasible models will then be validated using an experimental set up developed to emulate bulk fruit storage. The results reported in this Chapter are published in Nahor et al. (2003b).

In Chapter 3, the modelling methodology pursued with respect to the CA cool storage system will be addressed. The models of each of the components in the three sub-units will be formulated and implementation aspects of the modules as well as that of the global CA cool storage model will be presented. The results of this Chapter are presented in Nahor et al. (2002); Nahor et al. (2003c); Nahor et al. (2003d); Nahor et al. (2003e) and Nahor et al. (2004b).

Chapter 4 is devoted to the validation of the models developed in the preceding Chapter. First, the assessment of the models for the units will be carried out separately and then the global model will be validated by means of a pilot plant CA cool storage facility, using pear fruit. The results of this Chapter are published in Nahor et al. (2002); Nahor et al. (2003c); Nahor et al. (2003d) Nahor et al. (2003e) and Nahor et al. (2004b).

In Chapter 5, the developed methodology will, once more, be validated using an industrial setting (using apple fruit) by considering some important variables related to the different units. Here, the product loading strategy followed during the experiment will be considered.

In Chapter 6, a hypothetical CA cool storage will be considered and some practical operational situations will be investigated with respect to product quality and performance, design and optimisation of the mechanical plants as an application of the developed methodology.

Chapter 7 deals with the development of a methodology for the unique and accurate estimation of thermophysical properties of biological materials by using techniques of optimal experimental design. A hot wire probe set up will be developed and the heat conduction in the hot wire probe will be modelled by considering a 1D finite element geometrical model. The model will then be validated and further employed for the investigation of optimal heating profile and measurement location. The results of this Chapter are published in Nahor et al. (2001); Nahor et al. (2003a) and Nahor et al. (2004a).

Finally, Chapter 8 offers some general conclusions and future perspectives.

References

Anonymous. (2001). Jaarverslag van het Verbond van Belgische Tuinbouwveilingen. Leuven, Belgium.

Anonymous. Genesis 1, 16. In: The Bible (KJV).

Anonymous. Genesis 41. In: The Bible.

Anonymous. ASHRAE Fundamentals. (1993). American Society of Heating, Refrigerating and Air-Conditioning Engineers, Inc., Atlanta, USA.

Barton, P.I. (1992). The modelling and simulation of combined discrete/continuous processes. *Ph.D. Thesis,* Imperial College of Science, Technology and Medicine, London, UK.

Bishop, D. (1997). Controlled atmosphere storage. In: Dellino, C.V.J. (Ed.), Cold and chilled storage technology. BLACKIE A & P, London, UK, 53-92.

Cellier, F.E. (1979). Combined discrete/continuous system simulation languages – usefulness, experiences and future development. In: Ziegler, B.P., Elzas, M.S., Klir, G.J., Oren, T.I. (Eds.), Methodology in Systems Modelling and Simulation. Elsevier Science, London, UK, 201-220.

Cleland, A.C. (1985). RADS – a computer package for refrigeration analysis, design, and simulation, *International Journal of Refrigeration*, 8, 372-374.

Fahrland, D.A., (1970). Combined discrete event continuous systems simulation. *Simulation*, 14, 61-72.

Fidler, J.C. (1965). Controlled atmosphere storage of apples. The Institute of Refrigeration, London, UK 1-7.

Glöckner, G., Hofer, B., Kluge, C.H., Schroth, H.H., Wobst, E. (1990). Simulation of refrigerating plants for cold stores. *Refrigeration Science and Technology*, 1990-4, 487-493.

James, K.A. (1988). Dynamic mathematical modelling of refrigeration systems and heat pumps. *Ph.D. thesis*, Institute of Environmental Engineering, South Bank Polytechnic, London.

Kader, A.A. (1988). Respiration and gas exchange of vegetables. In: Weichmann J. (Ed.), Postharvest physiology of vegetables. Marcel Dekker Inc., New York, USA, 25-43.

Kreutzer, W. (1986). System simulation programming styles and languages. Addison-Wesley, Sydney.

Lovatt, S. (1992). A dynamic modelling methodology for the simulation of industrial refrigeration systems. *Ph.D. Thesis*, Massey University, Palmerston North, New Zealand.

Mack, L.R. Food Preservation in the Roman Empire. http://www.unc.edu/courses/rometech/public/content/Survival/Lindsay_Mack/Food_Preservation.htm, accessed on 07/08/03.

Mohsenin, N.N. (1980). Thermal properties of foods and agricultural products. Gordon and Breach, N.Y.

Nahor, H.B., Scheerlinck, N., Verniest, R., De Baerdemaeker, J., Nicolai, B.M. (2001). Optimal design of dynamic experiments for the parameter estimation of conduction heated foods. *Journal of Food Engineering*, 48, 109-119.

Nahor, H.B., Scheerlinck, N., Van Impe, J., Nicolaï, B.M. (2002). A simple model of a refrigeration plant for cool storage systems simulation. *Communications of the faculty of Agricultural and Applied Biological Sciences*, University of Ghent, Belgium, 67(4) 293-296.

Nahor, H.B., Scheerlinck, N., Van Impe, J., Nicolaï, B.M. (2003a). Optimisation of the Temperature Sensor Position in a Hot Wire Probe Set Up for Estimation of the Thermal Properties of Foods Using Optimal Experimental Design. *Journal of Food Engineering,* 57(1) 103-110.

Nahor, H.B., Schotsmans, W., Scheerlinck, N., Nicolaï, B. M. (2003b). Assessment and validation of existing gas exchange models for bulk storage of respiring produce. Submitted for publication in *Postharvest Biology and Technology.*

Nahor, H.B., Teshome, E.J., Scheerlinck, N., Van Impe, J.F., Nicolaï, B.M. (2003c). Prediction of dynamic behaviour of ca cool rooms using lumped parameter approach. *Acta Horticulturae*, 599, 213-219.

Nahor, H.B., Scheerlinck, N., Verboven, P., Van Impe, J., Nicolai, B.M. (2003d). Dynamic Simulation Of Controlled Atmosphere (CA) Cool Storage Systems For Pip Fruits. *Proceedings of the 21st International Congress of Refrigeration, Washington D.C, USA, (CD-edition, ISBN 2-913149-32-4).*

Nahor, H.B.; Scheerlinck, N.; Van Impe, J.; Nicolaï, B.M. (2003e). Combined discrete and continuous simulation of Controlled Atmosphere (CA) storage

systems. *Communications of the faculty of Agricultural and Applied Biological Sciences,* University of Ghent, 68(3) 17-21.

Nahor H.B., Scheerlinck N., Moles C.G., Banga J.R., Nicolaï B.M. (2004a). Implementation and validation of optimal heat generation profiles for simultaneous estimation of thermal food properties using a hotwire probe. Accepted to be presented in the *9th International Congress on Engineering and Food (ICEF9),* 7-11 March 2004, Montpellier, France.

Nahor H.B.; Scheerlinck, N.; Verboven, P.; Van Impe, J.; Nicolai, B.M. (2004b). Continuous/discrete simulation of controlled atmosphere (CA) cool storage systems: model development and validation using pilot plant CA cool storage. Submitted for publication in *International Journal of Refrigeration.*

Oren, T.I. (1977). Software for simulation of combined continuous and discrete systems: A state-of-the-art review. *Simulation*, 28, 33-45.

Pitt, A.J. (1997). Refrigeration plant. In: Dellino, C.V.J. (Ed.), Cold and chilled storage technology. BLACKIE A & P, London, UK, 53-92.

Rahman, M.S., Potluri, P.L. (1991). Thermal conductivity of fresh and dried squid meat by line source thermal conductivity probe. *Journal of Food Science*, 56(2), 582-585.

Reidy, G.A., Rippen, A.L. (1971). Methods of determining thermal conductivity in foods. *Transactions of the ASAE*, 14(2), 248-254.

Schenk, A. (2002). Advies plukdata en bewaaromstandigheden voor lang bewaring van applen en peren in 2002. Belgische Fruitrevue, 54(9), 30-32.

Sierenberg, R.W. (2001). Combined discrete/continuous modelling. In: Tijskens, L. M. M., Hertog, M. L. A. T. M., Nicolaï, B. M. (Eds.), Food process modelling. CRC Press, New York, USA, 87-101.

Tagawa, A., Kitamura, Y., Muramatsu, Y., Fusakaz A., Murata, S. (1996). Thermophysical properties of Adzuki beans by transient heat flow method using probe. *ASEA Annual International Meeting*. Paper # 966003.

Thompson, A.K. (1998). Controlled Atmosphere Storage of Fruits and Vegetables. CAB International, Oxon, UK.

Touloukian, Y.S., Liley, P.E., Saxena, S.C. (1970). Thermal conductivity: non-metallic liquids and gases. In: Thermophysical properties of matter 3. N.Y. 685p.

Touloukian Y.S., Powel, R.W., Ho, Y.C. (1978a). Thermal conductivity: non-metallic solids. In: Thermophysical of matter 2. N.Y. 1172p.

Touloukian Y.S., Powel, R.W., Ho, Y.C. (1978b). Thermal conductivity: metallic elements and alloys. In: Thermophysical of matter 1. N.Y.

www1. (2001). http://www.iarw.org/hq/aboutus/pdf/iarwcapacity01.pdf. Accessed August 07, 2003.

www2. (2001). http://www.coleacp.org /fo_internet/ en/documentation/rapports /rapport 2001/chiffrescles.pdf. Accessed on August 07, 2003.

PART I

A continuous discrete event simulation for CA cool storage facility

Chapter 2

Assessment and validation of existing gas exchange models for bulk storage of respiring produce

2.1. Introduction

It is a common practice nowadays to store fruit and vegetables in controlled atmosphere (CA) conditions in bulk to improve the shelf life of the produce. For proper design and optimisation of the cool storage facilities, model based simulation has lately become an important tool. Successful simulation of the whole installation depends on accurate modelling of the processes involved. The most important process affecting the concentration of the respiratory gases inside the cooled space is the gas exchange of the stored produce with its surrounding atmosphere.

The rate of gas exchange of the produce depends on several variables of the microenvironment surrounding the produce, namely, the temperature and the

concentrations of the respiratory gases. With respect to modelling and simulation of the cooled space of CA storage systems, expressing respiration rate as a function of these variables plays an important role in interrelating the entailed processes. This arises from the existence of a close relationship between gas exchange, heat generation and quality deterioration of the stored produce. Respiration heat generation is a direct result of gas exchange and respiration and quality deterioration share the same metabolic background. Hence, natural linking of the processes can be achieved when appropriate models are employed. The schematic representation of the above relationship can be depicted as in Figure 2.1.

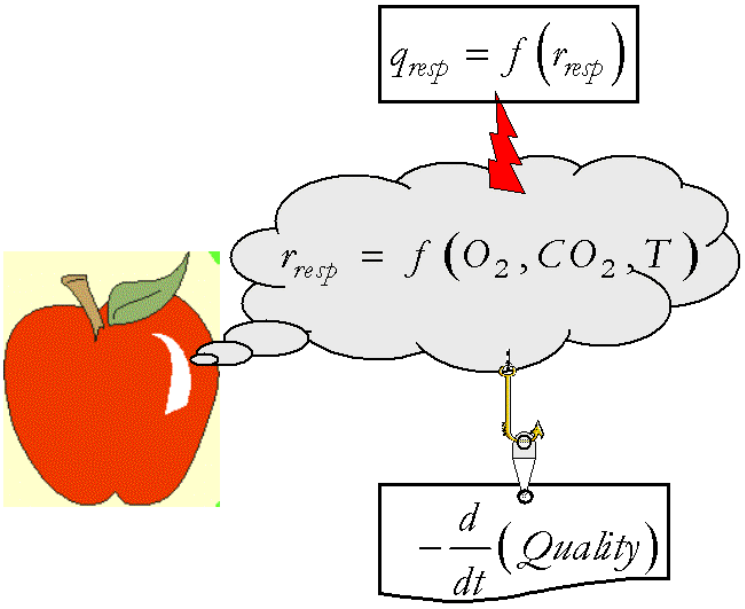

Figure 2.1 Relationship between gas exchange, heat generation and quality deterioration

The objective of this chapter is to assess the appropriateness of existing product respiration models for bulk storage of pome fruit in CA cool rooms. These models, not only account for gas exchange of the bulk-stored produce, but also serve as background models to hook up the product quality model. Moreover, since most of the models are developed using a single or a couple of fresh fruit for a short period, the influence of bulk storage and age of fruit are also investigated. The most

appropriate model will ultimately be included in a global CA storage model. The results presented in this Chapter are published in Nahor et al. (2003).

Accordingly, in Section 2.2, a literature review of existing gas exchange models, classified into empirical or semi-mechanistic[1], will be presented. Subsequently, assessment of the different models and the experimental set up employed in the present investigation and its model will be given in Section 2.3. Validation results of the selected models will be presented and discussed in Sections 2.4 and 2.5, respectively. Finally, conclusions will be drawn in Section 2.6.

2.2. Literature review

Several investigators have developed models, which account for the rate of respiration of various produce as a function of extrinsic variables (temperature and gas composition) for different purposes such as design of modified atmosphere packaging and controlled atmosphere storage. These models can broadly be classified as empirical or semi- mechanistic models.

Empirical models

Typical to empirical gas exchange models, as is true of any black box model, is that there is no well-defined model structure. Usually, it is determined by the nature of the produce and the nature and number of extrinsic variables considered during a specific experiment. Let us look at some of such models from literature.

Yang and Chinnan (1988) developed a model for O_2 consumption and CO_2 production rate as a quadratic function of O_2 and CO_2 concentrations and storage time for tomato. The model consisted of nine parameters, determined using regression analysis based on experimental observations and was validated using independent experimental data. The model was found to be in agreement with the observed data with a maximum root mean square error (RMSE) of 3.4%. Moreover, the firmness of tomato as a function of O_2 and CO_2 concentrations was described using a quadratic model involving six parameters that were determined experimentally. They suggested that models based on enzyme kinetics might be more appropriate for gas exchange of produce.

[1] Semi-mechanistic models refers here to models which involve some level of empiricism in formulating the model structure, yet, physical interpretation can be attributed to the model parameters.

Cameron et al. (1989) developed an exponential model for respiration of tomato as a function of O_2 concentration and time. Experimental data of O_2 depletion in time were curve-fitted to determine the model structure and estimate four empirical parameters. The rate of respiration was then calculated by differentiation of the obtained equation. The model was used for design of MA packaging systems.

Similarly, Raghavan and Gariepy (1989) developed a statistical model using experimental time histories of CO_2 and O_2 measurements for cabbage. Respiration rate and respiration quotient were expressed as a linear function of O_2 and CO_2 concentrations. The model consisted of three parameters.

Talasila et al. (1992) described the O_2 consumption rate of strawberries as a function of O_2 and CO_2 concentrations and temperature. The model was quadratic with respect to O_2 and CO_2 concentrations and exponential with respect to temperature, involving six parameters determined by non-linear curve fitting. For the gas concentrations and temperature range considered, the model was reported to adequately predict the O_2 consumption rate of freshly harvested strawberries.

Other more simplified models have also been developed, which, for example, use a single Arrhenius equation (Mannapperuma et al., 1989; Mannapperuma and Singh, 1994). Distinctive to all these models is that the structure of the model is an arbitrary function tailored to fit the experimental data. Hence, the estimated parameters are merely coefficients with no physical interpretation and only apply to the conditions specified in the experiment. Such models can hardly be adapted to situations other than the ones specified in the experiment by modifying the parameters, showing very limited flexibility and thus limited applicability.

Semi-mechanistic models

Even though respiration is a complex physiological process, which involves several enzymatic reactions that take place through various metabolic pathways and transport systems, semi-mechanistic models assume that respiration can satisfactorily be represented by a single enzymatic-mediated reaction (Chevillotte, 1973). Thus, Michaelis-Menten type enzyme kinetics, commonly applied to microbial respiration, with temperature dependence expressed using the Arrhenius equation were proposed.

This relationship is often extended to include the inhibitory effect of CO_2 on the uptake of O_2 and fermentation. There are three inhibition types identified in

literature (Chang, 1981), namely, the competitive, uncompetitive and the combination of the above two. In the *competitive* type inhibition, CO_2 (the inhibitor) and O_2 (the substrate) compete for the same active site on the enzyme, resulting in a dead-end enzyme-inhibitor complex. In the *uncompetitive* type, the inhibitor binds to the enzyme-substrate complex as it has formed, and again a dead-end ternary enzyme-substrate-inhibitor complex is produced. The combined type is when the inhibitor competes to bind to both the active sites of the enzyme and the enzyme-substrate complex. In the case where the competitive and uncompetitive inhibitions retain their relative activity, it is commonly called the *mixed* inhibition. A special case of the mixed type of inhibition is when the relative activity of the competitive and uncompetitive inhibitions is assumed to be the same. This is called the *non-competitive* inhibition. In the rest of this chapter, the terms competitive, uncompetitive, non-competitive and mixed will be used as defined above. Some efforts made to apply the Michaelis-Menten type model to describe the gas exchange of fruit and vegetables are cited henceforth.

Referring to the similarity of microbial respiration and that of fresh produce, Lee et al. (1991) proposed Michaelis-Menten type kinetics to model respiration of fresh produce. They advocated that at elevated concentrations of CO_2, the uncompetitive inhibition of CO_2 on the consumption of O_2 is a valid consideration as long as the product undergoes aerobic respiration. The model was extensively tested using published data of a wide variety of commodities as well as experimental data.

Later, Peppelenbos and van't Leven (1996) evaluated all types of inhibition (based on the Michaelis-Menten type kinetics) for modelling the influence of CO_2 levels on O_2 uptake as compared to no influence of CO_2. Both the non-competitive and mixed types of inhibition models gave best results for most of the products evaluated. Moreover, Peppelenbos et al. (1996) also developed and validated a model for CO_2 production, which assumes that simultaneous oxidative and fermentative processes take part in its (CO_2) production.

Hertog et al. (1998) developed a dynamic generic model describing the respiration in response to temperature and environmental gas conditions using the combined inhibition. The model describing the production of CO_2 by fermentation was extended to include the inhibition of CO_2 on fermentation. The model was validated using different types of produce, and the gas exchange pattern exhibited by different products was described sufficiently well.

Lammertyn et al. (2001) applied the non-competitive type inhibition to describe both the respiration rates of intact Conference pear fruit and pear cell protoplasts in suspension. In this comparative study, it was found that due to the incorporation of gas diffusion properties, the kinetic (Michaelis-Menten) constant was significantly larger for intact pears than protoplast suspension. The interesting inference that can be made from this result is that when fruit are packed together in bulk could there be an interaction effect that can significantly influence the kinetic parameter?

The advantage of the latter models is that the model structure is maintained when representing various gas exchange patterns of a variety of fruit and vegetables. This means that the involved parameters are attached to some physical meaning and thus, by adjusting these parameters the model could easily be adapted without modifying the structure. It must be emphasised that although enzyme kinetics based model incorporate some biochemical background, many issues such as gas diffusion in the fruit and through the cuticle as well as the effect of ethylene are not addressed. Therefore, care should be taken in interpreting the model parameters. It is obvious, however, that when presented to a specific experimental condition under which an empirical model is developed, the prediction accuracy of the semi-mechanistic models is less than or at best equal to the empirical model. Given that the model attempts to describe the metabolic pathways entailed during respiration through simplified enzyme kinetics, this relates to the fact that the model contains some information about the product quality.

The experimental data used to validate these models, be it empirical or semi-mechanistic, were obtained from experimental set ups which consider a single or a couple of fruit. Moreover, fresh or a few weeks old fruit were usually employed. This means that the influence of the interaction of the fruit in bulk storage and the age of the fruit might have influence on the estimated model parameters using data from the single fruit experiments. Thus, the need to assess and validate the existing models for their appropriateness in bulk storage and relatively longer storage time conditions.

2.3. Materials and method

2.3.1. Gas exchange models assessment

From the foregoing discussion, it is clear that the Michaelis-Menten type enzyme kinetic models are most appropriate model structures that enable to attain the stated

objectives. Here, the suitability of the different variants of the Michaelis-Menten model structures is assessed with respect to modelling gas exchange of bulk pome fruit.

At very low concentrations of CO_2 the rate of O_2 consumption can be described using the Michaelis-Menten kinetics with no inhibition (Lee et al., 1991).

$$V_{O_2} = \frac{V_{m,O_2} P_{O_2}}{K_{m,O_2} + P_{O_2}} \tag{2.1}$$

where V_{O_2} is the rate of O_2 consumption [mol kg^{-1} s^{-1}]; V_{m,O_2}, the maximum O_2 consumption rate [mol kg^{-1} s^{-1}]; K_{m,O_2}, the Michaelis Menten constant for O_2 consumption [kPa] and P_{O_2} the O_2 partial pressure [kPa]. The influence of CO_2 on the gas exchange rate of pip fruit has been studied by several investigators. Jurin and Karel (1963) observed the reduction in respiration at CO_2 concentrations above 5-6% on MacIntosh apples. Similarly, Fidler and North (1967) reported the influence of CO_2 on uptake of oxygen for various apple varieties. Moreover, Yearsley et al. (1997) observed a significant decrease in O_2 uptake at elevated CO_2 concentration (8%). On the contrary, Peppelenbos and van't Leven (1996) found no inhibitory effect of CO_2 on respiration of 'Golden Delicious' and 'Elstar' apples at 5% CO_2 concentration when applied for a short duration of time (4 days). de Wilde et al. (1999) showed that increased CO_2 partial pressure retarded respiration of Conference pears which was later confirmed by Lammertyn et al. (2001). The foregoing citations suggest that the inclusion of the inhibitory effect of CO_2 on O_2 uptake is relevant in the present inquiry.

After having evaluated a variety of fruit and vegetables, Peppelenbos and van't Leven (1996) advocated the simultaneous existence of the competitive and uncompetitive inhibition in respiration process. This means that the non-competitive (Eq. (2.2)) and the mixed type (Eq. (2.3)) models best describe the gas exchange process of fruit and vegetables, in general. These models are expressed mathematically as:

$$V_{O_2} = V_{m,O_2} \frac{P_{O_2}}{\left(K_{m,O_2} + P_{O_2}\right)\left(1 + \dfrac{P_{CO_2}}{K_{mn,CO_2}}\right)} \tag{2.2}$$

$$V_{O_2} = V_{m,O_2} \frac{P_{O_2}}{K_{m,O_2}\left(1+\frac{P_{CO_2}}{K_{mc,CO_2}}\right)+P_{O_2}\left(1+\frac{P_{CO_2}}{K_{mu,CO_2}}\right)} \tag{2.3}$$

where V_{m,O_2} is the maximal O_2 uptake rate [mol kg^{-1} s^{-1}] and K_{m,O_2}, K_{mn,O_2}, K_{mc,O_2}, K_{mu,O_2} are the Michaelis-Menten constants for O_2 consumption, non-competitive CO_2 inhibition, competitive CO_2 inhibition, and uncompetitive CO_2 inhibition [kPa], respectively.

The description of the CO_2 production rate consists of an oxidative and a fermentative part and can be stated as (Peppelenbos et al., 1996):

$$V_{CO_2} = RQ V_{O_2} + \frac{V_{m,CO_2,f}}{\left(1+\frac{P_{O_2}}{K_{m,O_2,f}}\right)} \tag{2.4}$$

where RQ is the respiration quotient; $V_{m,CO_2,f}$, the fermentative CO_2 production rate [mol kg^{-1} s^{-1}] and $K_{m,O_2,f}$, the Michealis-Menten constant for O_2 inhibition on fermentative CO_2 production rate [kPa]. The maximum O_2 consumption rate, V_{m,O_2}, (Eqs. (2.2) and (2.3)) and fermentative CO_2 production rate, $V_{m,CO_2,f}$, (Eq. (2.4)) were made temperature dependent according to Arrhenuis Law (Eqs. (2.5) and (2.6)); while Michaelis-Menten constants were assumed to be temperature independent (Hertog et al., 1998).

$$V_{m,O_2} = V_{m,O_2,ref} \exp\left[\frac{E_{a,O_2}}{R}\left(\frac{1}{T_{ref}}-\frac{1}{T}\right)\right] \tag{2.5}$$

$$V_{m,CO_2,f} = V_{m,CO_2,f,ref} \exp\left[\frac{E_{a,CO_2}}{R}\left(\frac{1}{T_{ref}}-\frac{1}{T}\right)\right] \tag{2.6}$$

with $V_{m,O_2,ref}$ and $V_{m,CO_2,f,ref}$ the maximal O_2 consumption and CO_2 production rates at reference temperature ($T_{ref} = 283\ \mathrm{K}$), respectively [mol kg^{-1}s^{-1}], and E_{a,O_2}

and E_{a,CO_2} the activation energies of O_2 consumption and CO_2 production [J mol^{-1}].

Furthermore, these representations exhibit generic behaviour in that when no inhibition is apparent for a given type of fruit, the corresponding kinetic parameters could easily be set to infinity to reduce the models to the simplest case of no inhibition representation (Eq. (2.1)). Therefore, here, both the combined and non-competitive type of inhibitions were considered for validation using experimental data from bulk-stored fruit.

2.3.2. Experimental set up

The developed experimental set up is shown in Figure 2.2. The set up consisted of a PVC box (755x573x1075mm) inverted on a 250mm high water-lock system to prevent leakage. 60 to 70 kg of fruit were placed inside the box and to ensure homogeneity, it was equipped with a fan and flow guide. After an adaptation period of 48 h, during which the box was flushed with a known concentration of gas, the box was completely sealed and the evolution of the concentration of the respiratory gases was measured at regular intervals of 15 minutes. Samples for measurements were acquired from the closed system by using an external pump, which circulated back the gas to avoid under-pressure conditions in the box. The gas concentration measurements were carried out with a gas chromatograph (CP2002–P, Varian-Chrompack, Bergen op Zoom, The Netherlands) equipped with a Molsieve 5Å molecular sieve column for analysis of O_2 and N_2 (accuracy 0.002%) and a HayesepA packed column for analysis of CO_2 (accuracy 0.03%). An automatic pump sampling system samples at a flow rate of 5-20 ml min^{-1} for 40s. The output of the gas chromatograph was expressed in percentages or mole fractions and was normalized. The total pressure was monitored during sampling with a pressure sensor (PTX 520-0, Druck, Barendrecht, The Netherlands) and partial pressures were obtained by multiplying the mole fractions and the total pressure. The temperature was measured with T-type thermocouples via a data logger (HP34790, Agilent technologies, U.S.A). A PC recorded the data collected by these instruments. Fresh Conference pears (*Pyrus Communis* L.) bought during the harvest period and fruit stored under ULO conditions (2.5% O_2, 0.7% CO_2 and -1°C) for 9 months were used so that the effect of age could be studied. The experiments were carried out at 1 and 7°C using the fresh and ULO-stored fruit and at 12°C using the fresh fruit only. In dealing with such a large set up, the problem of leakage is an inevitable phenomenon. In order to account for the leakage or possible gas diffusion through

the water lock system, the empty box was first run by changing the composition of the inside air to an initial concentration of 1.2 kPa O_2 and 12.8 kPa CO_2. The change in gas composition was followed in time and a leakage model was established.

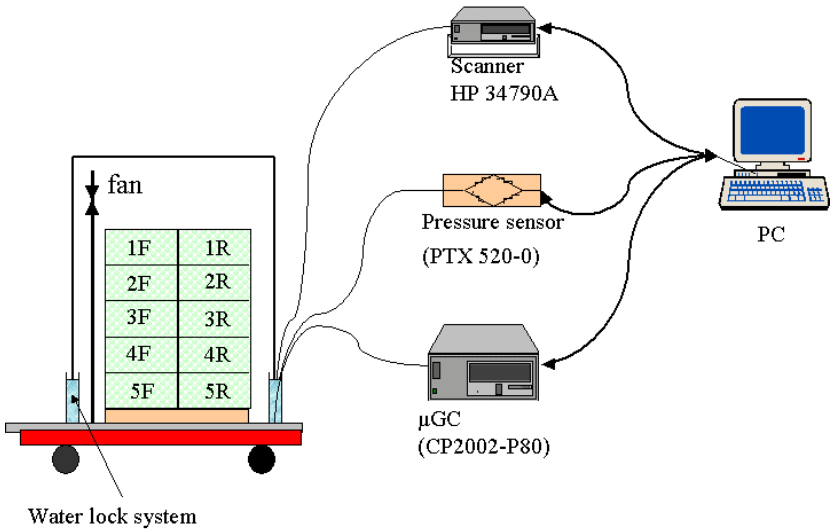

Figure 2.2 Schematic representation of the experimental set up

2.3.3. The gas exchange model

The evolution of O_2 and CO_2 concentration in the box was modelled by considering a mass balance in the box. The overall mass balance for O_2 and CO_2 concentration, assuming the gas composition obeys the ideal gas law, yields:

$$V\frac{dP_{O_2}}{dt} = -M_{pr}RTV_{O_2} + k_{O_2,leak} \qquad (2.7)$$

$$V\frac{dP_{CO_2}}{dt} = M_{pr}RTV_{CO_2} + k_{CO_2,leak} \tag{2.8}$$

where V is the free volume of the box [m^3]; P_{O_2} and P_{CO_2} the partial pressures of O_2 and CO_2, respectively [Kpa]; M_{pr} mass of stored product [kg]; R the universal gas constant [J mol^{-1} K^{-1}]; T temperature [K]; V_{O_2} and V_{CO_2} the O_2 consumption and CO_2 production rates, respectively [mol kg^{-1} s^{-1}]. The terms $k_{O_2,leak}$ and $k_{CO_2,leak}$ [mol s^{-1}] account for the influx of gas in or out of the box through leakage and/or diffusion and can be expressed as:

$$k_{O_2,leak} = \left(U_m A\right)_{O_2}\left(P_{O_2,amb} - P_{O_2}\right) \tag{2.9}$$

$$k_{CO_2,leak} = \left(U_m A\right)_{CO_2}\left(P_{CO_2,amb} - P_{CO_2}\right) \tag{2.10}$$

where U_m is the overall mass transfer coefficient [m s^{-1}]; A, the mass transfer area [m^2] and $P_{O_2,amb}$ and $P_{CO_2,amb}$, the ambient partial pressures of O_2 and CO_2, respectively [kPa]. As established earlier, for the rate of respiration of the fruit, V_{O_2}, the mixed and non-competitive types of inhibitions were considered (Eqs. (2.2)) and (2.3)). With regards to the CO_2 production rate, the model, which takes into account the oxidative and fermentative CO2 production, was used (Eq. (2.4)). The temperature dependence of the maximum consumption and production rates for O_2 and CO_2 in these equations (Eqs. (2.2) – (2.4)) were described using Eqs. (2.5) and (2.6), respectively.

The parameters for the models, obtained from literature (Lammertyn et al., 2001), are tabulated in Table 1. It can be observed, here, that the confidence interval of most of the kinetic parameters is large, sometimes even larger than the nominal value. This is inherent to the Monod type models in that during parameter identification the kinetic parameters can be highly correlated to the maximum consumption rate, hence, the problem of uniqueness (Versyck et al., 1997). The

models were implemented in MATLAB (The MathWorks Inc., Natick, Massachusetts).

Table 2.1. Model parameter values for individual pears (U: uncompetitive, M: mixed) (Lammertyn et al., 2001)

O_2 consumption		CO_2 production	
$V_{m,O_2,ref}$ [mol kg^{-1} s^{-1}]	(87.1±7.9)×10^{-9}	$V_{m,CO_2,f,ref}$ [mol kg^{-1} s^{-1}]	(43.0±6.5) ×10^{-9}
E_{a,O_2} [J mol^{-1}]	(64.6±4.7) ×10^3	E_{a,CO_2} [J mol^{-1}]	(58.5±8.9) ×10^3
K_{m,O_2} [kPa]	*U:* (6.2±0.9) ×10^3 *M:* (6.7±1.5) ×10^3	$K_{m,O_2,f}$ [kPa]	(0.69±0.2) ×10^3
K_{mc,CO_2} [kPa]	(24.6±71.1) ×10^3	RQ	0.76±0.03
K_{mu,CO_2} [kPa]	(44.8±31.4) ×10^3		
K_{mn,CO_2} [kPa]	(70.7±21.6) ×10^3		

2.4. Results

2.4.1. Estimation of leakage/diffusion parameters

From the empty box experiment the parameters $(U_m A)_{O_2}$ and $(U_m A)_{CO_2}$ were estimated using the optimisation tool of MATLAB (The MathWorks Inc., Natick, Massachusetts). The parameters were found to be 3.40×10^{-8} and -7.61×10^{-8} m^3 s^{-1}, respectively. Figure 2.3 shows the fitted experimental data from the empty box experiment. It is observed that the value for CO_2 is higher than that of O_2. This means that for the same concentration gradient the rate at which CO_2 leaks/diffuses is higher than that of O_2. Seemingly, due to smaller molecular size (with respect to leakage) and higher diffusivity of O_2 in water, the opposite phenomenon was expected. This could be explained by the higher solubility of CO_2 in water and as a result, it can be speculated that the interaction with the atmosphere was mainly by diffusion through the water lock system.

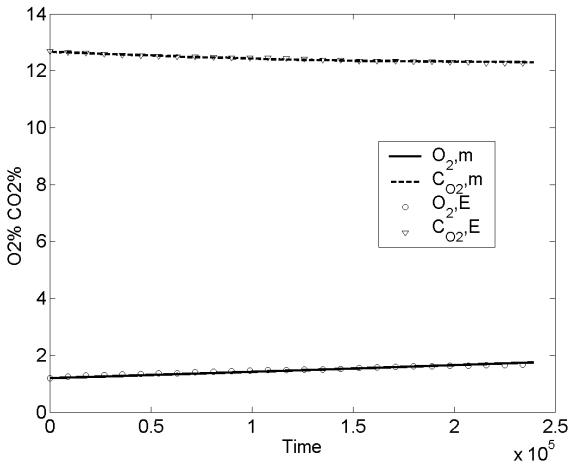

Figure 2.3 Fitted experimental data from the empty box experiment (m: Model; E: Experiment)

2.4.2. Validation of respiration models

Figures 2.4 – 2.8 show the measured and simulated respiratory gas concentrations at different temperatures and age of fruit, using the previously estimated leakage parameters. It can be observed that for pears, at relatively low levels of CO_2 concentration such as those used in CA conditions, the two models give similar results. At higher temperature (Figure 2.8), a slight distinction could be made between the two models at higher concentration of CO_2 (> 6%) and lower O_2 concentration (<4%). Comparing the RMSE between the experimental data and the two models, it can be observed that they are very close. In most of the cases, the non-competitive model gives slightly smaller RMSE. Nevertheless, this might not be significant in comparison to the biological variability observed in the large confidence interval of the parameters. Generally, as can be visually inspected and from the RMSE values, no preference could be made between the two models (non-competitive and mixed type), especially at lower temperatures.

At 1°C (Figures 2.4 and 2.5), it is observed that the models over-predict the measured concentrations of CO_2 and under predict that of O_2 when fresh fruit were used while they under predict the measured CO_2 concentration and over predict that of O_2 when older fruit were used. At 7°C (Figure 2.6 and 2.7), the model under-predicts the experimental results of CO_2 and over predicts that of O_2, in both cases.

However, an increase in O_2 consumption rate was observed with increasing age of the fruit at both temperatures. At 12°C (Figure 2.6) and using fresh fruit, the model seems to predict the experimental data well at lower concentrations while deviation is observed at concentrations of CO_2 >8%. The sudden change of slope in the measured O_2 concentration when it reaches around 1% level (Figure 2.5 and 2.7) is caused by the shift from aerobic to anaerobic respiration of the fruit. The fluctuation observed in the model predictions is due to the use of measured total pressure inside the box during the calculation of the partial pressures.

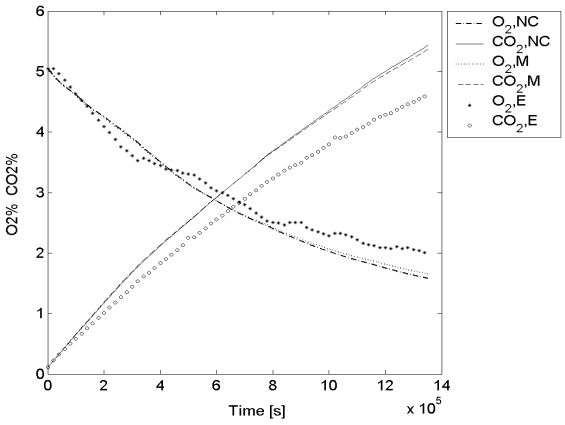

Figure 2.4 Measured and simulated CO_2 and O_2 concentrations [%] at 1°C using fresh fruit. RMSE(O_2,NC, O_2,E) = 0.24%; RMSE(O_2,M, O_2,E) = 0.21%; RMSE(CO_2,NC, CO_2,E) = 0.46%; RMSE(CO_2,M, CO_2,E) = 0.44%. (NC: Non-Competitive; M: Mixed; E: Experiment).

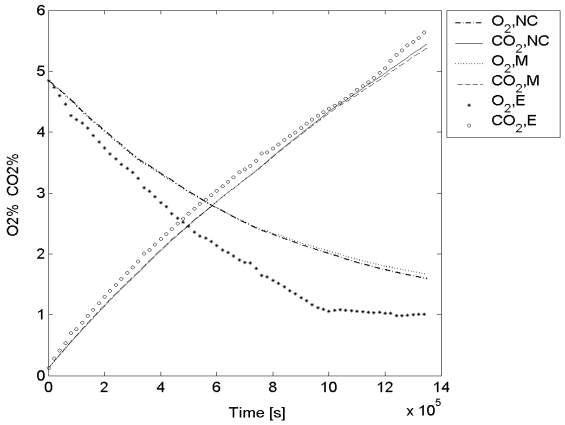

Figure 2.5 Measured and simulated CO_2 and O_2 concentrations [%] at 1°C using CA stored fruit. RMSE(O_2,NC, O_2,E) = 0.63%; RMSE(O_2,M, O_2,E) = 0.65%; RMSE(CO_2,NC, CO_2,E) = 0.15%; RMSE(CO_2,M, CO_2,E) = 0.16%. (NC: Non-Competitive; M: Mixed; E: Experiment)

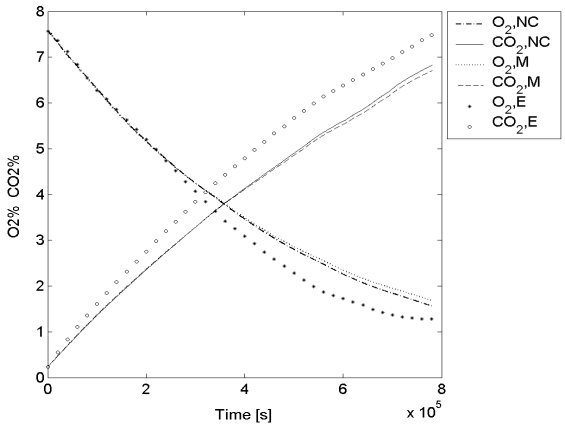

Figure 2.6 Measured and simulated CO_2 and O_2 concentrations [%] at 7°C using fresh fruit. RMSE(O_2,NC, O_2,E) = 0.36%; RMSE(O_2,M, O_2,E) = 0.42%; RMSE(CO_2,NC, CO_2,E) = 0.59%; RMSE(CO_2,M, CO_2,E) = 0.63%. (NC: Non-Competitive; M: Mixed; E: Experiment)

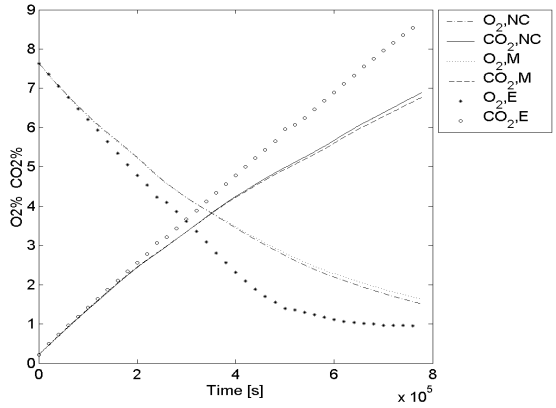

Figure 2.7 Measured and simulated CO_2 and O_2 concentrations [%] at 7°C using CA stored. RMSE(O_2,NC, O_2,E) = 0.92%; RMSE(O_2,M, O_2,E) = 0.97%; RMSE(CO_2,NC, CO_2,E) = 0.99%; RMSE(CO_2,M, CO_2,E) = 1.03%. (NC: Non-Competitive; M: Mixed; E: Experiment)

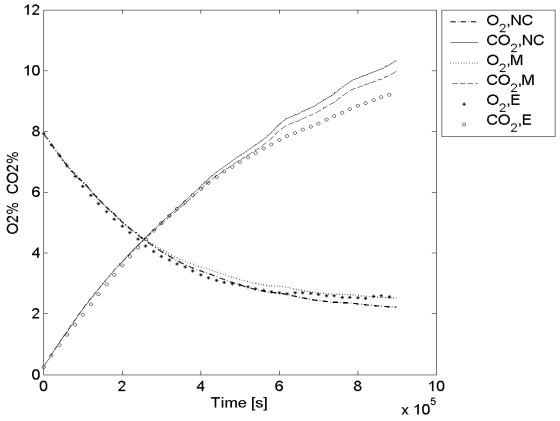

Figure 2.8 Measured and simulated CO_2 and O_2 concentrations [%] at 12°C using fresh fruit. RMSE(O_2,NC, O_2,E) = 0.15%; RMSE(O_2,M, O_2,E) = 0.16%; RMSE(CO_2,NC, CO_2,E) = 0.47%; RMSE(CO_2,M, CO_2,E) = 0.3%. (NC: Non-Competitive; M: Mixed; E: Experiment)

In order to confirm whether the observed higher respiration rate at 1°C and 7°C with the physiologically older fruit was due to biological variability or fruit age, the fruit used for the experiment at 7°C with the ULO-stored fruit were utilized for yet another replicate experiment. The result is depicted in Figure 2.9. A considerable increase in respiration rate was observed and hence, it is apparent that there is a significant effect on gas exchange of the fruit as they age.

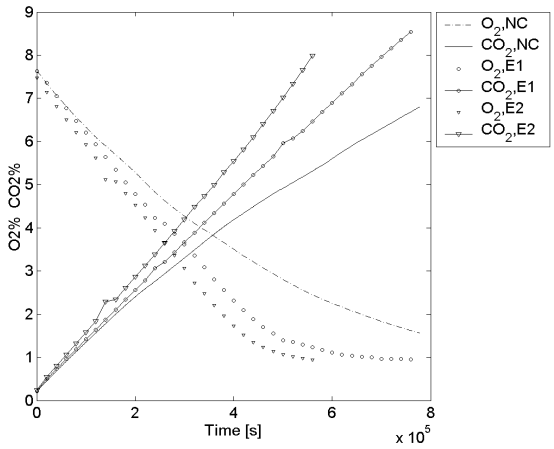

Figure 2.9 Effect of fruit age on gas exchange of pears (7°C) (NC: Non-Competitive; M: Mixed; E1: Experiment 1; E2: Experiment 2)

In general, at the fruit level, the kinetic parameter K_{m,O_2} contains the information not only about the respiration rate but also about the macroscopic gas diffusion through the pear tissue and skin (Lammertyn et al., 2001). It was also observed that there is a significant increase in diffusivity of O_2 and CO_2 through the flesh as well as the skin as the fruit age (Schotsmans, 2003). As a result, it can be inferred that the K_{m,O_2} value changes with fruit age. Moreover, due to these changes in diffusivity, the extent to which respiration may be inhibited by CO_2 or fermentation by O_2 might well be affected, consequently, altering the parameter values of K_{mn,CO_2} and $K_{m,O_2,f}$.

Subsequently, estimating these parameters from the experimental data at hand can explain to some extent the discrepancy between the model and experimental data.

When the estimated parameters lie within the bounds of the confidence interval of the nominal parameters, the observed discrepancy could be attributed to biological variability and otherwise to other effects such as fruit age or interaction effect of the fruit. One should be careful, here, that the large confidence interval involved in some of the parameters might not be due, solely, to biological variability, but also to the problem of uniqueness mentioned earlier related to the identification of the parameters.

In the estimation of the parameters, the non-competitive inhibition model was considered. Owing to the relatively low concentration of CO_2 and a high value of K_{mn,CO_2} as compared to K_{m,O_2} and $K_{m,O_2,f}$ it is assumed that the K_{mn,CO_2} value remains unaffected. This, on the other hand, avoids the parameters with very large confidence interval. Thus, the two other kinetic parameters of the model were estimated for 1°C and 7°C. The results are summarised in Table 2.2.

Table 2.2 Summary of the re-estimated kinetic parameters

Temperature [°C]	Age of fruit	K_{m,O_2} [kPa] $\times 10^3$	$K_{m,O_2,f}$ [kPa] $\times 10^3$
Confidence interval of nominal parameters		[5.3 7.1]	[0.49 0.89]
1	Fresh	7.0	0.48
	CA-stored	3.7	0.34
7	Fresh	5.4	0.87
	CA-stored	3.5	0.84

The estimated K_{m,O_2} values for the fresh fruit lie in the 95% confidence interval for 1°C and more or less at the boundary for 7°C, whereas for the CA-stored fruit it was found to be outside the confidence interval. A significant decrease in K_{m,O_2} is observed suggesting an increase in O_2 uptake rate with age. The estimated $K_{m,O_2,f}$ values lie in the 95% confidence interval except for the CA-stored fruit at 1°C, which was found to be lower. For the fresh fruit, it is apparent here that if there is any interaction effect of the fruit on their respiration rate, it is somehow concealed by the biological variability. Age, however, seems to influence the gas exchange significantly and, hence, should be taken into account when the model is considered to simulate long-term storage of fruit. It can be suggested here that in order to

include the observed influence the kinetic parameters can be expressed as a function of the physiological age of the fruit.

2.5. Discussion

In the past decade, Michaelis-Menten type models have extensively been used to represent gas exchange of a wide range of fruit and vegetables. The assessment made on two Michaelis-Menten type gas exchange models shows that no distinction could be made between both as to better describe the experimental data. This is mainly due to the larger variability in the observed rate of respiration as compared to the difference between the model predictions. Having found that both models describe experimental data of a wide range of horticultural produce well, Peppelenbos et al. (1996) proposed the non-competitive over the mixed type for simplicity. Lammertyn et al. (2001) suggested that the non-competitive type is more appropriate to represent the respiration of pears. This can be observed from the high uncertainty involved in the kinetic parameters K_{mc,CO_2} and K_{mu,CO_2} as compared to K_{mn,CO_2}. From the point of view of CA modelling this model could be preferred for having one degree of freedom less than the mixed type.

It was observed here that the age of the fruit had a significant influence on the gas exchange of the fruit. Peppelenbos and Rabbinge (1996) observed the same trend in Cox's Orange Pipin apples. This apparent increase in respiration could be attributed to the fact that more energy is required for maintenance of the aging cells. Moreover, if, at the fruit level, diffusion is the limiting factor, it can also be speculated that the increase in diffusivity of O_2 in the skin and cortex due to age (Schotsmans, 2003) could be the reason behind the increased respiration rate. Though it is not clear which one of the two (energy requirement for maintenance or increased diffusivity of O_2) has major contribution to the increased rate of fruit respiration, they both support the hypothesis that there is a significant increase in fruit respiration rate with age. This, in turn, suggests that the model parameters have some relation to the quality deterioration of the fruit. No interaction effect of the bulk fruit could be detected and if there was any, it was confounded with the biological variability. This could be observed from the estimated kinetic parameters for the fresh fruit, which lie more or less in the bounds of the 95% confidence interval of the nominal parameter data.

2.6. Conclusion

An assessment and validation of gas exchange models for pear fruit was presented. The Michaelis-Menten type gas exchange models were found to be appropriate to employ in CA storage system as compared to the empirical models. The advantage of such models is in their generic behaviour where a wide range of gas exchange patterns from a variety of fruit can be represented without altering the model structure. Moreover, as they attempt to consider simplified kinetics involved in metabolism, product deterioration models can be linked in some way to these models. Based the assessment of the different variants of the Michaelis-Menten kinetics, which consider different inhibition types, the non-competitive and mixed type were found to represent the gas exchange of fruit closely.

Then, the non-competitive and mixed type inhibitions were subjected to experimental data from bulk stored fruit. No distinction between the models could be made at the level of the considered CO_2 concentration. However based on literature recommendations and number of degrees of freedom, the non-competitive type of inhibition was found to be preferable. For those fruit where the inhibitory effect of CO_2 is not apparent, the kinetic parameter for inhibition could be taken as infinity. In this way, the model could still be valid to represent the gas exchange of pome fruit, which exhibit no inhibition by CO_2 at reduced levels of CO_2 concentration. Overall, both models were found to adequately represent the dynamic population behaviour of the bulk stored fruit.

The re-estimated values of the kinetic parameters K_{m,O_2} and $K_{m,O_2,f}$ using the experimental data for fresh fruit lied in the bounds of the confidence interval of the '*nominal*' parameters. Hence, no significant interaction effect (due to bulk storage) was apparent. On the other hand, significant influence of age of the fruit on their gas exchange rate was observed in that the re-estimated parameters for the aged fruit lied outside of the given confidence interval. Thus, when employed to simulate gas exchange in CA cool storage for longer storage periods, it is recommended that the kinetic parameters be expressed as a function of the physiological age of the fruit in order to include this effect (the experimental data at hand do not allow to establish this relationship). The change in kinetic parameters with fruit age is an indication that theses parameters are bound to have some relation with the quality deterioration of the fruit. In conclusion, the non-competitive type will be employed to represent the gas exchange of the stored produce in the present work.

References

Chevillotte, P. (1973). Relation between the reaction cytochrome oxidase–oxygen and oxygen uptake in cells *in vivo*. *Journal of Theoretical Biology*, 39, 277-295.

Cameron C.A., Boylan-Pett, W., Lee, J. (1989). Design of Modified Atmosphere packaging systems: modelling oxygen concentration within sealed packages of tomato fruit. *Journal of Food Science*, 54(6), 1413-1421.

Chang, R. (1981). Physical chemistry with applications to biological systems. MacMillan Publishers, New York.

de Wilde H.P., Woltering E.J., Peppelenbos, H.W. (1999). Carbon dioxide and 1-MCP inhibit ethylene production and respiration of pear fruit by different mechanisms. *Journal of Experimental Botany*, 50(335), 837-844.

Fidler, J.C., and North, C.J. (1967). The effect of conditions of storage on the respiration of apples. I. The effect of temperature and concentrations of carbon dioxide and oxygen on the production of carbon dioxide and oxygen. *Journal of Horticultural Science*, 42, 189-206.

Hertog, M.L.A.T.M., Peppelenbos, H.W., Evelo, R.G., Tijskens, L.M.M. (1998). A dynamic and generic model of gas exchange of respiring produce: the effects of oxygen, carbon dioxide and temperature. *Postharvest Biology and Technology*, 14, 335-349.

Jurin, V., Karel, M. (1963). Studies on control of respiration of MacIntosh Apples by packaging methods. Food Technology, 17(6), 104-108.

Lammertyn, J., Franck, C., Verlinden, B., Nicolai, B.M. 2001. Comparative study of the O_2 and CO_2 and temperature effect on respiration between 'Conference' pear cell protoplasts in suspension and intact pears. *Journal of Experimental Botany*, 52(362), 1769-1777.

Lee, D.S., Haggar, P.E., Lee, J., Yam, K.L. (1991). Model for fresh produce respiration in modified atmospheres based on principles of enzyme kinetics. *Journal of Food Science,* 56(6), 1580-1585.

Mannapperuma, J.D., Singh, R.P. (1994). Modelling of gas exchange in polymeric Packages of fresh fruit and vegetables. In: Singh, R.P., Oliveira, F.A.R. (Eds.), Process optimisation and minimal processing of foods. CRC Press Boca Raton, 437-458.

Mannapperuma J.D., Zagory, D., Singh, R.P., Kader, A.A. (1989). Design of polymeric packages for Modified Atmosphere storage of fresh produce. In: Fellman, J.K. (Ed.), Proceedings of 5th International Controlled Atmosphere Research Conference, Wenatchee, WA, 2, 225-233.

Nahor, H.B., Schotsmans, W., Scheerlinck, N., Nicolaï, B.M. (2003). Assessment and validation of existing gas exchange models for bulk storage of respiring produce. Submitted for publication in *Postharvest Biology and Technology*.

Peppelenbos, H.W., van't Leven, J. (1996). Evaluation of four types of inhibition for modelling the influence of carbon dioxide on oxygen consumption of fruit and vegetables. *Postharvest Biology and Technology*, 7, 27-40.

Peppelenbos W.H., Tijskens, L.M.M., van 't Leven, J. (1996). Modelling oxidative and fermentative carbon dioxide production of fruit and vegetables. *Postharvest Biology and Technology*, 9, 283-295.

Peppelenbos, H.W., Rabbinge, R. (1996). Respiratory characterstics and calculated ATP production of apple fruit in relation to tolerance of low O_2 concentrations. *Journal of Horticultural science*, 71(6), 985-993.

Raghavan, G.S.V., Gariépy, Y. (1989). Respiration activity of vegetables under CA. ASAE annual International Meeting, Québec, Canada, June 25-28.

Schotsmans, W. (2003). Gas diffusion properties of pome fruit in relation to storage potential. *Ph.D. Thesis* (557), Katholieke Universiteit Leuven, Leuven, Belguim.

Talasila P.C., Chau, K.V., Brecht, J.K. (1992). Effects of gas concentrations and temperature on O_2 consumption of strawberries. *Transactions of the ASAE*, 35(1), 221-224.

Versyck, K.J., Claes, J.E, Van Impe, J.F. (1997). Practical identification of unstructured growth kinetics by application of optimal experimental design. *Biotechnology progress,* 13(5), 524-531.

Yang, C.C., Chinnan, M.S. (1988). Modelling the effect of O_2 and CO_2 on respiration and quality of stored tomatoes. *Transactions of the ASAE*, 31(3), 920-925.

Yearsley, C.W., Banks, N.H., Ganesh, S. (1997). Effect of carbon dioxide on the internal lower oxygen limits of apple fruit. *Postharvest Biology and Technology*, 12, 1-13.

Chapter 3

A continuous-discrete event simulation model for a CA cool store facility: model development

3.1. Introduction

Consumer demand for fresh fruit and vegetables the whole year round has become the driving force for development of effective storage techniques to ensure product quality at the end of a relatively long storage period. Improvements of process operation with respect to product quality requirements can only be achieved by combining knowledge about the product and the process. Given the knowledge of various kinds of physiological activities, which bring about deterioration of the produce, optimal storage conditions can be influenced by the control of the immediate environment of the produce such as the temperature, humidity and gas concentrations. Improved control of these parameters can be ensured by proper design and optimal operation of the involved cool storage facility.

Any strategy to improve quality maintenance of the produce and/or optimal operation of the facility requires to be assisted by techniques, which allow

quantitative assessment of alternative cool store designs through prediction of the influencing variables. In this regard, predictive modelling and computer simulation play an important role.

Model-based dynamic assessment of complete cool/cold storage systems is comparatively a recent development, not that the transient effects were considered unimportant but the tremendous computation capacity required couldn't be met. With the drastically growing computational power, the development of methodologies for dynamic assessment emerged especially for the involved mechanical plants. Further, the incorporation of the discrete processes simulation (abrupt changes due to, for instance, controller action, door opening or defrosting) evidently contributes to increased prediction capacity of these models and their usefulness for the development of robust controllers for better manipulation of the variables. However, to date existing simulation models for cool/cold systems do not pertinently incorporate discrete event simulation.

So far, models developed for complete refrigeration systems are only applicable to conventional cool storage systems where only temperature and moisture are controlled. With the advent of CA storage, the evolution of the gas concentrations entailed in product respiration as well as the dynamics of the corresponding gas-handling unit became important. This requires the inclusion of adequate product respiration models to account, not only for the evolution of the gas concentrations but also the heat of respiration generated as a result of the ongoing physiological processes of the stored produce. Since the underlying mechanisms of respiration and quality deterioration (at least that of firmness loss) are believed to some extent to be similar (Hertog et al., 2001), product quality models can also be coupled to respiration models, to predict the quality degradation of the produce during storage. With such an approach, optimisation of the CA installation with respect to both plant performance and ultimate product quality is possible. The latter is of immense interest for growers due to the financial implication and is often not considered in simulation tools.

The main objective of this Chapter is to develop a model to simulate the dynamics of heat, moisture and gas exchange in the cooled space as well as that of the involved mechanical plants of a controlled atmosphere storage system. This objective will be met using a hierarchical modular approach implemented in an environment, which can handle discrete and continuous time events. Consequently, the model consists of three interacting units, namely, the cooled space, the

refrigeration system and the gas-handling unit. Accordingly, this Chapter is organised as follows. After a short literature review in Section 3.2, the model formulation of a CA cool storage is given in Section 3.3. This Section is divided into three sub-sections dealing with cooled space, the refrigeration system and the gas-handling unit. Subsequently, implementation aspects of the model will be discussed in Section 3.4. Finally, discussion and conclusions will be presented in Sections 3.5 and 3.6, respectively. The results of this Chapter are published in Nahor et al., 2002; Nahor et al., 2003a; Nahor et al., 2003b; Nahor et al., 2003c and Nahor et al., 2004.

3.2. Literature review

3.2.1. Complete refrigeration system models

Existing refrigeration system simulation models can broadly be classified into mechanical and thermal models (Cleland, 1990). The mechanical type models consider the mechanical refrigeration system in detail while ignoring the dynamics of the refrigeration users such as cool/cold rooms or freezers, usually known as applications. On the other hand, the thermal models attempt to take into account the real dynamics of the refrigeration users but use simpler models for the mechanical refrigeration system, normally by including less detail on the hydrodynamic behaviour of the plant. Models that consider both in detail have limited applicability due to their shear complexity, substantial requirement of data and prolonged computation times.

A large number of dynamic models have been developed for different subsystems of refrigeration (cold storage) facility (James and James, 1988; Touber, 1984; Yasuda et al., 1983; MacArthur, 1984; Amos, 1995; Wang and Touber, 1990; Lovatt et al., 1993; Hoang et al., 2003). The literature relevant to the present work mainly focuses on the complete refrigeration system thermal type simulation models.

The first complete simulation model that appeared may be that of Marshal and James (1975). The developed model considered a vegetable freezing plant. The refrigeration unit component models accounted for both mass and energy flows. The air space in the freezer was treated as eight perfectly mixed zones with an ordinary differential equation (ODE) representing the enthalpy of air in each zone. The complete model consisted of 46 ODE's and 105 algebraic equations. Predictions from the model fitted well experimental data.

A generic simulation model for industrial refrigeration systems was outlined by Cleland (1983). The model contained a variety of end users of the refrigeration plant from air-conditioned spaces to low temperature freezers. The air in each end user (application) was assumed to be perfectly mixed and was modelled by ODE's for temperature and humidity. The global model also contained product freezing and chilling models as well as thermal models of the refrigeration plant. The validation of this model was described by Cleland (1985a) in which data from New Zealand meat works was used. Model prediction of the air, freezing and chilling temperatures fitted experimental data with acceptable accuracy. Transients due to step changes in plant operation were poorly represented.

A general simulation model for refrigeration systems, apparently similar to that of Cleland (1985b), was described by Glöckner et al. (1990) denoted STASAN-PC. However, few details were given on the mathematical approaches used in the models or any testing of the model against measured data.

Hasse et al. (1996) developed a top-down model for dynamic simulation of cold storage plants. A mass and energy balance for the air in the cooled space was considered. The model treats the components of the refrigeration unit as well as those that are in the cool room such as the walls and other cold store structure, to predict the most important variables in a cold store operation process. Several operation conditions with respect to different controllers and defrosting strategy have been studied. Favourable agreement of the model predictions with experimental results was reported.

3.2.2. Product models

In CA storage modelling, it is important that quality issues about the product are included, because the quality determines the economic value of the stored produce. This means that the entailed physiological processes of the stored product, complex as they are, need to be represented to a certain extent. With regards to gas exchange a more detailed treatment was presented in Chapter 2.

Concerning product quality, some effort has been made in modelling some of the product quality attributes of pip fruit in relation to storage conditions. Various investigators pursued different approaches. Tijskens (1979) modelled the texture of Golden Delicious apples during storage in CA and air using an exponential decay to an asymptotic end value, describing the breaking force during compression of a

geometrical sample apple tissue. The model described the observed decrease in firmness well in both cases.

Later, Tijskens et al. (1997) developed a dynamic model that describes the decrease in firmness of 'Elstar' apples during different conditions of storage and transport, based on the effects of chemical and biochemical reactions on firmness. The effects of harvest maturity and ethylene have also been included. Fundamental kinetics has been pursued in the formulation of the model. The model was believed to allow optimisation of complete chains of product handling with respect to final expected firmness. Validation of the model was not carried out using experimental data.

A similar fundamental approach, but at cell level, was pursued by De Smet et al. (2002) to predict the mealiness-related texture changes of apple during CA and normal air storage. A number of ODE's were developed by considering mass balance of six chemical compounds pertinent to chemical processes and water transport phenomena at cell level. The model contained 12 parameters estimated using curve-fitting procedures for normal air and CA storage. Assuming the apples were stored at optimal storage temperature, the influence of temperature was not accounted for. The feasibility of the model was feebly tested using experimental data. It was reported that the model described the mealiness-related texture changes reasonably well.

A rather interesting approach was pursued by Hertog et al. (2001), to model the effect of modified atmospheres on the rate of firmness change in 'Braeburn' apples. A Michaelis-Menten type kinetics was proposed to represent the firmness loss during storage, similar to the one used to describe the gas exchange of the fruit. The kinetic parameters obtained for the model were comparable to the gas exchange parameters suggesting a common kinetic background of the two processes as found by other investigators as well (Knee, 1980; Amarante et al., 1997; Hertog et al., 2001; De Smet et al., 2002).

3.2.3. Implementation of complete refrigeration systems model

For implementation purposes of complete refrigeration systems, different software environments have been developed. Here, focus will only be given to the ones, which deal with dynamic simulation.

The package named RADS, made the first attempt at a generalized dynamic refrigeration system simulation environment (Cleland, 1985b). RADS allowed

dynamic simulation of almost any refrigeration system through the use of provided component models. Model equations were solved using a general ODE solver with fourth order error control. The package was first developed to handle continuous events only. However, in later versions discrete events have been addressed partially by checking conditions and changing each discrete state. It was not able to calculate the exact crossover of the discrete event, resulting in occurrence of the event one time step later. Moreover, when a discontinuous event lasts for a short time, the risk of jumping the event without being recognized was possible. RADS was developed in FORTRAN 77 (AISI, New York).

James (1988) developed a "Flexible Modelling Environment", FME using PASCAL (Jensen and Wirth, 1985). Separate files have been used to describe the model instances, which are linked after compilation. No general ODE solver was available within the FME, rather the models that require the solution of an ODE had to include the code to solve the ODE among the model evaluation. Moreover, no explicit provision was made to handle discrete events.

A software named STANSAN-PC SOFTWARE SYSTEM was developed by Glöckner et al. (1990). The software contains subroutines for refrigeration system and components of refrigeration end users. However, no details of the simulation environment has been given, nor on the paradigm pursued.

Lovatt (1992) developed an object-oriented environment for industrial refrigeration systems simulation, by the name 'RefSim', using *Top-Speed* Modula-2 (Wirth, 1982) that can handle both discrete and continuous time events. This simulation environment has solved many of the problems by previous softwares by using the hybrid programming language and inclusion of sophisticated ODE solvers.

Lately, general-purpose environments for simulation of various industrial installations have become available which allow discrete and continuous simulation built on object oriented programming languages. gPROMS (Process systems Enterprise, UK), EcoSimPro (EA International, Madrid, Spain) and PROSIM (Prosim BV, Zoetermeer, The Netherlands) can be mentioned as such modelling environments. These environments are equipped with powerful automatic solvers of systems of differential equations and feature an open architecture, which enables interfacing of external solvers, models and application softwares.

3.2.4. Discussion

From the preceding survey, it can be said that all the refrigeration system models developed so far apply for conventional cool room installations where a refrigeration unit is coupled to one or more applications in which only the temperature and, in few cases the humidity, are controlled. As a result, most of the existing models give little focus on the stored product in which the heat generation is simply represented by an empirical model. Moreover, the emphasis of these works was solely on performance of the plant operation aiming at maintaining the a priori determined settings. With the scheme of CA cool storage systems, the prediction of the concentration of the respiratory gases is required which necessitates the representation of the intricate gas exchange processes of the product with the environment. In turn, since quality deterioration and gas exchange of the stored produce are believed to be closely related, these models can be extended to include product quality indicators. Moreover, the dynamics of the gas handling plant needs to be included to accurately predict the respiratory gas concentrations and, on the whole, the overall performance of the system. Thus, since plant performance alone cannot guarantee increased conservation of product quality after the storage period, control of the processes entailed with respect to product quality ensures the overall objective of productivity.

Concerning the implementation of refrigeration system models, up to now, they are limited to custom-built simulation environments, tailored to fit a specific application. This restricted the ability to incorporate new models or control systems, thus undermining their flexibility. Most of the above discussed simulation environments suffer from the fact that discrete events are partially or not at all addressed. The use of sequential or structured programming languages makes the programs difficult to understand and causes them to be user-unfriendly. Thus, use of general-purpose simulation environments based on object-oriented and open architecture, which can handle both continuous and discrete time events seems a viable option. The advantage of such environments is not only on reducing the complexity through a modular and hierarchical approach but also the increased flexibility achieved through interfacing of other modules developed in compatible programming languages, owing to their open architecture.

3.3. Model formulation

The basis of virtually all theoretical process models are general conservation principles, which are applied to the fundamental quantities that are being conserved. When applied to mass, energy and momentum, result in the governing conservation equations. Having these first principle-based formulations, the most important question posed in modelling is the workable level of complexity to be considered.

Level of model complexity can be classified with regards to the number of states, reaction kinetics and the number of independent variables (Smets et al., 2002). In modelling CA cool storage systems, as in any modelling exercise, limiting the number of states requires identification and distinction of the most important processes and the ones with small influence on the system dynamics. This needs understanding of the physical, chemical and biological processes involved. The complexity regarding reaction kinetics comes into play when attempting to model the response of the stored produce to the environment they are stored in. Since the physiological processes involved are so complex to be represented by a simple chemical reaction(s), assuming only one limiting enzyme responsible for a specific metabolic process reduces the complexity greatly, yet providing significant insight on the metabolic activity of the product. The number of independent variables has to do with space and time discretisation. Especially in large systems, this becomes critical in relation to obtaining results in modest computation times. Thus, in choosing a modelling approach these factors are carefully considered based on the objective of the modelling exercise. In addition, the availability of data for simulation is important especially when the modelling aims at developing a simulation tool for a specific target of users.

The methodology commonly pursued in modelling large systems such as cool storage installations is the 'stirred tank' approach also known as the lumped parameter approach. This method assumes that there is no spatial variation at any instant in the transient processes. Of course this assumption is never satisfied exactly, however, the advantage of using such modelling approach is that the model is kept as simple as possible with acceptable accuracy and reasonable input data requirement. The distributed approach as a core methodology is not an option due to tremendous data requirement and decency of the computation times compared to the accuracy stipulated. However, it can be employed for some component sub-models with limited number of space discretisation elements. A trade-off between these two methodologies can be the zoning approach. This means that the system

under consideration is divided into a number of zones, each zone representing a perfectly mixed region, interconnected by the fluxes occurring between adjacent zones. This leads to a number of ordinary differential equations characterizing the salient state variables. The lumped parameter approach can generally be represented in state space formulation for continuous processes as:

$$\begin{aligned} \frac{d}{dt}\mathbf{x}(t) &= \mathbf{f}(\mathbf{x},\mathbf{u},\mathbf{d}) \\ \mathbf{y}(t) &= \mathbf{h}(\mathbf{x}(t)) \end{aligned} \tag{3.1}$$

where **x** is the vector of the state variables, **u** the vector of input variables, **d** the vector of disturbance variables and **y** the vector of output variables. **f**(*) and **h**(*) are usually vectors of non-linear functions. The consequence of a discrete change to the continuous time dependent behaviour of the mathematical model is that completely new initial value problem is posed after the discrete time event. Thus at time t^+, immediately after the time event the continuous behaviour of the system is generally described by:

$$\begin{aligned} \frac{d}{dt}\mathbf{x}'(t) &= \mathbf{f}'(\mathbf{x}',\mathbf{u}',\mathbf{d}') \\ \mathbf{y}'(t) &= \mathbf{h}'(\mathbf{x}'(t)) \end{aligned} \tag{3.2}$$

where all the new variables are as described above but after the discrete time event.

This Section is concerned with the formulation of the continuous/discrete component models of the CA cool storage system. It is divided into three main sub-sections dealing with the three units, namely, the cool room, the refrigeration plant, and the gas-handling unit. In each sub-section the component models considered in each unit will be described to some detail. Here, emphasis will be given to product model, which will, in turn, be divided into three modules, heat and moisture transfer, product respiration, and product quality models.

3.3.1. Cool room and accessories

The components of the cooled space can be classified as product and non-product components. The non-product components are the cooler, the surfaces that constitute the building envelope, and the medium, air. Here, the transient response of the individual components is formulated by an overall energy and mass balance.

This resulted in a module described by a set of ODE's for each component. The modules are then interconnected to formulate the sub-model for the unit. The modules representing the medium and the components of the cooled space model are discussed henceforth.

3.3.1.1 Room air model

Heat and mass is transferred among the cool store components (cooler, building envelopes, product) through a medium usually air. The energy and mass balance of the well-mixed mass of air results in the characterisation of the room air by temperature, moisture content and concentrations of the respiratory gases (O_2 and CO_2). To deal with spatial variability in the room when using lumped approach, the zoning approach can be pursued (Amos, 1995; Hasse et al., 1996; Tanner et al., 2002). Often, the smaller the size of the room, the better the level of homogeneity that can be achieved. This is true, assuming there is sufficient rate of air circulation and acceptable gradients are imposed on the system, usually through appropriate control system. Hence, in relatively smaller compartments such as a CA cool store, where homogeneous mixing of the air is expected, the use of single zone can be justified. For instance, Amos (1995) used 34 zones to represent an industrial apple cool store with a total volume of 34200 m³. The sizes of the zones ranged from 236 m³ to 4917 m³. Often, the size of industrial CA cool store for pip fruit is in the order of the smallest zone considered by Amos. Other assumptions considered include:

- The mass of dry air is considered constant
- Radiation heat transfer is ignored,
- Thermal properties of the medium as well as of the components in the cool room are considered constant (independent of temperature)
- Heat transfer coefficients were assumed constant.

The structure of the ODE's used to describe the time evolution of temperature, humidity and the respiratory gas concentrations (O_2 and CO_2) for a single zone are represented as follows.

$$\left(\rho V c_p\right)_a \frac{dT_a}{dt} = q_{(c \to a)} + q_r \tag{3.3}$$

$$M_a \frac{dX_a}{dt} = J_{m,(c\to a)} + J_{m,r} \tag{3.4}$$

$$V_a \frac{dc^g}{dt} = M_{pr} r_g + k_g \tag{3.5}$$

where ρ is the air density [kg m^{-3}]; V, the free volume [m^3]; c_p, the air heat capacity [J kg^{-1} °C^{-1}]; T_a, the air temperature [°C]; t, the time [s]; M_a, the mass of air [kg]; X_a, the air moisture content [kg kg^{-1}]; c^g, the gas concentration [mol m^{-3}]; M_{pr}, the mass of stored produce [kg]; r_g, the rate of gas accumulation [mol kg^{-1} s^{-1}] and k_g, the rate of gas flow [mol s^{-1}]. The terms q_r [W] and J_r [kg s^{-1}] (Eqs. (3.3) and (3.4)) are heat and moisture generation terms which represent for instance, the heat generated by people or the ventilators or any loading equipment in the cool room and for the latter, moisture generation by a sprayer or atomizer. The flux densities $q_{(c\to a)}$ [W] and $J_{(c\to a)}$ [kg s^{-1}] represent all the interactions (heat and moisture transfer rates) between the air and any component in the cool room and can generally be formulated as:

$$q_{(c\to a)} = UA\left(T_c - T_a\right) \tag{3.6}$$

$$J_{(c\to a)} = U_m A\left(X_c - X_a\right) \tag{3.7}$$

where U is the overall heat transfer coefficient [W m^{-2} °C^{-1}]; A, the heat or mass transfer area [m^2]; and T_c, the component temperatures [°C]; U_m, the overall mass transfer coefficient [kg m^{-2} s^{-1}]; X_c, the component moisture content [kg kg^{-1}]. The density, ρ and heat capacity, c of the air can be calculated by:

$$\rho_a = \frac{X_a + 1}{\frac{1}{\rho_{da}} + \frac{X_a}{\rho_v}} \text{ and } c_a = \frac{c_{da} + X_a c_v}{X_a + 1} \tag{3.8}$$

where ρ_{da}, ρ_v, c_{da}, and c_v represent the dry air and vapour density and specific heat, respectively. In Eq. (3.5), the term r_g is the rate of production or consumption of the respiratory gases (CO_2 and O_2) as a result of the respiring stored produce. As was discussed in Section 2.3.1 this was represented by Eqs. (2.2) and (2.4) for O_2 and CO_2, respectively. The term k_g stands for the gas transfer rate to and from the gas handling unit as well as the environment through leakage. The schematic representation of the heat and mass transfer processes in the cool room between the room air and the different components is shown in Figure 3.1.

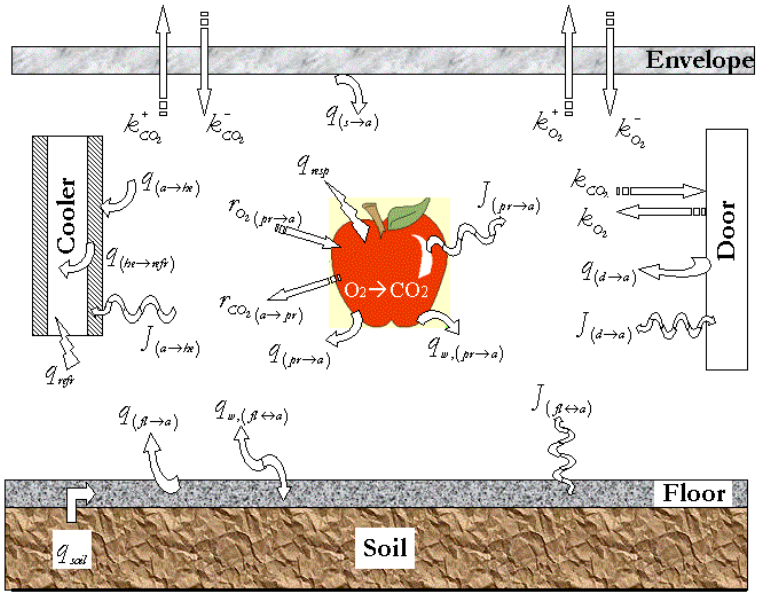

Figure 3.1 Schematic representation of the heat and mass transfer processes in the cool room

3.3.1.2 Heat exchanger (cooling battery) model

The most common heat exchanger employed in cool or cold rooms is the air blast cooling equipment. This equipment forms the boundary between the cool storage space and a refrigeration plant. The system layout of a given cold/cool storage facility is said to be direct when the evaporator of the refrigeration plant is placed inside the cooled space; in indirect systems an intermediate fluid, cooled by the evaporator of the refrigeration plant, is circulated in the heat exchanger placed inside the cooled space. The most common evaporator-expansion valve arrangements are *(i)* the direct expansion, *(ii)* the flooded, and *(iii)* the pump-circulated evaporator types. In industrial CA cool storage systems with direct system layout, the latter is often used. When an indirect system layout is employed, however, the refrigeration unit is usually equipped with a direct expansion evaporator. In all the cases, the thermal evaporator model is generally the same with some minor modifications with respect to the control of the refrigerant flow.

A two-zone model considering the refrigerant that flows inside the tubes as one zone and the tubes, fins and structure as another zone was considered. Assuming the

mass flow rate through the cooler constant, the energy balance for the refrigerant side reads as:

$$\left(Mc_p\right)_{refr}\frac{dT_{refr}}{dt} = q_{(be\rightarrow refr)} + q_{refr} \tag{3.9}$$

$$q_{(be\rightarrow refr)} = \left(UA\right)_{refr}\left(T_{be} - T_{refr}\right) \tag{3.10}$$

$$q_{refr} = \left(\dot{m}\, c_p\right)_{refr}\left(T_{in,refr} - T_{refr}\right) \tag{3.11}$$

where M is the mass of refrigerant [kg]; c_p, the refrigerant specific heat [J kg^{-1} °C^{-1}]; U, the overall heat transfer coefficient [W m^{-2} °C^{-1}]; $q_{(be\rightarrow refr)}$, the heat transferred from the refrigerant to the cooler [W]; A, the heat transfer are [m^2]; T_{be}, the cooler surface temperature [°C]; T_{refr}, the average refrigerant temperature [°C]; q_{refr}, the heat gained by the refrigerant [W]; $\dot{m}$, the refrigerant mass flow rate [kg s^{-1}] and $T_{in,refr}$, the inlet refrigerant temperature [°C]. In direct system layout where the evaporator of the refrigeration unit is placed in the cool room, Eq. (3.11) was formulated using enthalpy differences between the incoming and outgoing refrigerant obtained from the refrigeration unit model.

When considering the cooler side, condensation on the surface of the cooler is an inevitable occurrence. The condensation on surfaces can be described by four phases (Pieters and Deltour, 1997). In the beginning, condensation on the surface kicks off as soon as the temperature falls below the dew-point temperature of the air, until a certain threshold size (drop size in case of drop wise and film thickness in case of film wise condensation) is attained (phase 1). If condensation further continues, water drips and is driven out of the system at a rate the condensate is formed (phase 2). In case condensation stops, then evaporation may start (phase 3) and the droplet size/film thickness decreases until the surface becomes dry and thus no condensation (phase 4). In the case of an air cooler, since the temperature of the cooler is, in most cases, lower than freezing point, the condensed water is solidified into ice and is removed from the system during defrosting process. Of course at this point re-evaporation might occur to some extent before the water drips down to the gutter of the cooler. Here, the condensed water was assumed to be removed from the system completely; hence, no re-evaporation takes place. Moreover, the latent heat of freezing was accounted for by assuming that the all condensed water is solidified. The energy and mass balance on the airside yields:

$$\frac{d\left(\left(\left(Mc_p\right)_{he}+\left(Mc_p\right)_{w,he}\right)T_{he}\right)}{dt}=q_{(a\to he)}+q_{(refr\to he)}+q_{w,he} \tag{3.12}$$

$$q_{(a\to he)}=\left(hA\right)_{(a\to he)}\left(T_a-T_{he}\right) \tag{3.13}$$

$$q_{(refr\to he)}=-q_{(he\to refr)} \tag{3.14}$$

$$q_{w,he}=h_{fg}J_{m,he} \tag{3.15}$$

$$J_{m,he}=\frac{dM_{w,he}}{dt}=h_{m,he}A_{he}\rho_{da}E_{f,he}\left(X_a-X_{he}\right) \tag{3.16}$$

where $(Mc_p)_{he}$ is the thermal mass of the cooler (fluid and structure) [J °C^{-1}]; $(Mc_p)_{w,he}$, the thermal mass of the condensed water on the surface of the cooler [J °C^{-1}]; $q_{(a\to he)}$, the heat transferred from the medium to the cooler [W]; h or h_{he}, the cooler heat transfer coefficient [W m^{-2} °C^{-1}]; A *or* A_{he}, the cooler heat transfer area [m^2]; T_a, the air temperature [°C]; T_{he}, the cooler surface temperature [°C]; $q_{(refr\to he)}$, the heat transferred from the refrigerant to the cooler [W] $q_{w,he}$, heat of condensation [W], $J_{m,he}$, the condensation rate on the surface of the cooler [kg s^{-1}]; h_{fg}, the latent heat of evaporation or condensation[1] [J kg^{-1}]; $M_{w,he}$, the mass of condensed water on the surface of the cooler [kg]; t, the time [s]; $h_{m,he}$, the cooler mass transfer coefficient [m s^{-1}]; ρ_a, the air density [kg m^{-3}]; $E_{f,he}$, the factor for equivalent water covered surface; X_a, the air moisture content [kg kg^{-1}] and X_{he} the interface air moisture content on the surface of the cooler. One can note here that the variable X_{he} is a discrete variable in that its value is zero when there is no condensation and takes the saturation moisture value at T_{he}, the moment the dew point is greater than the cooler temperature. Moreover, since condensation may not occur on the whole surface of the cooler (depending on film or drop-wise condensation), an empirical correction factor, $E_{f,he}$ (Eq. 3.16) is introduced to account for the equivalent water covered surface area of the air cooler.

The temperature of the air blown out of the cooler, commonly called as pulse temperature, was calculated algebraically from the energy balance of the air around the air cooler as:

[1] The latent heat of freezing was accounted for by considering the fact that the latent heat of condensation is 7.5 times that of the latent heat of freezing. Hence, the latent heat of condensation is simply multiplied by a factor 1.125.

$$q_{(a\rightarrow be)} = \left(\dot{m}c_p\right)_a \left(T_a - T_p\right) \tag{3.17}$$

where $\dot{m}$ is the air mass flow rate [kg s^{-1}]; c_p, the air specific heat [J kg^{-1} °C^{-1}]; T_a, the air temperature [°C]; and T_p, the pulse temperature [°C]. Here, it is assumed that there is no air re-circulation, i.e., air re-circulation ratio is null[2]. The formation of ice on the surface of the tubes and fins of the cooler from condensing vapour undermines the performance of the cooler by reducing the effective heat transfer coefficient. Thus, defrosting operation is performed periodically by introducing a hot fluid into the cooler or using electrical heaters. The defrosting cycle of the cooler was modelled using a timer-based discrete heat load variable imposed on the cooler during the defrosting period. This load can be determined from observed temperature difference of the incoming and outgoing hot fluid used for defrosting or the dissipated power, in the case of the electrical heaters. The interval between subsequent defrosting actions was controlled based on a clock.

3.3.1.3 Surface model

The insulating walls, the ceiling and the floor are surfaces, which separate the cool store air from the outside. The mechanisms of the heat transfer through these surfaces may occur by convection (between air and boundary surfaces), conduction (through the surface material) and radiation. Several approaches of modelling thermal behaviour of insulating surfaces are discussed in Flores et al. (2001). Here, a lumped resistance and capacity approach within a single zone was pursued. The surface was considered as a one-dimensional slab in which the thermal capacity is lumped on one side and the change of temperature at this side is modelled. Radiation heat transfer between the surfaces was ignored. (To get a meaningful radiation heat flux, since the Stephan Boltzman constant is very small, it requires very high temperature gradient or very large surface area, in which neither is satisfied in the present case). Moreover, since CA rooms (often referred to as cells) are constructed inside building envelopes, they are not directly exposed to the sun, and thus the effect of solar radiation was neglected. Therefore, convection from the outside environment, conduction through the surface and convection inside the room, in the case of the walls and ceiling, and, conduction through the soil, concrete,

[2] Hoang (2003) estimated using CFD simulations a loss of 2.8% in flow rate due to air re-circulation in an empty cool cell. This value, however, can be different from one cool cell to another depending on factors such as the type fan, structure of cooler and the size of the cell.

floor slab and insulation and convection inside the room, in the case of floor were considered. Since insulation against moisture transfer from the soil to the concrete slab is often provided, penetration of moisture to the room through the floor is unlikely and thus can be neglected. The energy balance around a surface yields:

$$\frac{d\left(\left(\left(Mc_p\right)_s+\left(Mc_p\right)_{w,s}\right)T_s\right)}{dt}=q_{(a\to s)}+q_{(amb\to s)}+q_{w,s} \tag{3.18}$$

$$q_{(a\to s)}=\left(hA\right)_s\left(T_a-T_s\right) \tag{3.19}$$

$$q_{w,s}=h_{fg}J_{m,s} \tag{3.20}$$

$$J_{m,s}=\frac{dM_{w,s}}{dt}=h_{m,s}A_s\rho_a E_{f,s}\left(X_a-X_s\right) \tag{3.21}$$

where $(Mc_p)_s$ is the thermal mass of the surface [J °C^{-1}]; $(Mc_p)_{w,s}$, the thermal mass of the condensed/evaporated water [J °C^{-1}]; $q_{(a\to s)}$, the heat transferred from the medium to the surface [W]; q_{amb}, the heat transferred from the ambient to the surface [W]; $q_{w,s}$, the condensation/evaporation heat [W]; h, the heat transfer coefficient [W m^{-2} °C^{-1}]; A or A_s, the heat transfer area [m^2]; T_a, the air temperature [°C]; T_s, the inner surface temperature [°C]; h_{fg}, the latent heat of evaporation or condensation[J kg^{-1}]; J_m,s, the moisture transfer rate on the floor [kg s^{-1}]; $M_{w,s}$, the mass of condensed/evaporated water on/from the floor surface [kg]; t, the time [s]; $h_{m,s}$, the floor mass transfer coefficient [m s^{-1}]; ρ_a, the air density [kg m^{-3}]; $E_{f,s}$, the empirical factor for equivalent water covered surface; X_a, the air moisture content [kg kg^{-1}] and X_s the interface air moisture content on the surface of the floor. The term $q_{(amb\to s)}$ can take two forms depending on the surface, whether it is a wall/ceiling (Eq. (3.22)) or a floor (Eq. (3.23)).

$$q_{amb}=\left(U_{amb}A_s\right)\left(T_{amb}-T_s\right) \tag{3.22}$$

$$q_{amb}=\left(\frac{1}{R_{fl}}\right)\left(T_{soil}-T_s\right) \tag{3.23}$$

where U_{amb}, the overall heat transfer area at the outside of the surface [W m^{-2} °C^{-1}]; and T_{ambs}, the ambient temperature [°C]; R_{fl}, the overall soil and floor resistance [°C W^{-1}] T_{soils}, the deep soil temperature [°C]. When the total area of the surface is not available for condensation/evaporation (for instance, for floor due to the presence of bins or pallets), empirical factor $E_{f,s}$ was considered. The outside temperatures,

i.e., the temperature inside the envelope or that of the deep soil were assumed to be constant. However, when adjacent cells share a common wall, the dynamic room temperature of one cell was considered as a boundary condition to the other cell. As was observed at different occasions, condensation on the surfaces is unlikely and thus can be ignored, however, condensation or evaporation could occur on/from the floor. The four walls, the ceiling and the floor are instances of this class model.

3.3.1.4 Door model

The methodology employed by Lovatt et al. (1998) and Amos (1995) was pursued to model the instantaneous heat and water vapour transfer through open doors using algebraic equations. The model assumes that half the door size is used for entering airflow and the other half for exiting air flow ensuring total mass balance of the cool room and assuming that no pressure change occurs in the room. The model was extended to include the infiltration of the respiratory gases (CO_2 and O_2) during door openings. Two discrete random variables are involved, namely, the time and duration of door opening. These variables are determined using statistical techniques. Skewed (Poisson) distribution for opening frequency was used due to the fact that opening of the door during the day is obviously more frequent than at night. A normal distribution for the duration of opening was assumed. During door opening, which is determined by using the above-mentioned random variables, the following model equations are evaluated.

$$q_d = 0.5 A_d v_{a,d} \left(\rho c_p\right)_a \left(T_{amb} - T_a\right) \tag{3.24}$$

$$m_d = 0.5 A_d v_{a,d} \rho_a \left(X_{amb} - X_a\right) \tag{3.25}$$

$$k_{g,d} = 0.5 A_d v_{a,d} \left(c^g_{amb} - c^g_a\right) \tag{3.26}$$

where q_d is the heat infiltration through the door [W]; A_d, the door area [m^2]; $v_{a,d}$, the air velocity through the door [m s^{-1}]; ρ or ρ_a, the air density [kg m^{-3}]; c_p, the air specific heat [J kg^{-1} °C^{-1}]; T_{amb}, the ambient air temperature [°C]; T_a, the air temperature [°C]; m_d, moisture entering through the door [kg s^{-1}]; X_{amb}, the ambient air moisture content [kg kg^{-1}], X_a, the air moisture content [kg kg^{-1}]; $k_{g,d}$, the rate of gas flow through the door [mol s^{-1}]; c^g_{amb}, the ambient concentration of gas (O_2 or CO_2) [mol m^{-3}]; c^g_a, the gas concentration in the cool room [mol m^{-3}]. Note that this model is only employed during cooling phase and once the cell is set into ULO conditions, no door openings occur.

3.3.1.5 Product model

The product is the target element in CA cool storage practice. The prediction of interaction and response of the stored product with the environment is important to appropriately control the microenvironment at desired conditions. The product metabolic activity in response to the environmental conditions should also be represented not only in order to control the gas composition of the environment, which is the aim of CA storage, but also to characterize the state of the produce during storage to enable optimise environmental conditions with respect to product quality.

Accordingly, three sub-modules representing the heat and moisture transfer, the product respiration and product quality deterioration were developed and were interconnected to form the product model.

Heat and moisture transfer model

The product occupies most of the space in the cool room. In modelling the heat and moisture transfer between the medium and the product the distributed approach can be rejected due to the obvious reason of long computational time requirement. Apparently, a multi-zone lumped parameter approach seems a viable option. Nonetheless, due to increased degrees of freedom in the resulting model, and thus increased uncertainties involved with these required data, the ultimate accuracy gain might not be appreciable. Moreover, when incorporated in the large global CA cool storage system model, the computational load imposed by even the multi-zone model could influence the overall computational performance substantially. For instance, Amos, (1995) employed a multi-zone model to simulate the heat and moisture transfer in a pallet of apples packaged in carton boxes. The limited prediction accuracy of the model was attributed to the uncertainties entailed in the required parameters. Moreover, it was rejected as too complex to be integrated into a cool room model.

Thus, the heat and moisture transfer of the bulk-stored products was modelled based on single zone energy and mass balance. To predict the cooling dynamics of the product, the energy balance around the bulk product was used. In bulk storage, commonly the wooden bins or cartons are used. Here, it was assumed that the temperature of the packaging was the same as that of the product. However, since these packages can absorb substantial amounts of moisture, this was accounted for.

Only the energy released during condensation on the surface of the packaging is considered, i.e., the heat of absorption is neglected.

$$\frac{d\left(\left(\left(Mc_p\right)_{pr}+\left(Mc_p\right)_b\right)T_{pr}\right)}{dt}=q_{(a\rightarrow pr)}+q_{resp}+q_{m,pr}+q_{m,b} \tag{3.27}$$

$$q_{(a\rightarrow pr)}=\left(hA\right)_{pr}\left(T_a-T_{pr}\right) \tag{3.28}$$

$$q_{resp}=f_{resp}\,M_{pr}\,RQ\,r_{O_2} \tag{3.29}$$

$$q_{m,pr}=-J_{m,pr}h_{fg} \tag{3.30}$$

$$q_{m,b}=J_{m,b}h_{fg} \tag{3.31}$$

where $(Mc_p)_{pr}$ is the thermal mass of the product [J °C^{-1}]; $(Mc_p)_b$, the thermal mass of packaging [J °C^{-1}]; t, the time [s]; $q_{(a\rightarrow pr)}$, the heat transferred from the medium to the product [W]; q_{resp}, the respiration heat [W]; $q_{m,pr}$, the heat of evaporation from the product [W]; $q_{m,b}$, the heat of condensation on the bin [W]; h the product heat transfer coefficient [W m^{-2} °C^{-1}]; A, the product heat transfer area [m^2]; T_a, the air temperature [°C], T_{pr}, the product temperature [°C]; h_{fg}, the latent heat of evaporation or condensation [J kg^{-1}]; f_{resp}, the conversion factor, M_{pr}, the mass of the product [kg]; RQ, the respiration quotient; r_{O_2}, the rate of gas accumulation [kg kg^{-1}]; $J_{m,pr}$, the moisture transfer rate from the product [kg s^{-1}], $J_{m,b}$, moisture transfer rate to/from the package [kg s^{-1}]; c_v, the vapour specific heat [J kg^{-1} °C^{-1}]. The moisture transfer to and from either the product or the bin to the environment involves the partial vapour pressure around these objects. This was determined using the Equilibrium Moisture Isotherms (EMC) for the product as well as for the packaging (bin or carton).

$$J_m=\left(h_mA\right)\left(C_a-C\right) \tag{3.32}$$

where J_m represents $J_{m,pr}$ or $J_{m,b}$ and C represents C_{pr} or C_b, which are the moisture concentrations at the interface of the product and of the bin, respectively. Assuming the vapour behaves ideally the moisture concentrations can be expressed as a function of partial vapour pressure. The partial pressures were calculated from:

$$P=a_wP_{sat} \tag{3.33}$$

$$a_w = f\left(X_{db}\right) \tag{3.34}$$

where P is the air partial vapour pressure [Pa]; a_w , the water activity, P_{sat} , the saturated air vapour pressure [Pa]; X_{db} , dry base moisture content. The water activity, a_w, was determined from the EMC curve and the dry base moisture content, X_{db}, is time dependent variable given by:

$$M_{dm}\frac{dX_{db}}{dt} = J_m \tag{3.35}$$

where M_{dm} represents the dry matter weight [kg].

The advantage of the above-described model is that it requires only a small amount of input data.

Product respiration model

Respiration is responsible for the majority of the heat generated by the product. For the respiration model, reference is made to Chapter 2 where the model was extensively discussed and validated.

Product Quality model

Quality is subjective by nature and difficult to quantify. However, if it is to be modelled it needs to be quantified. Often, quality is determined by organoleptic attributes, physical properties, nutrients and level of microbial and toxicological contaminants. On the other hand, market and consumer perception of product quality is in terms of quality attributes such as colour, shape, taste, mouth feel and odour. In relation to pome (hard) fruit, firmness and colour are usually considered as attributes to quantify quality.

Here, the aim is to describe the relationship between external factors and product quality attributes. More often than not, this is approached by modelling a single product quality attribute. In the present work, the firmness model developed by Hertog et al. (2001) was adopted as an indicator of the quality of the stored produce. The reason for this was that, besides the model being semi-mechanistic, the kinetic parameters are shared with the respiration model resulting in decreased degree of freedom in the global CA model.

In this model, the total firmness loss was assumed to be a combined result of fermentative and oxidative metabolism. The uncompetitive type of CO_2 inhibition was used to describe the firmness loss associated to oxidative respiration and in the fermentation model, it was assumed that there was no inhibition by CO_2. The model can be stated as:

$$\frac{dF}{dt} = -\frac{dF_o}{dt} - \frac{dF_f}{dt} + F_c \tag{3.36}$$

$$\frac{dF_o}{dt} = \frac{F_{o,\max} P_{O_2}}{K_{m,O_2} + P_{O_2}\left(1 + \frac{P_{CO_2}}{K_{mu,CO_2}}\right)} \tag{3.37}$$

$$\frac{dF_f}{dt} = \frac{F_{f,\max}}{1 + \frac{P_{O_2}}{K_{mc,O_2,f}}} \tag{3.38}$$

The $F_{o,max}$ and $F_{f,max}$ are the maximum rates of firmness loss [N], related to respiration and fermentation, respectively, and F_c is a correction factor for apparent increase of firmness due to cooling [N]. The parameters K_{m,O_2}, K_{mu,CO_2} and $K_{mc,O_2,f}$ are the Michaelis-Menten constants [KPa] for O_2 uptake, uncompetitive CO_2 inhibition on O_2 uptake and O_2 inhibition of fermentation, respectively.

3.3.1.6 Accessories

Components classified as accessories are the different controllers, control elements such as valves, temperature sensors and ventilators. Various control strategies like those based on selective control, which involve a set of PI and PID controllers, On-Off controllers and phenomena related to the implementation of these controllers such as anti-reset windup are included in the model. The details of these components and their models are discussed in appendix A.

3.3.2. Refrigeration unit

The refrigeration unit is responsible for production of low temperature often by using the liquefiable vapour compression cycle. The most important components of

the cycle usually include the compressor, evaporator, and condenser. In modelling the refrigeration unit, Cleland and Cleland (1989) contended that in the case where mainly the load variations to the unit come from the applications (such as the cool rooms) a simple mathematical model based on thermal analysis could give accurate predictions. Darrow et al. (1991) have proved this hypothesis for a simple water chill refrigeration plant operated under variable load conditions. Model predictions fitted well experimental results. Moreover, Lopez and Lacarra (1999) applied this methodology to model industrial scale thermal storage systems for a winery plant with acceptable prediction accuracy.

In the present work, this methodology was adopted. The detailed structures, assumptions and justifications of the models are given in Cleland (1990) and Darrow (1991). However, for the sake of completeness the model structure of the components involved will be discussed briefly hereafter.

3.3.2.1 Evaporator

As discussed earlier the evaporator could be placed inside the room or not, depending on the system layout. In an indirect system layout the evaporator remains only part of the refrigeration cycle servicing the heat exchanger in the room through the secondary refrigerant. In this case, the component is usually insulated and the interaction is limited only with the secondary refrigerant. Considering a single zone, the energy balance, thus, yields:

$$\left(\left(Mc_p\right)_e + \left(Mc_p\right)_{refr}\right)\frac{dT_e}{dt} = -\left(UA\right)_e \Delta T_e + \dot{m}_{refr}\left(h_{e,in} - h_{e,out}\right) + \phi_e \qquad (3.39)$$

where $(Mc_p)_e$ is the evaporator thermal mass [J °C^{-1}]; $(Mc_p)_{refr}$ is the refrigerant thermal mass [J °C^{-1}] T_e, the evaporator temperature [°C]; U, the evaporator overall heat transfer coefficient [W m^{-2} °C^{-1}]; A, the evaporator heat transfer area [m^2], ΔT_e, the log-mean temperature difference [°C]; $\dot{m}_{refr}$, the refrigerant mass flow rate [kg s^{-1}]; $h_{e,in}$, the refrigerant enthalpy entering the evaporator [J kg^{-1}]; $h_{e,in}$, the refrigerant enthalpy exiting the evaporator [J kg^{-1}] and ϕ_e, the evaporator heat loss to the environment [W]. The term ΔT_e can be calculated by means of the log-mean temperature difference formula as:

$$\Delta T_e = \frac{\left(T_{refr,in} - T_{refr,out}\right)}{\ln \frac{\left(T_{refr,in} - T_e\right)}{\left(T_{refr,out} - T_e\right)}} \tag{3.40}$$

where $T_{refr,in}$ and $T_{refr,out,}$ are the secondary refrigerant inlet and outlet temperatures [°C], respectively.

3.3.2.2 Condenser

All the heat gain dealt with by the cooling system must be rejected at the condenser. Condensers could be water-cooled, air-cooled or, as a compromise between the two, evaporative cooled. The water used by a water-cooler condenser must be continuously recirculated through a cooling tower. On the other hand, an air-cooled condenser consists of a coil of finned tubes, over which air is drawn or blown. In evaporative condensers, the coil tubes are directly in the path of the air and water streams down. Evaporative cooling takes place directly on the outer surface of the tubes.

A single zone model of a condenser assumes that the de-superheating, condensation and liquid sub-cooling are one lumped-sum enthalpy change occurring at the condensation temperature (Cleland, 1990). Since the heat loss in the condensation process outweighs the two other processes, this assumption can be justified. The energy balance can, hence, be stated as:

$$\left(\left(Mc_p\right)_{cd} + \left(Mc_p\right)_{refr}\right)\frac{dT_{cd}}{dt} = -\left(UA\right)_{cd}\Delta T_{cd} + \dot{m}_{refr}\left(h_{cd,in} - h_{cd,out}\right) - \phi_{cd} \tag{3.41}$$

where $(Mc_p)_{cd}$ is the condenser thermal mass [J °C^{-1}]; $(Mc_p)_{refr}$ is the refrigerant thermal mass [J °C^{-1}]; T_{cd} , the condenser temperature [°C]; U, the condenser overall heat transfer coefficient [W m^{-2} °C^{-1}]; A, the condenser heat transfer area [m^2]; ΔT_{cd} , the log mean temperature difference [°C]; $\dot{m}_{refr}$, the refrigerant mass flow rate [kg s^{-1}]; $h_{cd,in}$, the refrigerant enthalpy entering evaporator [J kg^{-1}]; $h_{cd,in}$, the refrigerant enthalpy exiting condenser [J kg^{-1}] and ϕ_{cd} , the condenser heat loss to the environment [W]. The condense log-mean temperature difference, ΔT_{cb}, can be calculated from Eq. 3.40.

3.3.2.3 Compressor

The most common type of compressor in refrigeration is the reciprocating compressor. Recently, screw compressors are gradually replacing reciprocating compressors. Owing to the ability of these compressors to deliver higher compression rates, a smaller number of screw compressors is sufficient as compared to the reciprocating types (Billiard, 1999).

Due to the fast time response to changing suction and delivery pressures as compared to the overall system dynamics, compressors can be modelled algebraically (Marshal and James, 1975). Thus, the refrigerant mass flow rate can be calculated from:

$$\dot{m}_{refr} = V_{swept} \frac{\eta_v}{v} \tag{3.42}$$

where $\dot{m}_{refr}$ is the refrigerant mass flow rate [kg s^{-1}]; V_{swept}, the swept volume [m^3] and η_v, the volumetric efficiency of the compressor. The actual power used by the compressor is given by:

$$Q_{cp} = \dot{m}_{refr} \frac{\Delta h_{cp}}{\eta_{is}} \tag{3.43}$$

where Q_{cp}, is the compressor power, Δh_{cp}, the refrigerant enthalpy change in isentropic compression [J kg^{-1}] and the η_{is} is the isentropic efficiency of the compressor.

3.3.2.4 Holding tank

When an indirect system layout is employed, the cooled secondary refrigerant is stored in a buffer tank before it is pumped to the air blast coolers in the cool stores. This tank plays an important role in that it is a boundary equipment between the refrigeration unit and the cool rooms. In direct system lay out using liquid overfeed systems, the liquid separation tank plays similar role. The liquid refrigerant (primary) is stored in this tank before it is pumped to the individual evaporators inside the cool rooms. However, here it divides the refrigeration circuit into two, one circuit consisting the compressor, the condenser and the tank, and second circuit the evaporator and the tank itself. The reader is referred to Section 5.2.2.1, as to how this tank is incorporated into the evaporator model.

In the case of indirect system layout, the buffer tank (also called holding tank) is a horizontal cylindrical vessel divided into two compartments. The refrigerant returned from the end users enters in one of the compartments while the secondary refrigerant from the refrigeration unit into another, where flow from one compartment to another is also possible. The schematic representation of such a tank is shown in Figure 3.2.

The temperature of the two compartments can be modelled by applying an energy balance around each compartment.

$$\left(Mc_p\right)_1 \frac{dT_1}{dt} = \dot{m}_{chil}\, c_{p_1}\left(T_{in,chil} - T_1\right) + \dot{m}_{app}\, c_{p_2}\left(T_2 - T_{out,app}\right) \tag{3.44}$$

$$\left(Mc_p\right)_2 \frac{dT_2}{dt} = \dot{m}_{app}\, c_{p_2}\left(T_{in,app} - T_2\right) + \dot{m}_{chil}\, c_{p_1}\left(T_1 - T_{out,chil}\right) \tag{3.45}$$

where (Mc) is the thermal mass [J °C^{-1}]; T, the refrigerant temperature [°C], c_p, the refrigerant specific heat [J kg^{-1} °C^{-1}]; $\dot{m}_{app}$ and $\dot{m}_{chil}$ the refrigerant mass flow rates from the end users and the chiller unit, respectively [kg s^{-1}]; $T_{in,chil}$ and $T_{out,chil}$ the temperatures of the refrigerant entering and exiting the chiller unit, respectively [°C] and $T_{in,app}$ and $T_{out,app}$ the temperatures of the refrigerant to and from the end users, respectively [°C]. The subscripts 1 and 2 denote the two compartments of the holding tank. Assuming the specific heat of the secondary refrigerant is constant and by adding Eqs. (3.44) and (3.45) and rearranging, the temperature of the tank can be calculated by:

$$\left(M\right)_{1,2} \frac{dT_t}{dt} = \dot{m}_{chil}\left(T_{in,chil} - T_{out,chil}\right) + \dot{m}_{app}\left(T_{in,app} - T_{out,app}\right) \tag{3.46}$$

where $(Mc)_{1,2}$ represent the thermal mass of the buffer tank as a whole.

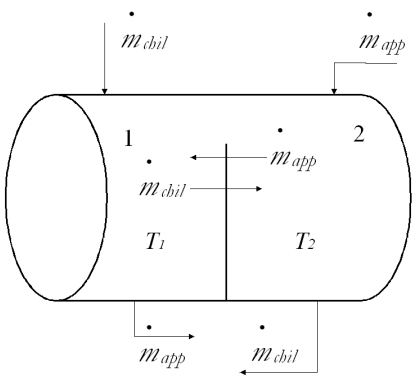

Figure 3.2 Schematic representation of the holding tank

3.3.3. Gas handling unit

In order to maintain the concentration of the respiratory gases at optimal levels, the excess CO_2 produced as a result of respiration should be removed. Various types of scrubbers have been employed such as the lime, renewable, temperature swing, water, and selective diffusion membrane scrubbers. The advantages and disadvantages of each of these scrubbers are discussed in Thompson (1998). Moreover, the time needed for the level of O_2 to reach an optimal concentration (<5%) can reduce the maximum storage life of the stored fruit. Thus, it is a common practice to flush with N_2 after the room has been sealed, commonly known as *pull-down* or *burning* operation.

In modern CA cool storage systems, Pressure Swing Adsorption (PSA) or Vacuum Swing Adsorption (VSA) systems are commonly used to scrub excess carbon dioxide from the cool rooms as well as generate nitrogen for pull-down operation. In this system a mixture of gas is fed to a column of bed packed with particles (adsorbent) and one component is preferentially adsorbed on the surface of the particles. The selectivity may depend on a difference in adsorption equilibrium (equilibrium driven) or in adsorption rates (diffusion driven). The latter is often used for CA purposes due to the involved short cycles and somewhat easier regeneration phase. This process essentially consists of two principal steps: *(i)* adsorption, during which the preferentially adsorbed species are picked up from the feed and *(ii)* regeneration or desorption during which these species are removed from the adsorbent by reducing

the total pressure, thus, regenerating the adsorbent for use in the next cycle. Often two columns are employed where one undergoes the adsorption step while the other column is in regeneration step. As the two columns switch there is a short pressure equalization step. The schematic representation of the principal steps is represented in Figure 3.3.

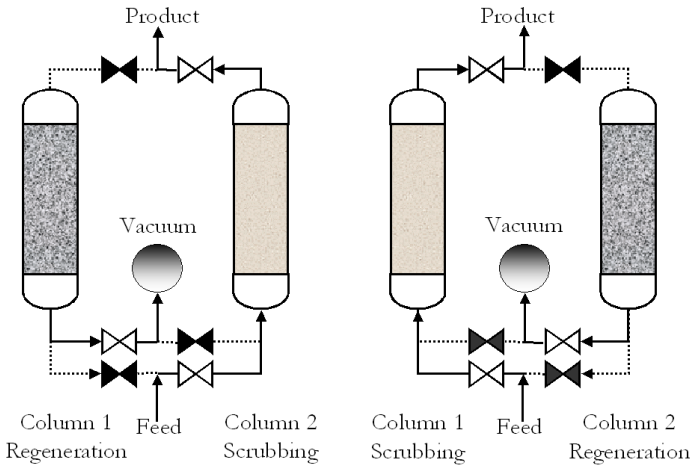

Figure 3.3 Schematic representation of the principal steps in PSA

Unlike many separation processes, PSA processes are more complex in that the process operates in transient conditions (Ruthven et al., 1994). Thus, a dynamic simulation model is more appropriate to obtain realistic results. A two-phase model, which accounts for the fluid phase and solid phase concentrations, was considered. In view of a kinetically controlled PSA process for CA storage, the following assumptions are considered.

- The fluid behaves ideally.
- Since the mass transfer resistance is the limiting factor, the axial dispersion was negligible.
- An isothermal process was assumed neglecting the temperature change due to the effect of heat of adsorption. Thus, the kinetic and equilibrium properties were considered constant.

- The pressure gradient across the bed was considered negligible and the process operates at a constant total pressure during adsorption and desorption. Therefore, the velocity change of the fluid was only due to the adsorbed particles.

- In a two-column adsorption unit, from the point of view of the cool room, only the adsorption step of the two columns is visible with very short intermittent gaps as the columns undergo a pressure equalization step. Hence, only the adsorption step was considered, ignoring the pressure equalization step.

Given the above assumptions, the flow pattern through an adsorption column can be represented by plug flow model. A mass balance for a component *i* over a differential volume element yields:

$$\frac{\partial v c_i^g}{\partial z} + \frac{\partial c_i^g}{\partial t} + \frac{1-\varepsilon}{\varepsilon}\frac{\partial \overline{q}_i}{\partial t} = 0 \tag{3.47}$$

where v is the velocity [m s^{-1}]; c_i^g, the gas phase concentration of component *i* [mol m^{-3}]; ε, the bed porosity; $\overline{q}_i$, the solid phase concentration of component *i* [mol m^{-3}]; z, the axial distance [m] and t, the time [s]. The velocity change through the bed operated at constant total pressure was obtained from the overall material balance.

$$C^g \frac{\partial v}{\partial z} + \frac{1-\varepsilon}{\varepsilon}\sum_{i=1}^{n}\frac{\partial \overline{q}_i}{\partial t} = 0 \tag{3.48}$$

where n is the total number of components and $C^g = \sum_{i=1}^{n} c_i^g$, which is not a function of the axial distance.

The solid phase mass transfer rates can be modelled by the simpler linear driving force (LDF) approximation or by a more detailed Fickian diffusion equation. Ruthven et al. (1994) argue that though a more detailed mass transfer model is needed especially for kinetically controlled processes, generally, the LDF model provides adequate accuracy for all operating conditions. In the present work, the LDF model was considered and it reads as:

$$\frac{\partial \overline{q}_i}{\partial t} = k_{m,i}(q_i^* - \overline{q}_i) \tag{3.49}$$

where $\overline{q}_i$, the solid phase concentration of component *i* [mol m^{-3}]; $k_{m,i}$, the effective mass transfer rate coefficient of component *i* [s^{-1}]; q_i^* , the equilibrium value of $\overline{q}_i$ [mol m^{-3}]. The adsorption equilibrium isotherm can be represented by the Extended Langmuir model for multi-component mixtures given by (Yang, 1997):

$$q_i^* = \overline{q}_{i,sat} \frac{b_i c_i^g}{1 + \sum_{i=1}^{n} b_i c_i^g} \tag{3.50}$$

where $\overline{q}_{i,sat}$ is the saturation value of $\overline{q}_i$ [mol m^{-3}] and b_i the Langmuir constant of component *i*. At the beginning of each adsorption step a clean bed was considered as an initial condition. At the entrance of the bed a constant inlet velocity, and thus flow rate, was assumed. The inlet concentration of a given component was obtained from the time dependent concentration of that component in the room. The initial and boundary conditions are represented in Eqs. (3.53) and (3.54), respectively.

$$\text{I.C.:} \quad c_i^g(z, t=0) = 0; \ \overline{q}_i(z, t=0) = 0; \ v(z, t=0) = 0 \tag{3.51}$$

$$\text{B.C.:} \quad c_i^g(z=0, t) = c_{i,a}^g(t); \quad v(z, t=0) = v_o; \ \left.\frac{\partial c_i^g}{\partial z}\right|_{z=L} = 0 \tag{3.52}$$

where *L* stands for the total length of the bed [m].

This model structure was applied to both carbon dioxide scrubbing and nitrogen generation units with appropriate kinetic and equilibrium parameters.

3.4. Implementation aspects

The energy and mass balance equations discussed above are relatively straightforward; their implementation, nevertheless, is not. Combining all the individual modules and testing each module is tedious and time consuming. Moreover, the involvement of combined continuous and discrete time events further complicates the implementation. The features needed for successful implementation could be identified as *(i)* object-oriented approach, *(ii)* combined discrete/continuous simulation paradigm and *(iii)* hierarchical design.

The appropriateness of the object-oriented modelling with such systems is that it correlates the structure of the real system to the structure of the simulation. Each

component of the real system is represented by a distinct component (an object) in the simulation. Thus, the interaction between real systems is identified with a corresponding interaction between objects. This structural and quantitative overlaying leads to a natural representation of the real system. Besides making model representation clearer, validation of individual modules is possible by extracting them from the larger system, making model implementation much easier.

In relation to simulation paradigms, three types have been identified as continuous, discrete and combined continuous and discrete system simulation (Kreutzer, 1986). In the continuous system simulation, the state variables change in a continuous way by slicing the time into arbitrary small steps. On the other hand, in a discrete-event simulation, an event is defined as an incident, which causes the system to change its state in some way. The events in a discrete-event simulator can occur only during a distinct unit of time during the simulation. The combined continuous and discrete system simulation, which is developed more recently, views system behaviour as predominantly continuous phenomenon, which possibly incorporates irregularities and discontinuities (Kreutzer, 1986). Between discrete events, the simulation proceeds in a continuous manner. The algorithm of the latter simulation paradigm is shown in Figure 3.4. In this algorithm, when a discontinuity is encountered, the exact time the discontinuity took place (crossover) is calculated after stopping the simulation. Then, the simulation is reinitialised starting from the obtained time.

Hierarchical design in simulation is one of the techniques used to cope with the complexity associated with a given system. Hierarchical simulation is a process whereby higher order components delegate functional responsibility to its composite sub-components (www 1, 2003). The higher level components are responsible for activating their respective child components in a meaningful sequence so as to model the correct behaviour of the system.

The implementation of the CA cool storage model was carried out using a general-purpose combined continuous/discrete simulation environment, EcosimPro (EA International, Madrid, Spain). It is equipped with an object-oriented modelling language named EL (EL modelling language manual) and powerful automatic solvers for systems of differential equations. A model for a component is represented by a module where discrete and continuous statements can explicitly be declared. The module can send and receive message through public variables of the type 'PORTS'. The Backus Naur Formalism (BNF) of a module in EcosimPro is shown in Figure 3.5. Hierarchical implementation is effected through aggregation of

components of the lower hierarchy into one component, which in turn serves as a subcomponent in the higher hierarchy. The BNF of one such component is shown in Figure 3.6.

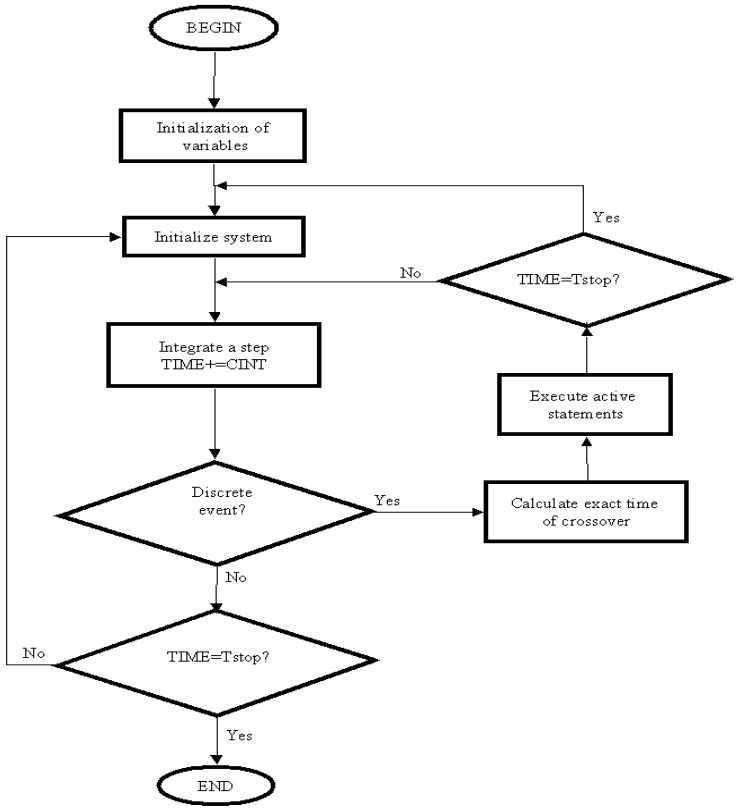

Figure 3.4 Algorithm of the combined continuous/discrete simulation paradigm

The modules employed in the CA cool room model and their hierarchy is shown in Figure 3.7 as implemented in the simulation environment. Moreover, component models can be created graphically using a CAD tool, SmartSketch (Intergraph Corporation, Huntsville, Alabama), customized for use with EcosimPro. To illustrate this, a component model made in SmartSketch at the level of hierarchy of the 'Cell' in Figure 3.7 is shown in Figure 3.8.

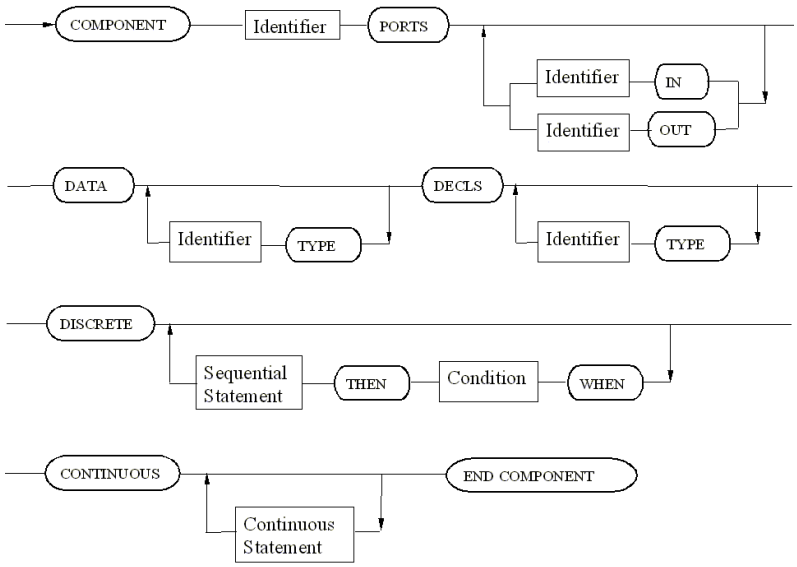

Figure 3.5 Backus-Naur Formalism of an ordinary EcosimPro component

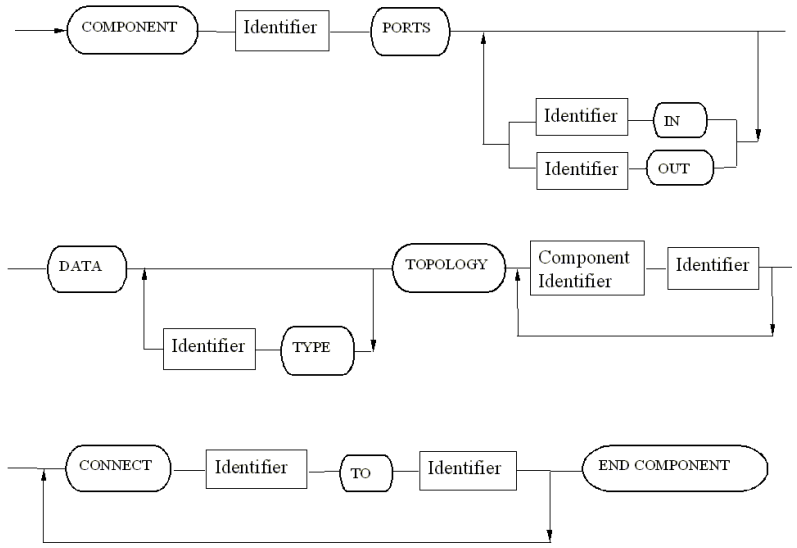

Figure 3.6 Backus-Naur Formalism of an aggregate EcosimPro component

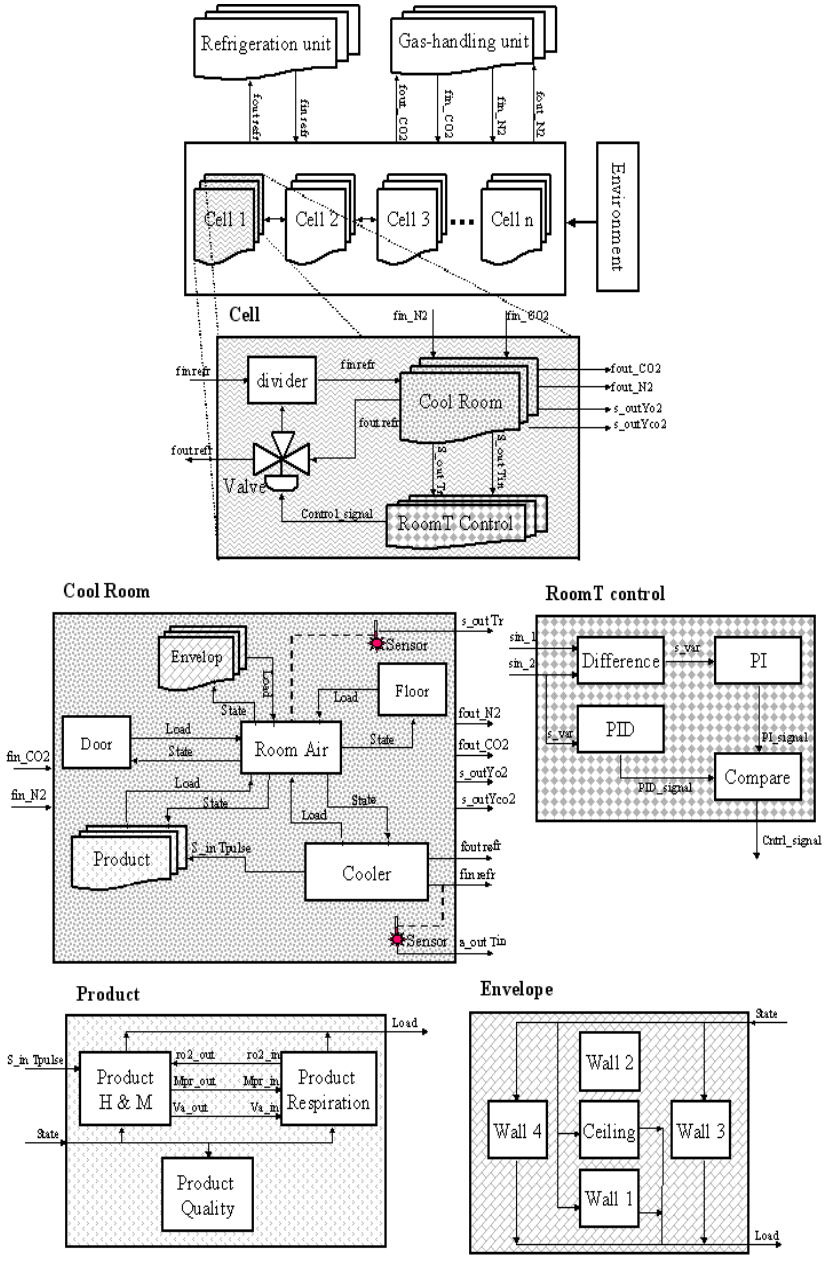

Figure 3.7 Hierarchical model structure of a CA cool storage facility

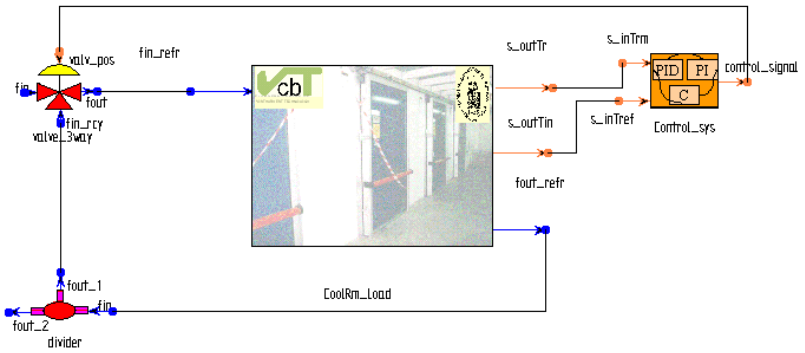

Figure 3.8 SmartSketch implementation of a cool room model

3.5. Discussion

It was attempted to develop a global CA cool storage model, where the involved interacting units and their components were represented in a modular fashion. To account for the evolution of the respiratory gases in the cool room, special focus was given to the product, by representing the gas exchange process of the produce with the environment using a semi-mechanistic product respiration model. This provided as well a background to hook up a product quality (firmness) model. The possible shortcomings of these models are that the involved kinetic parameters are not well established for a wide range of fruit. However, as more and more research is directed in this direction this limitation might not be of concern in the near future.

Unlike the cool room and refrigeration unit models, the gas handling unit model was based on distributed parameter approach. As PSA is a more complex separation process, the model, which has been considered, was tailored to fit the global CA storage system model by considering only the adsorption step and ignoring the intermittent steps between the switching of the two columns. Since no global model for CA cool storage system, which considers the gas-handling unit, appeared in literature so far, these assumptions couldn't be weighed against.

For the CA cool storage facility whose implementation structure is shown in Figure 3.7, the statistics of the implementation is shown in Table 3.1. To describe this facility (considering a only single cell), in total, 92 ODE's, 2 algebraic and 399 auxiliary equations were used. This amount is comparable to the amount of ODE's

used in the generic simulation model developed by Cleland (1983) and Cleland (1985a) for a meat processing plant which consisted of chilling, freezing, cold store and cutting rooms. The number of input data to the model stands at 177. Considering the number of equations involved this might not seem substantial. However, this Figure does not include those parameters for product and material properties that are provided to the model through tables. Most of these input parameters are those that can be found in manufacturer's manual. However, some parameters such as those related to the heat and mass transfer coefficients and some empirical factors can be subtle. Two data tables with a total of 78 parameters are part of the implementation.

Table 3.1 Implementation statistics of the CA cool storage model as depicted in figure 3.7.

Unit	Number of equations	Derivative variables	Algebraic (state) variables	Boundary variables	Auxiliary variables	Input data
Cell (single)	246	28	-	3	215	103
Refrigeration	27	4	2	1	20	28
Gas-handling[3]	2×142	2×3×10	-	-	2×82	2×23

Owing to the diversity (thus problem of compatibility) of the individual models involved and occurrence of combined discrete and continuous time events, the global CA cool storage model implementation is not straightforward. The model being implemented in a general-purpose object-oriented simulation environment, which can handle discrete and continuous time events, solves much of the problems encountered in the implementation of complete refrigeration systems in literature. This means that fitting the CA cool storage simulation model into such simulation environment ensures flexibility with respect to inclusion of new component models and inheritance of common behaviours from existing modules. Moreover, due to the open architecture of the simulation environment, existing models using compatible programming languages can be easily fused.

[3] In this unit two sub-units (the nitrogen generator and carbon dioxide scrubber, thus, 2×) are considered with each consisting 10 nodes (thus, 10×)

3.6. Conclusion

A global model for CA cool storage systems was presented. The model consists of three interaction components, namely, the cool room, the refrigeration and gas-handling units. In the cool room sub-model the product and non-product components were modelled using a lumped parameter approach based on the overall energy and mass balance around the components. Focus was rendered to the product by inclusion of a gas exchange model to account for the evolution of the concentrations of the respiratory gases as well as respiratory heat generation. Moreover, a product quality (firmness) model was incorporated to predict the quality deterioration of the product after the storage period. In modelling the refrigeration unit a methodology usually pursued for industrial simulation, which consider only the thermal effects (ignoring the hydrodynamic effects) was adopted. For the gas-handling unit a distributed model for a PSA process was developed by considering only the principal steps in the adsorption process.

The global CA model was implemented in a computational environment, which can handle discrete and continuous event simulation, EcosimPro (EA International, Madrid, Spain). Due to modular and object-oriented approach greater flexibility with respect to model modification and reusability was ensured. Moreover, in order to reduce complexity and increase intelligibility, a hierarchical design was considered. Finally, with such an approach, optimisation of the CA installation with respect to plant performance and ultimate product quality is possible.

References

Anonymous. EL Modelling Language Manual, 1992-2000, EA International.

Amarante, C. Banks, N.H., Ganesh, S. (1997). Permeance to gases, internal atmosphere modification and ripening of coated pears. *Proceedings of 7th International Controlled Atmosphere Research Conference*, UC Davis, CA, Vol. 2, Apples and Pears, 145-150.

Amos, N.D. (1995). Mathematical modelling of heat and mass transfer and water vapour transport in apple cool stores. *Ph.D. Thesis*, Massey University, Palmerston North, New Zealand.

Billiard, F. (1999). Fruit cold storage: techniques and equipment. *Acta Horticulturae*, 485, 61-70.

Cleland, A.C. (1983). Simulation of industrial refrigeration plants under variable load conditions, *International Journal of Refrigeration,* 6, 11-9.

Cleland, A.C. (1985a). Experimental verification of a mathematical model for simulation of industrial refrigeration plants. *International Journal of Refrigeration*, 8, 275-282.

Cleland, A.C. (1985b). RADS – a computer package for refrigeration analysis, design, and simulation, *International Journal of Refrigeration*, 8, 372-374.

Cleland, D.J., Cleland, A.C. (1989). Appropriate level of model complexity in dynamic simulation of refrigeration systems. *Refrigeration Science and Technology,* 1, 261-268.

Cleland, A.C. (1990). Food refrigeration processes, analysis, design and simulation. Elsevier Science Publ. Co. Inc., London.

Darrow, J.B., Lovatt, S.J., Cleland, A.C. (1991). Assessment of a simple mathematical model for predicting the transient behaviour of a refrigeration system. *Proceedings of 18th International Congress of Refrigeration*, Montreal, Canada, 1189-1192.

De Smet, V., Bariero, P., Verlinden, B.E., Veraverbeke, E.A., De Baerdemaeker, J., Nicolai, B.M. (2002). A mathematical model for development of mealiness in apples. *Postharvest Biology and Technology*, 25, 273-291.

Flores, E.S., Cleland, A.C., Cleland, D.J. (2001). Prediction of the dynamic thermal behaviour of walls for refrigerated rooms using lumped and distributed parameter models. *International Journal of Refrigeration*, 24, 272-284.

Glöckner, G., Hofer, B., Kluge, C.H., Schroth, H.H., Wobst, E. (1990). Simulation of refrigerating plants for cold stores. *Refrigeration Science and Technology*, 1990-4, 487-493.

Hasse, H., Becker, M., Grossmann, K., Maurer, G. (1996). Top-down model for dynamic simulation of cold-storage plants. *International Journal of Refrigeration.* 19(1), 10-18.

Hertog, M.L.A.T.M., Nicholson, S.E., Banks, N. (2001). The effect of modified atmospheres on the rate of firmness change in Braeburn apples. *Postharvest Biology and Technology*, 23, 175-178.

Hoang, M.L., Verboven, P., Baelmans, M., Nicolaï, B.M. (2003). Analysis of airflow, heat and mass transfer in chicory root cold store by means of computational fluid dynamics. *Proceedings of the 21st International Congress of Refrigeration, Washington D.C, USA, Paper N°. 484, (CD-ROM edition, ISBN 2-913149-32-4)*

James, K.A., James, R.W. (1988). Dynamic analysis of a heat pump using established modelling techniques. *Institute of Environmental Engineering Technical Memorandum N°. 98*, Polytechnic of the South Bank, London.

James, K.A. (1988). Dynamic mathematical modelling of refrigeration systems and heat pumps. *Ph.D. Thesis*. Institute of Environmental Engineering, South Bank Polytechnic, London.

Jensen, K., Wirth, N. (1985). Pascal User Manual and report, Springer, New York.

Knee, M. (1980). Physiological responses of apple fruit to oxygen concentrations. *Annals of Applied Biology*, 96, 243-253.

Kreutzer, W. (1986). System simulation programming styles and languages. Addison-Wesley, Sydney.

Lopez, A., Lacarra, G. (1999). Mathematical modelling of thermal storage systems for food industry. *International Journal of Refrigeration,* 22, 650-658.

Lovatt, S., Pham, Q.T., Cleland, A.C., Loeffen, M.P.F. (1993). A new method of predicting the time-variability of product heat load during food cooling – Part 1: theoretical considerations. *Journal of Food Engineering*, 18, 37-62.

Lovatt, S. (1992). A dynamic modelling methodology for the simulation of industrial refrigeration systems. *Ph.D. Thesis*, Massey University, Palmerston North, New Zealand.

Lovatt, S., Loeffen, M.F.P. (1998). Improved dynamic simulation of multi-temperature industrial refrigeration systems for food chilling, freezing and cold storage. *International Journal of Refrigeration,* 21(3), 247-260.

MacArthur, J.W. (1984). Transient heat pump behaviour: a theoretical investigation. *International Journal of Refrigeration*, 7, 123-132.

Marshal, S.A., James, R.W. (1975). Dynamic analysis of an industrial refrigeration system to investigate capacity control. *Proceedings of The Institute of Mechanical Engineers*, 189(44/75), 437-445.

Nahor, H.B., Scheerlinck, N., Van Impe, J., Nicolaï, B.M. (2002). A simple model of a refrigeration plant for cool storage systems simulation. *Communications of the faculty of Agricultural and Applied Biological Sciences*, University of Ghent, 67(4) 293-296.

Nahor, H.B., Teshome, E.J., Scheerlinck, N., Van Impe, J.F., Nicolaï, B.M. (2003a). Prediction of dynamic behaviour of CA cool rooms using lumped parameter approach. *Acta Horticulturae*, 599, 213-219.

Nahor, H.B., Scheerlinck, N., Verboven, P., Van Impe, J., Nicolai, B.M. (2003b). Dynamic Simulation Of Controlled Atmosphere (CA) Cool Storage Systems For Pip Fruits. *Proceedings of the 21st International Congress of Refrigeration, Washington D.C, USA, Paper N°. 482, (CD-ROM edition, ISBN 2-913149-32-4).*

Nahor, H.B.; Scheerlinck, N.; Van Impe, J.; Nicolaï, B.M. (2003c). Combined discrete and continuous simulation of Controlled Atmosphere (CA) storage systems. *Communications of the faculty of Agricultural and Applied Biological Sciences,* University of Ghent, 68(3) 17-21.

Nahor H.B., Scheerlinck, N., Verboven, P., Van Impe, J., Nicolai, B.M. (2004). Continuous/discrete simulation of controlled atmosphere (CA) cool storage systems: model development and validation using pilot plant CA cool storage. Submitted for publication in *International Journal of Refrigeration.*

Pieters, J.G., Deltour, J.M. (1997). Performances of greenhouses with the presence of condensation on cladding materials. *Journal of Agricultural Engineering resources*, 68, 125-137.

Ruthven, D.M., Farooq, S., Knaebel, K.S. (1994). Pressure swing adsorption. VCH Publishers Inc., New York.

Tanner, D.J., Cleland, A.C., Robertson, T.R. (2002). A generalised mathematical modelling methodology for design of horticultural food packages exposed to refrigerated conditions: Part 1, Formulation. *International Journal of Refrigeration,* 19, (1), 10-18.

Tijskens, L.M.M. (1979). Texture of golden delicious apples during storage. *Lebensmittel-Wissenschaft und-Technologie*, 12, 138-142.

Tijskens, L.M.M., Van Schaik, A.C.R., Hertog, M.L.A.T.M., De Jager, A., (1997). Modelling the firmness of Elstar apples during storage and transport. *Acta Horticalturae*, 485, 363-371.

Thompson, A.K. (1998). Controlled Atmosphere storage of fruit and vegetables. CAB International, New York.

Touber, S. (1984). Principles and methods for mathematically modelling the steady-state and dynamic behaviour of refrigeration components and installations. *Refrigeration Science and Technology*, 1984-2, 163-175.

Smets, I., Karina J.E., Versyck, K.J., Van Impe, J.F. (2002). Optimal control theory: a generic tool for identification and control of (bio)-chemical reactors. *Annual Reviews in Control*, 26(1), 57-73.

Wang, H., Touber, S. (1990). Distributed dynamic modelling of a refrigerated room. *International Journal of Refrigeration*, 13, 214-222.

Wirth, N. (1982). Programming in Modula 2. Springer, Berlin.

www 1: http://web.cs.mun.ca/~donald/msc/node11.html. Accessed on April 31, 2003.

Yasuda, H., Touber, S., Machielsen, C.H.M. (1983). Simulation model of vapour compression system. *ASHRAE Transactions*, 89 (2A), 408-425.

Yang, R.T. (1997). Gas separation by adsorption process. Imperial College Press, London.

Chapter 4

A continuous-discrete event simulation model for a CA cool store facility: model validation

4.1. Introduction

Dynamic simulation of a CA storage facility involves several interacting and coupled processes. The usefulness and applicability of such a simulation model for design and analysis depends on the amount and availability of the input data and the overall prediction quality of the model. Often, the main hindrance is the daunting amount of input data and their accuracy. Besides the number of variables involved, the availability of experimental data for all the variables complicates the validation procedure as most considered industrial facilities are not suited for measurement of the variables especially when closed circuits are involved as in the case of, for instance, the refrigeration cycle. Thus, the validation process should consider the selection of principal responses and those that are coupled to them. Moreover, sensitivity analysis of the parameters involved, especially those that are related to the

key variables, is of great importance for the overall applicability of the simulation model for design and analysis of CA cool storage systems.

The main objective of the present Chapter is to validate the global CA cool storage model described in the previous Chapter. The validation procedure considers the major units of the CA cool storage model independently in order to analyse the variables and input data more closely and then effort is made to validate the global model by interconnecting the units forming the global model. After a short survey of existing refrigerated storage facility models and the extent of their validation in Section 4.2, materials and methods employed in the validation of the model and its components will be described in Section 4.3. Next, the validation results of the main units of the model and subsequently of the global model, together with sensitivity analysis results will be presented (Section 4.4). Finally, in Sections 4.5 and 4.6, the validation of the models will be discussed and some concluding remarks will be drawn, respectively. The results of this Chapter are presented in Nahor et al. (2002); Nahor et al. (2003a); Nahor et al. (2003b) and Nahor et al. (2004).

4.2. Literature review

Here, the extent of validation of the complete refrigeration system simulation models cited in the literature review (Section 3.2) of the previous Chapter will be discussed. It should be noted that validation of such models often focus on the trend displayed by the model in comparison to the experimental data and no quantitative validation criteria is given. Hence, the fit between the model and the observation is usually evaluated through visual inspection.

The complete simulation model proposed by Marshal and James (1975) for a quick vegetable freezing tunnel contained 46 ODE's and 105 algebraic equations. The work made no mention of the model parameters. It was stated that principal responses were compared to experimental data, which resulted in modification of certain parameters. Since the objective of the modelling exercise was to investigate capacity control, the validation of the model focused on the refrigeration plant. Considering the liquid separator to be the key component with respect to capacity control of the refrigeration system, a comparison between plant and model has been made for the liquid separator pressure and feed rate. The model adequately represented the experimental data, which the authors advocate that a fair degree of confidence should be placed in the overall accuracy of the model due to this. Using the model, an alternative capacity control has been proposed.

The generic simulation model for industrial refrigeration systems outlined by Cleland (1983) offered no validation of the model. Later, the validation was described by Cleland (1985) in which data from New Zealand meat works was used. Some of the component models described in the previous work have also been updated. The model consisted of 100 ODE's. Model predictions of the air temperatures of the freezing, chilling, cold store and air-conditioned work areas fitted experimental data with acceptable accuracy. Transients due to step changes such as defrosting operation were poorly represented. Though simpler models were employed as compared to the ones used by Marshal and James (1975), the author argues that the discrepancy between model and experimental data was mainly due to data uncertainties rather than insufficiently detailed models of plant components.

The general simulation model for refrigeration systems by Glöckner et al. (1990) presented no details on the testing of the model apart from some simulation results of hypothetical situations. Nor the extent to which the model has been exposed to experimental data validation was described.

The top-down model for a dynamic simulation of cold storage plants developed by Hasse et al. (1996) was validated using experimental data from a canteen cold store with a volume of 165 m^3 and corresponding refrigeration unit. Comparison of model predictions and experimental data for the room air temperature, evaporator surface temperature and the room air relative humidity, using two controller strategies were presented. Favourable agreement of the model predictions with experimental result was obtained. The model parameters used in the model were given, though those ones that related to heat and mass transfer coefficients were not listed nor a method to calculate them was described.

From the foregoing discussion, it can be observed that validation of all the involved variables was difficult due to space and time restrictions. However, validation considering variables related, for instance, to air only without taking into account other variables that the air is interacting with and those processes that are coupled to them can decrease the level of confidence that one can place in such models.

4.3. Materials and methods

4.3.1. Cool room and accessories

4.3.1.1 The cool room

The cool room employed in this study was a laboratory scale cool room at the Flanders Centre of Postharvest Technology (Leuven, Belgium). The facility contains four CA (ULO's) and three conventional cool rooms. These are serviced by a chiller unit, working in an indirect system layout where glycol (35%) is used as a secondary refrigerant, and a VSA (Vacuum Swing Adsorption) gas-handling unit. The CA cool room employed has the dimensions 2.8 m wide, 4.25 m deep and 3.6 m high (Figure 4.1). The cooling unit is positioned at the back of the cool store and contains a cooling (5.5 kW) and a heating battery (4.6 kW). The latter is used for heating the room when needed. The cooling battery is constructed with a 10-pass, 6 streams bundle of tubes partitioned in to two blocks in series containing 2/3 the pipe bundle-size with four streams in one block and the rest 1/3 of the pipe bundle with two streams in the second block. The schematic representation of the arrangement of the cooling battery is depicted in Figure 4.2. Two axial fans of 40 cm are positioned at the back of the unit blowing air to the cooling battery.

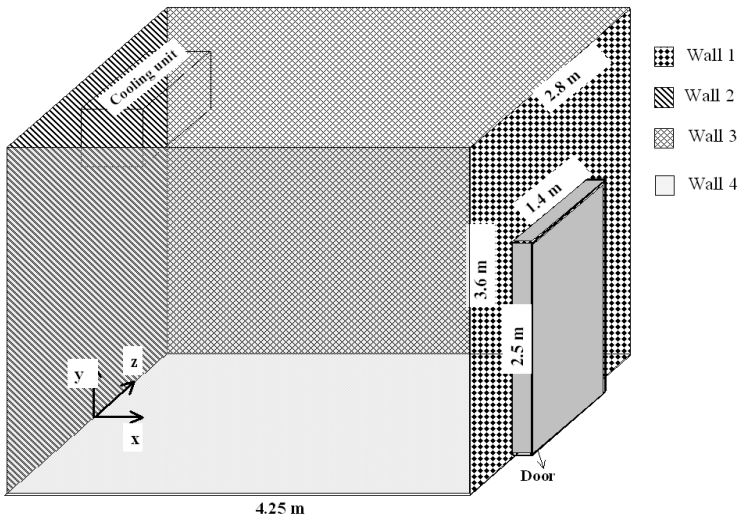

Figure 4.1 Schematic representation of the cool store

The cool room is equipped with a temperature control system, which consists of a PI and PID controllers. The PI controller is responsible to avoid over cooling of the air leaving the cooler unit, thus ensuring homogeneity in the room, by controlling the temperature difference between the inlet refrigerant and the cool room set at 10°C. The PID controller regulates the cool room temperature and the minimum of the two signals was implemented on the final control element, a three-way (mixing) valve that regulates the flow of fresh and recycled (from the cooler) refrigerant. During defrosting, the valve closes the flow of the fresh refrigerant and the refrigerant inside the cooler is heated up by a separate heat exchanger in the circuit using hot water from the central heating system of the building.

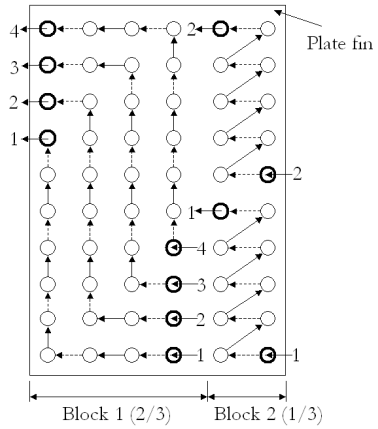

Figure 4.2 Schematic representation of the arrangement of the cooling battery

4.3.1.2 Model parameters

The thermal mass, heat transfer area, thermal properties and flow rates of air and refrigerant of the different components of the cool store were obtained from available material masses, manufacturer manuals and literature data. The literature data for the thermal properties of the components were obtained from the ASHRAE handbook (1993) and Incropera and De Witt (1990), unless otherwise stated. Product thermal, physical and kinetic parameters were obtained from Sperenger (1980), Schotsmans (2003), Veraverbeke (2001), Hoang (2003), Lammertyn et al. (2001), www 1 (2000). The values of the parameters used in the simulation are compiled in Appendix B.

The heat and mass transfer coefficients of the different components of the cool room were estimated from empirical correlations. Generally, the heat transfer coefficient is presented in the form of dimensionless Nusselt number. This dimensionless number is correlated to Reynolds and Prandtl number in case of forced convection where the Reynolds number is a function of velocity and geometry and the Prandtl number as a function of momentum and thermal diffusivities. The mass transfer coefficient is often estimated from the approximate Lewis relationship derived from the analogy between mass and heat transfer (ASHRAE, 1993).

$$Le = \frac{h}{h_m \rho c_p} = 1 \tag{4.1}$$

where h and h_m are the heat [W m^{-2} °C^{-1}] and mass [ms^{-1}] transfer coefficients, respectively. When using empirical correlations to calculate the heat transfer coefficient an error of 50% can easily be obtained (Incropera and De Witt, 1990). Since most of the other model parameters are found from literature and manufacturer manual, model tuning can only be carried out with respect to heat transfer coefficients. Thus, unless experimental verification is not performed, the tuning of these parameters was carried out by computing the coefficients from different empirical correlations. The one that gave the best result was then implemented. The correlations employed to calculate the different heat transfer coefficients will be discussed hereafter.

Heat exchanger

In cross flow heat exchangers the heat transfer coefficient is often affected by the arrangement of the bank of tubes, aligned or staggered, and type of fin. For a bank of inline tubes in block fins, the following correlation was used in this study to estimate the airside heat transfer coefficient (Hewitt et al. (1994)).

$$Nu = 0.3\,\mathrm{Re}^{0.625}\left(\frac{A_f - A_{pf}}{A_p}\right)^{0.375} \mathrm{Pr}^{0.333} F_1 \qquad 5\times10^3 < \mathrm{Re} < 1\times10^5 \text{ and } 5 < \left(\frac{A_f - A_{pf}}{A_p}\right) < 12 \tag{4.2}$$

where A_f is the total surface area of the fins [m^2]; A_{pf}, the surface area of pipes between fins [m^2]; and A_{pf}, the total surface area of the pipes [m^2]. F_1 is a factor for the number of tube rows and its value is 1 when the number of tubes in the transversal direction is more than 8. The Reynolds number, *Re*, is given by:

$$\mathrm{Re} = \frac{v_{\max} D_o \rho}{\mu} \tag{4.3}$$

where $v_{\max}$ is the maximum velocity [m s^{-1}], calculated from the ratio of the approach velocity of the air and the void fraction of the cooler block and D_o the external pipe diameter [m]. The effective heat transfer coefficient was then calculated from:

$$h_a = \frac{k_a Nu}{D_o}\left(\frac{\eta_f A_f + A_{bf}}{A_p}\right) \tag{4.4}$$

$$\eta_f = \frac{\tanh\left(\varphi\sqrt{\frac{2k_a Nu}{D_o W_f k_f}}\right)}{\varphi\sqrt{\frac{2k_a Nu}{D_o W_f k_f}}} \tag{4.5}$$

$$\varphi = 0.5 D_o\left(\frac{S_l}{D_o} - 1\right)\left(1 + 0.35\ln\left(\frac{S_l}{D_o}\right)\right) \tag{4.6}$$

where η_f is the fin efficiency; W_f, the fin width [m]; k_f, the thermal conductivity of the fin [W m^{-1} °C^{-1}] and S_l the transversal pitch of the pipes [m].

For the liquid side heat transfer coefficient, the following correlation was employed.

$$Nu = 0.023\,\mathrm{Re}^{0.8}\,\mathrm{Pr}^{0.4} \tag{4.7}$$

$$\mathrm{Re} = \frac{v_{refr} D_i \rho_{refr}}{\mu_{refr}} \tag{4.8}$$

$$h_{refr} = \frac{k_{refr} Nu}{D_i} \tag{4.9}$$

where v_{refr} is the velocity of the refrigerant inside the tubes calculated from the flow rate of the refrigerant.

$$v_{refr} = \frac{\dot{m}_{refr}}{N_{str} A_{cp} \rho_{refr}} \tag{4.10}$$

where N_{str} is the number of streams (number of pipes that feed the cooler) and A_{cp} the cross sectional area of the tubes [m^2]. The overall heat transfer coefficient was then calculated from:

$$U = \frac{1}{h_a} + \frac{D_o}{2k_p}\ln\left(\frac{D_o}{D_i}\right) + \frac{D_o}{D_i}\frac{1}{h_{refr}} \tag{4.11}$$

where k_p is the thermal conductivity of the pipe material [W m^{-1} °C^{-1}].

Walls, ceiling and floor

The surface heat transfer coefficient at the walls and floor inside the cool store were assumed constant and estimated from a correlation of a flat plate (Incropera and De Witt, 1990).

$$Nu = 0.664\,\mathrm{Re}^{0.5}\,\mathrm{Pr}^{0.333} \tag{4.12}$$

$$\mathrm{Re} = \frac{Lv\rho}{\mu} \tag{4.13}$$

$$h_s = \frac{kNu}{L} \tag{4.14}$$

where L is the characteristic dimension [m]. The air velocity near the surfaces was measured using an omni-directional transducer (TSI 8475, St. Paul, MN, USA). The overall heat transfer coefficient of the outer side of the wall was estimated from:

$$U_{amb} = \frac{1}{h_{amb}} + \frac{d_s}{k_s} \tag{4.15}$$

where d_s is the thickness of the surface [m] and k_s the corresponding thermal conductivity [W m^{-1} °C^{-1}]; and h_{amb} was estimated using Eq. (4.12). For the floor, different layers of construction and insulations were considered. A constant sub-soil temperature of 10°C at a depth of 8.8m was used (Pirard et al., 1993).

Product

Concerning heat and mass transfer coefficient for bulk storage of fruit in bins at low velocities, the well-known Ranz-Marshall (Ranz and Marshall, 1952) correlation, extended for combined forced and natural convection in a packed bed of spheres, can be employed.

$$Nu = 2 + 0.552\,\mathrm{Re}^{0.5}\,\mathrm{Pr}^{0.333} \tag{4.16}$$

In the computation of the Reynolds number, interstitial velocity inside the bulk of fruit in the bin was used. The average velocity value was obtained from air distribution studies performed on bulk storage inside bins (Hoang et al., 2000). In order to account for fruit with a shape different from that of a sphere, an equivalent

diameter was used as a characteristic diameter in the calculation of the Reynolds number.

The heat transfer area of the fruit was calculated based on correlations developed by Schotsmans (2003). The surface area of different pip fruit was expressed as a function of their characteristic dimensions. The correlations for pear and apple are given by Eqs. (4.17) and (4.18), respectively.

$$A = 6.29DH + 2.336D^2 - 1.766H^2 - 0.356D - 0.0357H + 0.011 \quad (4.17)$$

$$A = 8.8493D^2 - 0.8359D + 0.0325 \quad (4.18)$$

where H is the pear height [m] and D the maximum fruit diameter [m]. The specific surface area was calculated using available data for average[1] fruit characteristic dimensions and volume. The heat transfer area was estimated from the volume of fruit in the cool room. The pear Equilibrium Moisture Content was obtained from Nguyen et al. (2003) and that of the packaging from www 2 (2001).

4.3.1.3 Measurements and validation method

In order to assess the cool room model and possible tuning of the model parameters an empty room experiment was carried out. A cool room initially at ± 20°C was cooled to a set temperature of 1°C. The room was situated between two other rooms at 0.7°C and 12°C. The dynamics of the room air temperature was followed using type-T Teflon-insulated thermocouples (Omega Engineering, Inc., Stanford, USA) as shown in Figure 4.3. Only half of the room was scanned assuming symmetry. This assumption was checked by placing thermocouples on the other half of the room, symmetric to some selected positions (Figure 4.3). In total 108 thermocouples were employed. The positions of the thermocouples were chosen based on preliminary temperature measurements and air flow pattern studies (Hoang, 2003).

The thermocouples were connected to an HP 34970A data acquisition system (Agilent, Palo Alto, CA). The thermocouples were calibrated in a temperature controlled water-bath (F-26, Haake, Germany) and ice for a temperature range of 0 to 30°C. The data acquisition system was interfaced with a personal computer and

[1] These data were average values from the harvest of years 1998, 1999 and 2000 from 3 different orchards namely: Lendelede, Rillar and Velm, in Belgium. 100 fruit were sampled from each orchard every year for different apple and pear cultivars.

was controlled by Bench-link software (Agilent, Palo Alto, CA). A Pt100 situated at the back of the room, which is an integral part of the CA cool storage system, was used for temperature control (identified by the subscript *sys* from now on). The surface temperature of the cooler was measured on the fins at two positions, one at each block. In order to obtain a representative temperature of the room, the volume average of the measured temperatures was calculated using the formula:

$$T_{VA} = \frac{\sum_{e=1}^{n} T_e V_e}{\sum_{e=1}^{n} V_e} \tag{4.19}$$

where V_e and T_e represent the volume and temperature of a volume element. Relative humidity measurements were obtained from a RH meter (Siemens, Building Technologies Inc., Illinois, USA), which was also used for control purposes.

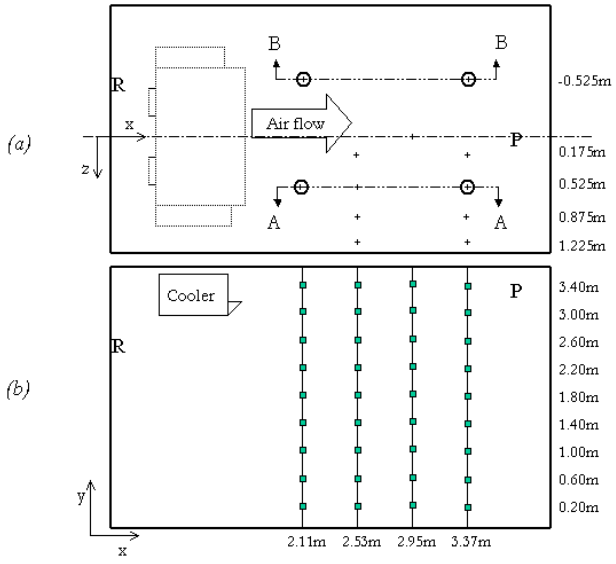

Figure 4.3 Sensor positions in the cool room for temperature measurement (a) Horizontal cross section, (b) Vertical cross section; (Circled positions were used to check symmetry; P: system pulse temperature sensor; R: system room air temperature and relative humidity sensor)

Furthermore, measurement of the heat flux through the envelope was carried out using micro-foil heat flow sensors (RdF Corporation, Hudson, England). The accuracy of the sensors was 5%. The measurement locations of the flux sensors are shown in Figure 4.4. Since the measurements were noisy, a Savitzky-Golay signal-filtering Matlab algorithm (The MathWorks Inc., Natick, Massachusetts) was employed to extract the available information.

The first measurement (at t=0) was used as an initial value in the simulation of the dynamic variables. In the case where several measurements for a given variable were carried out, an average value of the measurements was calculated as an initial value for the simulation.

In the present inquiry, because of the existence of different components and different approaches to model them, it is difficult to define a single and common validation criterion. The maximum performance expected from a model is an accuracy level equivalent to the measurement accuracy. This can be evaluated by comparing the Root Mean Square Error (RMSE) between the model predictions and measured data with the measurement accuracy. On the other hand, in dealing with the lumped approach, the quality of prediction of a given model can be evaluated with respect to the observed spatial variability. As a measure of spatial variability the distance between the weighted average of the observations and the minimum or the maximum observation can be calculated in terms of RMSE (in this case, the root mean square difference). This distance is then compared to the error between the weighted average and the model prediction. Here, in evaluating the performance of the different component models one or both of the above criteria will be employed. In summary, when the RMSE value between the weighted average and model prediction is equivalent to the measurement accuracy or less than the observed spatial variability, the accuracy of the model prediction can be asserted as acceptable. It should be emphasised here that the measurements are only a snap shot of reality. This means that the influence of random events and the stochastic nature of physics might not be represented by the present set of data. Thus, the focus should be as to whether the basic dynamics of the system as observed from the experimental data is in agreement with the dynamics of the model.

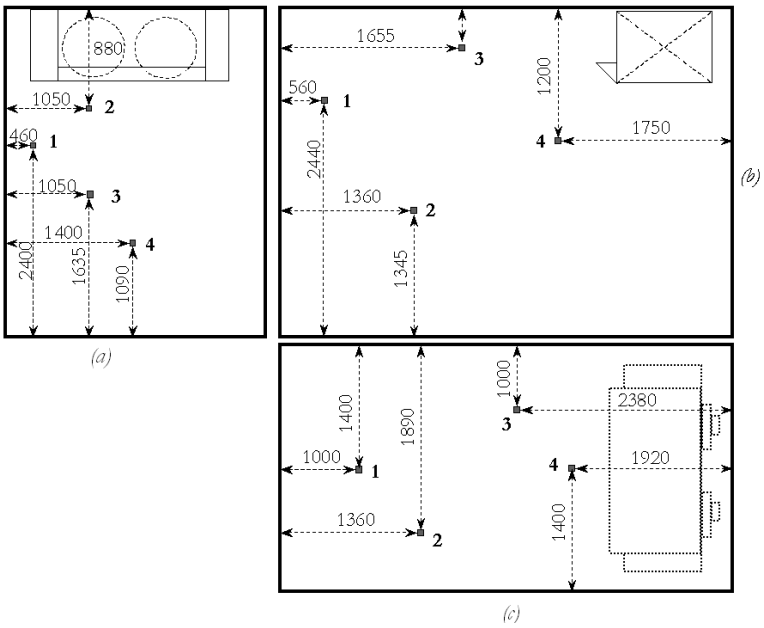

Figure 4.4 Heat flux measurement sensor positions (a) Wall 2; (b) Wall 3 and its mirror reflection represents Wall 4; (c) Ceiling and its mirror reflection represents Floor.

4.3.2. Refrigeration unit model

4.3.2.1 The experimental refrigerator

Since most industrial and pilot plant refrigeration systems were not built to suit for experimental purposes, the measurements one can do especially on the refrigeration cycle is very limited. As a result, a small experimental unit of 7.5 KW situated at the TME division (Mechanical Engineering Department – Katholieke Universiteit Leuven, Leuven, Belgium) was employed (Figure 4.5) to validate the refrigeration unit model. The system consists of a water-cooled double-pipe spiral condenser where the cooling medium was circulated via a pump. The evaporator, also a double-pipe spiral type, was insulated and glycol-water was pumped as a medium to be cooled. The unit was coupled to a 0.34 m^3 tank filled with glycol water to imitate the holding tank of the indirect system layout. The schematic representation of the experimental set up is shown in Figure 4.6.



Figure 4.5 Experimental refrigeration unit

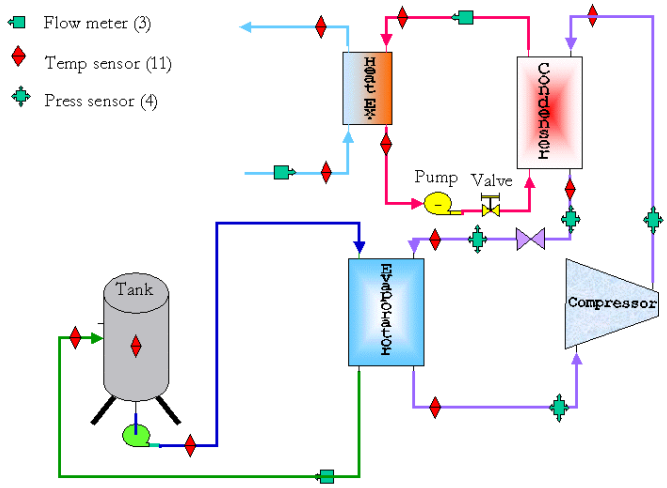

Figure 4.6 Schematic representation of the experimental set up

4.3.2.2 Model parameters

The thermal capacities of the components were calculated from available material masses, and material thermal properties were obtained from literature. The product of the effective heat transfer coefficient and heat transfer area for the condenser and

evaporator were estimated from steady state runs at operation conditions. The compressor swept volume was obtained from the manufacturer manual and the volumetric and isentropic efficiencies were estimated as a function of the pressure ratio from the steady state experiments. The results from the steady state experiments are summarised in Table 4.1.

The dependence of the volumetric efficiency of the compressor on pressure ratio (PR) can be approximated by a linear relationship (Figure 4.6). However, the isentropic efficiency of the compressor could be considered as constant. A trend is observed on the $(UA)_{cond}$ values as the pressure ratio increases. This was due to the fact that the desired pressure ratio was achieved by throttling the valve between and the condenser and the cooling water pump in the circuit (Figure 4.5). This obviously has some influence on the overall heat transfer coefficient of the condenser. The working pressure ratio during the experiments for validation was in the range of the first two runs (Table 4.1), and the average of these values was employed for simulation.

Refrigerant properties were determined using empirical formulae developed by Cleland (1986). For refrigerants not included in this work empirical formulae were developed partially in a similar way based on the refrigerant properties data obtained from ASHRAE Handbook fundamentals (1997). The values of the parameters used in the simulation are compiled in Appendix B.

Table 4.1 Estimated parameters using steady state runs

Run	*PR*	$(UA)_{cond}$ [W °C^{-1}]	$(UA)_{evap}$ [W °C^{-1}]	η_v	η_i
1	2.76	573	1723	0.740	0.48
2	2.78	698	1872	0.720	0.49
3	3.06	605	1633	0.716	0.51
4	3.56	616	2034	0.696	0.51
5	4.43	503	2005	0.65	0.50

4.3.2.3 Measurements and validation method

The water in the tank, initially at room temperature, was allowed to cool to about 2°C. K-type thermocouples (Omega Engineering, Inc., Stanford, USA) with an accuracy of ±0.5°C, pressure sensors, (4295AE20, Kristal Instrumente AG,

Winterhur, Switzerland) and magnetic flow meters (K-Mag10D1476, Bailey-Fischer & Porter GmbH, Göttingen, Germany), were used to measure the refrigerant and water temperatures, pressures and flow rates, respectively, at different locations (Figure 4.5). The measured data was logged by means of a 32-channel module attached to a SCXI-1300 (National instruments, USA) block. LABVIEW software was used to control the data acquisition and was linked to a MATLAB program (The MathWorks Inc., Natick, Massachusettes), which calculates the enthalpies and heat loads on the different components from the logged data using a database of refrigerant properties.

Validation criteria as defined in Section 4.3.1.3 were employed to evaluate the performance of the model. The first measurement (at t=0) was used as an initial value in the simulation of the dynamic variables. In the case where several measurements for a given variable were carried out, an average value of the measurements was calculated as an initial value for simulation.

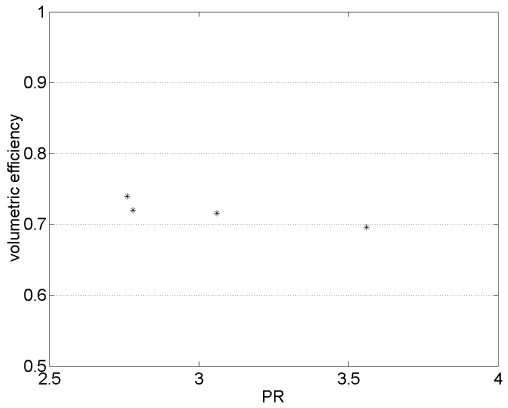

Figure 4.7 Volumetric efficiency of the compressor as a function of pressure ratio

4.3.3. Gas handling unit model

4.3.3.1 Model parameters

The parameters involved on the gas-handling unit include the physical (geometric) parameters of the bed, gas flow rate to the unit, duration of adsorption and desorption steps and kinetic and equilibrium parameters of the adsorbent material in

the beds. The physical parameters were obtained from manufacturer manuals and through physical measurements. The gas flow rate to the handling unit was measured using a float–type rotameter (Kytöyö Instruments, Muurame, Finland) and the duration of the adsorption/desorption process steps using a stopwatch. The kinetic and equilibrium parameters were obtained from literature (Valenzuela and Myers, 1989; Ruthven et al., 1994). Figure 4.8 shows the picture of the gas-handling unit.



Figure 4.8 Gas-handling PSA unit

4.3.3.2 Measurements

The direct validation of the model as an independent entity could prove to be difficult owing to the transient nature of the unit involving very short adsorption steps (60 s in the considered unit). This obviously necessitates gas concentration measuring devices that can continuously analyse the flow of gas from the columns (beds). However, during the pull-down operation the rate at which O_2 is removed is principally affected by the performance of the N_2 generation unit and later the removal of CO_2 by the CO_2 scrubber. The model could, thus, be validated indirectly

by means of the evolution of the concentrations of the respiratory gases inside the cool room.

4.3.4. Global CA cool storage model: measurement and validation method

For validation of the global CA cool storage model, a CA cool room described in Section 4.3.1.1 was loaded with 8 bins (1.0x1.2x0.75m), each containing ±380kg of Conference pears from Roeselare, Belgium. The loaded room measurement set up is shown in Figure 4.9. A total of 59 calibrated T-type Teflon-insulated thermocouples (Omega Engineering, Inc., Stanford, USA) were used to follow the dynamics of the room air and product temperatures. A fruit situated more or less at the centre of each bin was selected for product temperature measurement. The thermocouples were then connected to an HP 34970A data acquisition system (Hewlett-Packard Company, USA) as described in Section 4.3.1.3. Additional Pt100 temperature sensors, one situated at the back of the room to measure the room temperature and the other in front of the cooler (Figure 4.9) to measure the pulse temperature, were used by the system for control purposes (identified by the subscript '*sys*'). The accuracy of the temperature sensors was ±0.5°C. In order to obtain a representative temperature of the room, the volume average of the measured temperatures was calculated (Eq. (4.19)). The schematic representation of the room as partitioned for the volume average calculation is shown in Figure 4.10.

The relative humidity of the room was measured by a RH meter and a dew-point meter. The RH meter (Siemens, Building Technologies Inc., Illinois, USA), which is integral part of the CA cool storage system and used for control purposes, was situated at the back of the room near the Pt100 for room temperature measurement with accuracy of ±5%. The dew-point meter (General Eastern Instruments, MA, USA), positioned near the Pt100 for pulse temperature measurement (Figure 4.9), was calibrated using headspace air in equilibrium with different concentrations of salt solutions with ±3% accuracy. Capacitive type RH sensors (ESCORT junior, Tech Innovators, Oakland, Newzealand) were also used to record the relative humidity inside 4 of the bins with an accuracy of ±5%. Isolated volume of fruit with known weight was placed in each bin to estimate the moisture loss from the fruit.

The surface temperature of the cooler was measured at two positions as described in Section 4.3.1.3. Moreover, the in-coming refrigerant temperature was measured by system provided Pt100 temperature sensor. The gas concentrations in the room were analysed by a 1111D/000 paramagnetic O_2 analyser (Servomex Group Ltd,

USA) (±0.1% accuracy) and 2008SDH non-depressive infrared CO_2 analyser (Valtronics, CA, USA) (±0.05% accuracy) for oxygen and carbon dioxide, respectively.

The cooling process was started from initial temperature of ±20°C and cooled down to a set point of -1°C. Seven days later, the gas-handling unit was set into operation to pull the O_2 concentration down to a set point of 2.5%. The CO_2 level was controlled to a set point of 0.7%. The concentrations of the respiratory gases were measured (controlled) every two hours in the beginning and three hours in later stages. For O_2, the controller was set to a maximum N_2 injection time of 30 minutes or 2 minutes for every tenth of a percentage error, whichever comes first. For CO_2, a maximum scrubbing time of 10 minutes or 1 minute for every tenth of a percentage error, whichever comes first.

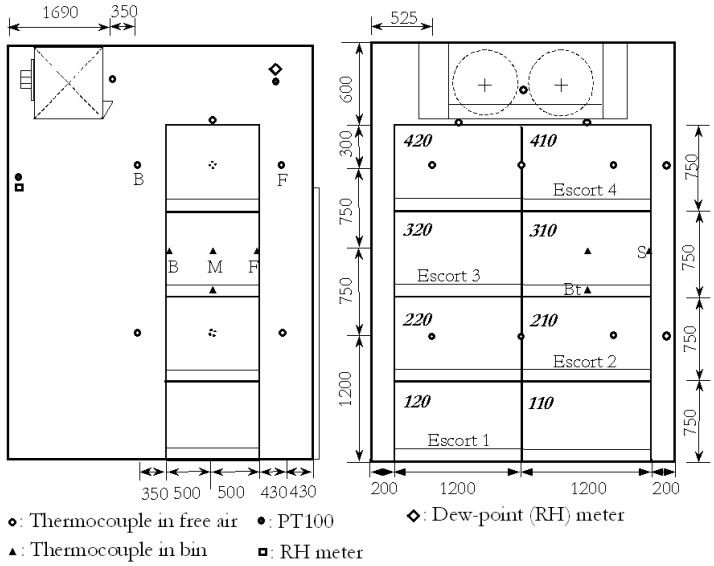

Figure 4.9 Loaded room measurement set up (B: Back, M: Middle, F: Front, S: Side, Bt: Bottom)

Validation criteria as defined in Section 4.3.1.3 were employed to evaluate the performance of the model. The first measurement (at t=0) was used as an initial value in the simulation of the dynamic variables. In the case where several measurements for a given variable were carried out, an average value of the

measurements was calculated as an initial value for simulation. The simulation was carried out on a Celeron 366Mhz, 128Mb Ram personal computer with Microsoft Windows NT OS.

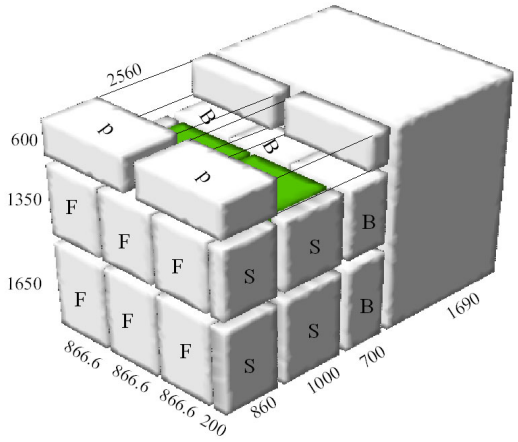

Figure 4.10 Cool room partition for volume average calculation (dimensions are in mm) (F: Front, S: Side, B: Back, P: pulse; the dark coloured section at the middle of the room represents the bins filled with fruit)

4.3.5. Sensitivity analysis

Owing to the inherent relatively large uncertainty involved with model parameters, a sensitivity analysis needs to be carried out especially to the transfer rate coefficients, which affect the cooling and moisture loss of the stored product. Since, in general, the relationship between model predicted values **y** and the model parameters **p** is not known, a first term approximation of the Taylor series can be used to express **y** as a function of **p** in the presence of small perturbation $\Delta\mathbf{p}$ in the model parameters.

$$\mathbf{y}(\mathbf{p}) = \bar{\mathbf{y}} + \left.\frac{\partial \mathbf{y}}{\partial \mathbf{p}}\right|_{\mathbf{p}_o} \Delta\mathbf{p} \tag{4.20}$$

where $\bar{\mathbf{y}}$ is the model prediction at nominal parameter values $\mathbf{p}_o$. By substituting Eq. (4.20) in the model equations and rearranging, the resulting system of equations can be solved, there by estimating the sensitivity $\partial\mathbf{y}/\partial\mathbf{p}$. However, when several model

variables are involved as in the case of the CA cool storage model, the resulting equations might get considerably complex affecting the stability of the numerical solution.

Alternatively, the absolute change $J^a_{i,j}$ of the model predicted value y_i with regards to small perturbation Δp_j in model parameters could be calculated from:

$$J^a_{i,j} = \left(\frac{\partial y_i}{\partial p_j} \right) \cong \frac{y_i\big|_{(p_j + \Delta p_j)} - y_i\big|_{(p_j - \Delta p_j)}}{2\Delta p_j} \tag{4.21}$$

where *i* and *j* denote the time and parameter indexes, respectively.

With the absolute sensitivity, the absolute change of the model prediction due to an increase or decrease of the parameter value by a unit value can be analysed. However, to compare the relative influences of different model parameters on model predictions, the relative sensitivity is often employed, formulated by the normalized partial derivatives of the model prediction y_i with respect to parameter p_j.

$$J^r_{i,j} = \left(\frac{\partial y_i}{\partial p_j} \right) \frac{p_j}{y_i} \cong \frac{y_i\big|_{(p_j + \Delta p_j)} - y_i\big|_{(p_j - \Delta p_j)}}{2\Delta p_j} \frac{p_j}{y_i} \tag{4.22}$$

The decision for controlling the critical model parameters that most severely influence the model prediction can then be made based on the comparison of the relative sensitivities between the different parameters. The limitation of the relative sensitivity, among others, is the 'division by zero' problem. This means that the relative sensitivity tends to be very large in the vicinity of zero for processes that cross the time-axis. In this case the relative sensitivity is not applicable.

4.4. Results

4.4.1. Cool room and accessories: model assessment

In this section an appraisal of the considered assumptions in formulation of the main cool room component models and possible tuning and analysis of the estimated parameters is carried out using the empty room experiment as described in Section 4.3.1. Moreover, the single zone consideration for the room air model is assessed by looking at the spatial temperature distribution in the cool room.

Simulations were carried out assuming a constant incoming secondary refrigerant temperature into the cooler unit.

Room air temperature and relative humidity

Figure 4.11 shows the comparison between symmetric positions in the empty room at steady state (after 100 min). As can be observed, the temperature difference between the symmetric points is evident at the middle section (in the interval y = [1.8 2.6]) than at the top or bottom with a maximum difference of less than 0.5°C. It can also be observed that the closer one gets to the cooler (x = 2.11) the less variation in temperature between symmetric points. These observations correspond with the distribution of the air velocity, as can be intuitively perceived. In general, since the maximum observed temperature difference is in the order of the accuracy of the thermocouples, the empty room can be considered symmetric with respect to air temperature. Thus, the calculation of the volume average room air temperature was based on measurements, which were obtained from one half of the room.

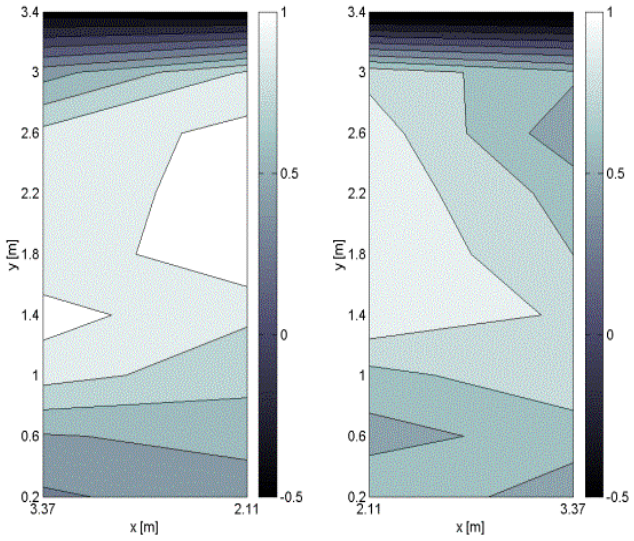

Figure 4.11 Symmetry in vertical cross section parallel to airflow direction in an empty cool room at steady state (for the positions in the empty cool room refer to Figure 4.3)

Figure 4.12 depicts the simulated and measured room air temperatures at different positions. The maximum temperature variation inside the room was more than 3°C during transient and about 2.0°C in steady state, as can be seen from the measured maximum and minimum profiles. The maximum RMSE between the volume average of the room and these temperatures was 1.91°C. The sensors for the maximum and the minimum temperatures were located right in front of the cooler (with coordinates (3.37, 1.4, 0.525)) and in the middle of the room (with coordinates (2.53, 3.4, 0.175)), respectively (Figure 4.3). The minimum temperature was less than that of the pulse temperature as measured by the Pt100, which was placed further down stream as compared to the sensor for the minimum temperature. It can also be observed that the calculated volume average temperature of all the thermocouples corresponds well with the Pt100 measurement (RMSE = 0.34°C), which was used as a sensor for the controllers. Even though much cannot be said about the model at this point, the prediction appears to be representative for the measured values in both the room air and pulse temperatures. This can be confirmed by the low RMSE values obtained (0.43°C and 0.63°C for the room and pulse temperatures, respectively) with respect to the calculated average temperatures of the measurements. These values are in the vicinity of the measurement accuracy and obviously less than the observed variability. Of course in a lumped system, one can easily tune the model to predict the experimental data, however in such cases where the room air temperature interact with several components it might not be easy to tune one state variable without disturbing another, especially when coupled systems such as heat and moisture transfer are present.

Figure 4.13 presents the room air relative humidity. At the beginning, as the room air starts to cool down, the relative humidity increases to a certain level due to the decrease of the saturation vapour pressure of the air. After about 1500 s, moisture removal by the cooler starts and the temperature effect was balanced or even exceeded by the decrease in partial vapour pressure where the relative humidity was observed to slightly decrease. At a stage where the cooler temperature was no more less than the dew point temperature of the room air temperature, the relative humidity reached to steady state value. This trend was observed in both the simulated and measured profiles. However, during much of the transient state, the model over predicts the experimental data. This discrepancy is reflected in the high RMSE value (8.8%), which exceeds the measurement accuracy (5%) considerably. In reality, when the cooling is on, condensation starts immediately on the surface of the pipes where refrigerant enters the cooler. This small, but significant, removal of moisture from the room air counteracts the temperature effect resulting in an

increase of the room air relative humidity at a slower rate. However, the model predicts constant vapour pressure of the room air until the predicted cooler temperature reaches the dew point temperature of the room air. This means that the removal of moisture from the room air by the cooler occurs earlier than the model can predict resulting in over prediction of the relative humidity. Nevertheless, at steady state the model prediction is observed to fit the experimental data well implying the amount of moisture removed in the end from the room air being the same in both cases.

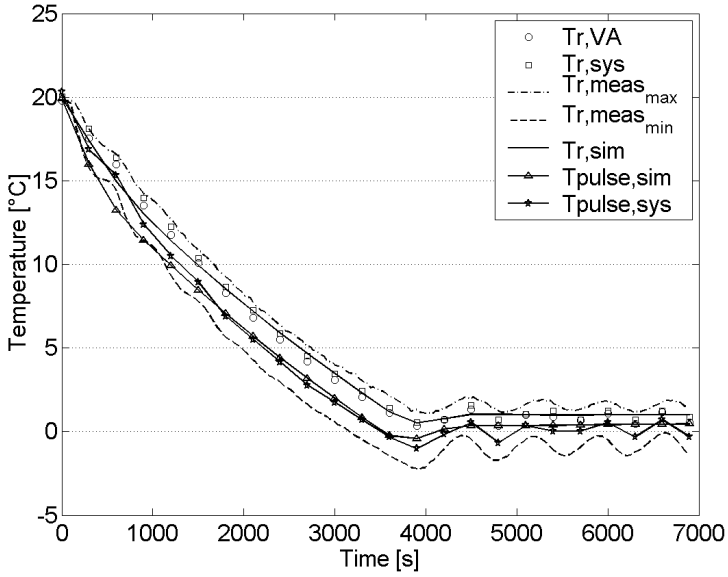

Figure 4.12 Air temperature in an empty room. T_r : room air temperature; Tpulse: pulse temperature RMSE($Tr_{,VA}$, $Tr_{,meas_{max}}$*) = 0.74°C; RMSE(*$Tr_{,VA}$, $Tr_{,meas_{min}}$*) = 1.91°C; RMSE(*$Tr_{,VA}$, $Tr_{,sim}$*) = 0.43°C; RMSE(*$Tpulse_{,sim}$, $Tpulse_{,meas}$*) = 0.63°C. (VA: volume average; sys: measurement from the system; meas: measurement; Sim: simulation).*

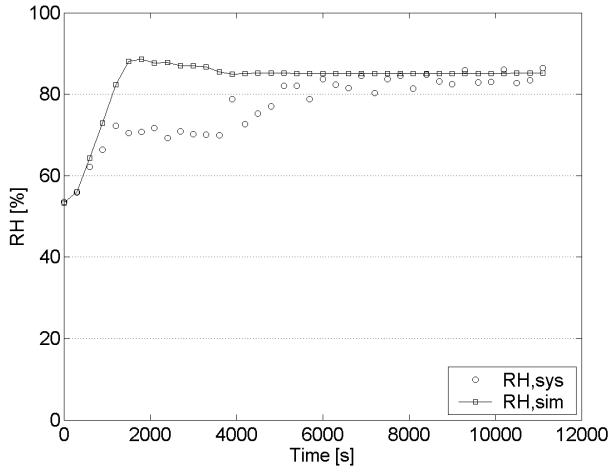

Figure 4.13 Air relative humidity in an empty room. RMSE = 8.8%. (sys: measurement from the system; Sim: simulation)

Cooler temperature

The cooler surface temperature as measured at the two blocks (Figure 4.2) and the simulated temperature profiles are shown in Figure 4.14. The temperature of the first block was higher than that of the second block. As the air enters the cooler unit, much of the energy of the air was dumped on the first block of the cooler (2/3 of the bundle of tubes). The second block (1/3 of the bundle of tubes), which has a supply of fresh refrigerant, deals with already cooled air and, hence, experiences less temperature increase as compared to the first one. As can be expected the model predicts the measurement from block one more closely. Owing to the lower temperature of the second block which might be lower than the dew point temperature of the air, condensation could occur on the surface as early as the beginning of the cooling process. Thus, the increase in relative humidity because of the lowering of the saturation vapour pressure of the air was balanced by the removal of moisture. This reinforces the explanation for the over prediction of the room relative humidity during the transient state by the model. The model predicts the surface cooler temperature with favourable agreement. The lower RMSE value of the model prediction, as compared to the minimum RMSE value of the measurements with respect to the weighted average temperature of the two positions, confirms this.

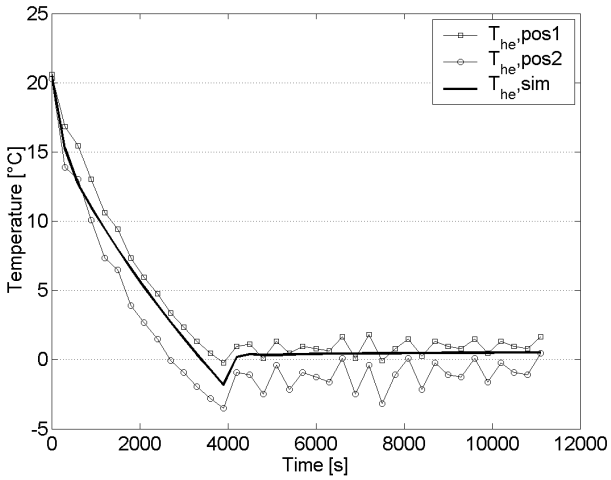

Figure 4.14 Cooler temperature. RMSE($T_{he,}$pos1, $T_{he,WA}$[2] *) = 0.82°C; RMSE(*$T_{he,}$pos2, $T_{he,WA}$ *) = 1.65°C; RMSE(*$T_{he,}$sim, $T_{he,WA}$ *) = 0.67°C; (pos1: block 1; pos2: block 2; Sim: simulation, WA: weighted average of the two positions)*

Envelope temperatures

Figures 4.15 – 4.19 show the temperatures and heat fluxes of wall 2, wall 3, ceiling and floor. First, the heat transfer coefficient used in the surface and floor models were estimated using empirical correlations, and using measured velocities near the surfaces. Later, the surface heat transfer coefficients were estimated using heat flux measurements and were found to be comparable for the walls but substantially different for the floor and ceiling. This could mainly be attributed to the accuracy of the velocity measurements owing to the high level of turbulence especially on the ceiling. The surface temperatures, after tuning the parameters based on the heat flux measurements, were well represented by the model as can be confirmed from the respective RMSE values which are comparable to the measurement accuracy. However, it can be observed that the model tends to overestimate the ceiling temperature during the transient state. In the formulation of the surface model, the ceiling was assumed to interact with the lumped room air temperature. In reality, however, the pulse temperature was responsible for the interaction with the ceiling, which is lower than the room air temperature. This could result in slight over

[2] The $T_{he,WA}$ is the weighted average of the temperatures $T_{he,}$pos2 and $T_{he,}$pos1.

estimation of the ceiling temperature by the model. From Figure 4.17, it can be observed that when the total mass of the floor (corresponding to 0.1m of floor thickness) was used, large deviation from the model prediction was obtained. This indicates that not all the floor thermal mass is affected by the room air temperature during the transient period. The layer of the floor actually interacting with the room air was found at 40% of the total thermal mass. Initially, the floor temperature was lower than that of the room air (Figure 4.18). As a result, an increase in temperature of the floor is expected at the beginning before it eventually starts to cool down. Here, this was not the case; rather the temperature decreases immediately after start. This indicates that there was an evaporative cooling involved caused by condensation on the floor prior to the start of the experiment. Moreover, as can be seen from Figure 4.19, the load imposed by the floor is more than 6 times that of the wall and more than 4 times that of the ceiling. This is due to the shear size of the thermal mass of the floor as compared to the other components of the empty cool room. This apparently significant influence, however, is substantially decreased by the presence of the stored produce in two ways: *(i)* much of the floor area is covered, reducing the heat transfer area and *(ii)* the product load is larger than the floor load.

Concerning the heat flux through the surfaces, the RMSE of the heat flux predictions were found to be higher than the measurement accuracy (5%) in most of the cases. The observed spatial variability in terms of RMSE was 0.9, 1.7, 2.2, and 3.9 W m^{-2} for wall2, wall3, ceiling and floor, respectively. These values are comparable to the prediction RMSE values (1.1, 1.3, 3.6, and 4.8 W m^{-2} for wall2, wall3, ceiling and floor respectively). Thus, the performance of the model in the observed trend can be considered sufficient, as can be inspected visually.

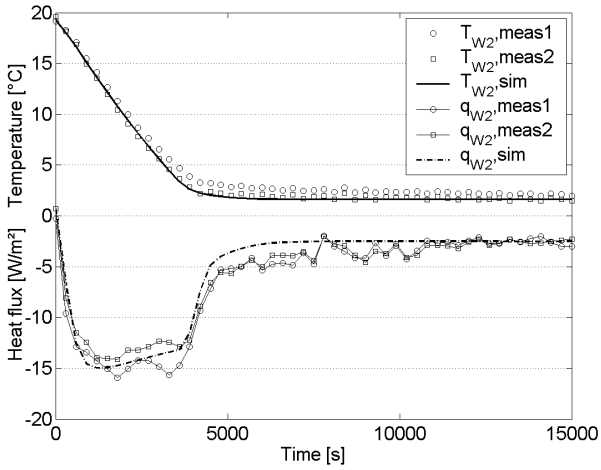

Figure 4.15 Wall 2 temperature and heat flux at 2 positions. RMSE($T_{w2,AV}$, $T_{w2,}$sim) = 0.49°C. RMSE($q_{w2,AV}$, $q_{w2,}$sim) = 1.1 W m^{-2}. (T_{w2} : wall 2 temperature; q_{w2}: heat flux through wall 2; meas1: measurement position 1; meas2: measurement position 2; sim: simulation; AV: average of measurements from 4 positions (Figure 4.4))

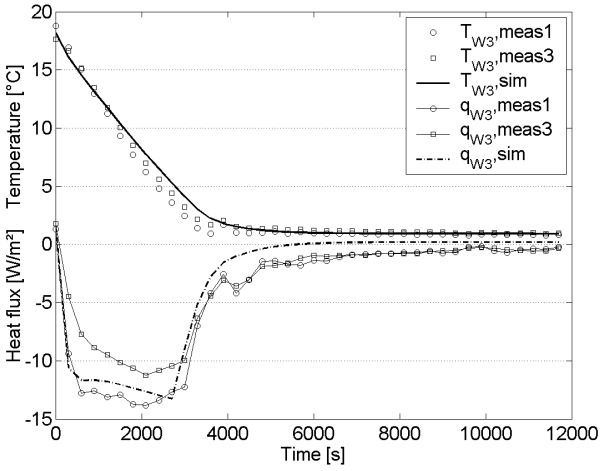

Figure 4.16 Wall 3 temperature and heat flux at 2 positions. RMSE($T_{w3,AV}$, $T_{w3,}$sim) = 0.53°C. RMSE($q_{w3,AV}$, $q_{w3,}$sim) = 1.3 W m^{-2}. (T_{w3} : wall 3 temperature; q_{w3}: heat flux through wall 3; meas1: measurement position 1; meas2: measurement position 2; sim: simulation; AV: average of measurements from 4 positions (Figure 4.4))

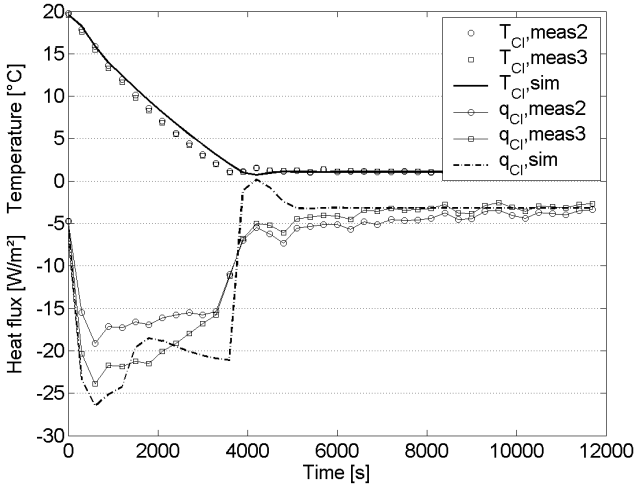

Figure 4.17 Ceiling temperature and heat flux. RMSE($T_{cl,AV}$, $T_{cl,sim}$) = 0.54°C. RMSE($q_{cl,AV}$, $q_{cl,sim}$) = 3.16 W m^{-2}. (T_{cl} : ceiling temperature; q_{cl}: heat flux through the ceiling; meas2: measurement position 2; meas3: measurement position 3; sim: simulation)

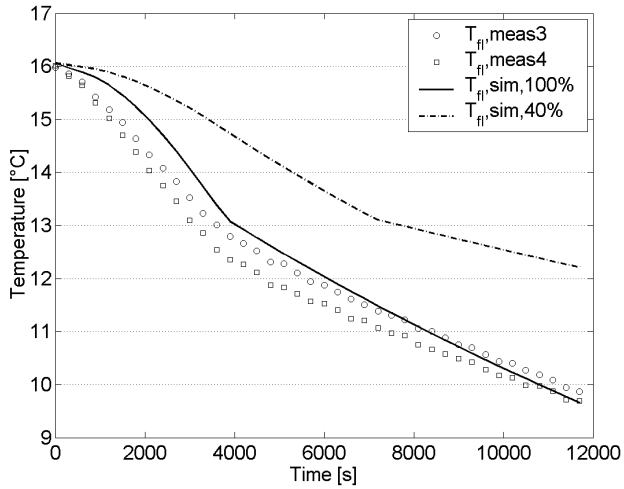

Figure 4.18 Comparison of different proportions of total floor thermal mass. . RMSE($T_{fl,AV}$, $T_{fl,sim,40\%}$) = 0.41°C. RMSE($q_{fl,AV}$, $q_{fl,sim}$) = 4.8 W m^{-2}. (T_{fl}: floor temperature; meas3: measurement position 3; meas4: measurement position 4; sim,100%: simulation with 100% floor thermal mass; sim,40%: simulation with 40% floor thermal mass)

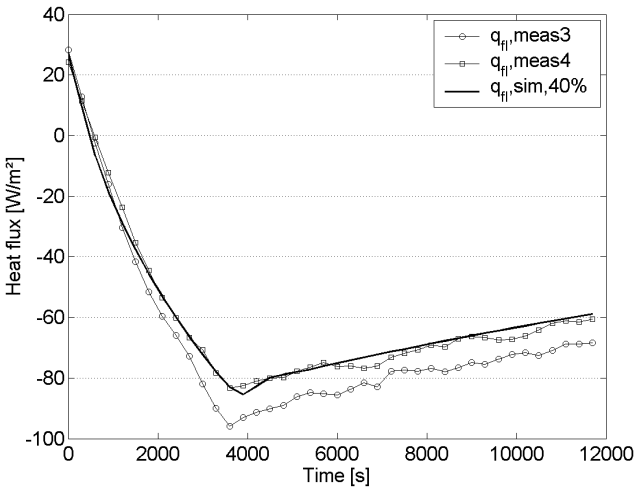

Figure 4.19 Floor heat flux at 40% of the total thermal mass at two positions. q_{fl}: heat flux through the floor (meas3: measurement position 3; meas4: measurement position 4; sim,40%: simulation with 40% floor thermal mass)

4.4.2. Refrigeration unit model validation

4.4.2.1 Validation results

Figure (4.20) shows the predicted and simulated temperatures of tank, evaporator and condenser temperatures. Evaluation of the model prediction capacity was carried out using statistical comparison by means of the Root Mean Square Error (RMSE). The RMSE values for three runs are summarized in Table 4.2.

Table 4.2 Root Mean Square Error of the predicted and simulated temperatures for different runs

RMSE values [°C]			
	Condenser	Evaporator	Tank
Run 1	2.22	0.88	0.23
Run 2	2.35	0.94	0.23
Run 3	1.68	0.5	0.23

The rather high RMSE values of the condenser and evaporator temperatures are mainly due to the inconsistency of the model at start up, where large variations were observed. Moreover, the fluctuations generated by the flow control provided by the expansion valve, especially near the end of the experiment, contributes to the obtained high RMSE values. However, as can be visually confirmed, for the rest of the process a favourable agreement between the model and the experimental data was obtained.

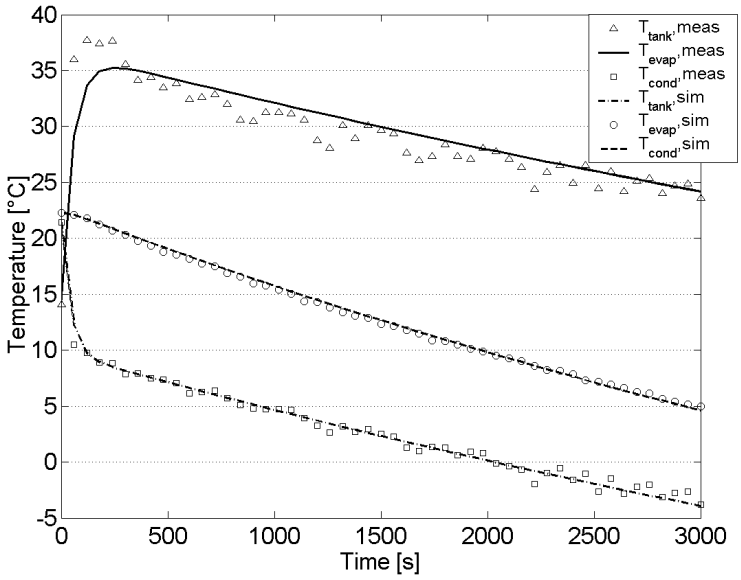

Figure 4.20 Evaporator, condenser and tank temperature in refrigeration unit

The observed slight deviation during start up in the evaporator temperature could be due to the considered assumption that refrigerant distribution is constant while actually there might be no or little refrigerant especially in the evaporator resulting in lower thermal mass. This discrepancy could be considerable for larger refrigeration systems. For the condenser, the main cause for the significant shoot in temperature at the beginning was the observed delay in the start up of the cooling water pump. Considering a more complex representation of the components could have improved the prediction accuracy during start up. However, in view of the added complexity and amount of input data, the advantage gained may be undermined.

The tank temperature, which forms a boundary between the refrigeration unit and the cooler inside the cool rooms, was predicted with acceptable accuracy. This is observed by the low RMSE values. This means that the uncertainty in the model prediction of the equipment temperatures was not propagated to the cooler of the cool room in case of indirect system layout.

4.4.2.2 Sensitivity analysis

The sensitivity of the condenser, evaporator and tank temperatures with respect to the overall heat transfer coefficients as well as the thermal masses of the condenser, evaporator and tank were investigated. The evaluation of the sensitivity was carried out based on the temperature measurement accuracy. The nominal parameter values considered for the simulation are tabulated in Table 4.3.

Table 4.3 Nominal parameter values considered for sensitivity analysis

	Condenser	Evaporator	Tank
UA [W °C^{-1}]	620	1800	-
MC (Thermal mass) [J °C^{-1}]	45268	70629	1529969

Figure (4.21) depicts the sensitivity of the condenser, evaporator and tank temperature in relation to condenser overall heat transfer coefficient. The condenser temperature was found to be more sensitive to changes in its overall heat transfer coefficient. A variation of 10% (equivalent to 62 W m^{-2} °C^{-1}) in overall heat transfer coefficient, the condenser temperature prediction can have an error of 6.2% relative to its value, which is equal to 2.2°C in absolute value. The variation in evaporation temperature in response to the variation in condenser overall heat transfer coefficient was less than 0.3°C in absolute value which is equivalent to 6.6% relative to its value. The tank temperature is barely sensitive (< 0.2°C absolute value for 10% parameter variation) to the variation in overall heat transfer of the condenser. Thus, only the condenser temperature has significant sensitivity, which is considerably higher than the limitation set by the measurement instrument (0.5°C).

In Figure 4.22, the sensitivity of the equipment temperatures to the evaporator overall heat transfer coefficient is shown. The evaporator temperature was found to be more sensitive as compared to condenser and tank temperature. Unlike the previous case a positive sensitivity is obtained. Given a variation of 10% in the parameter, which is equivalent to 180 [W °C^{-1}], a maximum over prediction of the

evaporator temperature of less than 0.2°C is expected. Thus, it can be asserted that the evaporator, condenser and tank temperatures are hardly sensitive to the variation in the parameter under consideration.

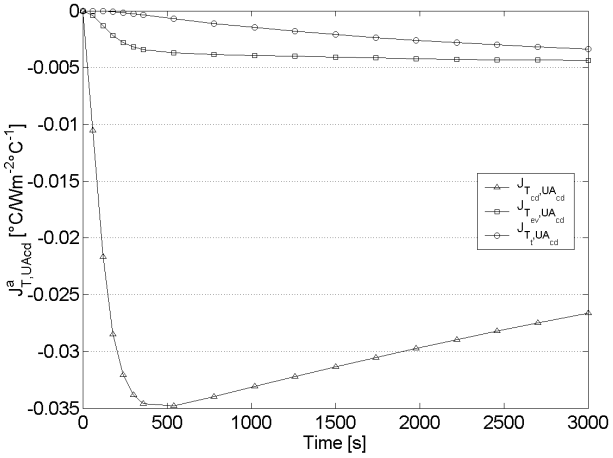

Figure 4.21 Absolute sensitivity of condenser, evaporator and tank temperature with respect to condenser overall heat transfer coefficient (UA) in refrigeration unit

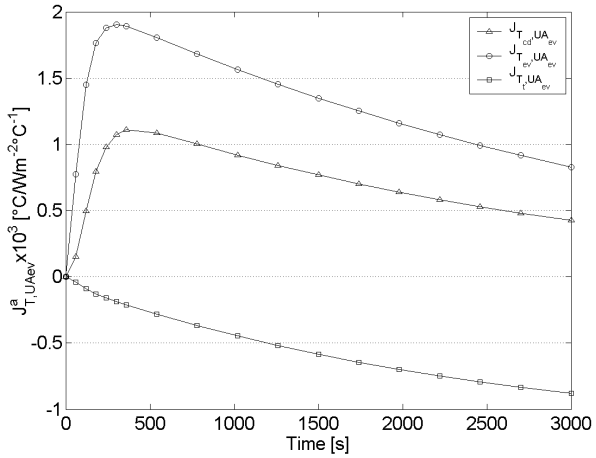

Figure 4.22 Absolute sensitivity of condenser, evaporator and tank temperature with respect to evaporator overall heat transfer coefficient (UA) in refrigeration unit

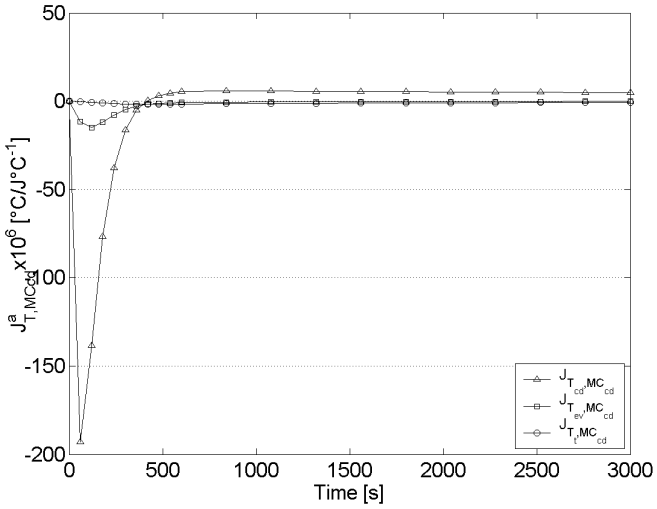

Figure 4.23 Absolute sensitivity of condenser, evaporator and tank temperature with respect to condenser thermal mass (MC) in refrigeration unit

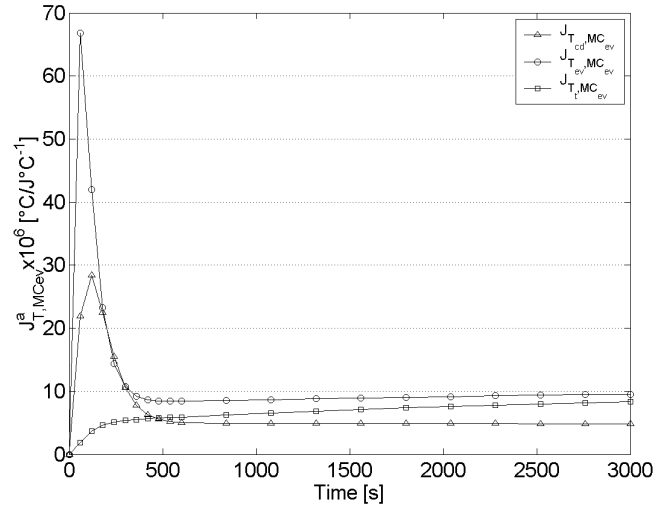

Figure 4.24 Absolute sensitivity of condenser, evaporator and tank temperature with respect to evaporator thermal mass (MC) in refrigeration unit

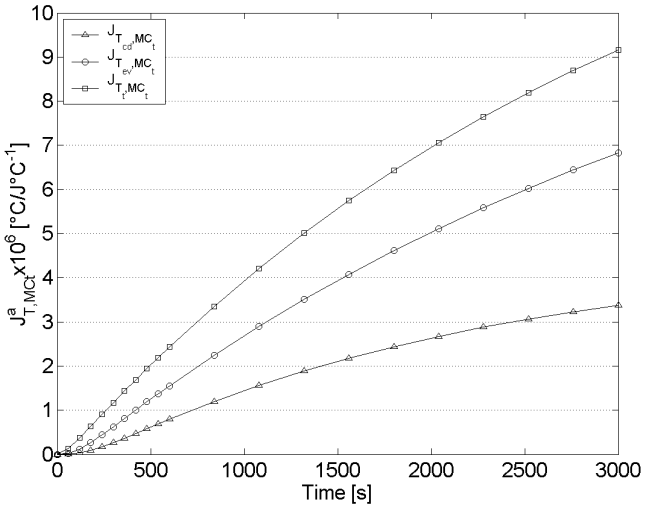

Figure 4.25 Absolute sensitivity of condenser, evaporator and tank temperature with respect to tank thermal mass (MC) in refrigeration unit

Figure 4.23 shows the sensitivity of the equipment temperatures to the thermal mass of the condenser. The sensitivity is maximal at the start up and rapidly decreases to a steady state for both condenser and evaporator temperature. A maximum error of 0.9°C in condenser temperature corresponding to 0.5% prediction error relative to its temperature was observed for a 10% change in thermal mass. The evaporator and tank temperatures were insensitive to the variation of the thermal mass of the condenser.

From Figure 4.24, it can be observed that the evaporator temperature shows larger sensitivity to variations to its thermal mass as might be expected. Here again the maximum sensitivity was limited to the start up with steep decent to steady state for evaporator and condenser temperatures. When a 10% variation in the thermal mass was introduced, a maximum error of 0.6°C in absolute value equivalent to 4.4% deviation was obtained. The condenser and tank temperatures were hardly sensitive with only less than 0.3°C and 0.04°C variation in absolute value, respectively when subjected to this perturbation.

The absolute sensitivity of the equipment temperatures with respect to tank thermal mass is shown in Figure 4.25. Here, unlike the rest, it can be observed that the

sensitivity increases with time implying that the heat load is not yet removed after 3000 s. A significant sensitivity of all the three temperatures was observed. A perturbation of 10% in the nominal value of the thermal mass brings about 1.4°C, 1.1°C, and 0.54°C (for tank, evaporator and condenser, respectively) in absolute value corresponding to 22.5%, 41.6% and 2.1% relative to their temperatures. This shows that the accurate knowledge of the thermal mass of holding tank is essential during the transient state with respect to accurate prediction of the equipment temperatures.

In summary, the condenser temperature has shown significant sensitivity to the thermal mass of the condenser (MC_{cd}), and to the product of overall heat transfer and area of the condenser (UA_{cd}) at start up, when subjected to 10% perturbation in the parameters. Moreover, the thermal mass of the tank (MC_t) has significant influence on the condenser temperature throughout the process. The evaporator temperature was found to be sensitive to thermal mass of the evaporator at start up and to the thermal mass of the tank (MC_t) throughout the process. Significant sensitivity of the tank temperature was observed only to the thermal mass of the tank (MC_t).

In order to identify the parameters most critically affect the accuracy of prediction the relative sensitivities of the condenser and evaporator temperature to the considered parameters are calculated. This is presented in Figure 4.26. It can be observed that for the condenser temperature, its thermal mass is a critical parameter. Indeed this was observed by the relatively high max error on the prediction when subjected to 10% perturbation. Concerning the evaporator temperature, in the beginning (t < 100 s), the parameter MC_{cd} is critical. However, assuming the error expected in the parameter is limited to 10%, it was observed that the maximum error expected on the prediction is insignificant as compared to the accuracy of the measurement instrument. The steady increase in the relative sensitivity of the parameter MC_t, suggests that the thermal mass of the tank is critical in the later stages of the process.

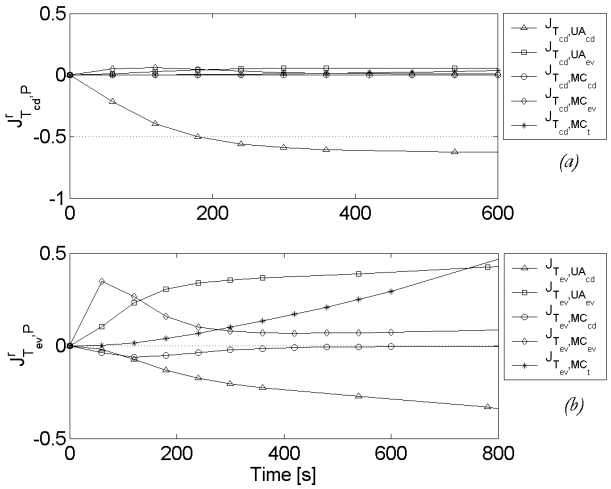

Figure 4.26 Relative sensitivity of (a) the condenser and (b) the evaporator temperatures with respect to the overall heat transfer of the condenser and evaporator and thermal masses of the evaporator, condenser and tank.

4.4.3. Global CA storage model validation

The validation of the global CA storage model, formulated by interconnecting the three sub-models as described in Section 4.4 (Figure 4.4), was carried out using loaded room experiment as described in Section 4.3.4.

4.4.3.1 Validation results

Room air

Figure 4.27 presents a comparison between the volume average of measured temperatures at different positions and the room temperature as measured by the Pt100 situated at the back of the room. The periodic peaks represent the defrosting actions. As can be expected, the volume average of the front side of the stack (Figure 4.9) was lower than that of the immediate backside temperature where the air gains energy from the product. The maximum temperature difference observed during the transient state was 3.5°C. In terms of RMSE value, the spatial variability during the steady state was 1.1°C. The temperature profile as measured by the Pt100 (also used for control purposes) is situated between these two. This is due to the

mixing occurring at a distance from the immediate backside between the air that has interacted with the product and the air that passes through the sides without entering the bins. The tendency of this temperature (T_r,sys) profile to be nearer to the backside volume average temperature profile could be due to the greater proportion of air passing through the bins. The effect of evaporative cooling on the air at the immediate backside is apparent at later stages (t < 1.5 d) where the room temperature, as measured by the Pt100, was observed to be higher.

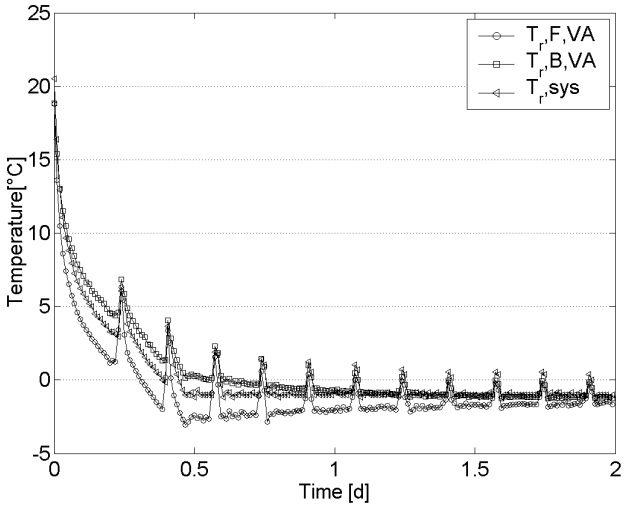

Figure 4.27 Spatial variation in room air temperature in loaded cool cell. (F: front grid; B: back grid; VA: measured volume average; sys: measurement from the system (Pt100))

In Figures 4.28 and 4.29, the measured and simulated room air and pulse temperatures, respectively, are shown. A good fit between the measured volume average temperature and that of the Pt100, for both the room and pulse temperatures was found. For the calculation of the volume average of the pulse temperature, no direct measurement was made (for the regions represented by P in Figure 4.10). Thus, the measurements of the thermocouples positioned immediately above the stack of bins and in front of the cooler were considered to derive a representative temperature (Figure 4.9). In both cases, a good agreement between model predictions and measured values was found, which is reflected in the low RMSE (<0.5°C). Moreover, the defrost operations (periodic peaks) were well represented in the room air as well as the pulse temperatures in both the transient

and steady state situations. It can be said that the model predicts the dynamics of the room air temperature with acceptable accuracy.

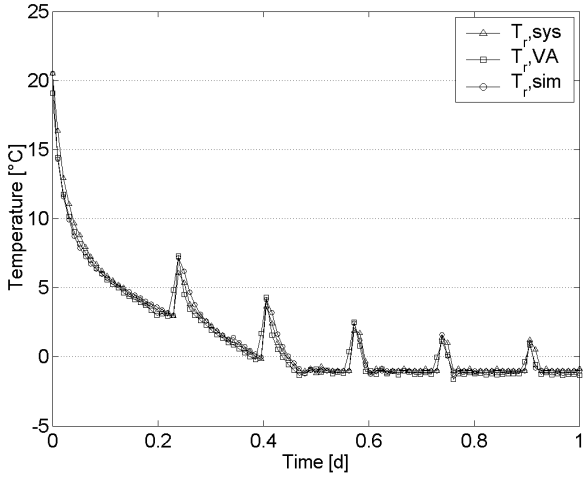

Figure 4.28 Air temperature in loaded cool cell. RMSE($T_{r,VA}$, $T_{r,}$sim) = 0.45°C. (VA: measured volume average; sys: measurement from the system (Pt100); sim: simulation)

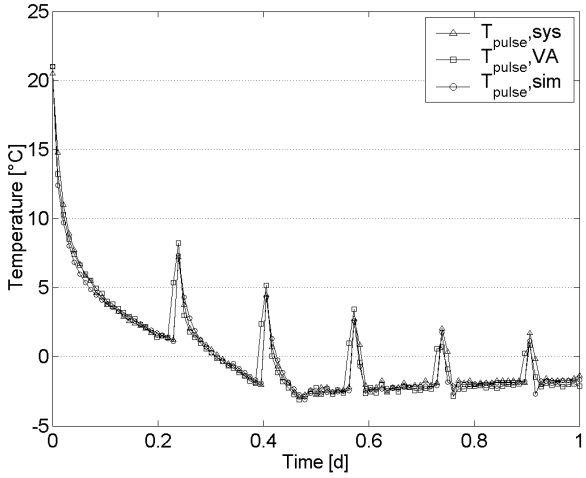

Figure 4.29 Pulse temperature in loaded cool cell. RMSE($T_{pulse,VA}$, $T_{pulse,}$sim) = 0.24°C. (VA: measured volume average; sys: measurement from the system (Pt100); sim: simulation)

Figure 4.30 presents the measured and simulated room air relative humidity. At the beginning, the increase in relative humidity was due to the combined effect of decrease in temperature and moisture release from the product phase to the air. Once removal of moisture has started by the cooler, a decrease in relative humidity was observed. A considerable (>6%) difference in measured relative humidity was observed between the RH meter and the Dew-point meter, positioned supposedly, where the maximum variability in room air relative humidity is expected. It is evident that at the beginning of the cooling process, the measurement from the dew point meter is higher due to drastic decrease in temperature. At steady state, however, both readings are expected to come close to each other where the room air temperature was uniform and a steady moisture removal was attained. Thus, the observed difference especially at steady state, which is slightly higher than the accuracy of the RH meter (5%), could not be attributed to spatial variation in the room. Calibration check done afterwards on the RH meter[3] showed that for RH values less than 80% it overestimates by 4%, and for RH values greater than 92% it underestimates by ±5%. Given the above observations, the variation at the beginning of the cooling process could be attributed to the spatial variation. On the other hand, this places a higher percentage difference between the RH meter and the model prediction, though the observed overestimation by the RH meter was within its limit of accuracy. Yet, the model prediction gives somewhat in between the two extreme relative humidity measurements closing to a steady value similar to both measurements. Considering the RMSE, the values between the model and the individual measurements is slightly higher than the respective measurement accuracy. However, taking the arithmetic average of the measurements the obtained RMSE with respect to model prediction (2.78%) is less than the accuracy as set by the dew point meter (3%). Hence, the model prediction gives acceptable representation of the dynamics of the relative humidity in the room with an accuracy level as set by the measuring instruments. Thus, efforts to improve the model in this regard would result in little or no advantage.

[3] Calibration of all sensors in the system is undertaken by a responsible company at regular interval of time.

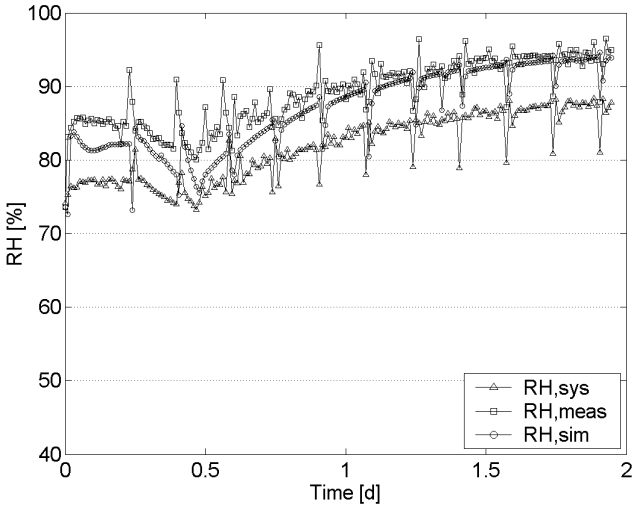

*Figure 4.30 Air relative humidity in loaded cool cell. RMSE(*RH,sim, RH,sys*) = 5.72; RMSE(*RH,sim, RH,meas*) = 3.56. (sys: measurement from the system RH meter; meas: measurement from the dew point meter; sim: simulation)*

Figures 4.31 and 4.32 show the concentration profiles of the respiratory gases inside the cool room. The first 7 days the room was in normal air where the door could be opened when needed. In this period, model predicts a decrease of O_2 concentration. However, since the door model was operational in this interval, as the door opens, fast equilibration of both, O_2 and CO_2 concentrations with the atmosphere was predicted. Once pull down operation starts, a steep decrease in O_2 concentration is evident due to the injection of N_2 into the cool room and to some extent consumption by the produce. In this period, a steady build up of CO_2 is observed. The model assumes a constant interval of time (two hours in this case) for control, during which the respiratory gas concentrations are checked and injection of nitrogen and/or scrubbing of excess CO_2 are performed for a calculated amount of time. However, in reality when there is a queue of rooms waiting to be checked the system could take longer time intervals than two hours. This could cause some discrepancy in model prediction as compared to observed concentrations.

Two simulated curves are shown in Figure 4.32 for CO_2 concentration. In the first case (P_{CO2}, sim_1), due to higher door opening frequency predicted by the model, the CO_2 concentration during the beginning of the ULO operation was much lower than the actual concentration in the room. As a result, after 20 days of simulation the CO_2 concentration is still below the set point, which left the scrubber idle. It is interesting to note here that a decrease in the rate of CO_2 build up after about 8 days was due to the hampered respiration resulting from the low O_2 concentration. In the second case (P_{CO2}, sim_1), the CO_2 produced by respiration was allowed to accumulate up until the beginning of the ULO operation. This was achieved by setting the door opening frequency to zero in order to see the performance of the scrubber model. It can be observed that from the moment the ULO operation starts the scrubber is set into action removing excess CO_2 reducing the concentration to ±0.82% after 13 days.

Considering the biological variability and relatively large time constant of the produce regarding their response, and the crude discrete (every 2-3 h) control of the equipment, it does not make sense to compare the model performance with the measurement accuracy. However, as can be visually inspected, the evolution of the O_2 concentration in the room was well represented by the model with maximum deviation of 1%. The effect of the over prediction of the door openings by the model is pronounced on the evolution of CO_2 due to its low concentration. However, considering this discrepancy, the model predicts the CO_2 concentration in the room satisfactorily. The prediction of the evolution of the respiratory gases being the result of the interaction of several modules, this can be considered as an indirect validation of these modules and especially the gas handling unit model. Simulation results of this unit are shown in Appendix C.

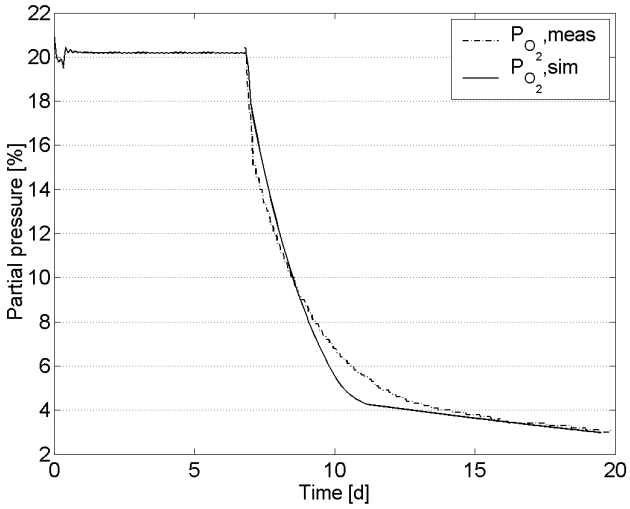

Figure 4.31 O_2 concentration in loaded cool cell (meas: measurement; sim: simulation)

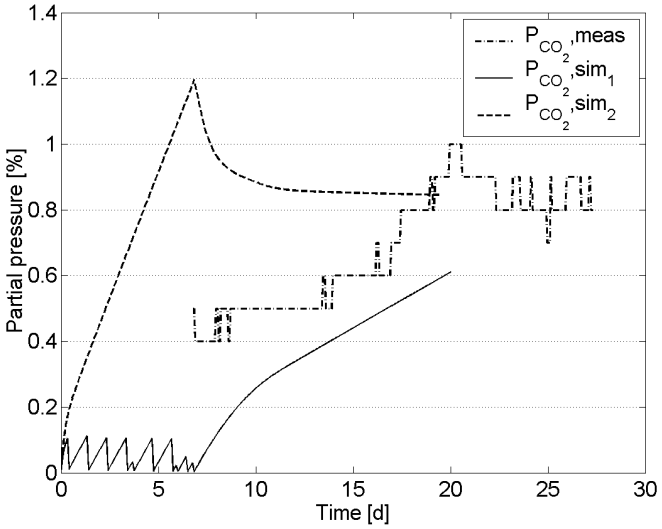

Figure 4.32 CO_2 concentration in loaded cool cell (meas: measurement; sim1: simulation with door model; sim2: simulation without door model)

Cooler and refrigerant

In Figure 4.33 the measured and simulated cooler surface temperatures are depicted. Evidently, since the air disposes much of the energy on the first block, the temperature was higher than that of the second block with a maximum difference of 4°C. Hence, it is logical that the model tends to simulate the temperature of the first block more closely. Due to the lower temperature of the second block, moisture removal from the air could occur earlier than the model can predict. This, on the other hand, influences the accuracy of the room air relative humidity prediction, as was also observed in the empty room analysis. This could, hence, be the possible reason for the above-observed discrepancy in prediction of the relative humidity as compared to the measurement from the RH meter at the beginning. The RMSE between the model prediction and the weighted average is slightly higher as compared to the measurement accuracy. However, considering the maximum RMSE value (1.34°C) of the measurements with respect to the weighted average temperature, the model provides sufficient representation of the cooler surface temperature (RMSE = 0.8°C).

In Figure 4.34 the measured and simulated secondary refrigerant temperatures entering the cooler are shown. This temperature is the result of the recycled refrigerant from the cooler and fresh refrigerant from the refrigeration unit as assorted by the mixing valve controlled by the PI and PID controllers. The fit between model predictions and the measured values was favorable, despite the high RMSE value. This was due to discrepancy of the model at the start and end of the defrosting action. The model assumes a load is immediately applied at the start of defrosting and removed immediately afterwards, which in reality is not true. The temperature of the fresh refrigerant from the refrigeration unit was barely variable due to the limited load on the unit during the experiment. (For this and some simulation results of the refrigeration unit, the reader is referred to Appendix C).

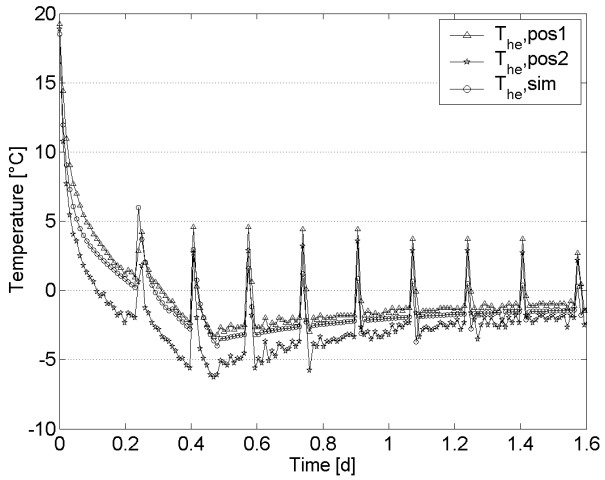

Figure 4.33 Cooler surface temperature in loaded cool cell. RMSE($T_{he,pos1}$, $T_{he,WA}$[4]) = 0.67°C; RMSE($T_{he,pos2}$, $T_{he,WA}$) = 1.34°C; RMSE($T_{he,sim}$, $T_{he,WA}$) = 0.84°C; (pos1: block 1; pos2: block 2; sim: simulation; WA: weighted average)

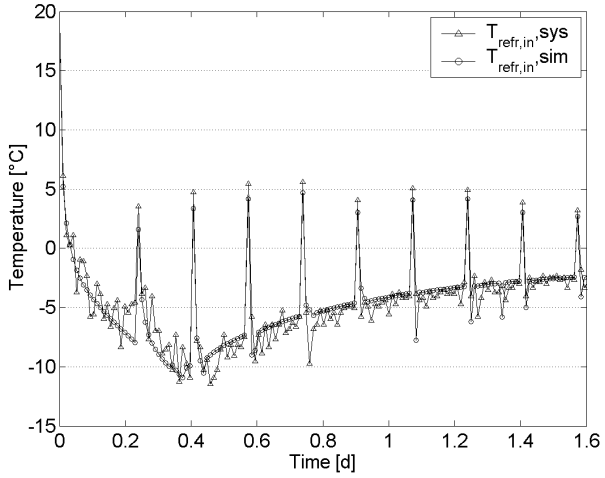

Figure 4.34 Refrigerant temperature entering the cooler. RMSE = 1.18°C. (meas: measurement; sim: simulation)

[4] The $T_{he,WA}$ is the weighted average of the temperatures $T_{he,pos2}$ and $T_{he,pos1}$.

Product

Significant difference in product temperature was observed due to both spatial variation and differences in the design of the bin (Figure 4.35). As the air was blown from the cooler, it bounces down hitting the opposite wall and was forced to pass through the lower bins, which, as a result, cool faster compared to the upper bins. The root mean square difference of the measured product temperatures in the open bins was 1.32°C. Moreover, the construction of the bin has substantial influence on the cooling rate of the product. After three days of cooling, while the open bins have already attained steady state conditions, the product temperature in the closed bin was 5°C higher.

Besides the difference in cooling rate, substantial difference in product initial temperature was also observed caused by the accumulation of the heat of respiration, owing to the limited interaction of the air, hampered by the much larger resistance of the closed bins. In the case where convective heat transfer is limited, high Biot number values are expected, suggesting the significant influence of conduction heat transfer. In such cases, the lumped parameter model is expected to poorly represent the measured values. The RMSE of the model prediction with respect to the average measured product temperature of the open bins was 0.9°C. Thus, the model simulation carried out assuming all bins were open type gives a sufficient representation of the product as compared to the observed variability.

Besides the limitations of the modelling approach, the inaccuracy of the product model parameters could be another reason for the observed discrepancy. For instance, the product heat transfer area estimated based on average fruit diameter could result in overestimation when fruit with bigger diameter were used or vice versa, which has significant influence in the cooling rate of the products. Another observation was that in reality, the product was actually interacting with the pulse air conditions rather than the room air conditions. This means that a plug-flow type model, which considers the pulse conditions as feed air conditions, could improve the model in this case. However, in the case where the room is completely filled with product, the plug-flow model may not yield better results. In such cases, a model with a couple of zones might give a better prediction of the product temperature and accounting, to some extent, the variability in the room air temperature.

The measured product moisture loss in the different bins ranges from 1.8-1.96% in the open boxes and 0.4% in the closed box with an overall moisture loss of 1.72 %

after a storage period of 38 days. The prediction by the model depicted in Figure 4.36 shows a moisture loss of 1.3 % after this period. The under prediction of the product moisture loss could be attributed to the limited accuracy of the product heat and mass transfer model. This means that, due to the existing evaporative cooling at the product surface, the air temperature at the interface was, in reality, colder than the bulk air resulting in lower vapour pressure at the surface of the product. This vapour pressure was then compensated by excessive moisture loss from the product. This phenomenon was not captured by the model which assumes the air temperature near the surface to be that of the room air or at best the average between the product and air temperatures (Note that the product temperature as predicted by the model was the centre temperature which was still higher than the surface product temperature). The above reasoning only holds when there is available free moisture at the product surface (or lower skin resistance to moisture transfer), which is the case with pears.

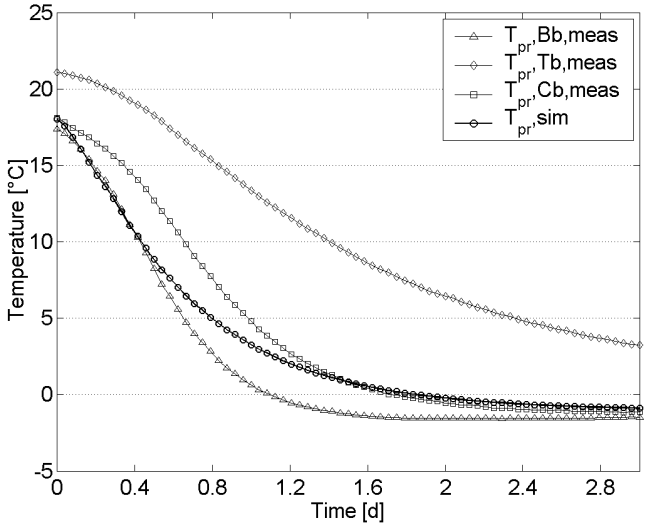

Figure 4.35 Product temperature. RMSE($T_{pr,AV}$, $T_{pr,sim}$ *) = 0.9°C (Bb: bottom bins; Tb: top bins; Cb: closed bin; meas: measurement; sim: simulation, AV: average of product temperature measurements of the open type bins)*

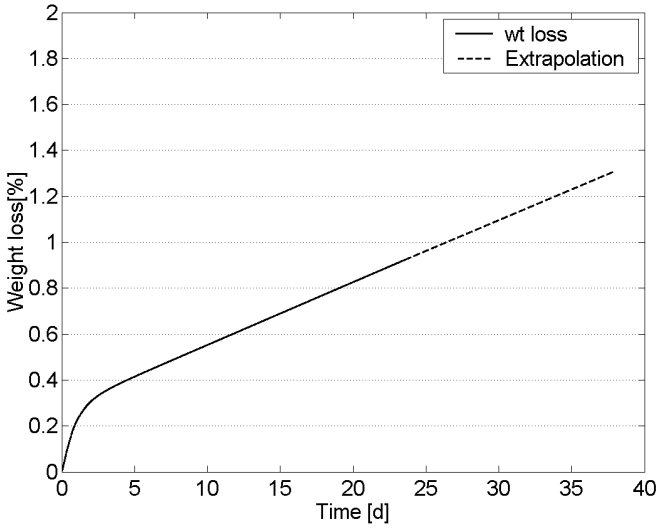

Figure 4.36 Simulated accumulated product weight loss

The product respiration heat generation as estimated from the rate of CO_2 production by the model and some literature sources is shown in Figure 4.37. The model seems to under estimate the CO_2 production rate and thus, the respiration heat generation, at the intermediate temperatures. This could be attributed to the biological variability reflected by the large confidence interval in the kinetic and equilibrium parameters in the respiration model (refer Chapter 2). On the other hand, during cooling period, reduced O_2 concentration and some build up of CO_2 were predicted. One can, hence, speculate that the possible reason for the observed under prediction of the CO_2 production as compared to the literature data could be this. In general, given the biological variability of fruit, the trend displayed by model prediction is representative of the respiration heat generation.

Since the performed experiments using Conference pear fruit for the validation of the global model (Section 4.3.4) was only for one month, it was not possible to get valuable data on the firmness of the fruit to evaluate the performance of the quality (firmness) model.

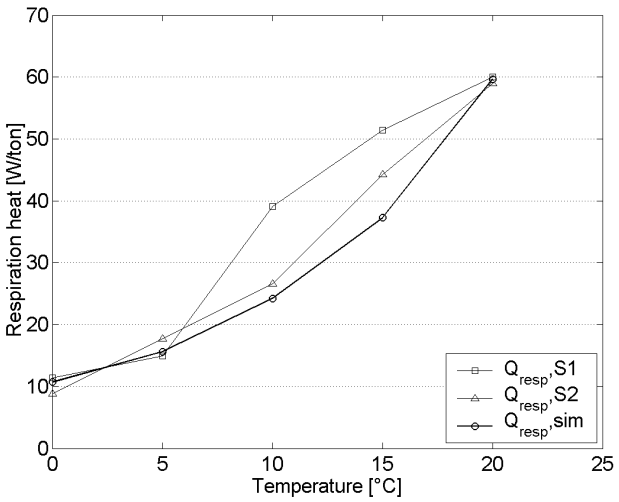

Figure 4.37 Respiration heat of apple as calculated from CO_2 production rate (S1: Sprenger Institute (1980); S2: USDA Handbook 66 (www 3, 2003); sim: simulation).

4.4.3.2 Sensitivity analysis

Sensitivity analysis of the global model was carried out considering some parameters of interest that could influence the heat and mass transfer significantly. The parameters chosen for the sensitivity analysis were model parameters (heat transfer coefficient around the cooler, h_{be} and around the product h_{pr}), the product heat transfer area A_{pr}, which is related to the characteristic dimensions of the fruit and the product initial temperature $T_{pr,i}$. This choice was based on the observation of their influence on model prediction quality during model tuning. The parameters considered and their nominal values are given in Table 4.4. The influence of these parameters on room air temperature, T_r, cooler temperature, T_{be}, product temperature T_{pr}, room air relative humidity RH_r and the moisture loss of the product *WtLoss* were studied. The significance of the sensitivity of a given variable with respect to a parameter was evaluated based on the measurement accuracy of that variable. The simulation of the global model was performed by deactivating modules such as the door and the defrost model. This was because of the fact that the abrupt change in the predicted variables brought about by these modules results in high sensitivity of the parameters instantaneously, obscuring the sensitivity of the parameters during continuous operation. In order to look at the sensitivity of the

parameters during transient and steady state conditions, the simulation was allowed to run until steady state was reached.

Table 4.4 Nominal values used for sensitivity analysis

h_{he} [W m^{-2} °C^{-1}]	h_{pr} [W m^{-2} °C^{-1}]	A_{pr}, [m^2]	$T_{pr,i}$ [°C]
21	0.965	170	18

Cooler heat transfer coefficient

Responses of the room air and cooler temperature to 10% perturbation and their sensitivity in relation to the cooler heat transfer coefficient are shown in Figure 4.38. It is apparent that the lower heat transfer rate was compensated by a larger temperature difference (between T_{he} and T_r) to bring about the required cooling of the room air, leading to a lower cooler temperature. This is depicted by the negative sensitivity of the cooler temperature at the beginning (due to faster cooling) and a positive one before it finally approaches to a zero value. Higher sensitivity was obtained during the cooling (transient) phase as compared to the steady state. This can also be seen in the absolute sensitivity curves that, after reaching a minimum, there is a drastic increase to the zero value as the temperature proceeds to the steady state. During the cooling phase, the room air temperature is apparently more sensitive than the cooler temperature. An error of 20% in cooler heat transfer coefficient, which is common to parameters estimated using empirical correlations, a maximum of 1.5°C and 0.63°C prediction error is anticipated for room air and cooler temperatures, respectively.

In Figure 4.39, the change in the room air relative humidity and its sensitivity with respect to cooler heat transfer coefficient is shown. The absolute sensitivity curve (Figure 4.39(b)) shows some fluctuations during the transient state. This is due to the fact that the condensation/no condensation events on the surface of the cooler at $p_j+\Delta p_j$ occur at different moments than at $p_j-\Delta p_j$. This creates differently behaving RH profiles (Figure 4.39(a)) during the transient state and as a result, the absolute sensitivity curve is bound to have the observed fluctuations. A maximum difference of 3% in relative humidity is observed to a perturbation of 10% in the parameter. The absolute sensitivity curve shows that a maximum of 4.4% prediction discrepancy can be obtained for an error of 20% in the cooler heat transfer coefficient. Since the accuracy of most RH meters is limited to 5%, this discrepancy

can still be considered as marginally significant. The observed positive sensitivity of the room air relative humidity implies that the temperature effect is more pronounced in comparison to the possible moisture removal by the cooler due to faster cooling.

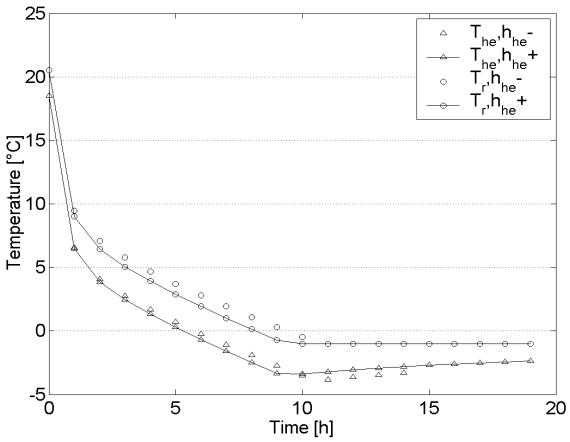

(a)

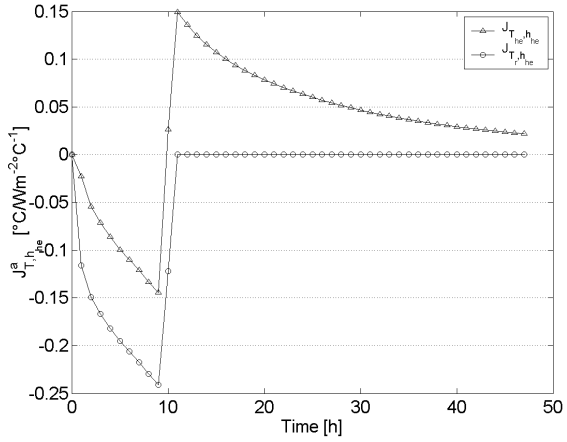

(b)

Figure 4.38 (a) Room air and cooler temperatures response to 10% perturbation and (b) their absolute sensitivity with respect to the cooler heat transfer coefficient

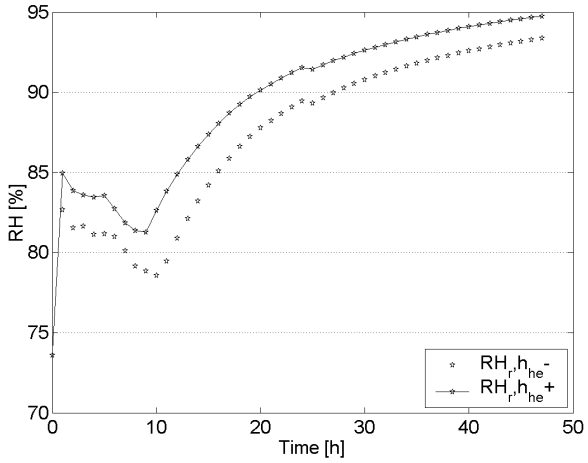

(a)

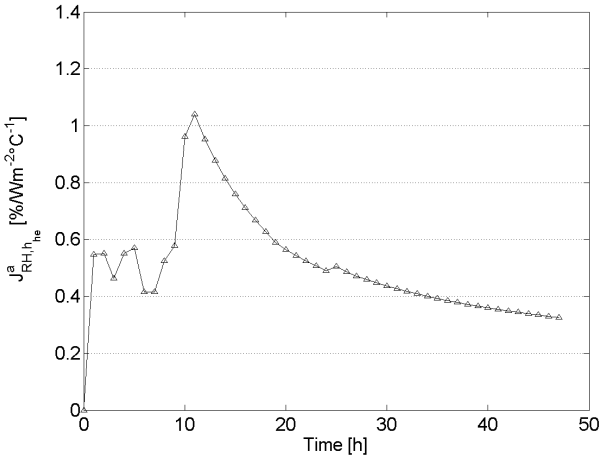

(b)

Figure 4.39 (a) Room air relative humidity response to 10% perturbation and (b) its absolute sensitivity with respect to the cooler heat transfer coefficient

Product heat transfer coefficient

The effect of a 10% perturbation of the product heat transfer coefficient on the room air, cooler and product temperature responses and their sensitivities are shown in Figure 4.40. For room air and cooler temperature, the effect was pronounced during the transient state. For the product temperature, it is observed that the effect starts after a lag phase, which corresponds to the cooling phase of the room air and the cooler. This can also be seen in the absolute sensitivity of the product temperature that after a gradual increase in sensitivity during the cooling phase an abrupt increase is observed to a maximum value and gradual decrease back to the time axis. When a high value of product heat transfer coefficient was employed, since faster removal of sensible heat and heat of respiration of the product was achieved, a larger load on the room air and ultimately to the cooler was imposed, leading to slower cooling rate of the variables. The absolute sensitivity curves show that the room air and cooler temperatures have similar sensitivities to changes in the product heat transfer coefficient. This is evident due to the fact that the same load picked from the product by the medium was disposed on the cooler. When an error of 20% is involved in the product heat transfer coefficient, a maximum of 1.7°C over prediction in room air and cooler temperature and 1°C under prediction in product temperature is expected.

Figure 4.41 presents the response and sensitivity of the room air relative humidity with respect to change in product heat transfer coefficient, respectively. No significant change in response is observed due to the imposed change in product heat transfer coefficient. The early decline in room air relative humidity when low value was used could be attributed to the early removal of moisture by the cooler due to faster cooling. From the absolute sensitivity, it is apparent that a maximum under prediction of 2.3% corresponds to 20% error in the product heat transfer coefficient. This value is smaller than the attached accuracy of 5% of most RH measurement sensors. Thus, the room air relative humidity can be considered insensitive to changes in product heat transfer coefficient.

The accumulated product weight loss profile in response to change in product heat transfer coefficient and its absolute sensitivity are shown in Figure 4.42. The effect of the change of the product heat transfer coefficient is apparent only during the product cooling phase. This is evident from the sensitivity curve where a decrease, after attaining a maximum value corresponding to a max of 0.02% over prediction for an error of 20% in product heat transfer coefficient, is observed after 20 hours

of cooling. The steep descent of the sensitivity to seemingly zero value means that the accumulated product weight loss in the end is the same in both cases.

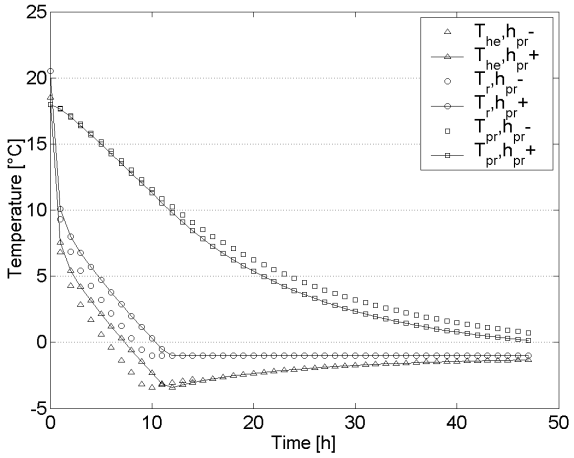

(a)

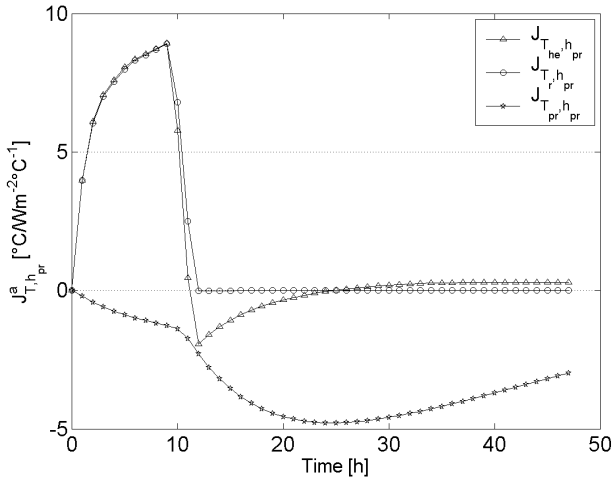

(b)

Figure 4.40 (a) Room air, cooler and product temperatures response to 10% perturbation and (b) their absolute sensitivity with respect to the product heat transfer coefficient

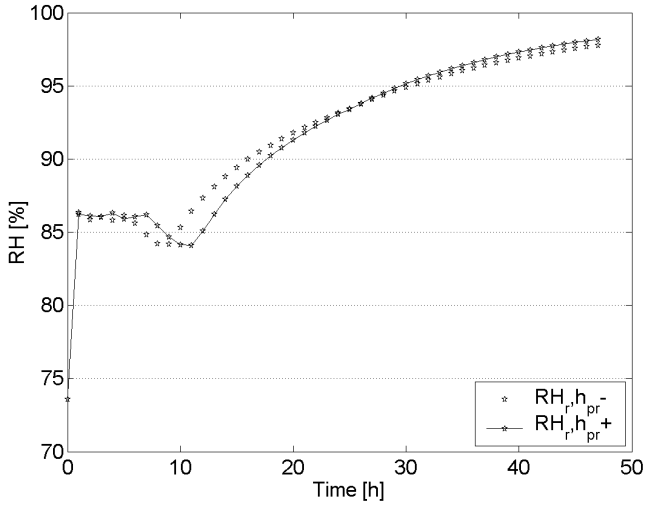

(a)

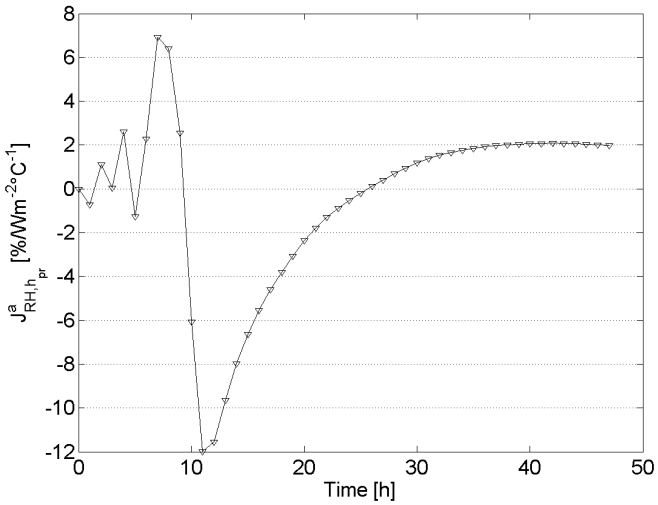

(b)

Figure 4.41 (a) Room air relative humidity response to 10% perturbation and (b) its absolute sensitivity with respect to the product heat transfer coefficient

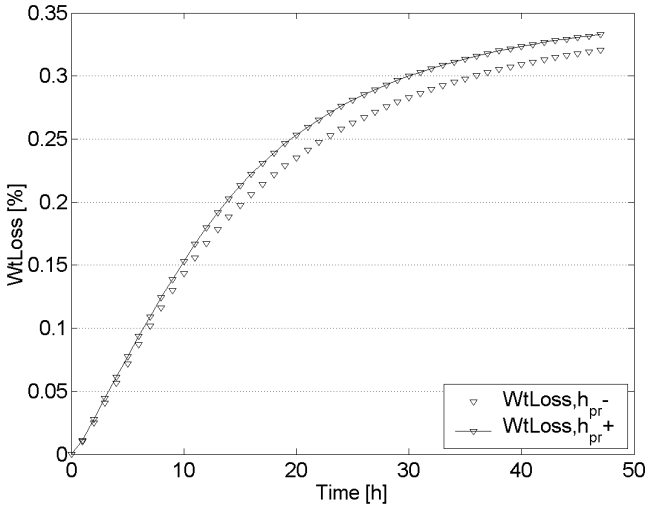

(a)

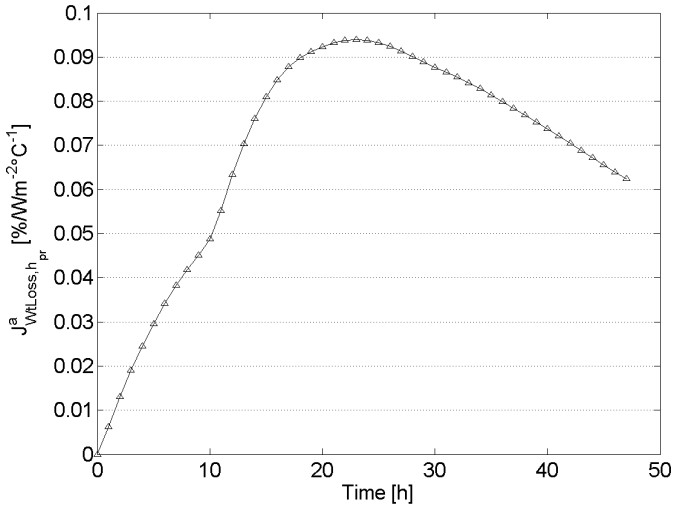

(b)

Figure 4.42 (a) Accumulated product weight loss response to 10% perturbation and (b) its absolute sensitivity with respect to the product heat transfer coefficient

Product heat transfer area

Figures 4.43 - 4.45 show the responses of the room air, cooler, product temperatures, room air relative humidity, and accumulated product weight loss and their respective sensitivities with respect to change in the product heat transfer area. Apparently, similar curves to those of the product heat transfer coefficient were obtained, as one may expect. It is to be recalled that the product heat transfer area was estimated using the specific surface area of the product calculated based on the average characteristic dimensions of the fruit (Eq. (4.17)). Owing to the biological variability, a large standard deviation on the mean values of these parameters is inherent. Consequently, the propagated error to the calculated heat transfer area was estimated to be as high as 40%. This implies that due to the high degree of uncertainty involved, even small sensitivity could influence the model prediction significantly. It should be emphasized here that practically, this high error in the estimation could occur on a particular harvest year or from a particular orchard where the fruit are in general smaller than the average fruit size. With such error on the heat transfer area, which is equivalent to 70 m^2 a maximum over prediction of 4.4°C in room, air and cooler temperature and 2.4°C under prediction in product temperature could be expected (Figure 4.45). This rather high sensitivity is limited in the transient state for cooler and room air temperature but still significant sensitivity exists after two days of cooling for the product temperature.

The room air relative humidity also shows a significant sensitivity for such a substantial error with a maximum under prediction of 7% (Figure 4.44). A steady error of around 1% seems to exist after 48 hours of cooling. As observed previously, the fluctuations on the absolute sensitivity curve (Figure 4.44(b)) during the transient state is due to the influence of the moisture transfer from the product as a result the introduced perturbation. This again creates differently behaving RH profiles (Figure 4.44(a)) owing to occurrence of the condensation/no condensation events on the surface of the cooler at different moments. For the accumulated product weight loss despite the large error on the heat transfer area only an over prediction of 0.05% is expected (Figure 4.45). As observed in the case of heat transfer coefficient, a steep descent in sensitivity implies that the two curves meet at the end.

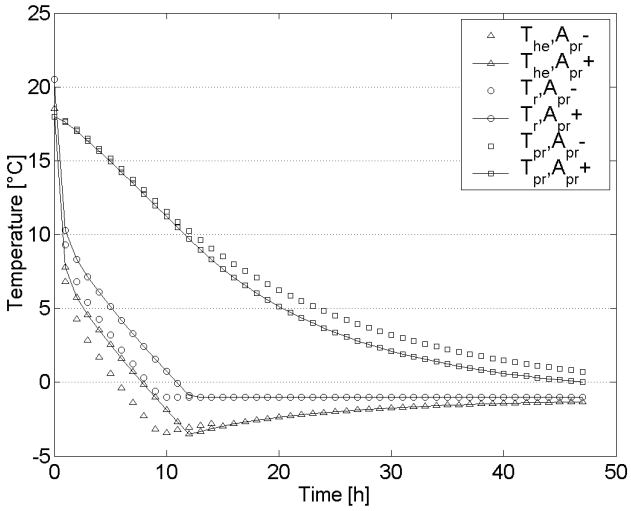

(a)

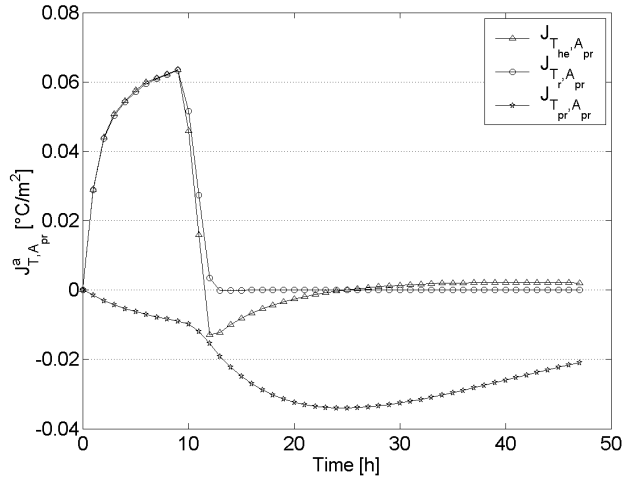

(b)

Figure 4.43 (a) Room air, cooler and product temperatures response to 10% perturbation and (b) their sensitivity with respect to the product heat transfer area

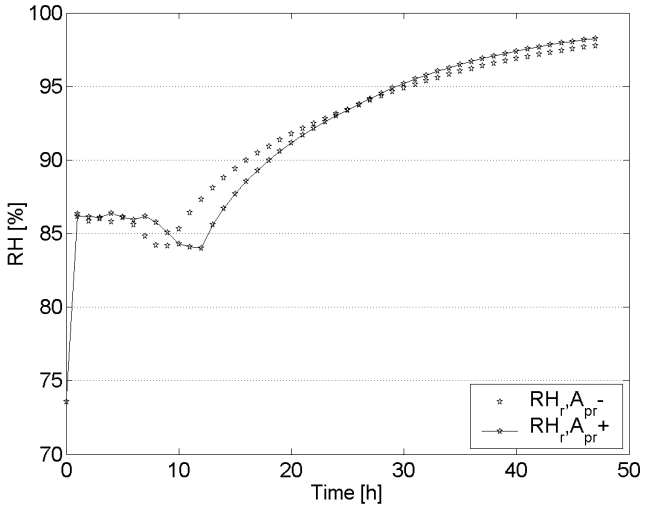

(a)

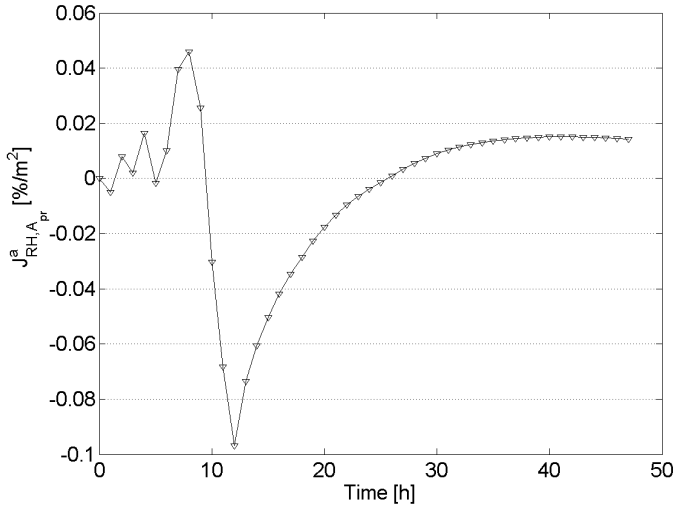

(b)

Figure 4.44 (a) Room air relative humidity response to 10% perturbation and (b) its sensitivity with respect to the product heat transfer area

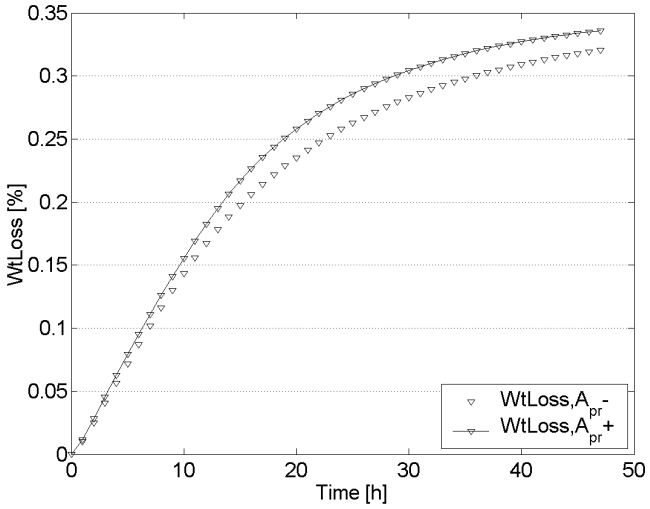

(a)

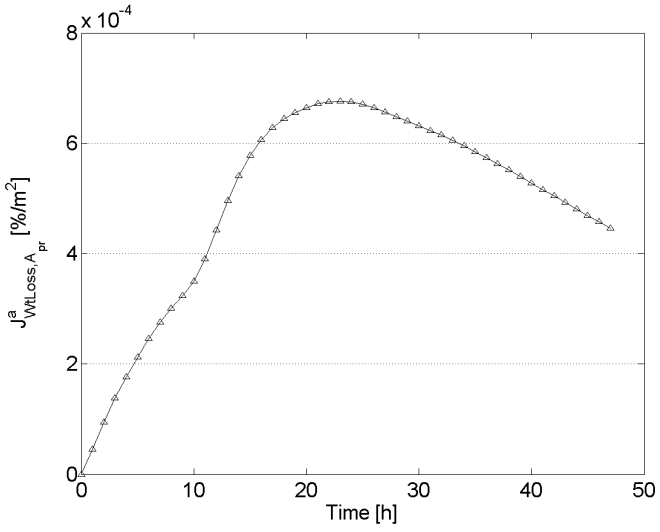

(b)

Figure 4.45 (a) Accumulated product weight loss response to 10% perturbation and (b) its absolute sensitivity with respect to the product heat transfer area

Product initial temperature

In Figure 4.46, the responses of the room air and cooler temperature at low (16.2°C) and high (19.8°C) initial product temperature are depicted. The transient state of both temperatures was affected substantially. In the case where a high initial product temperature was used the room air temperature needs four more hours to reach steady state as compared to low initial product temperature. The sensitivity suggests that both the cooler temperature and the room air temperature have similar sensitivity with a maximum value of 0.8°C $°C^{-1}$. Considering products loaded to a cool room 3°C higher, then a maximum of 2.4°C difference in the room air temperature is expected. Moreover, as maintaining uniform initial product temperature may not be evident, model predictions based on local product initial temperature measurement may show significant deviation from observed data. On the other hand, from a practical point of view, this means that an additional energy is disposed at the cooler at a rate of 6.4 kJ s^{-1} (considering only sensible heat removal) during the transient state, assuming 2 m^3 s^{-1} air flow rate through the cooler. Such rate of energy removal can impose a substantial load on the refrigeration unit. In an industrial application, pre-cooling of product as it arrives from the field is practiced or batch wise loading strategy is pursued to achieve fast cooling besides avoiding overloading of the refrigeration unit.

The initial product temperature has also a significant effect on the room air relative humidity during the transient state (Figure 4.47). It can be seen that moisture removal starts at the same moment but lasts longer for higher product initial temperature. During most of the transient state higher relative humidity is predicted for low product initial temperature, which, from practical point of view, affects the product moisture loss positively. Again, for 3°C difference in initial product temperature a maximum of 4.5% error in the prediction can be obtained, which is marginally significant.

In Figure 4.48, the product accumulated weight loss response and absolute sensitivity in relation to the different product initial temperatures is shown. The product weight loss response shows around 0.1% difference after only two days of cooling. The sensitivity shows that products introduced at 3°C lower, 0.07% gain in moisture loss can be achieved. It can be stated, hence, that the initial product temperature has a substantial impact on the performance of the refrigeration unit as well as on the quality of the stored product in relation to moisture loss.

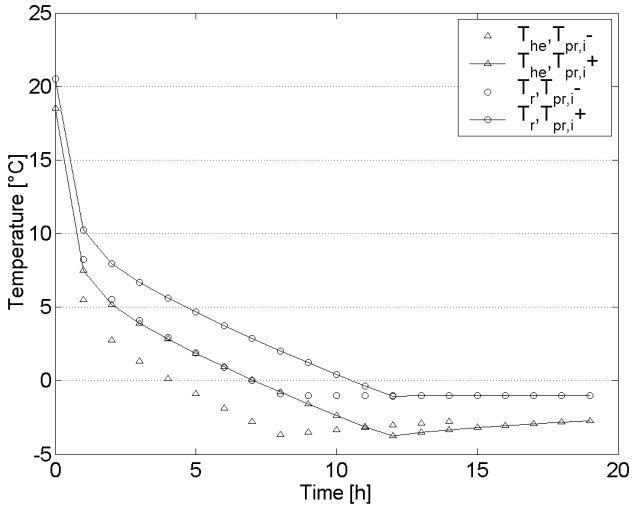

(a)

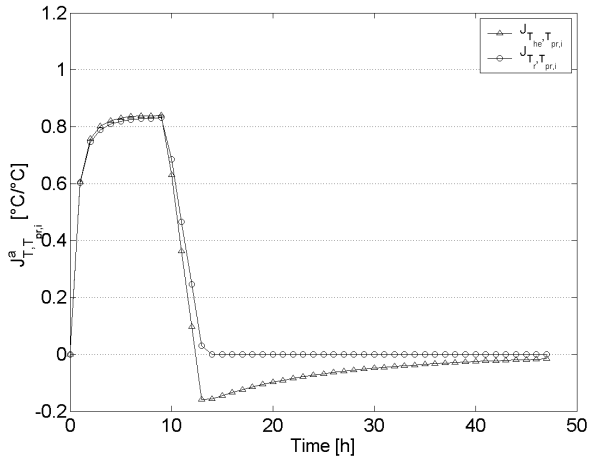

(b)

Figure 4.46 (a) Room air and cooler temperature responses and (b) their absolute sensitivity with respect to different product initial temperature ($\Delta T_{pr,i}$ = 3.6°C)

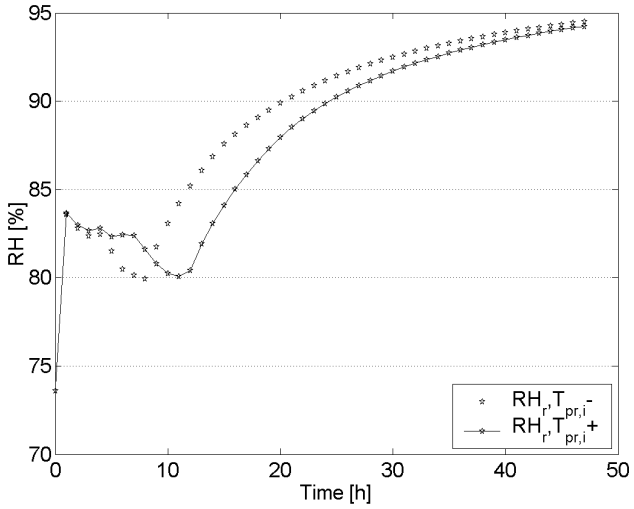

(a)

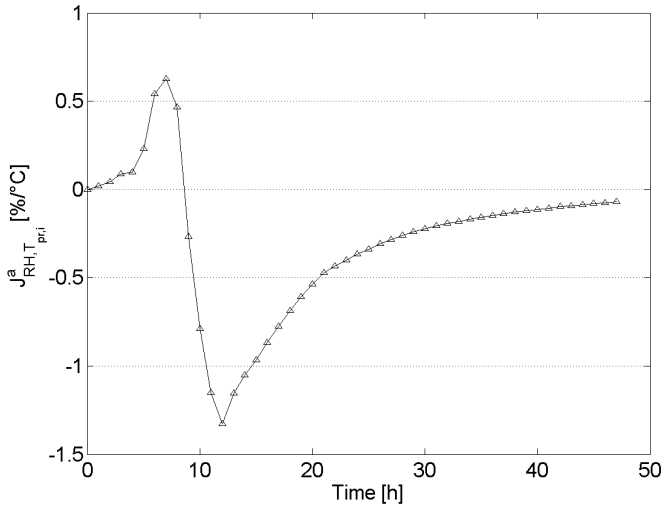

(b)

Figure 4.47 (a) Room air relative humidity response and (b) its absolute sensitivity with respect to different product initial temperature ($\Delta T_{pr,i}$ = 3.6°C)

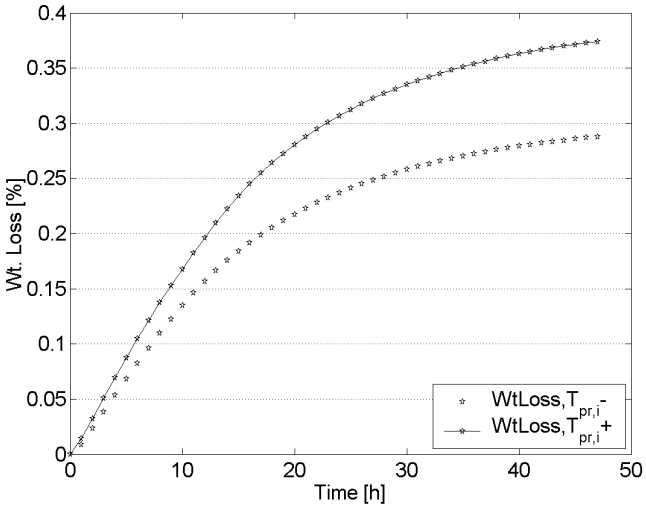

(a)

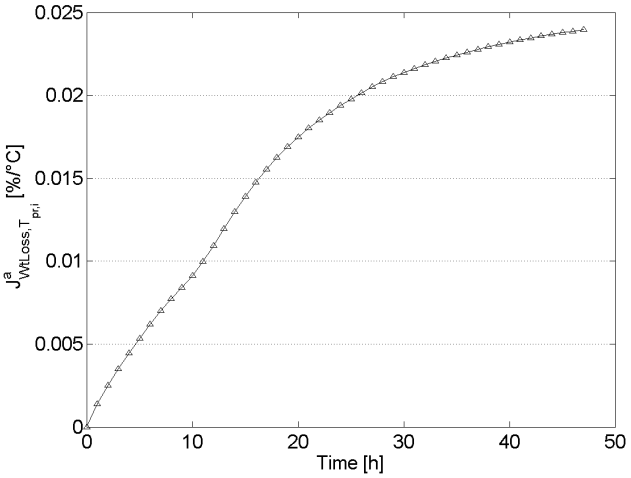

(b)

Figure 4.48 (a) Accumulated product weight loss product response and (b) its absolute sensitivity with respect to the initial product temperature ($\Delta T_{pr,I}$=3.6°C)

In summary, the room air and cooler temperatures were found to be sensitive to all the considered parameters and both have shown similar sensitivity. It was observed that the sensitivity was significant only during the transient state. Moreover, the product temperature was sensitive to its heat transfer coefficient and area. The room air relative humidity has shown marginal sensitivity to the cooler heat transfer coefficient and product initial temperature. Owing to the limitation of the relative sensitivity, very large values were obtained at temperatures near zero. The relative sensitivities of the room air relative humidity and the accumulated product weight loss are shown in Figure 4.49. During the transient state, the initial product temperature and the cooler heat transfer coefficient were more critical for the room air relative humidity (Figure 4.49(a)). The most critical parameter for the accumulated product weight loss was the initial product temperature (Figure 4.49(b)).

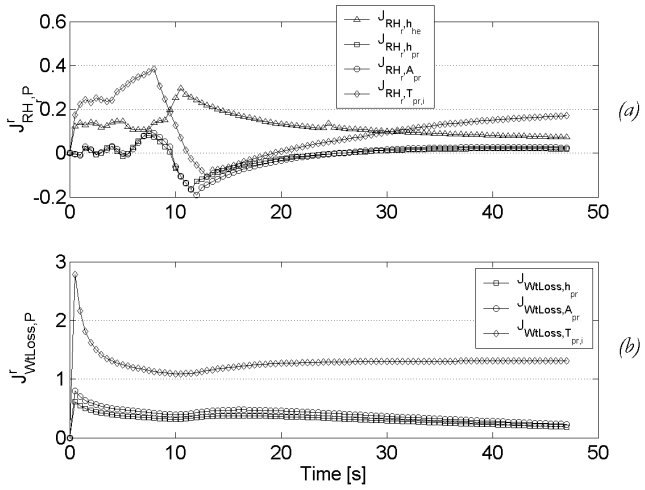

Figure 4.49 Relative sensitivity of (a) the room air relative humidity and (b) the accumulated product weight loss.

4.5. Discussion

An attempt was made to assess different aspects of the global CA cool storage model. The validation of such models using experimental data is often limited to some key model variables of some of the modules. This can be justified by the fact

that, besides the limitation to obtain experimental data for all the model variables, there are also space and time restrictions in obtaining and presenting the results. However, in systems where coupled processes exist, considering only one of the phenomena during validation would limit the confidence one can put on the overall prediction capabilities of the model.

Assessment of the cool room model using empty room experiments resulted in tuning of parameters related to heat transfer coefficients, especially related to the surfaces. The consideration of a single zone can be justified in the case of empty room where observed room air temperature variation was relatively small. The observed trend of the different component models suggests that the model can further be employed as an integral part of the CA cool storage model.

In the refrigeration unit model, the start up conditions were poorly represented. Similar results were reported by Darrow et al. (1991) using an experimental refrigeration unit. The higher sensitivity of the evaporator and condenser temperature to their respective thermal masses at start up suggests that accurate knowledge of the parameters is important during this phase. This braces the argument that the consideration of constant thermal mass of the equipment contributed to the observed discrepancy during start up. Nevertheless, in view of the large difference in time constants between the processes (cooling of the produce) in the cool room and the start up of the refrigeration unit, the observed discrepancy was insignificant. Lopez and Lacarra (1999) confirmed the adequacy of the model after applying it in industrial settings. Thus, the use of more elaborate models, which consider more phases or hydrodynamic effects, may not result in significant advantage with respect to the improvement of the accuracy of the model. One should note that in the situation considered the transient behaviour of the system was controlled by the load coming from the water tank. This was confirmed by the significant sensitivity of the evaporator and condenser temperatures to the change in thermal mass of the water tank. However, when the main source of load variation comes from within the refrigeration circuit the adequacy of the considered model may not hold.

As was observed, the main source of load variation in CA cool room before and most importantly after ULO conditions were set was the defrosting action. The accurate representation of this discrete process by the model contributes to the accurate prediction of the load imposed on the cooler and in turn, on the refrigeration unit. The representation of the cooler temperature by the model can be

considered adequate. However, the limitation of lumping the cooler was reflected on the discrepancy of prediction of the room air relative humidity. Given the arrangement of the cooler, modelling the two blocks as a series of coolers could improve the relative humidity prediction. This results in two separate temperature predictions for the two coolers. Nevertheless, the number of the ODE and DAE's used would be twice as many, increasing the model complexity to some extent.

Inconsistency in predictions related to the product, especially in the heat and mass transfer processes (product temperature and moisture loss) was observed. This can be attributed to the inadequacy of the model to describe the interaction between the room air and the stored biological material and the accuracy of the involved model parameters. The focus of attention in the whole Controlled Atmosphere cooling process being the product, requires some more discussion with respect to the adequacy of the proposed model.

Depending on the physiological nature of the produce, different responses to change in microenvironment could be obtained. Let's consider the following observations. For fruit with available free moisture content at the surface and/or less skin resistance (such as pears and chicory), product under cooling takes place during cooling leaving the air temperature surrounding the product lower than the bulk air. This results in lower vapour pressure of air surrounding the product, which in turn results in more removal of moisture from the product to compensate for the vapour pressure deficit. Consequently, there exists larger temperature gradient in the product temperature and excessive loss of moisture. On the other hand, for fruit with limited free moisture at the surface (such as apples and peaches) the vapour pressure deficit created by the product under cooling couldn't be sustained by the limited free water. It is, hence, compensated from the bulk air resulting in condensation on the skin of the fruit. Consequently, the heat of condensation released on the product raises the product surface temperature. It should be remembered here that in such instances further complication is introduced through the involvement of the fruit skin resistance where moisture tends to be transferred from the fruit flesh.

In her 1-D, two-phase CFD model, which considers the hydrodynamic effects, Hoang (2003), reported up to 2°C and 0.3% (after 2.5 h of cooling) under prediction in product temperature and moisture loss, respectively, during cooling of chicory and was attributed to the poor representation of the former phenomenon by the model. Moreover, Amos (1995) considered a multi-zone (150 zones) to model

cooling of apples in a carton (0.05 m^3) which considers both conduction and convection heat transfer modes. More often than not, the product temperature predictions were in good agreement with the measured data with maximum discrepancy of 2.5°C at times. Nevertheless, as big as 7.5°C differences in air temperature inside the box between measured and predicted values were observed, which was attributed mainly to the inaccuracy of the involved model parameters rather than model inadequacy. Moreover, the adequacy of the model in predicting, neither the air humidity nor product moisture loss, was reported. The model was reported to be too complex to be included in the full cool store simulation model.

The foregoing discussion suggests that the intricate phenomena taking place at the interface and inside the product cannot be captured by models that lump the product as one entity. Hoang, (2003) suggests that this phenomenon could adequately be represented by a 3D, 2-phase CFD model. This is further complicated by the accuracy in the involved model parameters related to the product. Sensitivity analysis showed that, owing to biological variability, the inherent high uncertainty in the model parameters invokes significant prediction inconsistency. Hence, though the distributed models, complex as they are, account for the spatial variability in the packaging (bin or carton), the improvement on the prediction accuracy, as stipulated by the current modelling objective, is not appreciated as compared to the simplistic lumped model. Wrapping up, the presented product model could be accepted as a working model in the simulation of CA cool storage facilities.

Another aspect of the product model was the prediction of the respiration rate and product quality during the storage period, which in turn affect the evolution of the respiratory gases in the cool room. The fact that these predictions yielded favourable agreement with the measured data and those acquired from literature, gives an indication that the respiration model and the interaction of the room air with the gas handling unit were well represented by the respective models, though no direct validation was provided for the latter. As far as our knowledge is concerned, no published work is available for comparison, which describes the performance of the gas-handling unit in relation to CA cool rooms.

Sensitivity analysis showed that room air, cooler and product temperatures were sensitive to heat transfer coefficients around the cooler and product during the transient state. This was established by considering the attached estimation accuracy of heat transfer coefficients when using empirical relationships. Due to biological variability, high uncertainty was attached to the heat transfer area. As a result, a

relatively large discrepancy could be expected in temperature as well as relative humidity, even when the sensitivity is low. The product initial temperature was found to present significant practical implications in relation to the cooling rate, moisture loss as well as imposed load on the refrigeration unit.

4.6. Conclusion

The validation of the global CA cool storage model described in Chapter 3 was presented in this Chapter. First, the sub-models were assessed individually to justify the considered assumptions and approximations in the formulation of the component models. The cool room model was appraised using empty room experiments, which resulted in modification of some model parameters especially related to the surfaces. In comparison to the experimental results, the trends displayed by the model were found to be satisfactorily in agreement with the measurements. Next, the refrigeration unit model was validated using an experimental set up tailored to imitate the situation of the cool storage system. Despite the observed inadequacy during the start up, the dynamic behaviour of the system was represented by the model with acceptable accuracy. Sensitivity analysis of model parameters revealed that the condenser and evaporator temperature were significantly sensitive to the thermal mass of the water tank, owing to the dominance of the transient behaviour of the system by the water tank. Moreover, the condenser temperature was sensitive to the overall heat transfer coefficients of the evaporator and condenser. In general, the proposed simple model gives acceptable accuracy, and thus is considered adequate for CA simulation.

Subsequently, a comprehensive direct and indirect validation of the global Controlled Atmosphere cool storage model, formulated by considering the sub-models and their interactions, was presented. More often than not, the most important discrete and continuous process events were represented with acceptable accuracy when compared to experimental data (i.e., with an accuracy level less than the observed variability of the different variables or at best with the accuracy level as set by the measurement instruments). Sensitivity analysis showed that the transient cooling phase was influenced by the accuracy of the heat transfer coefficients. Due to intrinsic biological variability, a greater uncertainty in the product heat transfer area was evidently contributing to larger discrepancy between model prediction and observed data. Moreover, the initial product temperature influenced the product cooling rate and moisture loss substantially with practical implication on cooling strategy. The change in accumulated moisture loss of the product by 0.07 % in two

days with 3 °C initial product temperature difference suggests that fast cooling of the product is advantageous in reducing the respiration and transpiration of the product. Fast cooling is often accomplished by forced ventilation, which increases the heat and mass transfer rate around the product. The change in accumulated moisture loss by 0.02 % for a change in product heat transfer coefficient by 10% on the other hand, implies the negative influence of the fast cooling. Therefore, in order to reap the full advantage of fast cooling, the use of cooling medium with very high (near saturation) relative humidity is mandatory. In general, as observed from the different validation results, the adequacy of the proposed model can be justified by its ability to represent the experimental data in most of the cases with acceptable accuracy.

Often product quality and product respiration are not considered in such simulation models and thus plant performance was only carried out in relation to the predetermined optimal storage conditions believed to bring about the best quality of the product at the end of the storage period. Thus, the advantage of the present simulation model is that optimisation of plant performance with respect to the final quality of the stored product could be carried out. To illustrate this, a model for fruit firmness, which is closely linked to the product respiration model, was employed. Moreover, prediction of the interaction between the cool room and the gas-handling unit enables to quantify the load imposed on the unit. The simulation model can thus be employed for sizing the gas handling unit and design of robust control strategy. Owing to the hierarchical and object oriented approach, more flexibility in introducing new models and reuse of existing modules was achieved. In general, the proposed combined discrete and continuous CA cool storage simulation model could be considered as a valid working model for design and optimisation of CA cool storage facilities.

References

Anonymous. ASHRAE Fundamentals. (1993). American Society of Heating, Refrigerating and Air-Conditioning Engineers, Inc., Atlanta, USA.

Anonymous. ASHRAE Fundamentals. (1997). American Society of Heating, Refrigerating and Air-Conditioning Engineers, Inc., Atlanta, USA.

Amos, N.D. (1995). Mathematical modelling of heat and mass transfer and water vapour transport in apple cool stores. *Ph.D. Thesis*, Massey University, Palmerston North, New Zealand.

Cleland, A.C. (1983). Simulation of industrial refrigeration plants under variable load conditions. *International Journal of Refrigeration,* 6, 11-9.

Cleland, A.C. (1985). Experimental verification of a mathematical model for simulation of industrial refrigeration plants. *International Journal of Refrigeration*, 8, 275-282.

Cleland, A.C. (1986). Computer subroutines for rapid evaluation of refrigerant thermodynamic properties. *International Journal of Refrigeration*, 9, 346-351.

Darrow, J.B., Lovatt, S.J., Cleland, A.C. (1991). Assessment of a simple mathematical model for predicting the transient behaviour of a refrigeration system. *Proceedings of 18th International Congress of Refrigeration*, 1189-1192.

Glöckner, G., Hofer, B., Kluge, C.H., Schroth, H.H., Wobst, E. (1990). Simulation of refrigerating plants for cold stores. *Refrigeration Science and Technology*, 1990-4, 487-493.

Hasse, H., Becker, M., Grossmann, K., Maurer, G. (1996). Top-down model for dynamic simulation of cold-storage plants. *International Journal of Refrigeration.* 19(1), 10-18.

Hewitt, G.F., Shires, G.L., Bott, T.R. (1994). Process heat transfer. CRC Press, London.

Hoang, M.L. (2003). Numerical computation of air, moisture and heat transfer in chicory root cold store. *Ph.D. Thesis* (554), Katholieke Universiteit Leuven, Leuven, Belguim.

Hoang, M.L., Verboven, P., De Baerdemaeker, J. and Nicolai B.M. (2000). CFD simulations of chicory root palloxes for cool storage. *Proceeding of Agricontrol2000:*

Modelling and Control in Agriculture, Horticulture and Post-harvested Processing. Wageningen, The Netherlands.

Incropera, F.P., De Witt, D.P. (1990). Fundamentals of Heat and Mass Transfer – 3rd Edition. John Willy & Sons, Inc., New York.

Lammertyn, J., Franck, C., Verlinden, B., Nicolai, B.M. 2001. Comparative study of the O_2 and CO_2 and temperature effect on respiration between 'Conference' pear cell protoplasts in suspension and intact pears. *Journal of Experimental Botany*, 52(362), 1769-1777.

Lopez, A., Lacarra, G. (1999). Mathematical modelling of thermal storage systems for food industry. *International Journal of Refrigeration,* 22, 650-658.

Marshal, S.A., James, R.W. (1975). Dynamic analysis of an industrial refrigeration system to investigate capacity control. *Proceedings of The Institute of Mechanical Engineers*, 189(44/75), 437-445.

Nahor, H.B., Scheerlinck, N., Van Impe, J., Nicolaï, B.M. (2002). A simple model of a refrigeration plant for cool storage systems simulation. *Communications of the faculty of Agricultural and Applied Biological Sciences*, 67(4) 293-296.

Nahor, H.B., Teshome, E.J., Scheerlinck, N., Van Impe, J.F., Nicolaï, B.M. (2003a). Prediction of dynamic behaviour of ca cool rooms using lumped parameter approach. *Acta Horticulturae*, 599, 213-219.

Nahor, H.B., Scheerlinck, N., Verboven, P., Van Impe, J., Nicolai, B.M. (2003b). Dynamic simulation of controlled atmosphere (CA) cool storage systems for pip fruits. *Proceedings of the 21st International Congress of Refrigeration, Washington D.C, USA, (CD-edition, ISBN 2-913149-32-4).*

Nahor H.B., Scheerlinck, N., Verboven, P., Van Impe, J., Nicolai, B.M. (2004). Continuous/discrete simulation of controlled atmosphere (CA) cool storage systems: model development and validation using pilot plant CA cool storage. Submitted for publication in *International Journal of Refrigeration.*

Nguyen, T.A., Verboven, P., Scheerlinck, N., Veraverbeke, E., Nicolai, B.M. (2003). An estimation procedure of effective diffusivity in pear tissue by means of numerical water diffusion model. *Acta Horticalturae,* 599, 541-548.

Pirard, G., Vancayemberg, F., Deltour, J. (1993). Rapport d'activités de décembre 1993. [Research activities report of December 1993] Centre d'Etude de la Regulation Climatique de Serres (IRSIA), Gembloux.

Ranz, W.E., Marshall, W.R. (1952). Evaporation from drops. *Chemical Engineering Progress,* 48, 141-173.

Ruthven, D.M., Farooq, S., Knaebel, K.S. (1994). Pressure swing adsorption. VCH Publishers Inc., New York.

Schotsmans, W. (2003). Gas diffusion properties of pome fruit in relation to storage potential. *Ph.D. Thesis* (557), Katholieke Universiteit Leuven, Leuven, Belguim.

Sprenger Institute (1980). Produktgegevens groente en fruit, Mededeling 30. Wageningen, The Netherlands.

Valenzuela, D.P., Myers, A.L. (1989). Adsorption equilibrium data handbook. Prentice Hall, New Jersey.

Veraverbeke, E. (2001). Changes in epicuticular wax structure and composition in relation to moisture loss of apple during posthrvest storage. *Ph.D. Thesis* (495), Katholieke Universiteit Leuven, Leuven, Belguim.

www 1: http://postharvest.ucdavis.edu/Produce/Producefacts/index.shtml. Accessed on March 4, 2000.

www 2: http://www.fpl.fs.fed.us/documnts/FPLGTR/fplgtr113/Ch03.pdf. Accessed on January, 23, 2001.

www 3: http://www.ba.ars.usda.gov/hb66/008respiration.pdf. Accessed on July 10, 2003.

Chapter 5

Validation using industrial CA cool storage facility

5.1. Introduction

The design of most CA cool storage facilities is performed based on steady state analysis and experience in which the average rate of heat, moisture and gas requirement is estimated. Moreover, optimisation of the facility is usually carried out based on experimental measurements, which can prove to be tedious and expensive besides its applicability to existing plants only. Using the methodology in Chapter 3, dynamic assessment of CA cool room and sizing of corresponding mechanical units can be carried out with small-added cost. Here, the global CA cool storage model will once more be validated using an industrial CA cool storage facility.

This Chapter is concerned with the validation of the developed methodology (Chapter 3) using an industrial controlled atmosphere cool storage facility. Hereto, several measured parameters will be compared to corresponding model predictions. In Section 5.2, the materials and methods employed will be described. Next (Section

5.3), the validation results of some important parameters will be presented. Finally, in Section 5.4 and 5.5, the obtained results will be discussed and some concluding remarks will be drawn, respectively.

5.2. Materials and methods

5.2.1. The CA cool storage facility

The cool storage facility employed in this study was one of the industrial facilities of the growers' cooperative (Belgische Fruitveiling) located in Glabbeek, Belgium (Figure 5.1). The facility consists of 62 ULO rooms (7.2m wide, 10.8m deep and 8.0m high), and a large cool room used as a buffer zone during the arrival and dispatch of fruit. These are serviced by a direct system refrigeration unit and gas-handling unit comprising nitrogen generator and CO_2 scrubber. The refrigeration unit uses a pump-circulated evaporator (liquid overfeed system) arrangement where liquid refrigerant is pumped to the evaporators from a liquid/vapor separator vessel. A level controller modulates the circulation pumps in such a way that depending on the refrigerant flow rate requirement it switches the pumps on or off. In case of very low refrigerant flow rate requirement, a by-pass valve is opened to return back part of the refrigerant into the vessel. The refrigerant flow (vapor and liquid) from the evaporators is directed to the separator vessel where the vapor is sucked by the compressor. Liquid refrigerant is supplied from the evaporative condenser to the vessel. The schematic representation of the liquid overfeed refrigeration system is shown in Figure 5.2. The gas-handling unit consists of central double vessel PSA N_2 generation unit and a single vessel CO_2 scrubber, where regeneration is carried out using normal air and flushed afterwards with very low O_2 air to avoid residual O_2 entering the cool room during the start of scrubbing. One scrubber unit services 6 to 8 cells, hence, in total there exist 8 scrubber units.



Figure 5.1 Controlled atmosphere storage facility (Glabbeek, Belgium)

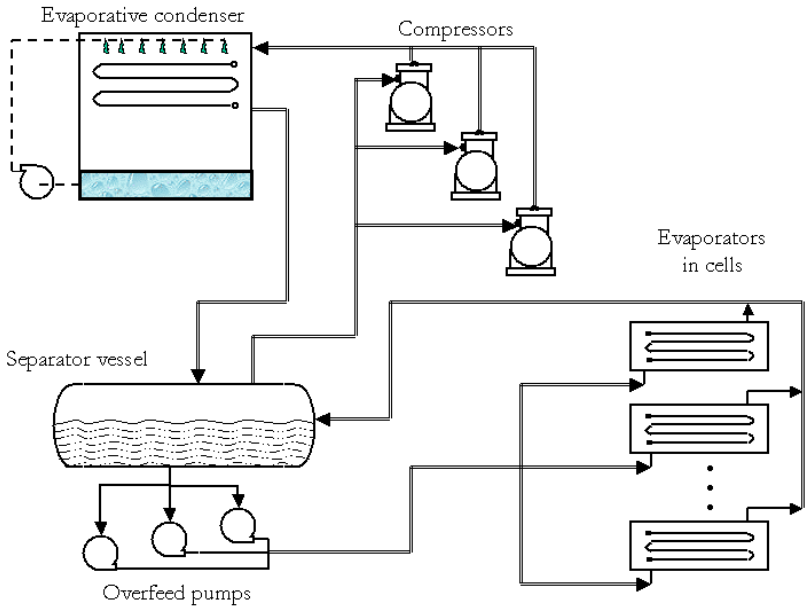

Figure 5.2 Schematic representation of the liquid-overfeed system of the cool storage facility.

5.2.2. Model formulation

The models of the different components as discussed in Chapter 3 were employed with slight modification of components such as the evaporator and its control

system, the product model (to encompass the loading strategy), the N_2 generator and CO_2 scrubber and their respective control mechanisms.

5.2.2.1 Evaporator

Basically, the same structure of model equations were employed as discussed in Section 3.3.1.2 and 3.3.2.1. However, for the pump circulated evaporator arrangement, a number of assumptions were considered.

- The model assumes a couple of zones; one zone represents the whole refrigerant side of evaporator and the liquid in the separator vessel. Another zone embodies the evaporator structure and the pipe work to and from the separator vessel.

- Vaporization in the evaporator is isothermal (negligible pressure drop within the evaporator).

- The liquid hold-up in the evaporators depends on the rate of heat transfer (increasing with the decrease of heat transfer rate). However, in the present arrangement where liquid refrigerant is deliberately over-supplied to the evaporator (typically 6 - 7 times the heat transfer rate (ASHRAE, 1994), the possible change in the rate of heat transfer creates negligible change in the liquid holdup in the evaporators. Thus, constant liquid and vapor hold-up amounts were assumed.

The schematic representation of the double zone model considered is depicted in Figure 5.3.

Concerning the control, the temperature in the room was controlled by means of an on-off control strategy. The refrigerant flow to the evaporator is regulated via a solenoid valve, based on the error between the set point and measured value of the room air temperature.

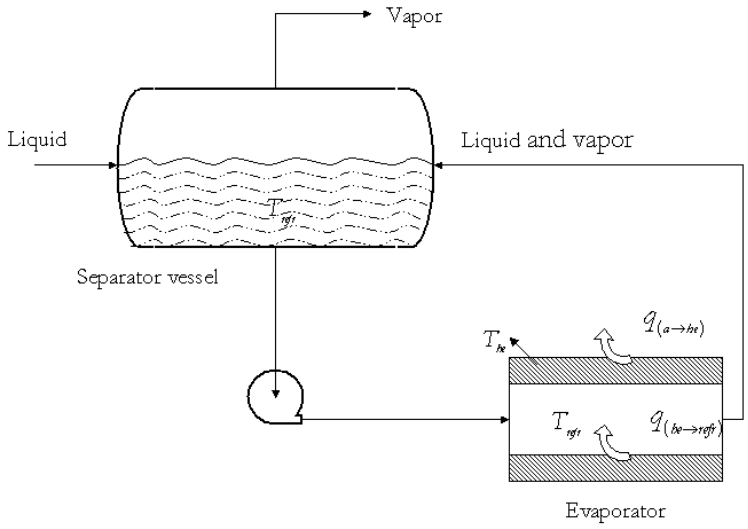

Figure 5.3 Schematic representation of the single zone model of a pump circulated evaporator

5.2.2.2 Product model

The model structure discussed in Section 3.3.1.6 was not altered; however, to implement the stepwise product loading in the room some data variables, such as the number of bins, were changed to a discrete variable incremented by the number of bins loaded at a certain moment in time. The already loaded bins, which reached steady state, were considered to be at the storage temperature while the dynamic product temperature variable switches to the new loaded bins. In case where the loading of a new batch is taking place before the preceding batch reaches steady state, a weighted average temperature based on the number of bins at steady state and those that are not was calculated. This calculated temperature would decay to the steady state value after some given period depending on its magnitude. It should be noted here that such a complicated simulation of the loading strategy could be implemented with relative ease due to the capability of discrete event handling of the software.

5.2.2.3 Gas handling unit

The nitrogen generator in the gas-handling unit of the present installation was constructed in such a way that the generated N_2 is stored in a buffer tank where it is injected to the cells from the tank as required. Assuming the capacity of the unit is large enough to satisfy the demands of the cells, the transients of the N_2 generator does not affect the dynamics of the concentration of the respiratory gases in the cell. Therefore, the dynamics of the nitrogen generator was not taken in to account, instead a constant flow rate of N_2 with a concentration of 97% was injected during the pull-down operation.

Concerning the single vessel CO_2 scrubber it was assumed that the maximum scrubbing time before the bed becomes saturated corresponds with the maximum allowed scrubbing time for a given cell. This time was set to 10 minutes (based on plant settings). This means that when the measured concentration of CO_2 (which was carried out in an interval of 30 minutes) in the cell goes above a certain set value the room air is scrubbed for a fixed time of 10 minutes and the unit goes in to regeneration phase. Regeneration time was also set to 10 minutes.

5.2.3. Measurements

A cool cell completely filled with 436 apple bins (1.2×1.0×0.75 m) of approximately 300kg each was considered for validation. The schematic representation of the loaded room set up is shown in Figure 5.4. The cool cell was set into operation on 17/09/2002 while it was still empty. Seven days later, loading of the product was commenced based on the loading strategy shown in Figure 5.5. A picture of the cell after loading of day 10 is also shown in Figure 5.6. This loading strategy was arbitrary, brought about by the allocation of different farmers in the available cool cells thought to bring about convenient operational condition during loading and unloading of the produce depending on a specific farmer's decision as to when to sell his produce.

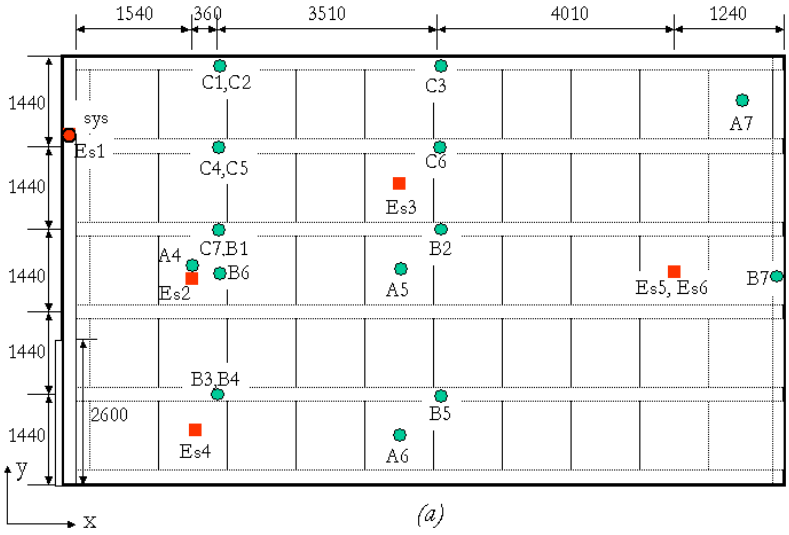

Figure 5.4 Experimental set up (the squares represent the bins); (a) top view; (b) lateral view; (Thermocouples A4, A6, and A7 were positioned inside bins; A5 inside a fruit at the centre of the bin. The Pt1000 used by the system was placed on the same position as Es1)

A total of 21 calibrated (±0.5°C) T-type Teflon-insulated thermocouples (Omega Engineering, Inc., Stanford, USA) were used to measure the room, product and evaporator surface temperatures which were connected to a Smartreader data logger (ATAL, AT Pumerend, The Netherlands) and the software TrendReader AXIOM (ATAL, ACR Systems Inc. (2000)) was used to interface with the logger. The surface temperature of the cooler was measured at three positions: at the side where the refrigerant enters and its symmetric position at the other side, and at the centre of the evaporator. Moreover, as integral parts of the system the room, evaporator surface, refrigerant and pulse temperatures were measured using Pt1000's (±0.1°C). Six capacitive type RH sensors (ESCORT Junior Tech Innovators, Oakland, New Zealand) with an accuracy of ±5% were employed to measure the relative humidity inside the bins as well as the free air. Room air respiratory gas concentrations were measured by sensors provided by the system. Moreover, the high and low pressure sides of the refrigeration unit were also measured by pressure sensors provided by the system. All the measurements were recorded in an interval of 30 minutes. The firmness of the apples was measured by taking 10 samples randomly every month and the firmness measurement was measured by a penetrometer (ART-Penetrometer, UP Umweltanalytische Product GmbH, Kolkwitz, Germany) after the apples were allowed to equilibrate with the atmosphere. The samples were picked during loading and placed near the sampling window of the cells prior to the start of ULO operation. The first measurement (at t=0) was used as an initial value in the simulation of the dynamic variables. In the case where several measurements for a given variable were carried out, an average value of the measurements was calculated as an initial value for simulation. Agreement of the model prediction with experimental data will be evaluated according to the validation criteria defined in Section 4.3.1.3. The simulation was carried out on a Celeron 366Mhz, 128Mb Ram personal computer with Microsoft Windows NT OS.

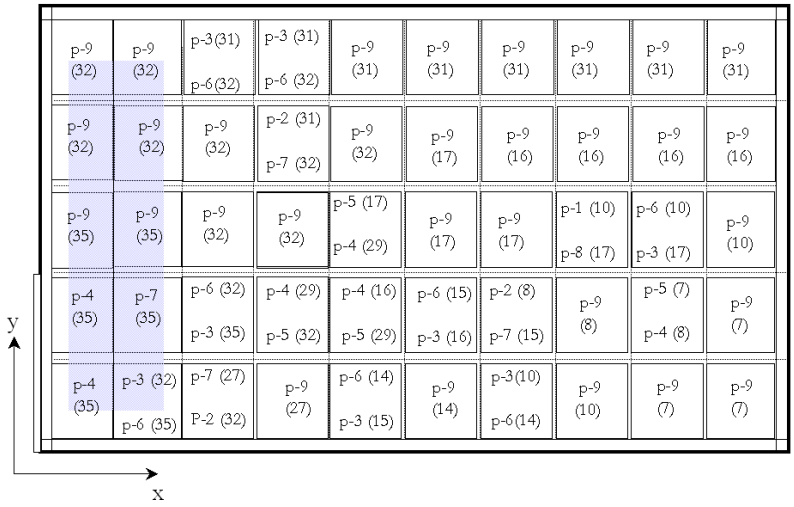

Figure 5.5 Loading of the cool cell. Each box represents a stack of maximum 9 bins and in each box, the number of stacks, preceded by the letter p, are shown. The number in brackets is the number of days since the start of the operation i.e., 17/09/02. For example, (p-6 (15) is read as: on day 15 after start of loading, 6 bins were stacked at this position)



Figure 5.6 Cell load condition on day 10 (after loading)

5.3. Results

5.3.1. Room Air

Figure 5.7 depicts the temperature variability in the cases of the empty and the loaded cool cell. The spikes represent the defrosting operation. During the first 7 days when the room was still empty, a maximum temperature difference of 2°C is observed between the air exiting and entering the evaporator (Figure 5.7a). When the cell is empty and at steady state, these positions (B6 and sys (Figure 5.4))could be considered as extreme locations as far as temperature variation is concerned and it was observed that the rest of the measured temperatures lie between these bounds. On the other hand, Figure 5.7b depicts the maximum and minimum temperature profiles in the cell when fully loaded and steady state was attained. A difference of 3°C exists where the maximum temperature was obviously found inside the void spaces of the bins located in front of the evaporator and at the middle of the stack. In terms of RMSE the observed spatial variability was 2.1°C. This result could be expected due to the synergic effect of the airflow pattern (formation of a dead zone) and the fact that the air reaching this location was loaded with energy removed from the bins. It should be noted here that higher temperature differences were observed during the transient state, especially, in the fully loaded condition. The introduced loading strategy reduces this variability to a large extent.

In Figure 5.8, the simulated and measured room air temperature at different product load levels is shown. Figure 5.8a corresponds to an empty cell prior to the start of loading. A favourable agreement between simulated and measured values is observed, both during transient and steady state conditions. As the product loading started in the 7th day, only 17.2% of the total capacity of the cell was filled up to the 10th day (Figure 5.5). The heat load from the product seems insignificant as no considerable change in room temperature in response to this load can be observed. Again, in this period the model prediction and simulation results are in good agreement. Figure 5.8c depicts the period where the cell was more or less half full. Even though there was product loading each day from day 14 on, the response of the room temperature is only visible on the 17th day. A slight over-prediction (< 1°C) of the room temperature by the model is observed during this day. This could be attributed to the positioning of the bins during loading such that buffering effect occurs (not all the stack interacts with the room temperature). This effect is clearly visible immediately after day 31 (Figure 5.8d). During this day, the bins loaded to the cell were placed on the far left row (from the door). A significant increase in

temperature was recorded by thermocouples C1, C2, and C3 (Figure 5.4) during this period. On day 29, 13 bins were loaded, which were only 20% of the bins loaded on day 31 (62 bins). Yet, the influence on the room air temperature as measured by the Pt1000 appears to be higher on day 29. This can either be due to their respective position in relation to the airflow or the effect died out before the following measurement was recorded. In general, as can be confirmed from the calculated RMSE, the agreement in the model prediction and measured values is within the limits set by the accuracy of the measuring instruments.

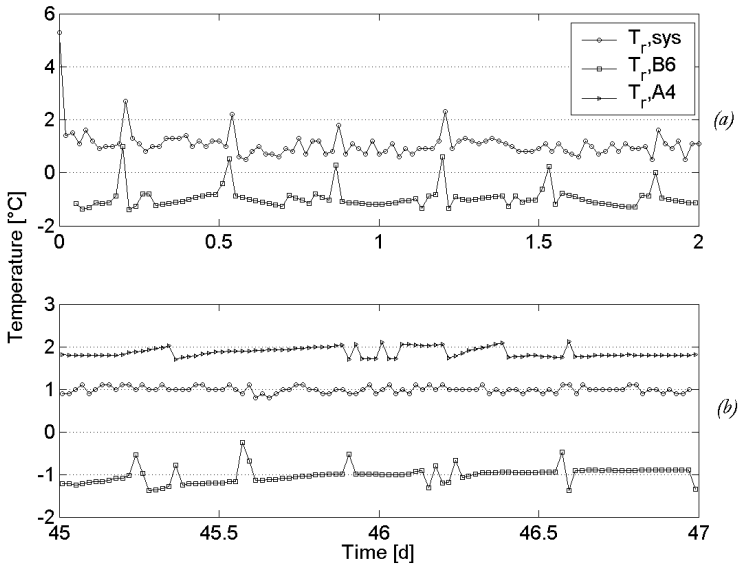

Figure 5.7 Variability in the cool cell during (a) empty and (b) loaded conditions RMSE = 2.1°C. (for the positions of the thermocouples B6, A4 and sys refer to Figure 5.4)

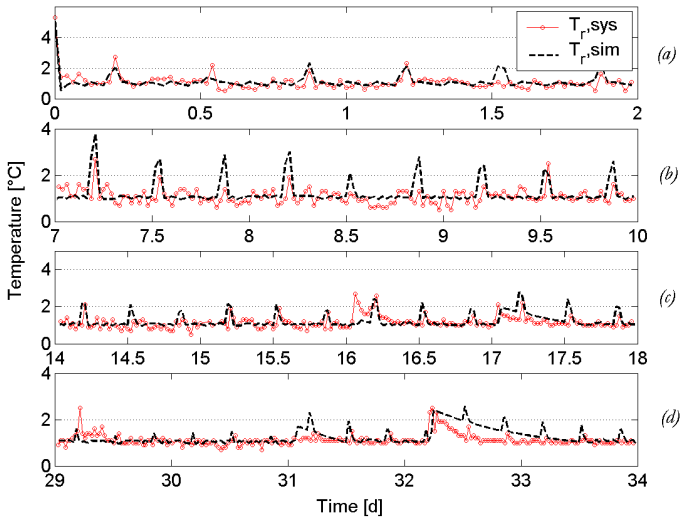

Figure 5.8. Measured and simulated room air temperature. RMSE = 0.42°C. (a) first two days corresponding to empty cell; (b) 17.2% loaded cell; (c) 45.4% loaded cell; (d) 90.3% loaded cell

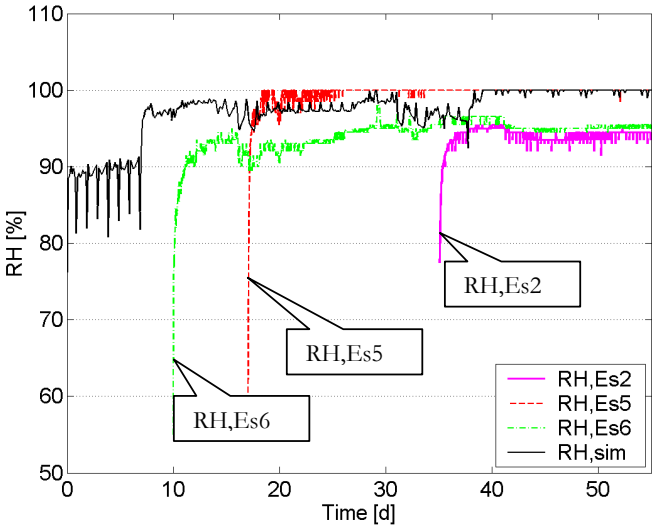

*Figure 5.9 Room air relative humidity profiles. RMSE(*RH,Es5, RH,sim*) = 4.2%. (Es2 and Es6 were positioned on top of the bin; Es5 was positioned at the centre of the bin (Figure 5.4))*

In Figure 5.9, the room air relative humidity as measured by the different Escort loggers and the simulated values are shown. According to the model prediction, at the beginning while the room was still empty, the relative humidity seems to stabilize at around 90%. As loading started (on day 7), it was observed that the influence of the heat load from the produce on the room air temperature was insignificant. Thus, the observed drastic increase in relative humidity was caused by the increase in absolute moisture content of the air due to the transpiration of the produce. As more and more produce was loaded, the relative humidity gradually increased to saturation. The measurement from the Escort logger Es5 that was placed inside the bin shows saturation while Es6 shows around 5% less than saturation, which can be attributed to measurement accuracy. After about 40 days when the temperature reaches steady state, the difference between the measured values was more or less within the bounds of the accuracy of the instruments. Moreover, the model prediction lies between the measurements from different locations. Thus, given these observations and the RMSE with respect to Es5, which lies in the limits of the accuracy of the measurement instrument, the model prediction can be considered as adequate representations of the observed experimental values. A decrease in relative humidity as recorded by Es2 and Es6 is observed at about 42 days. Since at that stage, the ULO operation was well underway, this cannot be attributed to door opening and the reason for this is not known.

Figures 5.10 and 5.11 show the concentration profiles of the respiratory gases inside the cell. During loading, when the control of the respiratory gases is not yet commenced, there was a constant aeration, lest there was accumulation of CO_2 beyond the optimal level. Therefore, the level of the respiratory gases stays practically the same as that of the atmospheric air. After 30 days, where the cell was full to 90 % its capacity, a slight increase of CO_2 concentration is observed despite the constant aeration. Once the ULO operation begins (41st day), a drastic build up of CO_2 to the set point (2.5%) in less than 3 days is observed solely due to respiration (Figure 5.10). An even more drastic decay of O_2 occurred due to the combined effect of respiration and injection of N_2 (Figure 5.10). The model and measured data seem to fit up to around 42nd day and the model starts to over predict the experimental observation thereafter in the case of CO_2 and under predict in that of O_2. This could be attributed to the accuracy of the involved parameters in the respiration model. Looking at the measured oxygen profile (Figure 5.11), after the set point of 5% O_2 concentration is reached the injection of N_2 stops and a strange increase in O_2 concentration is observed. Normally, after this point is reached (5% O_2), respiration takes it to the set point of 1% and it is controlled at this value

through aeration. This anomaly can only be due to some rather extensive leakage (for instance, a window left open) or faulty aeration valve. One can then speculate that the leakage might have started at the time when an offset between the model and the measured values is noticed. Relating to the unexplained decrease in relative humidity as measured by the Es2 and Es6 (Figure 5.9) at exactly the same time, the above speculation can be justified. It was observed that this increase in O_2 concentration has caused continuous high O_2 concentration alarms during the operation, which was only corrected after the 65th day and the set point of 1% was reached. During the burning operation the maximum discrepancy between model prediction and experimental observation was 0.6% and 3% for CO2 and O2 concentrations. Overall, taking into consideration the anomaly during the experiment, the model prediction is in good agreement with the observed values for both O_2 and CO_2 concentrations. This, in turn, gives an idea on the performance of, especially, the gas-handling unit model and that of the product respiration model.

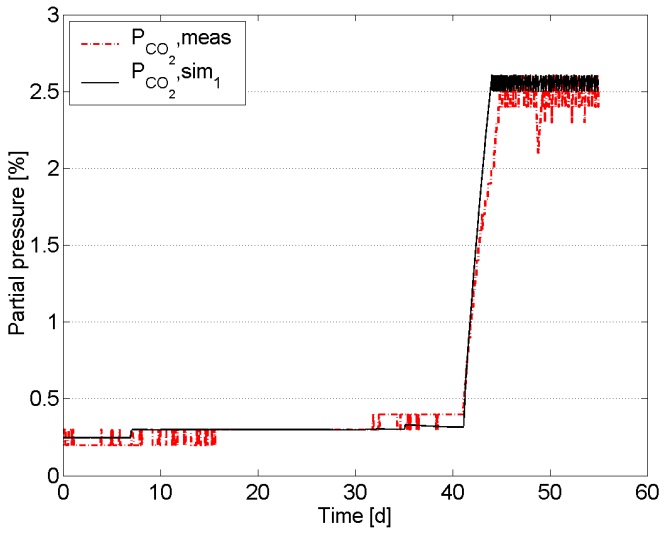

Figure 5.10 Measured and simulated CO_2 concentration profiles in an industrial loaded cell

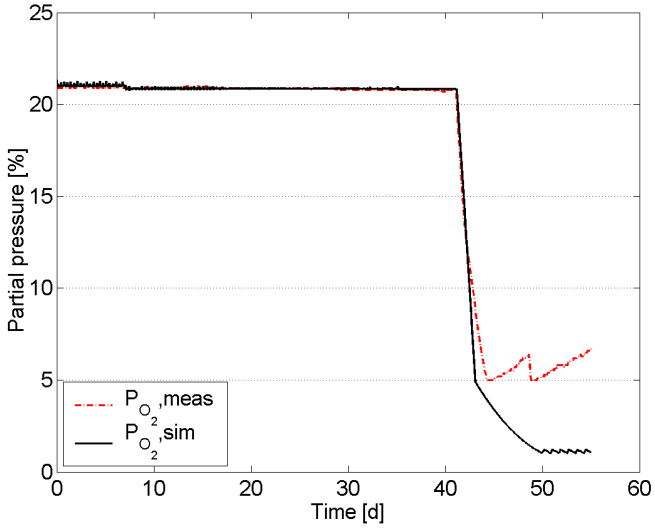

Figure 5.11 Measured and simulated O_2 concentration profiles of an industrial loaded cell

5.3.2. Evaporator and refrigerant

In Figure 5.12, the evaporator surface temperature as measured by three thermocouples positioned at the two sides and in the middle of the evaporator and simulated curves are shown. It is obvious that the temperature at the refrigerant entrance side (T_c,A1) is lower than that of the exit side (T_c,A3). During the pre-loading period, the model prediction appears to fit the experimental observation, as can be visually confirmed. As was observed in the room air temperature, the response of the evaporator to the product load during the first 15 days (which was ¼ the total capacity loaded in seven days) is insignificant (Figure 5.12a). As the product load grows to be significant, the evaporator surface temperature is observed to reduce slightly due to the opening of the refrigerant control valve to counteract the heat load (Figure 5.12b and c). The maximum temperature difference between predicted and measured evaporator surface temperature was 1 °C during the steady and 2.5°C during the transient states. Equivalent difference is also observed between the different measured evaporator surface temperatures. The overall RMSE between the model and the average of the three measurements (A1, A2, and A3) stands at 0.71°C. This is slightly higher than the measurement accuracy. The discrepancy especially during the brief transient condition due to loading at later stages (day 32

and later on day 36 (not shown in Figure 5.12) has contributed to this. However, a reasonable fit between the experimental data and model predictions obtained, suggesting adequate model performance.

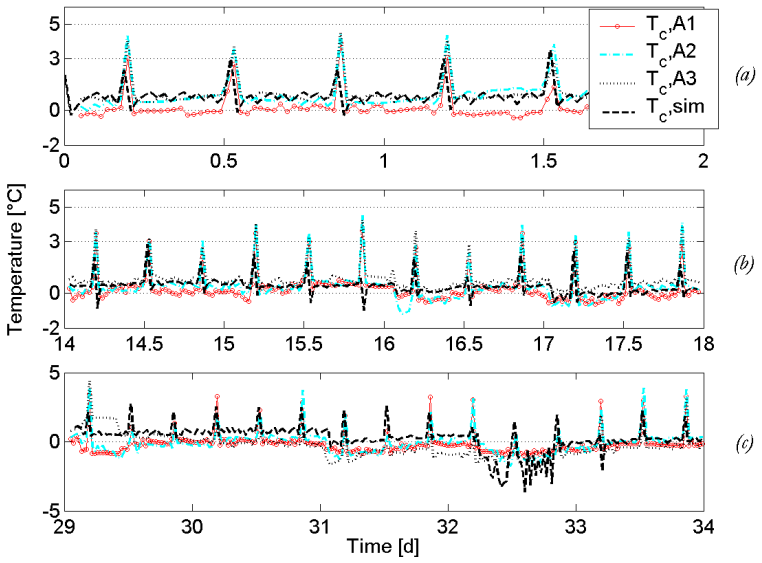

Figure 5.12 Cooler surface temperature RMSE($T_{c,AV}$, $T_{c,sim}$) = 0.71 °C. (A1: right (refrigerant entrance); A2: middle; A3: left, $T_{c,AV}$: average temperature of the measurements A1, A2 and A3) (a) first two days corresponding to empty cell; (b) 45.4% loaded cell; (c) 90.3% loaded cell

Figure 5.13 shows the refrigerant temperature inside the evaporator. Here, it can be observed that the defrosting action has a larger influence on the predicted refrigerant temperature as compared to the measurement. This can be explained by the fact that the sensor for refrigerant temperature was located outside the evaporator on the pipeline leading to the separator vessel. Thus, the influence of the defrost action is smaller than the model can predict which considers interaction of the refrigerant with the evaporator structure even during defrosting. At this instant, the discrepancy of the model as compared to the experimental data is significant which contributed to the high RMSE (1.79°C) obtained. Moreover, when the product imposes significant heat load on the cooler (also due to impeded airflow) the model under predicts the refrigerant temperature during the transient state. This can be explained by the fact that the dryness ratio of the refrigerant leaving the evaporator was

considered constant assuming the oversupply of refrigerant is maintained by leaving the control valve open. However, when the load is higher, more refrigerant evaporates, increasing the refrigerant dryness ratio and thus, the enthalpy. In the whole, despite the high RMSE due to the above limitations as can be visually inspected, favourable agreement between the model prediction and measured refrigerant temperature in the evaporator is observed.

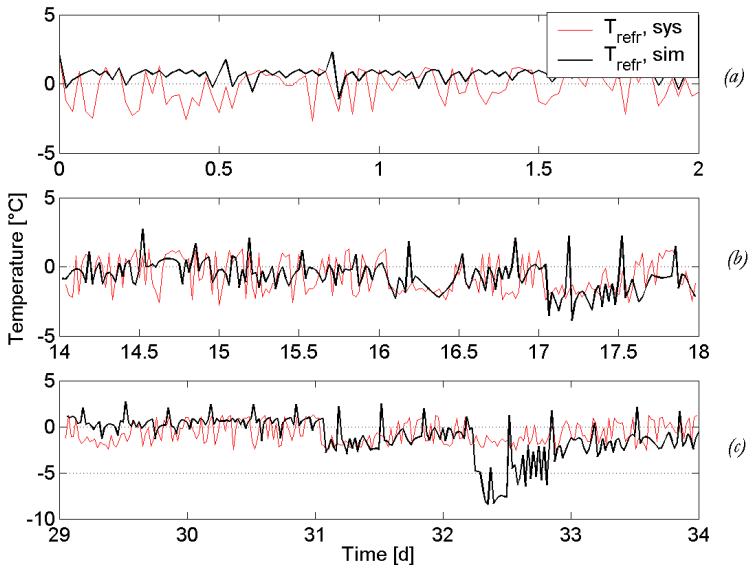

Figure 5.13 Refrigerant temperature in the evaporator. RMSE = 1.79°C (a) first two days corresponding to empty cell; (b) 45.4% loaded cell; (c) 90.3% loaded cell

5.3.3. Product

In Figure 5.14, the product temperature profile of the different batches and the product loading profiles are depicted. Each peak represents the initial product temperature of a batch and then the cooling profile is shown until next batch is loaded. Referring to Figure 5.14a, during loading in the 14th day, the temperature of the air inside one of the bins loaded the same day (T_{bin},A6) shows a higher temperature than the predicted product temperature. This discrepancy can be attributed to spatial difference due to the fact that the measured bin was located at

the far right section where relatively slower product cooling rate is expected. Product temperature measured in the batch loaded during the 17th day (where 43 bins were loaded) shows that the product temperature attained the set point after about three days. This is also predicted by the model but at a slightly different cooling rate. During the transient state, the model under predicted the measured values. Several factors might contribute for this discrepancy. The obvious reason can be the spatial variability. The position of the measured bin being at the middle of the room and at the middle of the stack, the cooling rate can indeed be slower than that of the bins at other positions. The extreme case can be the position of the bin where Es5 was placed. This bin was located at the far end of the room and at the top of the stack down stream the pulse air. As can be observed from the profile of this sensor (placed at the middle of the bin and was measuring the air inside the bin (Figure 5.4)), there is a drastic cooling of the air inside the bin. Another reason could be related to the lumped capacitance approach, in that the assumption that the product temperature is uniform may not hold where higher velocities resulting in high heat transfer coefficients exist. Overall, although a discrepancy of about 2-3 °C can be expected between model prediction and reality, the model gives a rather good estimation of the cooling rate of the product and prediction of the product temperature of the loaded batch, with relatively low RMSE (0.84°C) computed between days 17 and 21.

In Figure 5.15, the measured and simulated curves of firmness loss of the fruit are shown. The observed trend of the model to predict lower firmness values, besides biological variability, could be due to the fact that the firmness measurements were carried out while the fruit are still at much lower temperature than the atmospheric (though the protocol stipulates temperature equalization between sample and room temperature). It should be noted that this measurement result is only from a limited number of fruit (10 apples) and given the biological variability the fit between model prediction and measurement was remarkable. For comparison, the firmness loss of Jonagold apples stored under optimal conditions obtained from literature (Schotsmans, 2003) is also shown. Apparently, considerable difference between the two measurements is observed, especially in the beginning. This larger difference could be explained by the fact that during loading of the cell, which took about 5 weeks, the apples were stored in atmospheric air. This is portrayed by the drastic firmness loss of the apples in the first 8 weeks, which apparently incurred a final firmness difference of more than 10 N.

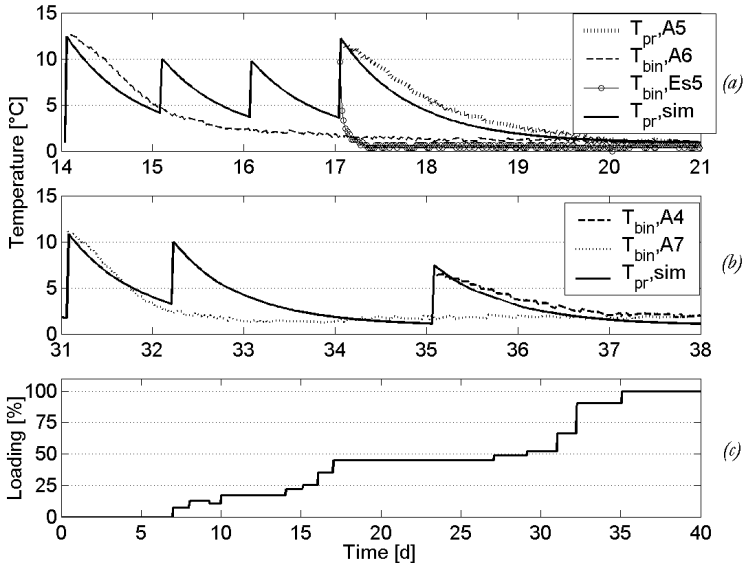

Figure 5.14 (a) Product temperature profile during loading of days 14 to 17 RMSE($T_{pr,}$A5, Tpr, sim*) = 0.84°C; (b) product temperature profile during loading of days 31 to 35; (c) product loading profile. (bin: the air inside the bin; pr: product centre)*

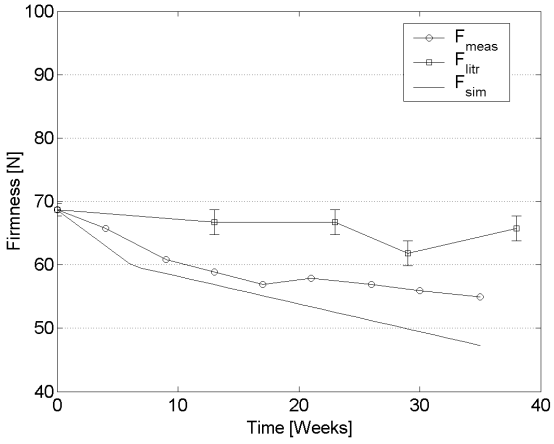

Figure 5.15 Firmness loss profile of the stored Jonagold apples during storage (meas: measured, lit: literature, sim: simulation)

5.4. Discussion

The complete validation of such a model using industrial facility is constrained by the collection of substantial amount of data on a relatively longer period of time. Considering the accessibility, resource (as well as logistical) and time limitations, one always finds a pragmatic solution of validating the proposed model. Here, some experimental data collected pertaining to the room, refrigeration unit and gas handling unit (indirectly) were exploited to carry out the validation of the proposed model. The level of validation provided by complete industrial cool/cold simulation models in the literature is limited to very few variables focussing rather on the one of the involved units, usually the refrigeration unit (Martial and James, 1975; Cleland, 1985; Glöckner et al., 1990; Hasse et al., 1996). In comparison, the validation provided in the present work takes into account more variables considered critical in all the involved units, giving special emphasis to the ones which form a boundary and are responsible for the interaction between the units and those that drive the dynamics of the installation as a whole. Moreover, due to the leeway of the model to simulate practical and real working conditions such as the stepwise product loading, it was possible to validate the model using experimental data that considers the transients involved.

The consideration of a single zone for the cool cell space can be justified by the observed spatial difference. In comparison to the pilot scale CA cool storage facility employed previously (Chapter 4) higher spatial variability was observed (2.1°C as compared to 1.1°C). It is evident that better agreement between model prediction and the measured room air variables was observed in the case of the pilot plant. This is rather associated with the accuracy of the model parameters. In the case of the industrial facility, crude approximations of some model parameters especially related to heat transfer coefficient of air around the product and to the gas-handling unit had to be made. Therefore, consideration of more zones might not improve the obtained accuracy, as more parameters with large uncertainty related to the interaction between zones will be introduced.

The product model has shown moderate accuracy pertaining to the prediction of the product temperature during the transient condition. This discrepancy can be explained, besides the accuracy of the model parameters, by the validity of the uniform product temperature assumption. The dimensionless number which relates the internal and external (in relation to the product phase) heat transfer is the Biot number (hV/kA_s). For air flow over an apple (considered as a sphere) a heat transfer

coefficient of about 3 W m^{-2} °C^{-1} would constitute the margin for justification of the lumped assumption (Bi < 0.1). This heat transfer coefficient corresponds to a Reynolds number in the order of 2×10^2. It should be noted here that depending on the correlation used to estimate the heat transfer coefficient this value might vary. The velocities that correspond to this order of Re values are in the vicinity of the velocity values that can be found inside a bin (Hoang, 2003). To that end, the assumption of uniform product temperature is marginally valid which affects the accuracy of the lumped model.

5.5. Conclusion

A validation of the global CA cool storage model using an industrial facility was presented in this Chapter. First, minor modifications to some of the modules were carried out pertinent to the control systems of the evaporator and gas-handling unit and to the product model to accommodate the product-loading schedule. Then some selected important variables were compared to experimental data in empty, partially loaded and fully loaded conditions. As often as not, model predictions of the most important discrete and continuous variables were found to agree well with the experimental data. The maximum spatial difference at steady state in the room at empty and fully loaded conditions was found to be 2 and 3 °C, respectively. The observed discrepancy between the model results and experimental data was smaller than this value. The room air relative humidity was represented with the level of accuracy set by the measurement instruments. Moreover, a good agreement between simulated and measured values of the concentrations of the respiratory gases was obtained. It was observed that the operational anomaly caused considerable influence on the O_2 concentration (what it should be as compared to what was observed) profile and also influenced the CO_2 concentration and the room air relative humidity. Even though including prediction of such malfunctions in the model could prove to be difficult or even impossible, when using such simulation tool for design purposes, such irregularities and their influence on the plant and stored product can be analysed in order to include safety issues which provide critical levels for high and/or low level alarms. The largest difference between model prediction and observed data were found for the product temperature profile. This was attributed to the model assumptions, which assumes uniform temperature distribution in the product phase, besides to the spatial variability and accuracy of the model parameters. It was demonstrated here that the complicated product loading strategy and the transients involved with it could successfully be simulated

owing to the discrete event simulation capabilities of the software. In conclusion, the global CA cool storage model, once more, demonstrated to be a pragmatic working tool for simulation of CA cool storage facility.

Reference

Anonymous. ASHRAE Handbook, Refrigeration systems and applications. (1994). American Society of Heating, Refrigerating and Air-Conditioning Engineers, Inc., Atlanta, USA.

Cleland, A.C. (1985). Experimental verification of a mathematical model for simulation of industrial refrigeration plants. *International Journal of Refrigeration*, 8, 275-282.

Glöckner, G., Hofer, B., Kluge, C.H., Schroth, H.H., Wobst, E. (1990). Simulation of refrigerating plants for cold stores. *Refrigeration Science and Technology*, 1990-4, 487-493.

Hasse, H., Becker, M., Grossmann, K., Maurer, G. (1996). Top-down model for dynamic simulation of cold-storage plants. *International Journal of Refrigeration.* 19(1), 10-18.

Hoang, M.L. (2003). Numerical computation of air, moisture and heat transfer in chicory root cold store. *Ph.D. Thesis* (554), Katholieke Universiteit Leuven, Leuven, Belguim.

Marshal, S.A., James, R.W. (1975). Dynamic analysis of an industrial refrigeration system to investigate capacity control. *Proceedings of The Institute of Mechanical Engineers*, 189(44/75), 437-445.

Schotsmans, W. (2003). Gas diffusion properties of pome fruit in relation to storage potential. *Ph.D. Thesis* (557), Katholieke Universiteit Leuven, Leuven, Belguim.

Chapter 6

Application: plant performance/ design and product quality evolution

6.1. Introduction

In Belgium, most of industrial CA cool storage facilities are owned by fruit growers cooperatives, which provide service to their members. Assumed to suite operational and fluctuating market conditions during selling of the fruit, various customs of loading of the cool cells are practiced. In general, two loading strategies can be identified.

(i) Batch wise loading and

(ii) Step wise loading of the cells.

In the batch wise loading strategy, each batch arriving in the station is pushed into a cool cell until it is full to its capacity and the process continues to the next cell and so forth until the available cells are filled. This type of loading strategy is practiced in

facilities owned by growers' cooperatives in France (Luc Machiels, personal communication). On the other hand, in stepwise loading, the arriving produce is distributed into the available or allocated cool cells and the cells are progressively filled as the growers bring in their produce. This allows to fill the cool cells almost at the same time and can take up to 1 month to fill the allocated cells. This type of loading strategy is pursued by the installations owned by the growers' cooperatives in Belgium.

In this Chapter, the validated CA cool storage model will be used to investigate different working conditions and their influence on final product quality and mechanical plant design/performance by considering various customs of product loading schemes. Accordingly, in Section 6.2, a hypothetical CA cool storage facility will be described, which will be used in the simulation of the two product loading strategies. Section 6.3 discusses the effects of these considerations both from product and plant design/performance point of view. Finally, in Section 6.4, these factors together with some operational and commercial issues will be discussed. In Section 6.5, some concluding remarks will be given.

6.2. Materials and methods

Here, in order to investigate the implication of the stepwise and batch wise loading strategies, a hypothetical industrial CA cool storage facility with 10 ULO cells was considered. The dimensions of the cells and the cooling capacity of the evaporators in the cells were assumed to be the same as the one described in Section 5.2.1.1 with a total capacity of 430 bins of size 1.2×1.0×0.75 m, filled with Jonagold apples. It was assumed that 430 bins full of product arrive at the facility every other day for storage. Then, in stepwise loading, the bins are distributed to the 10 cool cells, and the cells are filled at the end of day 18. This means 43 bins were loaded in each cell every other day. The profile of such loading scheme is shown in Figure 6.1. In the batch wise loading, a single cell is loaded to its capacity at a time, as the produce arrive. That is, all the 430 bins were loaded to a single cell and the next batches are loaded to the next cell and so forth until all the cells were filled. The products were assumed to be introduced at a uniform temperature of 10°C and all the cells are at the set point temperature of 1°C. In both cases, the ULO operation starts when a cell is full and 2 days after storage product temperature is attained. This means that for the step wise loading the operation will start at almost the same time for all the cells. While for the batch wise loading, each cell is '*burned*' as the above stated

conditions are fulfilled for that cell. For comparison purposes cost of energy of refrigeration will be calculated using the following formula.

$$C_{refr} = \frac{qp}{\eta_{COP}} \tag{6.1}$$

where C_{refr} is the cost of refrigeration, € ton^{-1}; q, the chilling and storage heat load per ton of stored produce, kJ ton^{-1}; p, the price of electricity (= 0.08 € kWh^{-1}) and η_{COP} the coefficient of performance of the whole cooling plant which was assumed to be 2.5 (Bert Verlinden, personal communication). Moreover, in order to quantify the firmness loss of the apples in terms of money, the grading system as shown in Figure 6.2 was defined. This was based on the '*Belgische Fruitveiling'* quality grading system for Jonagold apples, (www 1, 2003). In this grading, the A1, A2, A3 and A4 represent apples with 50, 33, 25, and 20% red colour, respectively. On the other hand, the ++, +, Y and R represent the base (background) colour and the firmness of the fruit, ++ being the extremely green base and extremely firm apple and R the yellow and soft apple. The simulation was carried out on a Celeron 366Mhz, 128Mb Ram personal computer with Microsoft Windows NT OS.

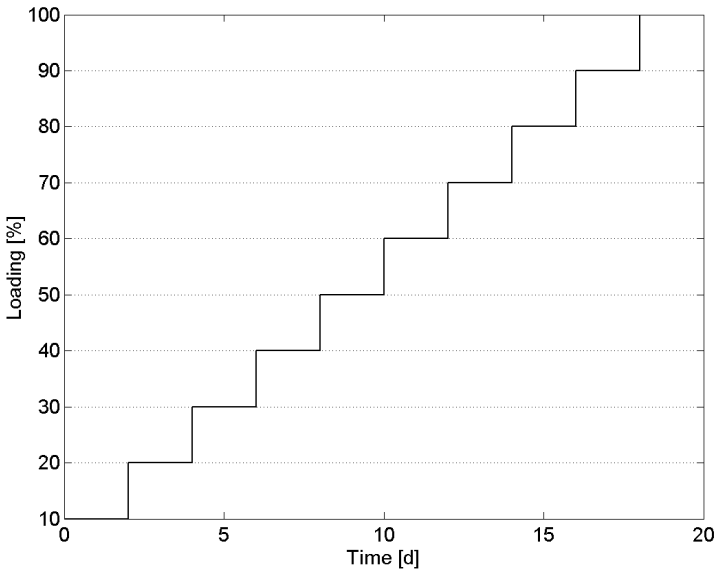

Figure 6.1 Hypothetical stepwise product loading profile

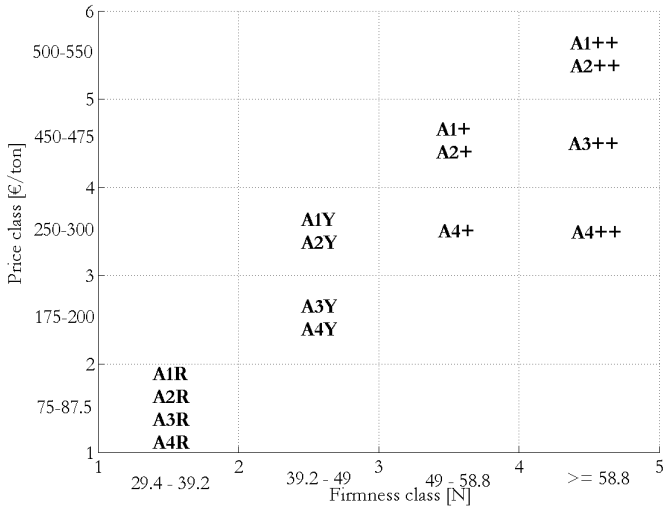

Figure 6.2 Quality grading system based on appearance and firmness (A1: at least 50% red colour, A2: at least 33% red colour; A3: at least 25% red colour; A4: at least 20% red colour; ++: extremely green base and extremely firm; +: greenish-yellow and firm; Y: yellow; R: ripe)

6.3. Results

6.3.1. Effect of loading strategy on product quality

6.3.1.1 Product cooling rate

In Figure 6.3, the product temperature profiles and their respective room air temperatures are depicted for the two loading strategies. For the case of the full load condition (batch wise loading), the air temperature is observed to rise, since the load imposed by the product is higher than the available cooling capacity of the specific cell. On the other hand, for the stepwise loading (i.e. 10% load condition) the effect of the produce is apparent on the room temperature. Obviously, slower product cooling rate is expected in the fully loaded condition. However, in comparison, in cooling 10% of the full load condition the apparent gain in cooling rate is only less than 50%. This is due to heat transfer limitations, in that, though there is extra cooling capacity able to take more heat load, the rate of heat removal from the product is the limiting factor. Thus, the control system tries to keep the room

temperature at the required set point by controlling the cooling capacity via the control valve. It should be noted here that the cooling rate obtained for the full load condition is comparatively more dependent on the available capacity of the individual evaporators in each room. Nonetheless, from the product point of view the step wise loading appears to be advantageous as it provides faster cooling.

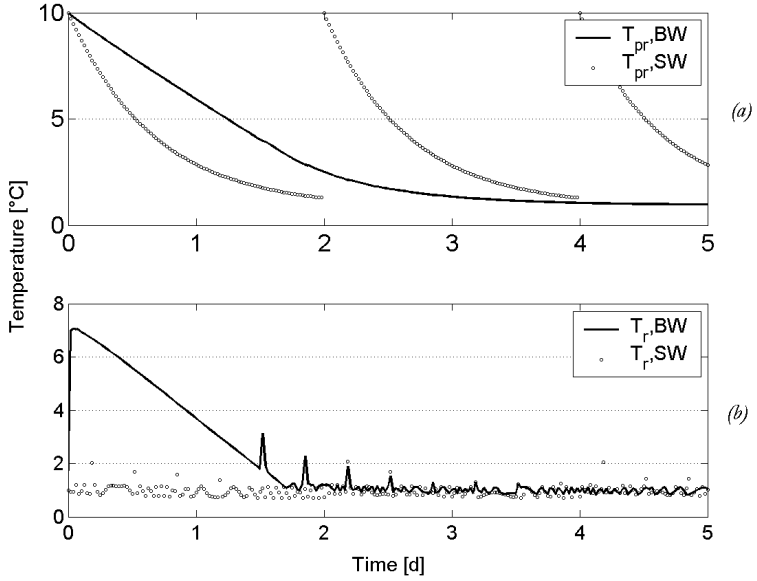

Figure 6.3 (a) Typical product profiles in one of the cells of the batch wise and step wise loading conditions (b) corresponding room air temperatures (BW: batch wise; SW: stepwise)

6.3.1.2 Product weight loss

The accumulated weight loss and their respective room air relative humidity are depicted in Figure 6.4 for both strategies. A higher rate of moisture loss is observed for the full load condition at the beginning, because of low room air relative humidity as well as high temperature. Once at steady state, a constant rate moisture loss was attained. On the other hand, for the stepwise loading, a slower rate of moisture loss is observed at the beginning. However, due to the reduced relative humidity each time product was loaded, a higher rate of moisture loss was observed until the end of product loading and stabilizes to a constant rate similar to the full load condition. When extended to a storage period of 180 days, 2.5% and 2.3%

cumulative moisture loss was predicted for the stepwise and batch wise loading strategies, respectively. This slight difference, which can hardly be explained, is evidently much less than the prediction accuracy of the employed models. These values correspond with the reported moisture loss of 2.5 – 3.0% (Veraverbeke et al., 2003) in practice for Jonagold apples. No apparent advantage of one strategy over the other was observed in relation to moisture loss, as both stabilize to the same rate of moisture loss.

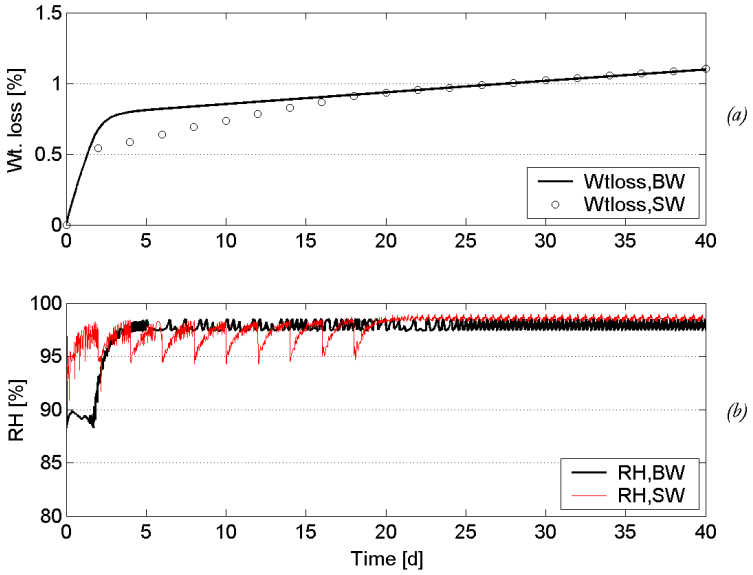

Figure 6.4 (a) Accumulated weight loss of the batch wise and the stepwise loading conditions and (b) their respective room air relative humidity's (BW: batch wise; SW: stepwise)

6.3.1.3 Product firmness loss

Figure 6.5 shows the firmness loss of the stored produce of the two loading strategies and their respective room air concentrations of the respiratory gases. The advantage of the batch wise over the step wise loading is that once the room is full and once it attains the product set point temperature the '*burning*' operation can start (in practice this is about 5-10 days after filling depending on the size of the cool cells). While in the stepwise loading, the '*burning*' operation cannot start until all the cells are full. The observed difference in firmness is the maximum that can occur,

that is the difference in firmness between the first batch loaded in the batch wise and stepwise schemes. This difference closes to zero for the last batch, as in both cases the '*burning*' operation starts at about the 25th day after the start of loading of the first batch. Overall, considering the whole produce and the biological variability (and thus the accuracy of the model) the observed difference may not be significant. However, as it is proven that fruit stored under optimal respiratory gas concentrations exhibit higher firmness than in normal air, this difference may be significant when lengthy stepwise loading periods are considered. Hence, it might be interesting to quantify the financial implication of the observed difference. At storage time of 120 days (4 months), the firmness of the first batch of the batch wise–loaded fruit is around 60 N and that of the stepwise-loaded, 57 N. It is evident that there is a strong correlation between the firmness and the background colour of the fruit. Hence, there is a fair chance that these fruit lie in different quality groups, for instance in the high price category (500 - 550 € ton^{-1}) and the second level price category (450 – 475 € ton^{-1}) (Figure 6.2). This means a difference in selling price of 50 – 75 € per ton. Assuming a cool cell contained 130 tons of fruit an apparent loss of 6500 € per cell is incurred.

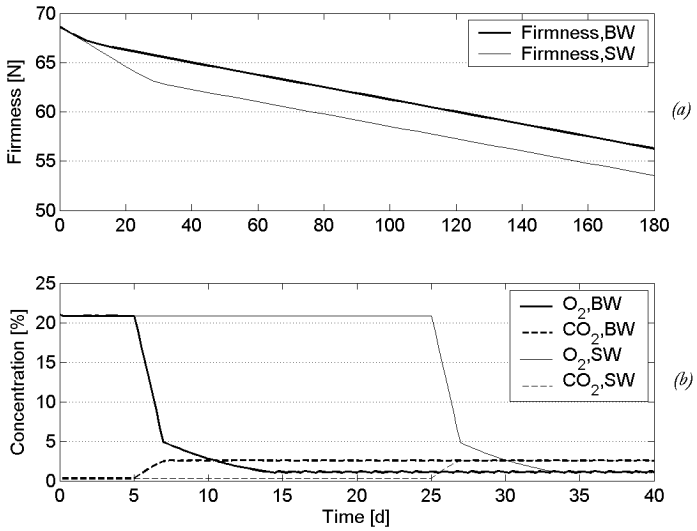

Figure 6.5 (a) Firmness loss of stored produce of the first cell of the batch wise and in one of the cells of the stepwise loading schemes (b) their respective respiratory gas concentration profiles. (BW: batch wise; SW: stepwise)

6.3.2. Effect of loading strategy on mechanical plants' performance/design

6.3.2.1 Refrigeration unit

The effect of the product loading strategy on the refrigeration unit is depicted in Figure 6.6a. In the case of the batch wise product loading condition, the heat load imposed on the refrigeration unit is delivered from the cell(s) that are packed to their capacity (product heat load and losses) and the rest of the cells to maintain their room air temperature set point (losses). In this case, less load fluctuation is observed as compared to the stepwise loading scheme where the heat load comes from the 10 partially filled rooms. This is because of the fact that in the case of stepwise loading, instantaneous high capacity requirement is demanded from all the cells operating in parallel while the plant is left idle on other instances.

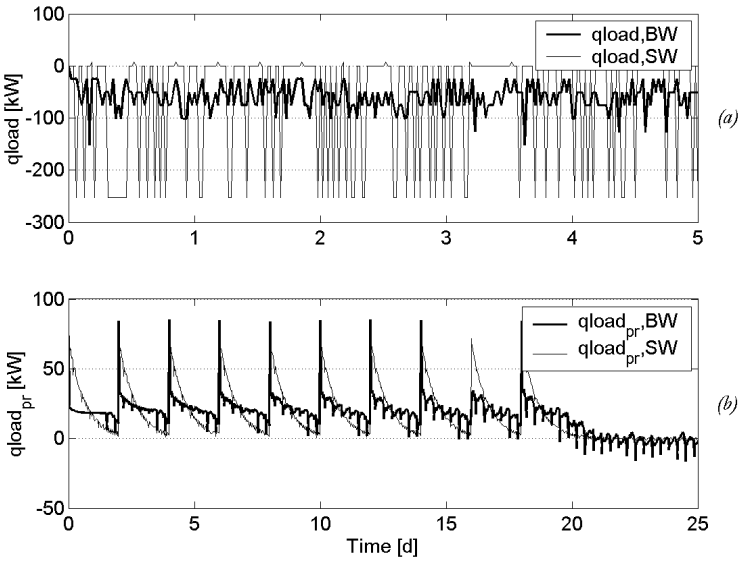

Figure 6.6 (a) Heat load on the refrigeration plant with 10 ULO cells for batch wise and the stepwise loading conditions and (b) their respective product heat load. (BW: batch wise; SW: stepwise)

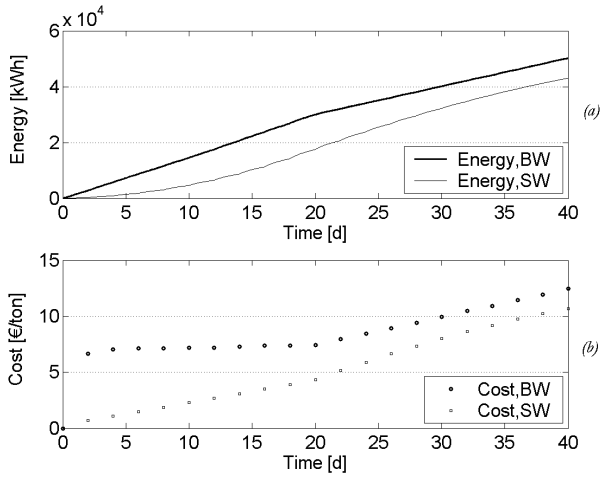

Figure 6.7 (a) Cumulative cooling and storage heat for the batch wise and the stepwise loading conditions and (b) their respective cost per ton of product. (BW: batch wise; SW: stepwise)

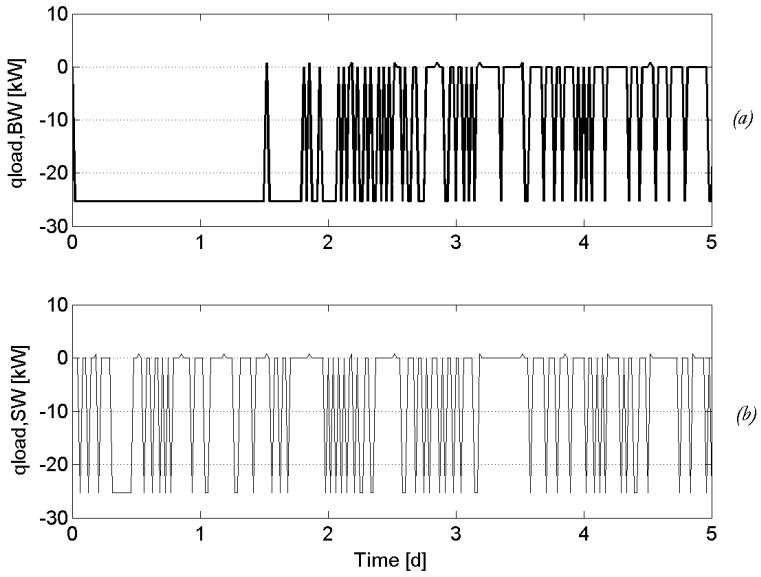

Figure 6.8 Individual cell refrigeration loads for (a) batch wise loading and (b) stepwise loading conditions. (BW: batch wise; SW: stepwise)

The major heat load is imposed by the product field heat (latent and sensible) and respiration heat. In Figure 6.6b, the product heat load component is shown for the two cases. In the case of the batch wise loading condition, a peak and drastic decrease is observed at each loading event. This drastic decrease at the beginning was caused by the heating up of the room temperature, thus decreasing the driving force, and resulting in a lower heat load. Subsequently, a slower rate of decrease is observed as compared to the stepwise loading condition. In order to estimate the energy usage by the refrigeration unit, the area under the heat load curves (Figure 6.6a) was calculated. This is depicted in Figure 6.7a where the evolution of the cumulative energy usage during the storage period is shown. This comparison shows that operationally the stepwise loading is profitable. It should be noted here that the energy needed to keep the unloaded rooms at the set point room air temperature in the case of the fully loaded condition is considerable (for the last room it was more than 18 days running) and can be reduced by setting them in to operation at the appropriate time. In Figure 6.7b the cost of cooling and storing is shown per ton of produce. In the case of batch wise loading, it is observed that there is a large increase in the cost per ton of produce at the beginning and afterwards a gentle increase as more and more products are loaded. This shows that the load imposed on the refrigeration unit at the beginning was higher compared to the stepwise loading. It should be noted that if extrapolated to 180 days of storage, there exists only a marginal difference in the total cost to cool and store 1 metric ton of produce (Jonagold apple in this case), which amounts to ±45 € ton^{-1}.

From the design point of view, the available refrigeration capacity for the stepwise loading scheme was not efficiently used, as the plant remains idle for most of the time and thus operating at sub-optimal conditions. This scenario is caused by the excess capacity of the individual evaporators (coolers) in the cool cells, which suggests a smaller capacity coolers could be proposed implying smaller capacity refrigeration plant as a whole. On the other hand, in the case of the batch wise loading, though the unit is not idling, the maximum capacity could not be utilized. Given that the cooling rate depicted in Figure 6.3a is to be maintained, the individual capacity of the cooler should be retained. As can be read from Figure 6.8a, during the first two days the maximum capacity of the cooler was employed. However, since the load is distributed in time taking only one cell at a time, again, implies a smaller capacity refrigeration unit. However, it should be noted here that the idealised considerations depicted such as the product arriving every other day may not be realistic. Hence the latter implication may not hold in operation conditions other than these.

6.3.2.2 Gas handling unit

N_2 generation unit

In Figure 6.9, the N_2 requirement for the '*burning*' operation in each case of the loading schedule with their respective O_2 concentration profiles is shown. It is to be recalled that the N_2 generator was attached to a buffer tank from where the injection to the rooms was carried out. Since in the case of the step wise loading the cells are set into ULO operation at the same time, the load on the N_2 generator is obviously, 10 times (from the 10 cells) higher as compared to batch wise product loading schedule. In reality, the assumption that the cells get filled at the same time is hardly met. Thus, for instance, the requirement in the stepwise loading can be reduced by 50% if the burning operation of the cells was scheduled in an interval of 10 hours instead of at the same time. This means that the '*burning*' of the last room will start 90 hours after the first one (injection time of less than 50 hours for each cell as can be seen from Figure 6.9c), which might have slight but not considerable effect on the firmness loss of the fruit. This shows that the way the cool rooms are loaded has substantial implication on the size of the equipment and thus the investment cost.

In design considerations, these two situations depict the required minimum and maximum N_2 generation capacity and, hence, the demand for N_2 generation falls between these limits. Practically, the capacity of the N_2 generation unit is determined by optimising the gas flow rate (99-97% N_2) to the cells and the time required to pull down the O_2 concentration to less than 5% (typically 30-50 h). This depends on the size and capacity of the cells, the type of produce and the loading situations. Thus, for a given cell capacity, the optimal gas flow rate and pull-down time, and thus the size of the unit, can be determined by simulating different loading situations and by using various produce using the present tool.

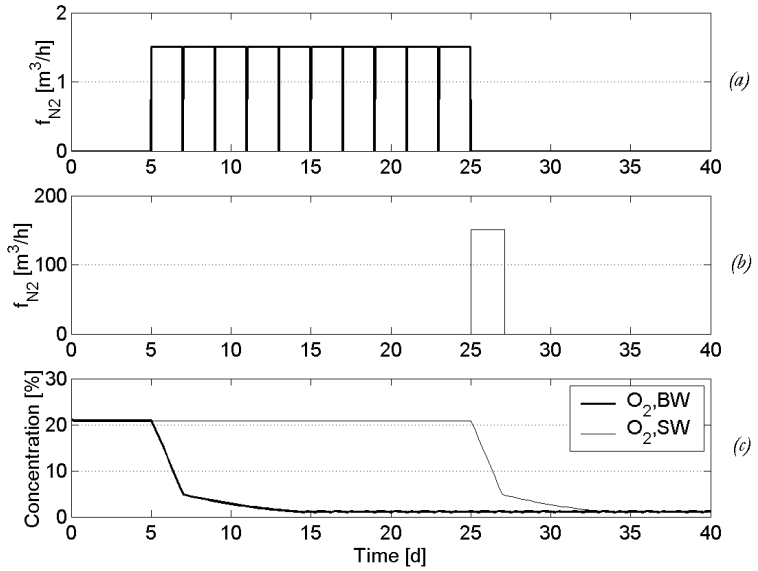

Figure 6.9 (a) N_2 requirement in batch wise product loading for 10 cells (b) N_2 requirement in step wise loading for 10 cells (c) respective O_2 profiles in the first cell of the batch wise scheme and in one of the cells in the stepwise scheme (BW: batch wise; SW: stepwise)

CO_2 scrubber

In Figure 6.10, the rate of CO_2 production in the 10 cells and the respective CO_2 concentration profiles for the two product loading schedules is shown. It is observed that at the end of the loading period (day 20) there exists a difference of more than 120 kg_{CO2} d^{-1} in rate of CO_2 production. At this moment, more than half of the batch-wise-loaded cells already attained the set point concentrations of the respiratory gases where the rate of respiration is more than 70 % slower. When the step-wise-loaded cells were set into ULO operation (day 25), a drastic decrease in CO_2 production is observed before it stabilizes to the value of 73 kg_{CO2} d^{-1} that is the value obtained in batch wise loading, as can be read from Figure 6.10a. This rate is the load the scrubber unit should remove from the cells during the storage period of the fruit.

During the transient state of the respiratory gas concentrations, it was observed that for the stepwise loading (cells operate in a parallel mode), a single scrubber could not

handle the load causing a long queue and, as a result, considerable build up of CO_2 in the cells. Thus, the results as shown in Figure 6.10 was obtained by using two scrubbers for the stepwise loading scheme, handling 5 cells each. However, during the steady state the scrubbers were idling most of the time. In the case of the batch wise charging, only one scrubber could handle the load with a maximum of three cells being in the queue at times. This means a maximum delay of 40 minutes (the scrubber needs 20 min per cell, 10min for scrubbing and 10 for regenerations) and without substantial effect on the concentration of the CO_2 in the cool cells. When the total amount of operation time of the scrubber was calculated, it was found 300.67 and 200.33 h (for both scrubbers) for the batch wise and stepwise schemes, respectively during the storage period of 40 days. This is understandably so because in the case of batch wise loading the scrubber starts working at much earlier time (day 7 as compared to day 25) and is operating one at a time and maintaining the rooms at the set point. This means that during the transient period, the batch wise scheme incurs higher operational cost. However, it should be emphasised that the cost incurred by the whole gas-handling unit is insignificant as compared to the refrigeration cost (For instance, the adsorbed kW of a unit that can handle 300kg_{CO2} d^{-1} is about 1.8. This means that for the 300.67 hours of operation during 40 days, a cost of 0.32 € ton^{-1} is incurred).

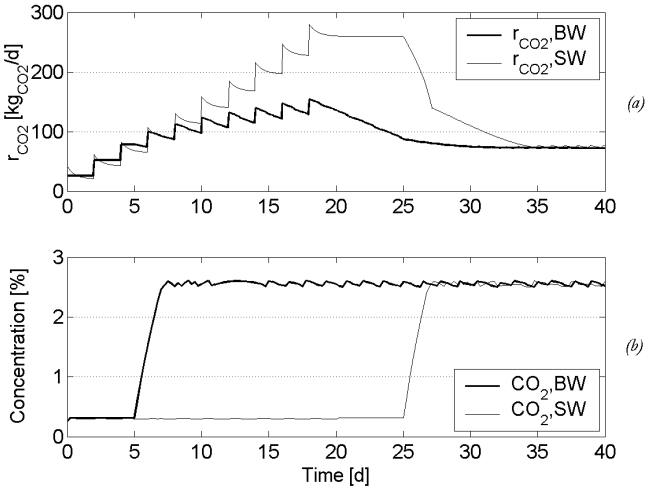

Figure 6.10 (a) Rate of CO_2 production for step wise and batch wise product loading (b) respective CO_2 profiles in the first cell of the batch wise scheme and in one of the cells in the stepwise scheme (BW: batch wise; SW: stepwise)

6.4. Discussion

As an application of the global CA cool storage model, the implication of some practical operational issues, related to product loading strategies, to the product quality, mechanical plants performance and design aspects was investigated. With regards to product quality, it was found that no difference in cumulative moisture loss was observed. However, the batch wise product loading was apparently advantageous with regards to firmness loss of the produce. In general, the influence of the considered product loading schemes on the product quality was apparent. Concerning the refrigeration plant, less load variation was observed in the batch wise loading but it was marginally energy intensive over the stepwise product loading strategy. Considering sizing of the refrigeration plant, the batch wise scheme required high capacity individual evaporators as compared to the stepwise loading. However, overall, the capacity of the refrigeration unit is not affected by the product-loading scheme. During transient situations, higher plant capacity was required for the gas-handling unit (N_2 generator and CO_2 scrubber) in the case of the stepwise loading scheme, due to parallel working mode of the cells. Nevertheless, 33% higher operational time was required for the CO_2 scrubber when batch wise product loading strategy was used.

In operational and market situations other aspects are considered in practice, where the decision to go for either one of the strategies is based upon. This has to do with the freedom of decision the growers stipulate as to when to sell their produce. When this flexibility is required, the stepwise loading strategy is ideal because *(i)* the cell(s) a grower hires are not shared and he can load them at his own picking rate and *(ii)* does not interfere with other growers' decision and can sell his produce at his own choosing when he thinks the price is profitable. On the other hand, when collective decisions drive the market the batch wise loading is preferred because of its simplicity in scheduling, the available storage space and somewhat easier operational condition with respect to loading of the product.

The light this investigation sheds on these choices is that at what cost, besides the operational conditions and flexibility, are these decisions made. From this perspective, the decision can be weighed in its multi facets of product quality, plant performance and operational and market conditions. Based on that, other loading strategies can be designed which for instance consider the combination of the two strategies, achieved by allocating some of the available storage space to stepwise and the rest to batch wise product-loading strategies.

6.5. Conclusion

In conclusion, it was demonstrated that the global CA cool storage model could be used for sizing (design) and evaluation of plant performance taking into consideration the implication on the product quality. Other areas of application include development of new control strategies and tuning of controller parameters and model based product control. Concerning the latter, since sensor based automatic control of product quality can prove to be difficult, the control of the *'a priori'* known optimal set points can be assisted by model based product quality control. In this case, the response from the quality models is fed to the controller for better maintenance of the microenvironment for overall plant optimal operation and increased final product quality.

Reference

Veraverbeke, E.A., Verboven, P., Van Oostveldt, P., Nicolai, B.M. (2003). Prediction of moisture loss across the cuticle of apple (*Malus sylvestris* subsp. *mitis* (Wallr.)) during storage: Part 2. Model simulations and practical applications. *Postharvest Biology and Technology*, 30(1), 89-97.

www 1. http://www.bfv.be/media/pdf/Brochure%20EN.pdf. Accessed on August 30, 2003.

PART II

Optimal experimental design for estimating thermal properties of biological materials

Chapter 7

Optimal experimental design for estimating thermal properties of biological materials

7.1. Introduction

The accurate knowledge of thermal properties of foods and agricultural products play an important role in successful modelling and simulation of heat transfer processes in an effort to extend their shelf life. The involved thermophysical properties are the thermal conductivity k, the density ρ and the heat capacity c. The latter two can be brought together as one parameter, namely, the volumetric heat capacity. Besides the estimation of these parameters based on the chemical composition using empirical equations, various measurement methods involving steady or transient state heat transfer exist. Among others, the transient hot wire probe method emerged as the method of choice owing to its accuracy and is therefore extensively used (Bristow et al., 1994). In this method, a needle with a heating wire is inserted in the sample and the heating is started. The thermal conductivity (and with some modification, the volumetric heat capacity) can then be

calculated from the time-temperature data measured in the probe or at some position in the product.

Recent interests are directed towards the simultaneous estimation of the thermophysical properties by means of single or dual heat probe methods (Moysey et al., 1977; Chang et al., 1980; Bristow et al., 1994; Tagawa et al., 1996). Commonly recognized as important properties contributing to the parameter estimation accuracy are both quality and quantity of the experimental data. High quality data are mostly acknowledged as experimental observations featuring low measurement error. Moreover, the persistency of excitation of the system evoked by the applied experimental input (in this case the heat generation) noticeably contributes to the unique and accurate estimation of the involved parameters. This means that if the dissipated power fails to excite the probe-food system, the measured signal may not be sufficiently rich to estimate the parameters simultaneously. Likewise, the degree of excitation may not be equal at every location in the sample, leading to the existence of an optimal measurement position associated to a given heat generation profile applied. It is, hence, worthwhile to evaluate the *information content* of an experiment with respect to these factors.

This Chapter deals with the application of optimal experimental design techniques to the estimation of thermophysical properties of biological materials. It is concerned with the design of optimal experiments, heating strategy and measurement position in particular, that contribute to unique and accurate estimation of the parameters simultaneously. The developed methodology can ultimately be employed for accurate and simultaneous estimation of not only thermal properties but also other product parameters such as those involved in respiration and product quality models. Accordingly, this Chapter is divided into six sections. In Section 7.2, the state-of-the-art on measurement techniques and application of optimal experimental design will be discussed. In Section 7.3, first the experimental set up employed in the present study will be described, followed by the discussion on the conduction heat transfer model structure and the geometrical model. Finally, the theoretical framework of the optimal experimental design and its application to the problem at hand will be presented. In Section 7.4, the resulting model will be validated using dynamic and static profiles and investigation of these profiles with respect to their information content will be carried out using theoretical (mathematical) experiments. Moreover, the optimal sensor position for a given heating strategy will be identified and implementation of the obtained results will be carried out. Subsequently, optimisation of parameterised profiles will be performed by means of modern global optimisation algorithms followed by experimental implementation of the optimal

heating profile obtained. The results will be summarised and discussed in Section 7.5 and conclusions will finally be drawn in Section 7.6. The results presented in this Chapter are published in Nahor et al. (2001), Nahor et al. (2003) and Nahor et al. (2004).

7.2. Literature review

Since the hotwire probe method proved to provide reputable results, a great deal of effort has been made towards simultaneous estimation of thermophysical parameters of various substances (e.g., soil, various food products) using this method. Both steady state and transient methods were applied. Steady state heating methods require maintenance of a constant temperature gradient within the sample, thus longer heating time. This can trigger water movement in response to the applied temperature gradient, thereby altering the thermal property one is attempting to measure. For this reason transient methods are usually preferred.

The hotwire probe method, which was developed by Hooper and Chang (1952), approximates the line source method. The latter was first developed by Stalhane and Pyk in 1931. In this method, the probe is inserted in a medium, whose parameters are to be estimated, initially at uniform temperature. The heater is turned on and the rate at which the applied heat is transmitted away from the probe depends on the thermal properties of the medium. One or more of the thermal properties can be determined by analysing the temperature response adjacent to the heat source or at a sensor located some distance away from the heat source. Often the methods of analysis are based on approximate analytical solution of the heat conduction equation for an infinite line heat source applied to a homogeneous isotropic medium, which is at uniform initial temperature. Due to this reason, the application of heating is limited to constant heating or instantaneous heat pulses. For the latter, since it is practically difficult to achieve instantaneous heating the ideal case has been extended for short duration pulse heating. The approximate solutions of the conduction equation for these heating profiles (ideal and extended versions) commonly employed in literature are summarized in Table 7.1.

Hereafter some of the major contributions to the state-of-the-art in estimating thermal properties of various loose-filled materials will be considered in some detail. It should be mentioned at this stage that it is not the intention to give an exhaustive list of investigators and their work; rather the representative methodologies employed by the wide range of investigators will be outlined. Moreover, the application of the optimal experimental design in various fields of study will be cited.

Chang et al. (1980) estimated the thermal conductivity and the specific heat of grain dust using single and dual probe hot wire methods. The infinite line source approximation for constant heating has been employed. To compensate for the finite diameter of the heating element a delay t^0 has been introduced which was determined from the experimental data. The dual probe has been used to estimate the specific heat. The results obtained by regression analysis from the single and dual probes for thermal conductivity, were compared and reported to be in good agreement.

Table 7.1 Summary of approximate solutions used for the hot wire probe method (for the symbols, refer to the nomenclature list)

Heating	**Equation**
Constant	$\Delta T = \frac{Q_l}{4\pi k} \ln \frac{t_2}{t_1}$
Instantaneous pulse	$\Delta T(r,t) = \frac{q}{4\pi k t \rho c} \exp(-\frac{r^2}{4kt})$
Short duration pulse	$\Delta T(r,t) = \frac{Q_l}{4\pi k} \text{erfc}\left(\frac{r}{\left(4(k/\rho c)t\right)^{\frac{1}{2}}}\right)$ for $0 < t < t_o$ $\Delta T(r,t) = \frac{Q_l}{4\pi k}\left\{\text{erfc}\left(\frac{r}{\left[4(k/\rho c)(t-t_o)\right]^{\frac{1}{2}}}\right) - \text{erfc}\left(\frac{r}{\left(4(k/\rho c)t\right)^{\frac{1}{2}}}\right)\right\}$ for $t \geq t_o$

Larson (1988), simultaneously estimated the thermal parameters of soil using a multi-needle probe (one heating and two sensors) applying the instantaneous pulse heating method. He used curve-matching procedures to estimate the parameters at different moisture contents. Achievement of shorter observation times and avoidance of thermal gradients were reported by using pulsed heating as compared to constant heating.

An in depth review of the hot wire probe method and parameter estimation procedures has been given by Bristow et al. (1994). They discussed the application of the method to determine the thermal parameters of soils. In their study, short duration pulse heating was used and the measurements were analysed using the

equations both for the instantaneous heating and the extended theory for the short duration heating. The results from both theories were compared. Several factors that influence the estimation procedure such as the sensor position (with respect to heating wire) and duration of the pulse heating were also investigated. Linear and non-linear regression analyses were used as parameter estimation techniques. Concerning the comparison of the instantaneous heating and the extended theory, they demonstrated that the former is not adequate to estimate the thermal conductivity, though the volumetric heat capacity can be estimated with acceptable accuracy. This, they reasoned, is attributed to the fact that the maximum temperature difference obtained during the heating period, which contains the information for estimating the volumetric heat capacity, was approximately the same for the two theories. The time occurrence of the maximum temperature difference contains the information regarding the thermal conductivity, which was found to be significantly different. Statistically significant differences in estimated thermal conductivities were observed when varying the pulse width for both the single and dual probes and they reported that the reason was unclear. Concerning the heat capacity, despite the observed trend with increasing pulse width, this was not statistically significant at 95 and 99% confidence interval. Moreover, the estimated values appeared to be smaller than those computed using the composition of the soil. They also reported that no significant difference in thermal properties was observed due to probe spacing away from the heating probe. Errors in positioning the probe can cause errors on the estimation of the heat capacity significantly. Other sources of error have also been investigated.

Later in 1995, Bristow et al. investigated different parameter estimation procedures such as those that use a single point and non-linear model fit algorithms using the dual probe method. From their investigation they concluded that the non-linear model fit algorithm proves to be more versatile especially when the data collection involves considerable noise. They also proposed that an appropriate finite probe model in place of the approximate infinite line heat source method could be appropriate. An in depth error analysis of the heat pulse method for measuring soil thermal properties has been carried out by Kluitenberg et al. (1995).

A somewhat different approach was pursued by Tagawa et al. (1996) in their attempt to estimate the thermophysical properties of beans as a function of temperature, using the transient single probe method by applying constant heating. They considered a probe of finite diameter instead of the approximation that the probe is a line heat source. This resulted in the inclusion of additional parameter, namely, the contact resistance. A non-linear least square method was used to estimate four

parameters defined by one or more of the thermal parameters including the contact resistance. The non-linear simultaneous equation solving techniques were employed to solve for the thermal parameters. Neither comparison to estimates mentioned in the literature nor verification by an independent measurement was carried out.

From the above discussion, it is clear that the endeavours of the investigators are directed towards using approximate analytical solutions of the governing equations. Due to the rigidity of the method, only limited types of heating profiles have been investigated. Moreover, their purely experimental approach restricted more investigation towards factors affecting the estimation process such as optimal sensor position and optimal heating duration.

Parameter estimation quality in terms of its accuracy and confidence depends on the quality and quantity of the experimental data. Besides, the *information content* of the experimental data induced by the applied experimental inputs also influences the parameter estimation quality noticeably when experimental data are presented to the parameter identification algorithm. Optimal experimental design techniques have been applied in several fields to investigate the information content of an experiment (see, e.g., Versyck et al., 1997; Bernaerts et al., 2000, for examples in predictive food microbiology).

In heat transfer, Taktak et al. (1993) applied optimal experimental design for estimation of thermal properties of composite materials using finite and semi-infinite body and employing the approximate analytical solution. On one side of the body was subjected to a constant flux produced by a heater and the second boundary was maintained at constant temperature. Experimental optimisation with respect to the heating time and the sensor location were carried out.

The experimental design methodology aims at finding experimental modus operandi such as initial conditions, experimental inputs, sensor location, which guarantee unique estimation of the model parameters with greatest statistical confidence. However, this technique has not yet been exploited in food technology with respect to estimation of thermophysical properties of biological materials in general, thus the present work.

7.3. Materials and methods

In this Section, the materials and methods used to develop the methodology for simultaneous estimation of the thermophysical properties of biological materials uniquely and with great statistical confidence, will be presented. First, the experimental set up and its design and implementation will be described. Next, the

underlying theories of heat conduction and the methods to solve the model equations will be discussed. Subsequently, the theoretical framework of optimal experimental design for parameter estimation and its application to the problem at hand will be explained.

7.3.1. Experimental set up

In this work, a dual probe hot wire set up was developed. The set up consists of a hot wire probe constructed from a stainless steel hypodermic needle 21G x 2" (Terumo, The Netherlands) which encases an insulated constantan (Cu55/Ni45) resistance wire (Good fellow Cambridge Ltd., UK) with 0.07mm diameter. Constantan was selected for its distinct characteristics that the resistance is practically independent of temperature. The remaining space in the needle hole was filled with a heat tolerant resin (810 electrical resin, Schotchcast, Germany). The probe was inserted at the geometrical centre of a container (D=35 mm and L = 90 mm) filled with medium. A T-type thermocouple was used to measure the temperature in the medium at a known distance from the heating probe. Electrical current was supplied to the heating probe by a DC power source (HP E3632A, Agilent technologies, U.S.A.), which is equipped with a multi-meter to measure the voltage and current. For the acquisition of the time temperature data and the applied power a data logger (HP 34970, Agilent technologies, U.S.A.) was used. As heat transfer media, agar and tylose gels were selected for the fact that their thermal properties are similar to that of most food substances. Agar gel was prepared by adding a weighed amount of agar (Merck, Dermstadt, Germany) in water in such a way that the mixture will have moisture content of 98% wet basis. The thermophysical properties of agar gel are the same as that of de-iodised water (van Haneghem, 1981). At 20°C, these parameters are $\rho c = 4.18\times10^{6}$ $\mathrm{Jm^{-3}°C^{-1}}$ and $k = 0.6$ $\mathrm{Wm^{-1}°C^{-1}}$ (Incropera and De Witt, 1990). Tylose is a methylcellulose gel prepared by mixing the tylose powder with water to give final moisture content of 77% wet basis. The properties of tylose gel are $\rho c = 3.712\times10^{6}$ $\mathrm{Jm^{-3}°C^{-1}}$ and $k = 0.56$ $\mathrm{Wm^{-1}°C^{-1}}$ (Riedel, 1960). These thermophysical properties of the food simulants were assumed to be the nominal parameters. The schematic representation of the employed set up and the detail of the hot wire probe are shown in Figures 7.1(a) and (b), respectively. In order to control the hardware for the dynamic heat generation profile and the synchronization of the data acquisition from the different measuring devices, a code was developed using the LabView data acquisition environment (National instruments Co., Austine Texas).

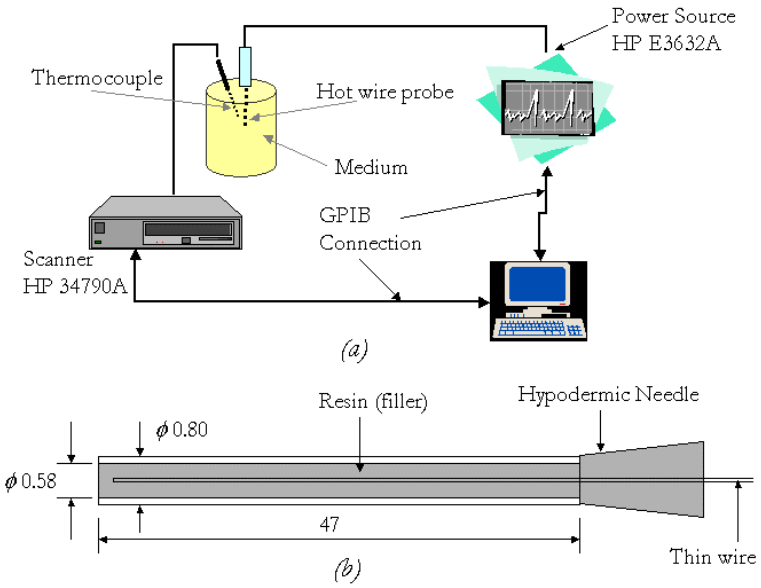

Figure 7.1 (a) Schematic representation of hot wire probe set up, (b) Details of the heating probe (dimensions in mm)

7.3.2. Conduction heat transfer model

A quantitative description for conduction heat transfer is given by means of the Fourier equation. For transient three-dimensional flow with heat generation and constant parameters, it reads as:

$$\rho c \frac{\partial T}{\partial t} = k\nabla^2 T + Q(t) \tag{7.1}$$

where ρc is the volumetric heat capacity [J m^{-3} °C^{-1}]; T the temperature [°C]; t the time [s]; k the thermal conductivity [W m^{-1} °C^{-1}] and Q the volumetric heat generation [W m^{-3}]. The initial condition for the Fourier equation can be described as a spatial function at $t = 0$.

$$T(x, y, z, t) = T_0(x, y, z) \quad \text{at} \quad t = 0 \tag{7.2}$$

At the boundary Γ of an object, different types of heat transfer conditions can take place. The most common in thermal food processing applications is the convective boundary condition given by:

$$-k\left(\frac{\partial T}{\partial n}\right) = h\left(T - T_{\infty}\right) \text{ on } \Gamma \tag{7.3}$$

where n is the outward normal to the surface; h the heat surface transfer coefficient [W m^{-2} °C^{-1}] and T_{∞} the surrounding temperature [°C].

7.3.3. Finite element model

The conduction heat equation can be solved using analytical or numerical methods. With respect to the estimation of thermal properties, analytical methods are restricted to simple geometries and limited, often to static, heat generation profiles. To overcome these limitations, numerical methods are preferred.

The finite element method is a numerical procedure for solving physical problems governed by partial differential equations. In this method, a geometrical model is defined and subdivided into a finite number of elements, which are interconnected by a finite number of nodes (Zienkiewicz, 1994). Next, the unknown temperature is approximated by low order polynomials that interpolate in the nodal values. The polynomial is represented in terms of a linear combination of *shape functions*. Applying the Galerkin weighted residual method results in the following first order system of differential equations.

$$\mathbf{C}\frac{d\mathbf{u}}{dt} + \mathbf{K}\mathbf{u} = \mathbf{f} \tag{7.4}$$

where **C** is the global capacitance matrix, which is a function of the volumetric heat capacity; **K** the global conductance matrix, which is a function of the thermal conductivity and heat transfer coefficient; **f** the global load vector, which is a function of the input parameters and boundary conditions, and **u** the vector which contains the approximate temperatures at the nodes. For numerical details of the finite element method, the reader is referred to, e.g. Segerlind (1984).

The geometric model of the hot wire probe set up considers the detailed components of the heating probe, namely the heating wire, the filler resin, the needle

wall, as shown in the schematic representation, Figure 7.2. A 1-D finite element model consisting of 42 nodes and 41 1-D axi-symmetric linear iso-parametric elements was obtained. The heat generation *Q(t)* was applied on the heating element during problem solving. The finite element model was implemented in MATLAB (The MathWorks Inc., Natick, Massachusetts).

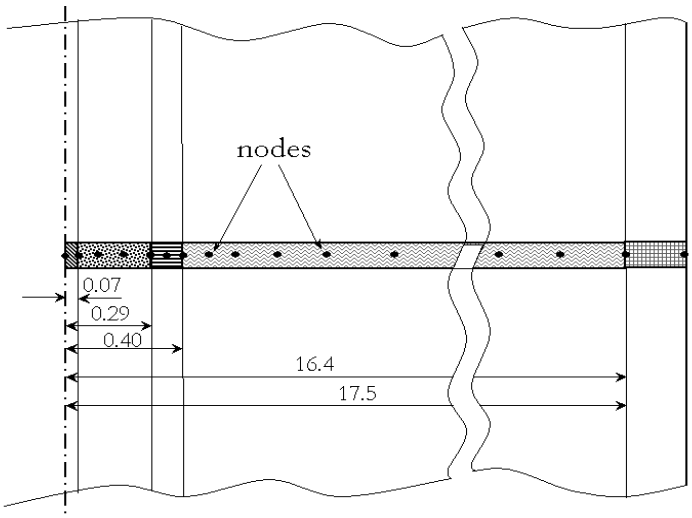

Figure 7.2 1-D axi-symmetric geometric model (Dimensions in mm)

: Constantan wire, : Resin, : Stainless steel, : Medium, : Copper

7.3.4. Model validation method

Validation of the proposed model was carried out using agar gel and tylose as media. Several static and dynamic heat generation profiles, shown in Table 7.2, were implemented. The simulated temperatures and measured output were compared, and as a measure of agreement between the two quantities, root mean square errors were calculated as:

$$\mathrm{RMSE} = \left[\frac{1}{n} \sum_{i=1}^{n} \left(T - T_m \right)^2 \right]^{\frac{1}{2}} \tag{7.5}$$

where n is the number of data points; T the predicted temperature value [°C] and T_m the measured temperature value [°C].

Table 7.2 Dynamic and static heat generation profiles for validation

Heating profile	**Medium**	**Profile category**	**Power [W] and t [s]**	**Final time t_f [s]**
AS1	Agar	Static	0.3	300
TS2	Tylose	Static	0.5	300
AB1	Agar	Dynamic	0 $0 \le t \le 38$ 0.5 $38 < t \le 96$ 0 $96 < t \le 136$ 0.5 $136 < t \le 196$ 0 $196 < t \le 238$ 0.5 $238 < t \le 300$	300
TB2	Tylose	Dynamic	0 $0 \le t \le 40$ 0.45 $40 < t \le 140$ 0 $140 < t \le 200$ 0.45 $200 < t \le 300$	300
AP1	Agar	Dynamic	0 $0 \le t \le 40$ 7.5 $40 < t \le 44$ 0 $44 < t \le 104$ 7.5 $104 < t \le 108$ 0 $108 < t \le 200$ 7.5 $200 < t \le 204$ 0 $204 < t \le 300$	300
TP2	Tylose	Dynamic	0 $0 \le t \le 40$ 3.75 $40 < t \le 52$ 0 $52 < t \le 252$ 3.75 $252 < t \le 264$ 0 $264 < t \le 300$	300

7.3.5. Optimal experimental design for parameter estimation: Theoretical framework

7.3.5.1 Parameter estimation

Once the structure of the model is determined, it is useful to study the structural (theoretical) identifiability, which verifies the possibility to uniquely identify all model parameters given perfect measurement data. It can be shown that the above-defined model is structurally identifiable using the Taylor series approach developed by Pohjanpalo (1978) (unpublished result). Structural identifiability, however, does not guaranty in practice that unique parameter values can be determined from any set of experimental data (Bernaerts, 2002). Practical parameter identifiability requires persistently exciting inputs yielding data that contain sufficient information to allow unique parameter estimation. In this respect, optimal experimental design techniques for parameter estimation have been developed with the objective of defining the experimental procedure such that parameters can be estimated uniquely and with greatest statistical confidence. Optimisation of the experimental procedures include initial conditions, experimental inputs, sensor location and the like.

Parameter estimation is an iterative procedure, in which parameter values are searched in such a way that some identification cost functional is minimized. The identification functional quantifies the deviation between the model predictions and the experimental data. Often, a quadratic identification functional $\Im$ is used (Eq. (7.6)),

$$\Im = \int_0^{t_f} \left(\mathbf{y} - \mathbf{y_m}\right)^{\mathrm{T}} \mathbf{Q} \left(\mathbf{y} - \mathbf{y_m}\right) dt \tag{7.6}$$

with $\mathbf{y}$ the vector of model predictions; $\mathbf{y}_m$ the vector of measured outputs; $\mathbf{Q}$ a user supplied square weighing matrix and t the time. Considering a perfect model structure and noise free data set, the parameter estimation procedure yields the nominal parameter vector $\mathbf{p}^*$. However, depending on the magnitude of the noise involved, a change in one parameter can sometimes be compensated almost completely by a proportional shift in another and gives rise to the problem of uniqueness. The effect of noise on the unique estimation of the parameters can be illustrated by means of mathematically simulated data by considering some noise and plotting the functional $\Im$ against the parameter plane. Figures 7.3(a) and (b) show

the functional and contour plots respectively, using a noise with a standard deviation of 0.05°C. As can be seen from these plots, depending on the initial guess the optimisation procedure can end up in one of the several local minima, which give different parameter combinations. Using these parameter combinations, when the predicted temperatures and the measured data are plotted, a satisfactory fit is obtained, even though the parameters deviate considerably from the nominal ones, leading to the problem of uniqueness. Since experimental data used for parameter estimation are always noise corrupted, optimal experimental design techniques are employed to foster the quality of the parameter estimation through optimal choice of experimental input and procedure.

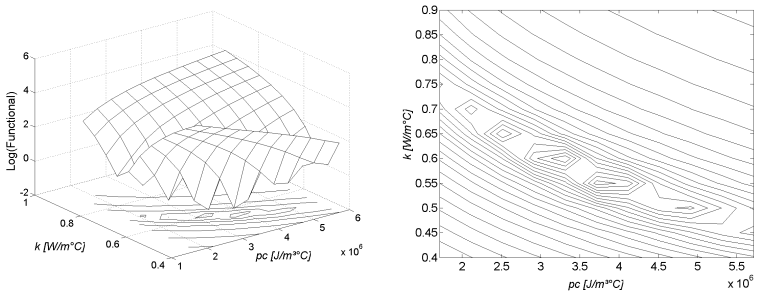

(a) *(b)*

Figure 7.3 Functional and contour plot using noise corrupted measured data (a) Functional plot, (b) Contour plot

7.3.5.2 Optimal experimental design

In the functional $\Im$ (Eq. (7.6)), the vector of temperature predictions, **y(p)** is an unknown function of the parameter vector **p** and can be linearised by using a first order Taylor expansion with respect to **p**, around the nominal parameter vector $\mathbf{p}^*$.

$$\mathbf{y}(\mathbf{p}) \cong \mathbf{y}^* + \left.\frac{\partial \mathbf{y}}{\partial \mathbf{p}}\right|_{p=p^*} \Delta \mathbf{p}^{\mathrm{T}} \tag{7.7}$$

with $\mathbf{y}^* = \mathbf{y}\left(\mathbf{p}^*\right)$. The vector $\mathbf{y}_m$ is the set of measured temperatures. In practical situations, noise and other errors always corrupt these measured data. This leads to a

relative measurement error that can be modelled by Gaussian white noise (Munack, 1989). Hence,

$$\mathbf{y}_m = \mathbf{y}^* + \mathbf{w} \tag{7.8}$$

where **w** is Gaussian white noise. This is characterised by a zero mean

$$E[\mathbf{w}] = 0 \tag{7.9}$$

and covariance function

$$E\left[\mathbf{w}(t_1)\mathbf{w}^T(t_2)\right] = \delta_{t_1 t_2}\boldsymbol{\Phi} \tag{7.10}$$

where $\boldsymbol{\Phi}$ is a positive definite matrix and $\delta_{t_1 t_2}$ is the Dirac delta function. **Q** is usually chosen as the inverse of the error covariance matrix. This implies that the more the measurement is corrupted by noise, the less it will count in the information criterion (Versyck et al., 1997).

After substitution of Eqs. (7.7) and (7.8) in Eq. (7.6) and applying the expected value operator, the following expression is obtained (Munack, 1989).

$$E(\Im) = \Delta\mathbf{p}^T \left[\int_0^{t_f} \left(\frac{\partial \mathbf{y}}{\partial \mathbf{p}}\right)^{\mathrm{T}} \mathbf{Q} \left(\frac{\partial \mathbf{y}}{\partial \mathbf{p}}\right) \, dt \right] \Delta\mathbf{p} + 2t_f \tag{7.11}$$

The term in square brackets in Eq. (7.11) is the *Fisher Information Matrix* (Munack, 1989),

$$\mathbf{F} = \int_0^{t_f} \left(\frac{\partial \mathbf{y}}{\partial \mathbf{p}} \right)^{\mathrm{T}} \mathbf{Q} \left(\frac{\partial \mathbf{y}}{\partial \mathbf{p}} \right) dt \tag{7.12}$$

The matrix $(\partial \mathbf{y}/\partial \mathbf{p})$ contains the sensitivity functions and quantifies the dependence of temperature predictions on the parameter values relative to the nominal parameter set $\mathbf{p}^*$.

With respect to the problem at hand, the parameter vector $\mathbf{p}$ has two elements namely the thermal conductivity and the volumetric heat capacity, $\mathbf{p} = [k, \rho c]$. The vector of predicted temperatures at n measurement positions is read as $\mathbf{y} = [u_1 \ldots u_n]$. The sensitivity matrix $(\partial \mathbf{y}/\partial \mathbf{p})$ can therefore be expressed as:

$$\frac{\partial \mathbf{y}}{\partial \mathbf{p}} = \begin{bmatrix} \frac{\partial u_1}{\partial \rho c} & \cdots & \frac{\partial u_n}{\partial \rho c} \\ \frac{\partial u_1}{\partial k} & \cdots & \frac{\partial u_n}{\partial k} \end{bmatrix}^T \tag{7.13}$$

Since only one online temperature measurement is available, Eq. (7.13) reduces:

$$\frac{\partial \mathbf{y}}{\partial \mathbf{p}} = \begin{bmatrix} \frac{\partial u}{\partial \rho c} & \frac{\partial u}{\partial k} \end{bmatrix} \tag{7.14}$$

The user supplied weighing matrix $\mathbf{Q}$ is often chosen as the inverse of the error covariance matrix and is given by:

$$\mathbf{Q} = \mathrm{diag}\left(\frac{1}{\sigma_1^2}, \frac{1}{\sigma_2^2}, \cdots, \frac{1}{\sigma_n^2} \right) \tag{7.15}$$

In the case where the standard deviation σ is the same for all the state variables, Eq. (7.15) reduces to:

$$\mathbf{Q} = \frac{1}{\sigma^2} \mathbf{I}_n \tag{7.16}$$

where **I** is the identity matrix and the subscript *n* denotes the size of the covariance matrix ($n \times n$).

Substituting Eq. (7.14) and (7.16) in Eq. (7.12) yields,

$$\mathbf{F} = \frac{1}{\sigma^2} \int_0^{t_f} \left[\frac{\partial u}{\partial \rho_c} \quad \frac{\partial u}{\partial k} \right]^{\mathrm{T}} \left[\frac{\partial u}{\partial \rho_c} \quad \frac{\partial u}{\partial k} \right] dt \tag{7.17}$$

Eq. (7.17) can be written as:

$$\mathbf{F} = \begin{bmatrix} F_{11} & F_{12} \\ F_{21} & F_{22} \end{bmatrix} \tag{7.18}$$

where

$$F_{11} = \frac{1}{\sigma^2} \int_0^{t_f} \frac{\partial u(t)}{\partial \rho_c}^2 dt \tag{7.19}$$

$$F_{12} = F_{21} = \frac{1}{\sigma^2} \int_0^{t_f} \frac{\partial u(t)}{\partial \rho_c} \frac{\partial u(t)}{\partial k} dt \tag{7.20}$$

$$F_{22} = \frac{1}{\sigma^2} \int_0^{t_f} \frac{\partial u(t)}{\partial k}^2 dt \tag{7.21}$$

These elements of the *Fisher Information Matrix* can be solved numerically in the time domain by using the implicit Euler method:

$$\left(F_{11}\right)_{t+\Delta t} = \left(F_{11}\right)_t + \Delta t \frac{1}{\sigma^2} \left(\frac{\partial}{\partial \rho_c} u\left(t + \Delta t\right) \right)^2 \tag{7.22}$$

$$\left(F_{12}\right)_{t+\Delta t}=\left(F_{21}\right)_{t+\Delta t}=\left(F_{12}\right)_{t}+\Delta t\frac{1}{\sigma^{2}}\left(\frac{\partial}{\partial\rho c}u\left(t+\Delta t\right)\right)\left(\frac{\partial}{\partial k}u\left(t+\Delta t\right)\right) \tag{7.23}$$

$$\left(F_{22}\right)_{t+\Delta t}=\left(F_{22}\right)_{t}+\Delta t\frac{1}{\sigma^{2}}\left(\frac{\partial}{\partial k}u\left(t+\Delta t\right)\right)^{2} \tag{7.24}$$

Since in general no analytical expression for the sensitivity functions $\partial u(t)/\partial\rho c$ and $\partial u(t)/\partial k$ exist, they are computed from the differential Eq. (7.4) given above. It is convenient to rewrite Eq. (7.4) to denote the explicit dependency of **C, K, f** and **u** on ρc and k:

$$\mathbf{C}\left(\rho c\right)\frac{d}{dt}\mathbf{u}\left(\rho c,k\right)+\mathbf{K}\left(k\right)\ \mathbf{u}\left(\rho c,k\right)=\mathbf{f}\,. \tag{7.25}$$

C, K and **u** can be expanded around the nominal parameter set $\mathbf{p}^{*}$ using a first order Taylor expansion:

$$\mathbf{C}\ \left(\rho c\right)\cong\mathbf{C}^{*}+\left.\frac{\partial\mathbf{C}}{\partial\rho c}\right|_{\rho c^{*}}\Delta\rho c \tag{7.26}$$

$$\mathbf{K}\left(k\right)\cong\mathbf{K}^{*}+\left.\frac{\partial\mathbf{K}}{\partial\mathbf{k}}\right|_{k^{*}}\Delta k \tag{7.27}$$

$$\mathbf{u}\left(\rho\mathbf{c},k\right)\cong\mathbf{u}^{*}+\left.\frac{\partial\mathbf{u}}{\partial\rho\mathbf{c}}\right|_{\rho c^{*},k^{*}}\Delta\rho c+\left.\frac{\partial\mathbf{u}}{\partial k}\right|_{\rho c^{*},k^{*}}\Delta k \tag{7.28}$$

where, $\mathbf{C}^{*}=\mathbf{C}\left(\rho c^{*}\right)$, $\mathbf{K}^{*}=\mathbf{K}\left(k^{*}\right)$ and $\mathbf{u}^{*}=\mathbf{u}\left(\rho c^{*},k^{*}\right)$.

Substituting Eqs. (7.26) – (7.28) in Eq. (7.25) and collecting like terms yields:

$$\mathbf{C}^* \frac{d\mathbf{u}^*}{dt} + \mathbf{K}^* \mathbf{u}^* = \mathbf{f} \tag{7.29}$$

$$\mathbf{C}^* \frac{d}{dt}\left(\frac{\partial \mathbf{u}}{\partial \rho c}\right) + \mathbf{K}^* \left(\frac{\partial \mathbf{u}}{\partial \rho c}\right) = -\left(\frac{\partial \mathbf{C}}{\partial \rho c}\right)\frac{d\mathbf{u}^*}{dt} \tag{7.30}$$

$$\mathbf{C}^* \frac{d}{dt}\left(\frac{\partial \mathbf{u}}{\partial k}\right) + \mathbf{K}^* \left(\frac{\partial \mathbf{u}}{\partial k}\right) = -\left(\frac{\partial \mathbf{K}}{\partial k}\right)\mathbf{u}^* \tag{7.31}$$

$\partial \mathbf{C}/\partial \rho c$ and $\partial \mathbf{K}/\partial k$ can be constructed by direct differentiation of the corresponding elemental matrices and subsequent assembly.

Now, Eqs. (7.30) and (7.31) are of the general structure,

$$\mathbf{C}^* \frac{d}{dt}\mathbf{x} + \mathbf{K}^* \quad \mathbf{x} = \mathbf{g} \tag{7.32}$$

where $\mathbf{x}$ is $\partial \mathbf{u}/\partial \rho c$ or $\partial \mathbf{u}/\partial k$ and $\mathbf{g}$ is $-\left(\partial \mathbf{C}/\partial \rho c\right)\left(d\mathbf{u}^*/dt\right)$ or $-\left(\partial \mathbf{K}/\partial k\right)\mathbf{u}^*$. Eq. (7.32) can be solved in the time domain using the implicit Euler scheme.

$$\left(\frac{\mathbf{C}^*}{\Delta t} + \mathbf{K}^*\right) \mathbf{x}_{t+\Delta t} = \frac{\mathbf{C}^*}{\Delta t}\mathbf{x}_t + \mathbf{g}_{t+\Delta t} \tag{7.33}$$

7.3.5.3 Optimal design criteria

In order to quantify the quality of the estimation, certain scalar quantities of the *Fisher Information Matrix* are employed. Several optimal design criteria have been suggested (Mehra, 1974; Walter and Pronzato, 1990).

- the modified A–criterion: maximises the trace of the *Fisher Information Matrix* given by [max(trace (**F**))]
- the D–criterion: maximises the determinant of the *Fisher Information Matrix* [max(det (**F**))], aiming at minimising the geometric mean of the identification error.
- The E-criterion: minimises the largest error, that is the minimum eigenvalue of the *Fisher Information Matrix* is maximised, given by [max(λ_{min} (**F**))].
- the modified E–criterion: minimizes the ratio of the largest (λ_{max}) to the smallest (λ_{min}) eigenvalue of the *Fisher Information Matrix*, given by $\min(\Lambda(\mathbf{F})) = \min([\lambda_{max}(\mathbf{F}) / \lambda_{min}(\mathbf{F})])$.

The clear advantage of the modified E-criterion over the rest is that the minimum value is unity. This means that for the case of two parameters, the contours of the identification functional are circles. The possible shortcoming of this criterion is that it does not take in to account the individual values of λ_{max} and λ_{min}. A criterion value close to unity may be obtained whereas the largest error is still large, i.e., the smallest eigenvalue is still small. In such a case, combining it with other optimal design criteria such as the E-criterion, which aims at minimizing the largest error ($\max(\lambda_{min})$) is advisable (VanRolleghem et al., 1995). In the present work, three criteria are used, the modified A–criterion, the D–criterion the modified E-criterion.

The above-developed algorithm of optimal experimental design was implemented in MATLAB.

7.4. Results

7.4.1. Model Validation

Comparisons of model predictions and experimental results of various static and dynamic heat generation profiles (Table 7.2) are presented in Figures 7.4 – 7.6.

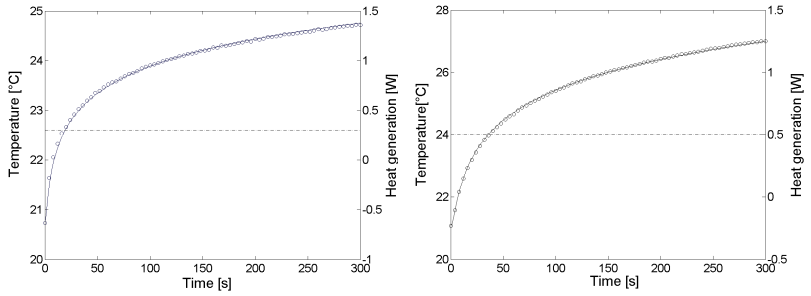

(a) *(b)*

Figure 7.4 Simulation for constant heat generation profile (a) for agar gel (AS1), RMSE = 0.03°C (b) for tylose (TS2), RMSE = 0.02°C (—: model prediction, ◦◦◦◦◦◦: measurement, ------: heat generation)

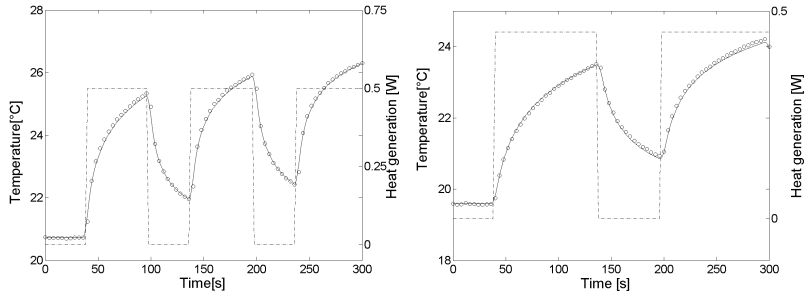

(a) *(b)*

Figure 7.5 Simulation for block-type heat generation profile (a) for agar gel (AB1), RMSE = 0.06°C (b) for tylose (TB2), RMSE = 0.04°C (—: model prediction, ◦◦◦◦◦◦: measurement, ------: heat generation)

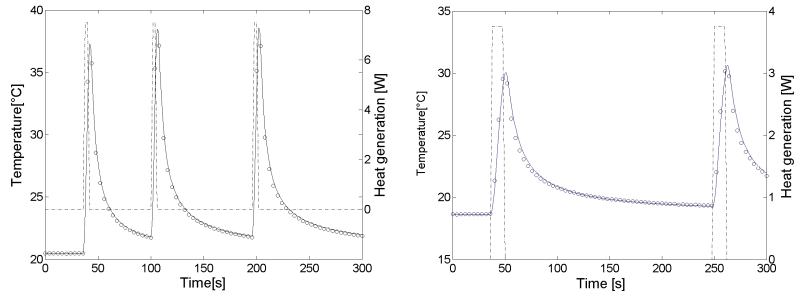

(a) *(b)*

Figure 7.6 Simulation for pulse-type heat generation profile (a) for agar gel (AP1), RMSE = 0.34°C (b) for tylose (TP2), RMSE = 0.26°C (—: model prediction, ∘∘∘∘∘: measurement, -----: heat generation)

In Figure 7.4, a constant heating profile was employed with 0.3 and 0.5W power for agar gel and tylose, respectively. In both cases, the model prediction and the measured values are in good agreement. Besides the apparent good fit, the RMSE values suggest that the accuracy of prediction is in the order of magnitude of the measurement accuracy, which was 0.5°C.

Figures 7.5 and 7.6 depict the implementation of dynamic heating profiles, block type and short duration pulse heating. In both cases, good agreement between predicted and measured values was found. Likewise, the RMSE values are with in the bounds of the measurement accuracy. Here, it is observed that as the dynamic behaviour of the heating profile increases, the RMSE values also increase. This is because the measurement frequency during the abrupt changes in temperature of the medium, caused by the sudden application of heating, was not enough.

It can, therefore, be concluded that the proposed finite element model is appropriate and, hence, can be employed for further investigations using optimal experimental design.

7.4.2. Optimal experimental design for parameter estimation: Optimal heating profile.

As mentioned earlier, the aim of optimal experimental design is to find the optimal experimental protocols such as the optimal heating profile, heating duration, and so forth. The focus here is to achieve an informative experiment by using an appropriate heating profile. This means that the level of the persistency of excitation

of the probe-food system evoked by a given heating profile is investigated through application of optimal experimental design. First, the heating profiles employed for validation were investigated for their information content with respect to the estimation of the parameters k and ρc, by simulating numerical experiments. This was achieved by introducing a realistic additive noise (σ = 0.05°C) to the model predictions. For comparison purposes a constraint has been set to the proposed heating profiles in such a way that for all cases the same amount of energy is applied. This can be mathematically expressed as:

$$E = \int_{t_o}^{t_f} Q(t)dt = 90\,\mathrm{J} \tag{7.33}$$

Moreover, the *Fisher Information Matrix* can be formulated using absolute, semi-relative and relative sensitivities (Munack (1989)). The relative sensitivity can be described as:

$$\left(\frac{\partial \mathbf{y}}{\partial \mathbf{p}}\right)_{ij} = \left(\frac{\partial y_i}{\partial p_j}\right)\left(\frac{p_j}{y_i}\right) \tag{7.34}$$

Here, the relative and absolute sensitivities were considered to calculate the optimal design criteria A, D and Modified E.

Figures 7.7 - 7.12 show the functional and contour plots of the studied profiles using agar gel and tylose as a medium. The values of the considered criteria are summarised in Table 7.3.

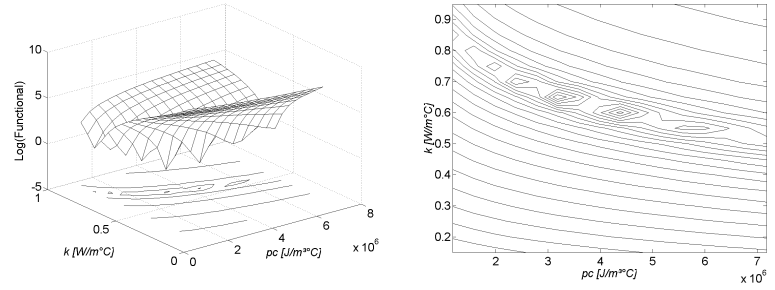

Figure 7.7 Functional and contour plot for constant heating profile using agar (AS1)

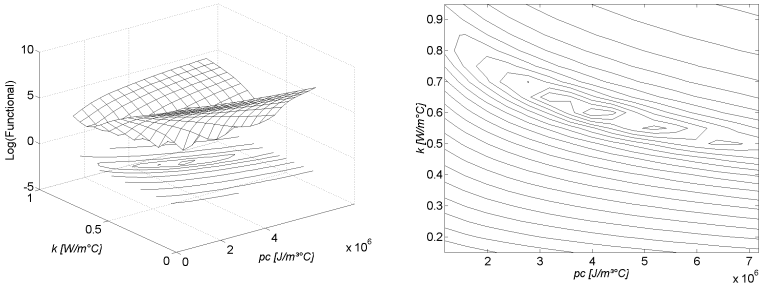

Figure 7.8 Functional and contour plot for block-type heating profile using agar (AB1)

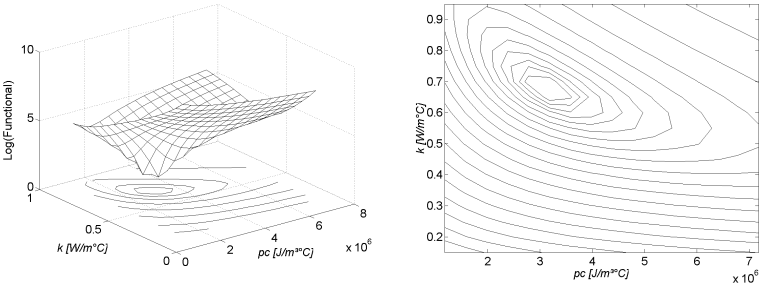

Figure 7.9 Functional and contour plot for short duration pulse heating profile using agar (AP1)

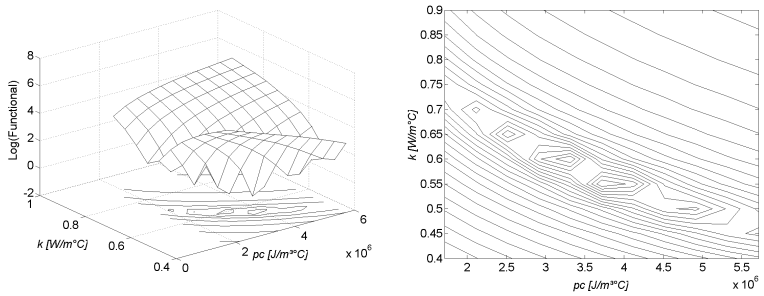

Figure 7.10 Functional and contour plot for constant heating profile, using tylose (TS2)

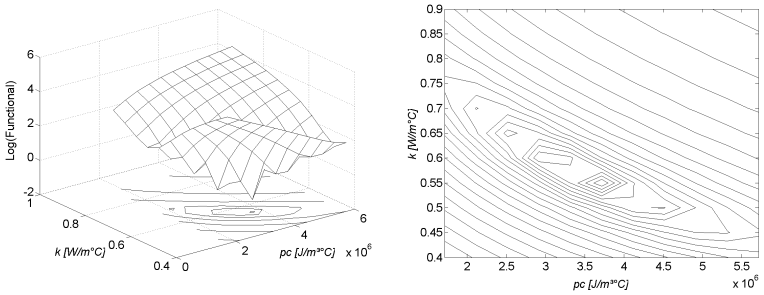

Figure 7.11 Functional and contour plot for block-type heating profile using tylose (TB2)

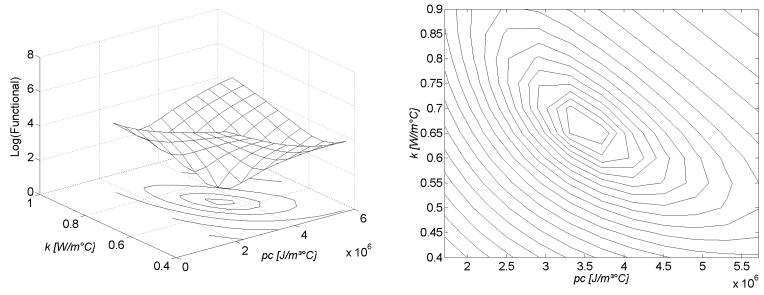

Figure 7.12 Functional and contour plot for short duration pulse heating profile using tylose (TP2)

Table 7.3 Absolute and relative values of the proposed criteria

Heating profile	Medium	Mod. E-criterion		D-criterion		Mod. A-criterion	
		Absolute	**Relative**	**Absolute**	**Relative**	**Absolute**	**Relative**
AS1	Agar	$1.32x10^{16}$	287.5	$3.84x10^{-4}$	$7.71x10^{3}$	$2.26x10^{6}$	$1.49x10^{3}$
AB1	Agar	$3.15x10^{15}$	69.24	$1.80x10^{-3}$	$3.27x10^{4}$	$2.37x10^{6}$	$1.53x10_{3}$
AP1	Agar	$3.13x10^{14}$	9.93	$6.30x10^{-2}$	$4.82x10^{5}$	$4.43x10^{6}$	$2.4x10^{3}$
TS2	Tylose	$3.11x10^{15}$	81.02	$5.90x10^{-3}$	$6.24x10^{4}$	$4.30x10^{6}$	$2.31x10^{3}$
TB2	Tylose	$9.65x10^{14}$	28.24	$2.40x10^{-3}$	$4.09x10^{4}$	$1.52x10^{6}$	$1.11x10^{3}$
TP2	Tylose	$1.37x10^{14}$	5.25	$4.60x10^{-2}$	$4.75x10^{5}$	$2.50x10^{6}$	$1.88x10^{3}$

Application of the optimal experimental design theory on the simulated theoretical experiments shows that a minimum value for the modified E-criterion was obtained (Table 7.3) when the short duration pulse heating profile was applied for both agar gel and Tylose. The D- and A- criteria also gave maximum values for this heating profile. For this profile, even though the theoretically attainable value of unity is not obtained with respect to the Modified E- criterion, it is observed from the cone-like structure of the functional plot (and circle-like contours) (Figures 7.9 and 7.12) that a unique identification of the parameters is possible irrespective of the initial guess. Observing the trend of the criteria for the considered profiles, in general, the information content of the profiles increases as one goes from the constant to the short duration pulse profile for both media. This result strongly suggests that informative experiments can be obtained by applying block-type profiles preferably with short duration heating irrespective of the medium used.

7.4.3. Optimal experimental design for parameter estimation: Optimal sensor position.

7.4.3.1 Computational results

For a given type of heat generation profile, factors that influence the information content of an experiment might be the duration and magnitude of the heat generation power, and the measurement position. This means that given, for instance, a constant heat generation profile, what should be the power dissipated and for how long should this power be dissipated to evoke the appropriate excitation of the system to enable estimating the parameters with greater statistical confidence? Moreover, as the degree of excitation might not be the same at all the points in the sample, then where should the time-temperature measurement be taken?

In order to address these questions, two types of heating profiles were chosen, namely the constant and a short duration pulse with the peak at the beginning of the experiment. These profiles were chosen for they are commonly employed in parameter estimation experiments using the hot wire probe. Moreover, the latter was found to provide more informative experiments.

First, the heat generation power was kept constant at 0.5W and 7.5W for 4s for constant and short duration pulse heating, respectively. The modified E-criterion was computed for several combinations of measurement positions and final times (durations). Discrete measurement positions are selected based on the finite element mesh and an interval constraint of [60 600 s] was defined for the final time. Subsequently, the final time was set to 300s and again the Modified E-criterion was computed for a combination of magnitudes of heat generation and measurement positions. An interval constraint of [0.3 12 W] was defined for the magnitude of heat generation. In these investigations, tylose was used as a medium.

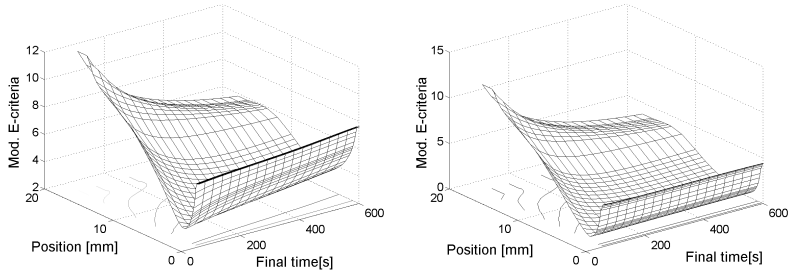

(a) *(b)*

Figure 7.13 Modified E-criterion as a function of position and final time for (a) constant heating (b) short duration heating

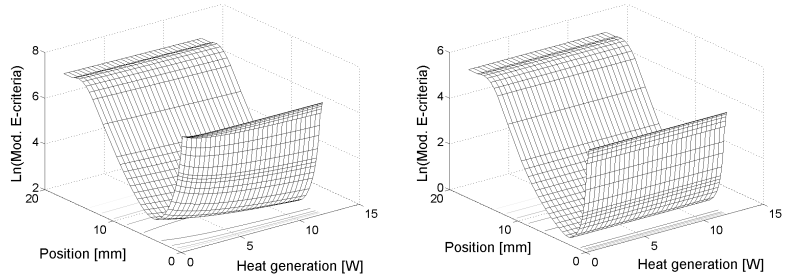

(a) *(b)*

Figure 7.14 Modified E-criterion as a function of position and magnitude of heat generation for (a) constant heating (b) short duration heating

In Figures 7.13(a) and (b) the effect of the measurement position and the final time are shown. The minimum value of the modified E-criterion obtained with a constant profile was equal to 15.53 at a distance r = 4mm from the centre of the probe with a final time of 210s. On the other hand, when using the pulse heat generation profile, the minimum value of modified E-criterion obtained was 1.22 at r = 3mm with a final time of 300s. In both cases, it can be observed that the influence of the measurement position is more pronounced than that of the final time. Moreover, the optimal measurement position remains the same irrespective of the final time for a given heating profile.

In Figures 7.14(a) and (b), the effect of the magnitude of the heat generation, with a fixed final time of 300s, is shown. The modified E-criteria obtained were 8.10 at r = 4mm and 1.21 at r = 3mm for the constant and pulse profiles, respectively. It was found that the modified E-criterion is minimal when the magnitude of the heat generation is maximum for both profiles. However, the value of the modified E-criterion varies from 1.21 to 1.24 corresponding to the maximal and minimal magnitudes of the heat generation for pulse and from 8.10 to 15.80 for constant profiles. This indicates that the effect of the magnitude of the heat generation is not significant, especially in the case of the pulse profile. It should be noted here that as the magnitude of the heat generation increases, the temperature of the product increases considerably. This causes significant property changes of the substance, which are not accounted for in the model (Fourier), leading to inaccurate estimation of the parameters. As in the previous case, the measurement position remained a more influencing factor than the magnitude of heat generation and optimal

measurement position stayed the same irrespective of the magnitude of the heating profile.

It can be concluded that the measurement position is a more important factor with respect to the information content of an experiment as compared to the duration or the magnitude of the heat generation for a given heating profile. In all cases, the value of the minimum modified E-criterion is smaller for the pulse profile as compared to the constant, confirming once again the previously obtained result that short duration pulse gives a more informative experiment. Moreover, the value of the modified E-criterion for the pulse profile is almost equal to unity, which means that according to this criterion, the profile is close to optimal.

Supplementary to the fact that the measurement position is the main influencing factor, an optimal measurement position can be determined for a wide spectrum of thermophysical properties of biological materials. For this purpose, a Monte Carlo simulation (Sobol, 1994) was used to pick a random combination of parameters to form the parameter vectors. Numerical experiments were performed using these parameter vectors and the modified E-criterion was calculated. Optimal measurement position was then obtained by minimising the criterion for the chosen parameter vector. The mean value for k was chosen to be 0.5 $Wm^{-1}°C^{-1}$ with a standard deviation of 0.2 $Wm^{-1}°C^{-1}$. This choice was based on the fact that the thermal conductivity of most biological materials lies in the interval [0.1 0.9]. For the volumetric heat capacity a mean value of 3 x 10^6 $Jm^{-3}°C^{-1}$ with standard deviation of 1 x 10^6 $Jm^{-3}°C^{-1}$ was chosen. Thousand Monte Carlo runs were performed for each heating profile, where parameter samples were drawn from a normal distribution. The results are summarized in Table 7.4.

Table 7.4 Results of the Monte Carlo simulations for optimal measurement position

	Heat generation profile	
	Constant	**Pulse**
Optimal Measurement Position *r* [mm]	4.72 ± 0.07	3.28 ± 0.04
E-Criterion	19.00 ± 0.51	1.23 ± 0.06

It was observed that the optimal sensor position varies with the type of heating profile employed and is closer to the heating probe (centre) when short duration pulse heating was applied. Moreover, the observed low standard deviation attached to the optimal sensor position implies that the optimal sensor position only depends on the heating strategy pursued irrespective of the medium employed.

7.4.3.2 Implementation

The major draw back encountered here was the accurate positioning of the sensor at the theoretical optimal location. The attainable accuracy of positioning of the sensor was ±0.8mm. This represents 24% and 17% of accuracy with respect to the optimal distances of 3.24 and 4.72mm, respectively. Thus, analysis was carried out to observe how the value of the modified E-criterion changes when a shift of ±1mm in the radial direction of the optimal position was introduced. A maximum increase (in the value of E-criteria) of 5 (from 15.5 to 20.1) and 1 (from 1.2 to 2.1) was observed for the constant and short duration pulse heating, respectively. This shows that the optimality of the sensor position is not affected significantly when the sensor is placed in the vicinity of the optimal position with accuracy of 1mm.

Measurements were carried out using tylose as a medium. The time-temperature response recorded was presented to a parameter estimation algorithm and the thermophysical properties were estimated. Table 7.5 summarizes the obtained results.

Table 7.5 Parameter estimates for tylose using optimal sensor location

Profile	Optimal position r [mm]	Actual position r [mm]	Estimates		δk [%]	$\delta \rho c$ [%]
			k [$Wm^{-1}°C^{-1}$]	ρc [$Jm^{-3}°C^{-1}$]		
Constant	4.72±0.07	4.2	0.5795	$3.54x10^6$	3.48	4.62
Pulse	3.28±0.04	4.0	0.5775	$3.91x10^6$	3.12	5.43

The maximum deviation of the parameter estimates from the nominal values was 3.5% for k and 5.4% for ρc. No discernible difference has been observed in the parameter estimation accuracy attained when using constant or short duration heating profiles. In order to show the uniqueness of these estimates the corresponding objective functionals are presented in Figures 7.15(a) and (b). There is clearly only one minimal value that can be attained irrespective of the initial guess. The estimation procedure leads, hence, to unique parameter values. Altogether, the results obtained show that using appropriate heating profile and the experimental time-temperature data collected from the optimal measurement position, accurate and unique estimates can be obtained.

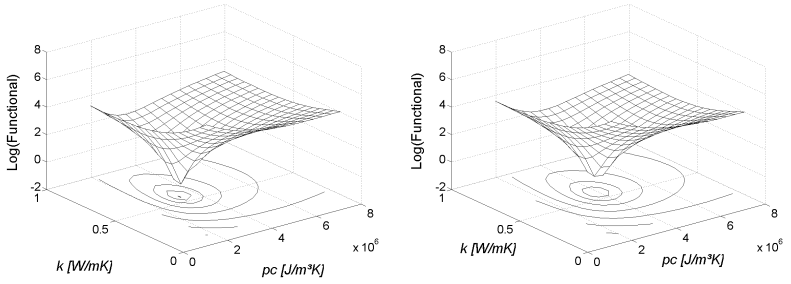

Figure 7.15 Objective functional plot for (a) constant heating and (b) short duration heating profiles

7.4.4. Optimisation of parameterised input heating profile

7.4.4.1 Computational results

A more general approach can be pursued by defining a general block-type heating profile through characteristic parameters such as the amplitude, duration and frequency of the peaks. This can be achieved by piecewise discretisation of the input profile preferably using simple basis functions such as ramps or steps. This leads to substantial number of degrees of freedom transforming the problem into a finite dimensional non-linear programming problem. Moreover, the measurement position could also be considered as an additional degree of freedom along with the characteristic parameters. This requires computationally more powerful algorithms to solve the parametric optimisation problem under several imposed constraints, which may ensure global optimal solution.

Global optimisation methods, which can handle such multi-dimensional optimisation problem, can broadly be divided in to deterministic and stochastic global optimisation methods. The deterministic methods are those that can provide a level of assurance that a global minimum will be located. However, no algorithm can solve with certainty a global optimisation problem in a finite time. Stochastic methods, on the other hand, rely on probabilistic approaches, which may not guarantee convergence of the global solution due to the involvement of random elements. However, the advantage of the stochastic methods is that they can locate the vicinity of the global solutions with relative efficiency though the global optimality cannot be guarantied.

Nevertheless, since the modified E-cost has a global minimum known *a priori*, reaching this global value ensures the global optimality of the solution. In the present work, two stochastic strategies for global optimisation were employed, namely, the Integrated Controlled Random search method (Banga and Casares, 1987) and the Stochastic Ranking Evolution Strategy (Runarsson and Yao, 2000).

Parametrisation of the input heating profile was realized by discretising the input profile into 10 steps. (Only step function was considered since it was established that in general block-type profiles give informative experiments. Note that pulse is a block profile with very short heating duration). As the discretisation step decreases the number of degrees of freedom increases and then higher computational power is required. It was demonstrated in Nahor et al. (2001) that a heating profile with three pulse peaks already gives less information than one with two peaks, thus the choice of ten discretisation steps. Two cases were considered with respect to the measurement position, in the first case the measurement position was let free to be optimised being an additional degree of freedom. Alternatively, the position was fixed to 4mm in the second case. Additional constraints were applied on the magnitude of the heat generation in such a way that a restricted temperature increase is invoked in the product. This avoids excessive heating, which can result in considerable change of the thermal parameters of the medium. The optimal heat generation profiles obtained for the two cases are presented in Figures 7.16(a) and (b).

In the first case where the optimisation procedure was left to determine the optimal profile as well as the measurement position, the *a priori* known global minimum has been attained. Pulse heating with two peaks, one at the beginning and one at the end of the experiment, was identified as optimal profile with the optimal sensor position located at 2.25mm from the centre of the probe. In the second case where the measurement position is imposed (fixed at 4.0mm) the best solution was found at a slightly higher value than the global minimum. In this instance, a single peak pulse at the beginning with 'gradual' decrease was found as best profile. Thus, when the measurement position is altered, a different heating profile is obtained, which is in keeping with the previous result.

7.4.4.2 Implementation

The optimal input dynamic heating profile designed at the simulation level could not easily be reproduced practically due to the limitation of the control of the involved hardware and the acquisition frequency in the experimental set up. For this reason, the theoretically obtained time intervals were adjusted in a manner the experimental

set up would handle. Here, only the heating profile with global minimum of unity was implemented. The implemented variant of the theoretical profile is presented in Figure 7.17.

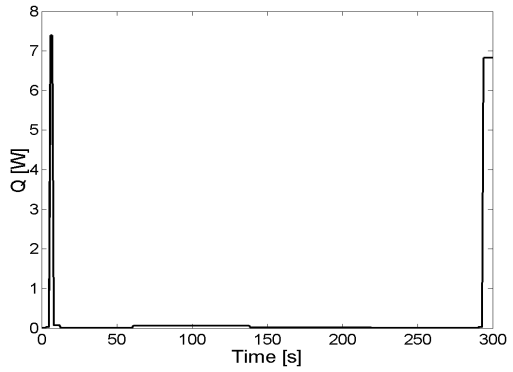

(a)

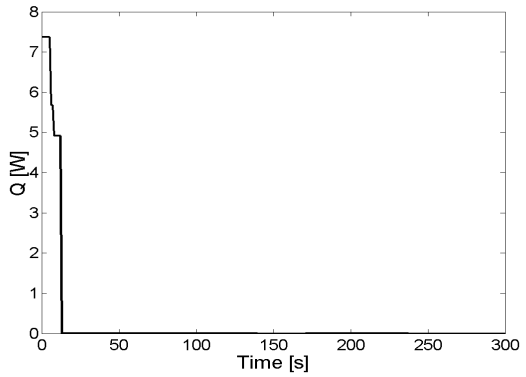

(b)

Figure 7.16 Optimal heating profile from parameterised optimisation (a) DOF = 11; Measurement location = 2.25mm (free); Mod E-cost = 1.0; (b) DOF = 10; Measurement location = 4.0mm (fixed); Mod E-cost = 1.32

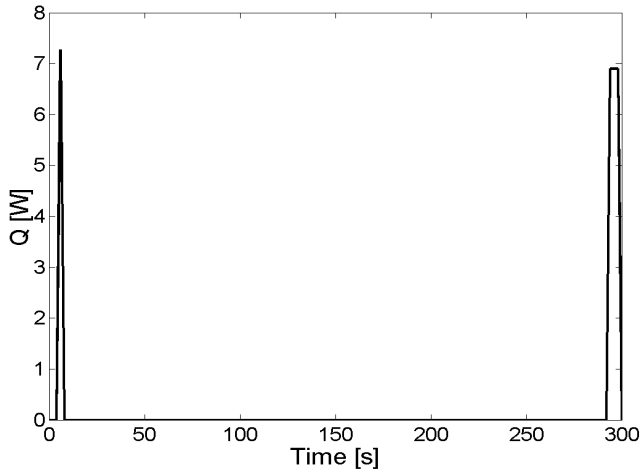

Figure 7.17 Implemented optimal heating profile. (Optimal meas. location 2.25mm; Actual meas. location 1.55mm)

The parameter estimates and their accuracy obtained by implementing the above profile are summarized in Table 7.6.

Table 7.6 Parameter estimates for tylose using optimal heating profile and optimal sensor location

Estimates		δk [%]	$\delta \rho c$ [%]	Mod. E-criteria
k [$Wm^{-1}°C^{-1}$]	ρc [$Jm^{-3}°C^{-1}$]			
0.53	3.93×10^6	5.62	5.82	2.71

It can be observed that by adjusting the theoretically optimised profile for practical implementation the modified E-criteria value is changed to some extent. The deviation of the estimated parameters is in the order of magnitude of the results obtained from previous implementation. In order to ensure that the parameters are estimated uniquely, the corresponding functional plot is shown in Figure 7.18.

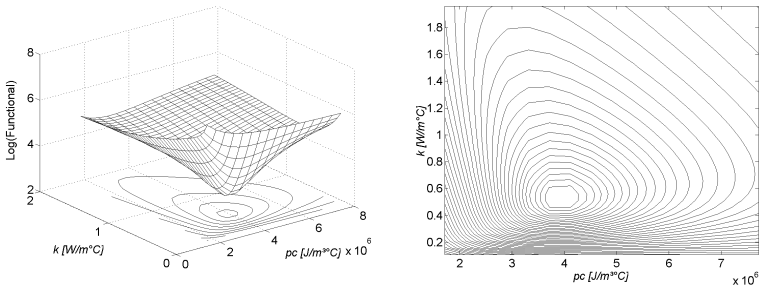

Figure 7.18 Functional and contour plots of the implemented optimal profile

The cone-like structure of the functional leads to unique estimation of the parameters irrespective of the initial guess in the parameter estimation procedure.

7.5. Discussion

In literature, the estimation of thermophysical properties of loose filled and porous materials using the hot wire probe method has been carried out by approximating the finite diameter probe by a semi-finite line heat source so as to tailor an analytical solution of the governing equation. Nevertheless, the type of heating profile that can be employed is limited. As opposed to this, the use of an appropriate model of the hot wire probe, as in this Chapter, enabled the implementation of various types of heating strategies. The application of optimal experimental design provides a basis to evaluate the information content of a given experimental protocol theoretically and facilitates the design of informative experiments. Bringing together the features of the former and the latter approaches, theoretical evaluation of different experimental protocols has been possible.

Using purely experimental approach, Bristow et al. (1994) have reported that for the short duration pulse heating, no statistically significant difference was observed in the estimates by changing the magnitude of the dissipated heat. In the contrary, they found out that by varying the pulse width a significant difference in estimates were obtained especially in the thermal conductivity. They reported that the reasons for this are unclear. In light of the results obtained in this work, it can be explained as follows. As the width of the pulse increases the heating profile changes from pulse-type to block-type heating. Further, if the pulse width is increased to the final time of the experiment, it results in a constant heating profile. It was observed that for a given measurement position the informative nature of the profiles decreases as we

go from the short duration pulse to constant heating. Moreover, the optimal sensor location is displaced away from the centre of the heat source with changing heating profile, again, from the short duration pulse to constant heating. It can then be speculated that the change in estimates observed by Bristow et al. (1994) with increasing pulse width was due to the decrease of the information content of the experiment as a result of both of the above stated phenomena. This leads to several local minima in the parameter plane, which causes the parameter estimation procedure to get stuck in one of the local minima.

Optimal measurement position for the most commonly employed heating profiles was found to be at some distance away from the heating probe. The relatively lower information content of the data observed in the vicinity of the heating probe (i.e., higher value of modified E-criterion) suggests that care must be taken in simultaneous estimation of parameters using the single probe method concerning the level of noise involved and the nature of parameter estimation procedure. The parameter estimates obtained from the implementation of the optimal experiment protocol showed a maximum deviation of 5.4%. The number of experiments carried out would not allow to attach statistical uncertainty to the estimates. Bilskie et al. (1998) report that the maximum deviation of 5.1 and 5.9% for Al_2O_3 and glycerol, respectively using the dual probe method. These values are comparable to the maximum deviations obtained. It should be noted that the nominal values used here are values estimated using other methods obtained from literature or calculated by summation of constituent parts using published results. Thus, the presupposition that these parameters are nominal can be questioned. Nevertheless, using the present methodology, it can be said with certainty that the estimates are unique (Figures 7.15 and 7.18) irrespective of the nature of the parameter estimation procedure or initial guess. It is evident that more experimental work is needed to establish the accuracy of the estimates. Yet, the relatively large deviation observed on the estimates can be attributed to the '*implementability'* of the optimal heating profile. This means that the inherent limitations of the experimental set ups with respect to the frequency of measurement and control of the involved hardware can lead to substantial loss of information due to the inability to capture the full dynamics especially in a fast changing heating profiles. This leads to loss of accuracy in the estimates in spite of the fact that a given profile can theoretically be proven to give the maximum information. It was observed that when a carefully selected measurement position is used (given that the sensor could be positioned with acceptable accuracy around the optimal location) the simplest heating strategy could yield the same or even better accuracy of the estimates. Thus, through careful choice of heating strategy and

measurement position one can achieve both the accuracy and uniqueness of the estimates.

In the present study only food simulants were considered to investigate the application of optimal experimental design methodology to foster the accuracy of the estimation of thermal properties. In dealing with real biological materials factors such as non-homogeneity and anisotropy come into play. This might thus require the reconsideration of the assumptions used in building the model, which were based on the homogeneity of the media. To the author's knowledge there is no standardised heterogeneous food simulant available. Moreover, another aspect that needs attention in the processes of optimal experimental design when dealing with real biological materials is the design robustness. This means that the achievable parameter estimation quality when the design is based on erroneous nominal parameter values that deviate from true process parameters. This is often the case, since it is evident that the parameters to be estimated are not known in the beginning. Versyck (2000) has shown that optimal experimental design based on incorrect nominal values can lead to loss of accuracy in the estimates. This can be surmounted through iterative design cycle where the estimates from the first iteration cycle are considered as nominal parameters in the proceeding iteration cycle. The progress of the iteration can be stopped when user specified criterion is met, for instance, when the estimated parameter sets in two subsequent iterations are sufficiently close. In the present case, since the nominal parameters of the employed simulants were assumed to be accurately known, such iterative procedure was not deemed necessary. Finally, in the implementation of the theoretically obtained optimal modus operandi, the statistical confidence of the estimated parameters should be established through repetitions.

7.6. Conclusion

A methodology based on the optimal experimental design technique was presented to enhance the uniqueness and accuracy of the simultaneous estimation of the thermal properties of biological materials using a hot wire probe set up. The hot wire and its environment were first modelled using the finite element formulation of the conduction equation and the model was validated against experimental data obtained from static and dynamic experiments. Besides appropriate representation of the reality, this modelling approach provided much flexibility with respect to the application of different heating strategies as compared to the commonly employed approximate analytical approach.

The optimal experimental design technique, which is based on the *Fisher Information Matrix,* was applied to evaluate the information content of several proposed heating strategies. This was carried out by simulating numerical experiments. Results showed that short duration pulse-like heating profiles provide informative experiments. Subsequently, the effect of different factors such as measurement position, magnitude of heat generation profile and duration were investigated using two types of heating strategies, namely, the constant heating and short duration pulse heating profiles. It was found that for a given heating profile, the measurement location was the most important factor. Thus, the optimal measurement position was identified for a range of thermophysical properties (for a given profile) using Monte Carlo simulations. The optimal position was found to be at some distance away from the heating source and was different for different heating profiles. Subsequently, experimental time-temperature data have been collected around the optimal measurement locations using the constant and short duration heating profiles. The maximum deviation of the parameter estimates with respect to the nominal ones was found to be 5.4%. Though the number of experiments carried out did not enable to estimate the uncertainty on the estimates, it was shown that the unique identification of the parameters was possible.

Further, modern global optimisation methods were employed to optimise parameterised heat generation profiles with respect to the type and magnitude of heating and measurement position. Parameterisation was realised through discretisation of the input heating profile by using steps. When the measurement position was let as an additional degree of freedom, the optimal profile (short duration pulse heating with two peaks) was obtained with a modified E-criteria value of unity. Moreover, when the measurement position was fixed, a profile close to optimal (short duration pulse heating with one peak) was obtained (Modified E-criteria value of 1.32). In implementing the theoretically obtained optimal experiment from the global optimisation, adjustments were needed due to the limitations of the set up. The implementation of the adjusted profile also produced estimates with similar deviations as above.

In general, it can be concluded that the application of optimal experimental design for the estimation of thermal properties of biological materials fosters the uniqueness and accuracy of the estimates. Due to the limitations in implementing theoretically obtained experimental designs, both a careful choice of simpler profiles to implement as well as optimal measurement position is needed to achieve unique as well as accurate estimates. More test substances and real foodstuffs (such as fruit tissues) should be considered to validate the results of the present study and to

assess the potential of this methodology to design more robust measurement instrument for estimation of thermophysical properties of biological substances.

References

Banga, J.R., Casares, J.J. (1987). Integrated controlled random search: application to a wastewater treatment plant model. *IChemE Symposium Series*, 100, 183-192.

Bernaerts, K. (2002). Dynamic experiment design and validation in predictive microbiology: optimal estimation of two-parameter microbial growth kinetics as function of temperature. *Ph.D. Thesis* (519), Katholieke Universiteit Leuven, Leuven Belgium.

Bernaerts, K., Versyck, K.J., Van Impe, J.F. (2000). On the design of optimal dynamic experiments for parameter estimation of Ratkowsky-type growth kinetics at sub-optimal temperatures. *International Journal of Food Microbiology*, 54(1-2), 27-38.

Bilskie, J.R., Horton, R., Bristow, K.L. (1998). Test of dual-probe heat-pulse method for determining thermal properties of porous materials. *Soil Science*, 163(5), 346-355.

Bristow, K.L., Bilskie, J.R., Kluitenberg, G.J., Horton, R. (1995). Comparison of techniques for extracting soil thermal properties from dual-probe heat pulse data. *Soil Science,* 160(1), 1-7.

Bristow, K.L., Kluitenberg, G.J., Horton, R. (1994). Measurement of soil thermal properties with a dual-probe heat-pulse technique. *Soil Science Society of America Journal*, 58, 1288-1294.

Chang, C.S., Lai, F.S., Miller, B.S. (1980). Thermal conductivity and specific heat of grain dust. *Transactions of ASAE*, 23(5), 1303-1306, 1312.

Hooper, F.C., Chang, S.C. (1952). Development of the thermal conductivity probe. *Heating, Piping, and Air Conditioning*, 24(10), 125-129.

Incropera, F.P., De Witt, D.P. (1990). Fundamentals of Heat and Mass Transfer – 3rd Edition. John Willy & Sons, Inc., New York.

Kluitenberg, G.J., Bristow, K.L., Das, B.S. (1995). Error analysis of heat pulse method for measuring soil capacity, diffusivity, and conductivity. *Soil Science Society of America Journal*, 59, 719-726.

Larson, T.H. (1988). Thermal measurement of soils using a multi-needle probe with a pulsed-point source. *Geophysics*, 53(2), 266-270.

Mehra, R. (1974). Optimal input signal for parameter estimation in dynamic systems: survey and new results. *IEEE Trans Automatic Control*,19(6), 753-768.

Moysey, E.B., Shaw, J.T., Lampman, W.P. (1977). The effect of temperature and moisture on the thermal properties of Rapeseed. *Transactions of ASAE,* 20(3), 461-464.

Munack, A. (1989). Optimal feeding strategy for identification of monod-type models by fed-batch experiments. In: Fish, N.M., Fox, R.I., Thomhill, N.F. (Eds.) Computer applications in fermentation technology, modelling and control of biotechnological process. Elsevier, Amsterdam, 195-204.

Nahor, H.B., Scheerlinck, N., Verniest, R., De Baerdemaeker, J., Nicolaï, B.M. (2001). Optimal design of dynamic experiments for the parameter estimation of conduction heated foods. *Journal of Food Engineering*, 48, 109-119.

Nahor, H.B., Scheerlinck, N., Van Impe, J., Nicolaï, B.M. (2003). Optimisation of the temperature sensor position in a hot wire probe set up for estimation of the thermal properties of foods using optimal experimental Design. *Journal of Food Engineering,* 57(1) 103-110.

Nahor H.B., Scheerlinck N., Moles C.G., Banga J.R., Nicolaï B.M. (2004). Implementation and validation of optimal heat generation profiles for simultaneous estimation of thermal food properties using a hotwire probe. Accepted to be presented in the *9th International Congress on Engineering and Food (ICEF9),* 7-11 March 2004, Montpellier, France.

Pohjanpalo, H. (1978). System identifiability based on the power series expansion of the solution. *Mathematical Biosciences*, 41, 21-33.

Reidel, L. (1960). Eine prufsubstanz für gefrierversuche. *Kaltetechnik*, 12, 222-226.

Runarsson, T.P., Yao, Xin. (2000). Stochastic ranking for constrained evolutionary optimisation. *IEEE Transactions on evolutionary computation*, 4(3), 284-294.

Segerlind, L.J. (1984). Applied finite element analysis. John Wiley & Sons, New York.

Sobol, I.M. (1994). A primer for the Monte Carlo method. CRC Press, Inc.

Stalhane, B., Pyk, S. (1931). New method for measuring the thermal conductivity coefficients. *Teknisk Tidskrift*, 61(28), 389-393.

Tagawa, A., Kitamura, Y., Muramatsu, Y., Fusakaz A., Murata, S. (1996). Thermophysical properties of Adzuki beans by transient heat flow method using probe. *ASEA Annual International Meeting*. Paper N°. 966003.

Taktak, R., Beck, J.V., Scott, E.P. (1993). Optimal experimental design for estimating thermal properties of composite materials. *International Journal of Heat and Mass Transfer*, 36(12), 2977-2986.

van Haneghem, I.A. (1981). Een niet-stationaire naaldmethode (warmtegeleiding, warmtecapaciteit, contactweerstand). *Ph.D. Thesis*, Wageningen University and Research Center, Wageningen, The Netherlands.

VanRolleghem, P.A., Van Daele, M., Dochain, D. (1995). Practical identifiability of a biokinetic model of activated sludge respiration. *Water Research*, 19(11), 2561-2570.

Versyck, K.J., Claes, J.E, Van Impe, J.F. (1997). Practical identification of unstructured growth kinetics by application of optimal experimental design. *Biotechnology progress*, 13(5), 524-531.

Versyck, K.J. (2000). Dynamic input design for optimal estimation of kinetic parameters in bioprocess models. *Ph.D. Thesis*, (436) Katholieke Universiteit Leuven, Belgium.

Walter, E., Pronzato, L. (1990). Qualitative and quantitative experiment design for phenomenological methods: A survey. *Automatica,* 26(2), 195-213.

Zienkiewicz, O.C., Taylor, R.L. (1994). The Finite Element Method-(Volume-1)-4th Edition. McGraw-Hill Book Co. London, England.

Chapter 8

General conclusions and future research

8.1 General conclusions

Conventional cool storage systems have now been replaced by controlled atmosphere facilities for the storage of a wide range of horticultural products especially those that are stored for a relatively longer period, such as pome fruit. The challenge to meet the growing consumer demand and stringent regulations drives the quest for better design, operation and control of CA cool storage systems. Use of predictive modelling and computer simulation is indispensable for efficient and cost effective sizing of the involved equipment and design of robust control systems.

Successful simulation of the involved processes and physical systems in controlled atmosphere storage depends on the use of an appropriate modelling methodology and natural implementation of these processes and entities. The main objectives of the present research as defined at the onset were: (*1) To develop a methodology for modelling and simulation of controlled atmosphere cool storage systems considering (i) the heat, moisture, and gas exchange in the cooled space, (ii) the quality evolution of the stored produce and (iii) the dynamics of the involved mechanical plants. A hierarchical and modular implementation*

approach using a combined continuous and discrete simulation environment will be pursued and (2) to develop a methodology for estimation of thermal properties of biological materials, based on the application of optimal experimental design techniques for unique and accurate estimation of the parameters simultaneously.

8.1.1 CA cool storage system simulation

To achieve the first objective, the CA cool storage system model was developed in which the interacting units and their components were represented in a modular fashion. The system was divided into three sub-units namely: *(i)* the cooled space, *(ii)* the refrigeration unit and *(iii)* the gas-handling unit. The components in the cooled space were further classified as product (respiring produce) and non-product (cooler, envelope, and air) entities. The dynamics of the heat and mass transfer of the non-product components were formulated by an overall energy and mass balance by considering the zoning approach, which resulted in a description of the modules by a set of ODE's for each component. The stored produce being the focus of attention, a special emphasis was rendered and was represented through three sub-models, which describe the heat and moisture transport, the gas exchange and quality deterioration. Assessment of existing product respiration models revealed that Michaelis-Menten type models describe the gas exchange better and allow direct linking of product quality models as both are believed to have a common metabolic background. Moreover, processes involving discrete time event such as door opening, defrosting operation and control strategies involving on-off, PI and PID controllers and their implementation aspects were included in the model. In total the cooled space model for a single cell was represented by 26 ODE's. Regarding the refrigeration unit, since the dynamics of the system is dominated by the load variations imposed by the end users (the cool cells), the use of a model that considers the thermal effects only (ignoring the hydrodynamic effects) was justified. Accordingly, an energy balance around the main components of the refrigeration unit (condenser, evaporator, compressor and a holding tank in case of indirect system layout) was performed by using the zoning approach. The unit was represented by 4 ODE's and 2 algebraic variables. Pertaining to the gas-handling unit, the process involved in modern systems is pressure swing adsorption. Accordingly, a two phase, isothermal plug flow model was proposed where the solid phase mass transfer was described by a linear driving force model. The extended Langmuir isotherm was used to represent the adsorption equilibrium. This unit was described by 3 PDE's. Finally, the individual modules were arranged to form the

sub-models and in turn, the global CA cool storage system model was formulated by interconnecting these sub-models.

Implementation of the CA cool storage model was carried out using a general purpose simulation environment EcosimPro (EA International, Madrid, Spain) which can handle combined continuous/discrete processes. The difficulties encountered in most of previous works in implementing such diverse modules such as complete representation of discrete events and flexibility with respect to the inclusion of new component models was addressed. As a result, the use of object-oriented approach together with discrete events simulation, gave rise to natural representation of the real system. Besides making model representation clearer, validation of individual modules was possible by extracting them from the larger system, making model implementation much easier. Moreover, due to the open architecture, existing models developed using compatible programming languages were easily fused.

The validation of the proposed models was first carried out by considering the individual units separately using experimental data obtained from various experimental set-ups. The cool room model was appraised using empty room experiments from a pilot scale CA cool storage facility. Heat flux measurements on the surfaces resulted in modification of heat transfer coefficients related to the surfaces, especially to the ceiling and the floor, previously estimated using measured velocities and empirical correlations. It was found that the thermal mass of the cooler interacting with the medium was found at 40% of the thickness of the floor. In comparison to the experimental results, the trends displayed by the models of the different components were in line with the experimental results. Next, the refrigeration unit model was validated using an experimental set up tailored to imitate the situation of an indirect cool storage system. The dynamic behaviour of the system was represented by condenser, evaporator and tank water temperatures predicted by the model with RMSE (Root Mean Square Error) values of 2.08, 0.77, 0.23 °C, respectively. The observed high RMSE value of the evaporator was attributed to the discrepancy during start up. However, since the time constant of the refrigeration unit (typically 5-6 min) is much less as compared to the one from the cool room (typically more than 3 h) the influence of the start up condition has insignificant effect on the dynamics of the cool rooms. Sensitivity analysis of the model parameters revealed that the condenser and evaporator temperature were significantly sensitive to the thermal mass of the water tank, owing to the dominance of the transient behaviour of the system by the water tank. In general, the proposed

simple model gives acceptable accuracy especially with respect to the water tank, which forms the boundary between the cool room and the refrigeration unit, thus considered adequate for CA simulation.

Subsequently, a comprehensive direct and indirect validation of the global controlled atmosphere cool storage model, formulated by considering the sub-models and their interactions, was presented. The simulated variables that characterize the room air (temperature, humidity and concentration of the respiratory gases), the cooler and refrigerant temperatures and the variables related to the product (temperature, moisture loss and firmness loss) were compared to experimental results. As observed from the different validation results, the adequacy of the proposed model was justified by its ability to represent the most important discrete and continuous process events with an accuracy less than the observed variability of the different variables (2 °C for room air, 1.5 °C for cooler surface temperature, 1.5°C for product temperature and 5% for RH) or at best with the accuracy level as set by the measurement instruments (0.5 °C for temperature and 5% for RH). Thus, it was concluded that little or no advantage is achieved by including more zones or phases. Sensitivity analysis showed that the transient cooling phase was influenced by the accuracy of the heat transfer coefficients. Due to the intrinsic biological variability, a greater uncertainty in the product heat transfer area was evident contributing to a discrepancy between model prediction and observed data. Moreover, the initial product temperature influenced the product cooling rate and moisture loss substantially with practical implication on cooling strategy. It was concluded that fast cooling of the product, which reduces respiration as well as transpiration of the produce should always be accompanied by very high (near saturation) relative humidity of the cooling medium.

The model was further validated using an industrial CA storage facility. First, minor modifications to some of the modules were carried out pertinent to the control systems of the evaporator and gas-handling unit and to the product model to accommodate the product-loading schedule. Then some selected variables, which characterize the cool room, refrigerant and evaporator and the gas-handling unit were compared to experimental data in empty, partially loaded and fully loaded conditions. As often as not, model predictions of the most important discrete and continuous variables were found to agree to the experimental data with a maximum difference less than the observed spatial variability and/or the accuracy as set by the measurement instruments. The largest difference between model prediction and observed data were found for the product temperature profile. This was attributed

to adequacy of the model, which assumes uniform temperature distribution in the product phase, besides the spatial variability and accuracy of the model parameters. The eminence of the present simulation model as compared to the complete refrigeration systems simulation models developed so far is that actual practical operation conditions such as the stepwise loading of the product and the involved transients can be simulated, providing actual picture of the real world. In conclusion, the global CA cool storage model, once more, demonstrated to be a pragmatic working tool for simulation of CA cool storage facility.

Finally, the global CA cool storage model was used to investigate the implication of some practical operational issues related to product loading strategies (stepwise and batch wise) to the product quality, mechanical plants performance and design aspects. With regards to product quality, it was found that no influence of the considered product loading schemes could be detected on the product weight loss. Moreover, the observed difference in firmness after a storage period of 180 days was only less than 5N. Thus, it is concluded that the influence of the loading strategy is only marginal. Concerning the refrigeration plant, less load variation was observed in the batch wise loading but was marginally energy intensive over the stepwise product loading strategy thus, higher energy cost. Considering sizing of the refrigeration plant, the batch wise scheme required high capacity individual evaporators as compared to the stepwise loading. However, overall, the capacity of the refrigeration unit does not appear to be affected by the product-loading schemes considered. During transient situations, a higher capacity was required for the gas-handling unit (N_2 generator and CO_2 scrubber) in the case of the stepwise loading scheme, due to parallel working mode of the cells. However, the required operational time was 33% larger for the CO_2 scrubber when batch wise product loading strategy was used.

The advantage of the present simulation model is that owing to the inclusion of models that describe the gas exchange and quality deterioration of the stored produce, it was possible to carry out optimisation of the plant performance with respect to the final quality of the stored produce. It was demonstrated that appraisal of the implication of practical industrial operational procedures directly on the product quality and energy saving issues was achievable. It was revealed that the stepwise loading strategy, customarily believed to bring about superior product quality, was in fact found to produce less quality fruit in terms of firmness. This shows that alternative operation procedures should be sought through use of such tools for improvement of the final product quality in long-term storage. Moreover, prediction of the interaction between the cool room and the gas-handling and

refrigeration units enables to quantify the imposed load, which facilitates appropriate sizing and optimisation of the units. Thus, by employing the developed tool, the optimisation of operational conditions and sizing of the plant as a whole, which ultimately leads to increased productivity and profitability, could be attained.

The potential application of the present simulation model, besides the sizing of the gas handling and refrigeration units, is for the design of robust control strategy and model based product quality control. Concerning the latter, since sensor based automatic control of product quality can prove to be difficult, the control of the *'a priori'* known optimal set points should be assisted by model based product quality control where the response from the quality models is fed to the controller for better maintenance of the micro environment for overall plant optimal operation. In general, the tangible contribution of the present thesis is a valid working combined discrete and continuous CA cool storage simulation model, which could be applied for design and optimisation of CA cool storage facilities.

8.1.2 Optimal experimental design for parameter estimation

To achieve this objective, a hot wire probe set up was developed. The heat transfer in the probe and its environment was first modelled using a finite element formulation of the heat equation. The model was successfully validated against experimental data obtained from static and dynamic experiments. The model was then further employed to investigate the optimality of a given heating profile and sensor location by using optimal experimental techniques. Results have shown that short duration pulse profiles provide informative experiments. Among the factors investigated for their effect on the information content of an experiment (such as the measurement position, magnitude of heat generation profile and duration of experiment), the measurement location was found to be the most important factor. Thus, the optimal measurement position was identified for a range of thermophysical properties (for a given profile) using Monte Carlo simulations. The optimal position was found to be at some distance away from the heating source and was different for different heating profiles. Subsequently, experimental time-temperature data have been collected around the optimal measurement locations using the constant and short duration heating profiles. The maximum deviation of the parameter estimates with respect to the nominal ones was found to be 5.4%. Though the number of experiments carried out did not enable to estimate the uncertainty on the estimates, it was shown that the unique identification of the parameters was possible.

Further, modern global optimisation methods were employed to optimise parameterised heat generation profiles with respect to the type and magnitude of heating and measurement position. When the measurement position was let as an additional degree of freedom, the optimal profile (short duration pulse heating with two peaks) was obtained with modified E-criteria value of unity. Moreover, when the measurement position was fixed a profile close to optimal (short duration pulse heating with one peak) was obtained (Modified E-criteria value of 1.32). In implementing the theoretically obtained optimal experiment from the global optimisation, adjustments were needed due to the limitations of the set up. The implementation of the adjusted profile also produced estimates with similar deviations as above.

This work revealed that the application of optimal experimental design for the estimation of thermal properties of biological materials fosters the uniqueness and accuracy of the estimates. Moreover, careful choice of practically *'implementable'* heating profiles and respective optimal measurement position is indispensable to achieve both unique and accurate estimates.

8.2 Future research

Below, some recommendations for future research are compiled.

8.2.1 CA cool storage system

- When using the Michaelis-Menten type model to represent the gas exchange of bulk stored fruit it was found out that the kinetic parameter depend on the age of the fruit. Some effort should be made to express this parameter as a function of the physiological age of the fruit.

- The product heat and moisture exchange model has shown only moderate accuracy. This was due to the intricate thermal and hydrodynamic phenomena, taking place inside the bins and at the interface and inside the product, which cannot be captured by models that lump the product as one entity. Therefore, a closer look into airflow inside and around different bin types and arrangements with different produce by advanced airflow models is needed. This might require a specialized set up for carrying out experiments. However, since these elaborate distributed models take into consideration the spatial distribution and local effects, a method should be

developed to link the results with the lumped parameter models used in the global CA model.

- The quality model as it is now only predicts one quality attribute and thus further investigation and incorporation of quality models for prediction of different quality attributes, which can be used for development of control strategies for minimizing quality deterioration is essential.

- To widen the usability of the simulation model, modules for different kinds of refrigeration unit and gas handling unit arrangements and the involved unit operations need to be developed.

- The usefulness of such simulation model as a tool highly depends on the availability and amount of input data. Thus, in order to craft the present CA simulation model as a practical tool, additional effort should be put in reducing the amount of input data by implementing knowledge base systems, which widens the usability of the tool for different user target groups. Moreover, development of a user friendly GUI is indispensable.

- It is apparent that lumped assessment of the entailed processes in CA cool storage systems results in setting the global design parameters in relation to the facility as a whole, during the preliminary design phase. However, for detailed and robust design, especially that of the cooled spaces requires dynamic distributed analysis of the heat and mass transfer processes. Hence, some endeavour towards linking CFD simulation models is required to realize a tool that can be used in the whole design phases of the CA cool storage facility.

8.2.2 Optimal experimental design for parameter estimation

- More test substances and real foodstuffs (such as fruit tissues) should be considered to establish the optimal experiment protocol for simultaneous and accurate estimation of a wide range of biological materials.

- Once the optimal measurement position is identified, the challenge is to accurately position the sensor at this coordinate. Hence, design of an automated set up for accurate positioning of the temperature sensor probe is required.

- To expand the applicability of the present methodology to different materials and systems, an exciting challenge will be the design of an automated system to estimate thermal parameters, driven by model based optimisation-heating procedure.

- To assess the potential of this methodology for the design of more robust measurement instruments for estimation of thermophysical properties of biological substances.

- Application of the above-developed methodology for simultaneous and unique estimation of the bulk product respiration model parameters.

Appendix A

Cool room accessory models

In this Appendix, the accessory models related to the different types of controllers and their implementation aspects, and the control valve, are presented.

A.1 Control strategies and controllers

The most common configurations when dealing with information gathering and decision implementation are closed loop and open loop control. The choice of an adequate configuration depends, among others, on the structure of the decision making process. Feedback control is one of the simplest and by far the most common closed loop control strategy employed (Ogunaike and Ray, 1994). The task of a controller is to compare the process signal to the set point and issue an appropriate signal to the final control element such as the control valve. How the controller calculates what command signal to issue for a given value of error is what differentiates one controller from another. There are three basic types of controllers that are conventionally used for continuous feed back control: Proportional, Integral and Derivative; and the on-off control for discrete feed back control.

The operation of the Proportional, Integral and Derivative controllers is calculated according to the following relations, respectively.

$$C(t) = P_{offset} + G_p \varepsilon(t) \tag{A.1}$$

$$C(t) = P_{offset} + \frac{1}{\tau_I} \int \varepsilon(t) dt \tag{A.2}$$

$$C(t) = P_{offset} + \tau_D \frac{d\varepsilon(t)}{dt} \tag{A.3}$$

where $C(t)$ is the control signal, $\varepsilon(t)$ the error, P_{offset}, the offset value, and G_p, τ_I, and τ_D are the proportional gain, integral time and derivative time, respectively. The three actions described above are used individually (only proportional) or combined in the P, PI or PID controllers. The proportional controller recognises the size of the deviation and reduces the large part of the overall error. The integral controller sums up the small errors over time and reduces the final error (offset error) in a system. The derivative part counteracts the proportional and integral terms when the sensor output changes quickly and thus helps reduce an overshoot.

These controllers can be arranged into simple single-input single-output types often used in evaporator or individual compressor control or into sophisticated multiple-input multiple-output strategy controllers. In laboratory scale CA cool rooms and air-conditioned conference rooms, where stringent control of the temperature and humidity is stipulated, the latter is employed in what is commonly known as the 'auctioneering' control. Here, feedback signals from different process variables are used to calculate different control signals, which are compared in some way, for issuance, of the control signal.

Implementation of the controllers involve strategies to avoid the phenomena known as p-jump related to the proportional controller, anti reset wind up related to Integral controller, and noise effects on the derivative controller.

In the CA cool storage model, the four types of controllers and their implementation aspects, as described above, were implemented. For the anti-reset windup problem, the integral follow up scheme was implemented. This was carried out by introducing an additional feedback path through the integrator, which modifies the input error to the integral controller. The actuator error, i.e., the difference between the actual actuator output and the desired control action, was used as a modifying feedback to the integrator. Moreover, a low pass filter for the derivative action was implemented to filter out high frequency noise, which have large slopes, compared with the more

slowly varying primary signal dominating the output of the differentiator. A scheme to avoid the p-jump that causes the control element to open briefly due to the change of the error in the positive direction while the error is still negative was also implemented.

A.2 Control valve model

Often, a control valve is employed as a final control element to change the dynamic behaviour of the heat and mass transfer in the cool storage system. In general, two types of control valves are used, the mixing valve (3-way valve) and the throttling valve. The flow rate through a valve was represented in terms of a flow fraction defined as a function of the normalized control signal. For a mixing valve, the energy and mass balances were given by:

$$\left(\rho V c_p T\right) = \left(\rho V c_p T\right)_1 + \left(\rho V c_p T\right)_2 \tag{A.4}$$

$$\rho V_{total} = \left(\rho V\right)_1 + \left(\rho V\right)_2 \tag{A.5}$$

where ρ is the density, V the volume flow rate, c_p the heat capacity, T the temperature, V_{total} the total volumetric flow rate and 1 and 2 represent the flows from the two directions of the valve. Assuming that the densities and heat capacities of the mixing fluids are equal, and introducing the flow fraction, equations (A.4) and (A.5) reduce:

$$T = fT_1 - \left(1 - f\right)T_2 \tag{A.6}$$

$$V_1 = fV_{total} \text{ or } V_2 = \left(1 - f\right)V_{total} \tag{A.7}$$

where f is the flow fraction.

For throttling valve the flow rate can be represented as:

$$V = fV_{\max} \tag{A.8}$$

where V_{max} is the volume flow rate when the valve is completely open. Depending on the characteristics, a valve can be distinguished as linear, quick opening, or quick closing.

For a linear valve, the flow fraction is equal to the normalized control signal.

$$f = s; \text{ where } s = \frac{S}{100} \tag{A.9}$$

where S is the control signal from the controller and s the normalized control signal. To model the quick opening and quick closing valves, usually quadratic functions are employed. These functions are characterized by a given maximum slope at normalized control signal of zero for the quick opening and one for the quick closing valves.

Furthermore, valves require a finite interval of time to travel from limit to limit. This means that for a given target flow fraction, the valve will open or close at a rate determined by the limit-to-limit travel interval. Thus, the actual flow fraction characteristic function, f, is determined not only by the characteristic selection, but also on the limit-to-limit travel interval. Alternatively, an opening or closing strategy can be imposed on the control valve, especially in the case of on-off control, on top of the limit-to-limit travel interval.

Reference

Ogunnaike, B.A., Ray, W.H. (1994). Process dynamics, modelling and control. Oxford University Press, New York.

Appendix B

CA cool storage model parameters

In this Appendix, the parameters employed in the simulation of the CA cool storage model are compiled. A number with a curl bracket in the description column of the tables indicates the source from which the parameters are obtained. When the parameter is obtained from literature, a number in a square bracket appears indicating the reference number in the reference list. For instance, [3] signifies a parameter obtained from reference 3. The legend of the numbers in the curl brackets is as follows.

- {1} - Manufacturer manual or calculated from data given in manufacturer manual. The model numbers and manufacturers of the equipment are given with the respective data tables.
- {2} - Empirical estimation from correlations, which might involve measured data.
- {3} – Directly or indirectly measured.

B.1. Global parameters

Symbol	Description	Value	Unit
Mwt_{H2O}	Molecular weight of water [4]	0.01802	kg mol^{-1}
P_{tot}	Atmospheric pressure [4]	101.3	kPa
R	Universal gas constant [4]	8.314	J mol^{-1} K^{-1}
$h_{fg,0}$	Latent heat [1]	2500.8	kJ kg^{-1}

B.2. The cool room model parameters

B.2.1. Control System

Schatten N.V., Brussels, Belgium.

Symbol	Description	Value		Unit
		Pilot plant	Industrial plant	
ON-OFF				
Umin	Low limit of output {1}	0	0	--
Umax	High limit of output {1}	1	1	--
PI				
k	Proportional gain of PI controller {1}	25	--	--
T_I	Integral time constant (reset time) {1}	240	--	s^{-1}
T_r	Anti-windup time constant {1}	1	--	s^{-1}
Umin	Low limit of output {1}	0	--	--
Umax	High limit of output {1}	100	--	--
PID				
k	Proportional gain of PID controller {1}	75	--	--
T_I	Integral time constant (reset time) {1}	180	--	s^{-1}
T_r	Anti-windup time constant {1}	1	--	s^{-1}
T_D	Derivative time constant {1}	90	--	s
Umin	Low limit of output {1}	0	--	%
Umax	High limit of output {1}	100	--	%

B.2.2. Door

SALCO B.V., Zwaagdijk-Oost, The Netherlands.

Symbol	Description	Value		Unit
		Pilot	Industrial	
H_d	Door height {1}	2.5	3.5	m
T_{out}	Outside air temperature {3}	12	10	°C
W_d	Door width {1}	1.4	2.6	m
$v_{a,d}$	Velocity of air entering room during door opening {3}	0.02	0.02	m s^{-1}

B.2.3. Floor

Schatten N.V., Brussels, Belgium.

Symbol	Description	Value	Unit
		Pilot & industrial	
$E_{f,fl}$	Equivalent water covered surface {2}	0.6	--
k_{fl}	Effective thermal conductivity of concrete [1]	2.6	W m^{-1} °C $^{-1}$
t_{fl}	Floor thickness {1}	0.1	m
h_{fl}	Floor surface heat transfer coefficient {3}	8	W m^{-2} °C $^{-1}$
c_{fl}	Concrete heat capacity [1]	900	J kg^{-1} °C $^{-1}$
k_{soil}	Soil thermal conductivity [1]	1.12	W m^{-1} °C $^{-1}$
t_{soil}	Soil thickness [6]	8.8	m
T_{soil}	Soil temperature 8.8m deep [6]	10	°C
ρ_{fl}	Concrete density [1]	2400	kg m^{-3}

B.2.4. Walls and ceiling

Roma-Dam-Systems GmbH, Thurheim, Germany.

Schatten N.V., Brussels, Belgium.

Symbol	Description	Value		Unit
		Pilot	Inds	
W_r	Room width {1}	2.8	7.2	m
L_r	Room length {1}	4.25	10.8	m
H_r	Room height {1}	3.6	8.0	m
T_{out}	Outside air temperature {3}	12	10	°C
t_s	Wall thickness {1}	0.12	0.12	m
ρ_s	Wall density {1}	40	40	kg m^{-3}
k_w	Wall thermal conductivity {1}	0.022	0.022	W m^{-1} °C^{-1}
$c_{p,s}$	Wall specific heat [1]	1045	1045	J kg^{-1} °C^{-1}
$h_{in,w1}$	Wall 1: inside {3}	6.5	10	W m^{-2} °C^{-1}
$h_{in,w2}$	Wall 2: inside {3}	3.5	10	W m^{-2} °C^{-1}
$h_{in,w3}$	Wall 3: inside {3}	3	9.6	W m^{-2} °C^{-1}
$h_{in,w4}$	Wall 4: inside {3}	3	9.6	W m^{-2} °C^{-1}
$h_{in,cl}$	Ceiling: inside {2}	29	38	W m^{-2} °C^{-1}
$h_{out,w1} = h_{out,w2}$	Wall 1 and 2: outside {2}	0.166	0.166	W m^{-2} °C^{-1}
$h_{out,w3}$	Wall 3: outside {2}, {3}	3	9.6	W m^{-2} °C^{-1}
$h_{out,w4}$	Wall 4: outside {2}, {3}	3	9.6	W m^{-2} °C^{-1}
$h_{out,cl}$	Ceiling: outside {2}	0.166	0.166	W m^{-2} °C^{-1}

B.2.5. Heat exchanger

Pilot: Goedhart Cooling Equipment[1] B.V., Sint-Maartensdijk, The Netherlands.

Industrial: ZLE 16.5 – 8 – 420, Helpman B.V., Groningen, The Netherlands.

[1] This cooler is a customized one and thus has no model number. The data are given in the manual of the cool room by Schatten N.V., Brussels, Belgium.

Symbol	Description	Value		Unit
		Pilot	Industrial	
A_{he}	Cooler surface heat transfer area {1}	49	590	m^2
A_{refr}	Refrigerant side heat transfer area {1}	3.97	22.6	m^2
$(Mc)_{he}$	Cooler thermal mass {1}	34971	786233	J °C^{-1}
$(Mc)_{refr}$	Refrigerant thermal mass {1}	74618	337000	J °C^{-1}
$E_{f,he}$	Equivalent water covered surface {2}	1.0	1.0	--
F_1	Factor for number of tube rows [2]	1	1	--
h_{he}	Air side heat transfer coefficient {2}	21	45	W m^{-2} °C^{-1}
U_{refr}	Refrigerant side overall heat transfer coefficient {2}	417	1040	W m^{-2} °C^{-1}

B.2.6. Product

Symbol	Description	Value		Unit
		Apple (Indus.)	Pear (pilot)	
ρ_{pr}	Product density [9]	800	1000	kg m^{-3}
$\rho_{pr,bulk}$	Product bulk density [9]	475	600	kg m^{-3}
c_{pr}	Product heat capacity [9]	3460	3800	J kg^{-1} °C^{-1}
k_{prs}	Bulk thermal conductivity [9]	0.3	0.25	W m^{-1} °C^{-1}
$D_{pr,skin}$	Skin moisture diffusivity [9]	4.08	4.08	1×10^{15}m^2 s^{-1}
t_{peal}	Fruit peal thickness [11]	0.0112	0.0112	mm
h_{pr}	Heat transfer coefficient {2}; [3]	4.2	0.96	W m^{-2} °C^{-1}
x_{pr}	Moisture content wet base [9]	0.87	0.85	--
$A_{pr,}$	Specific surface area [8]	84	82	m^2 m^{-3}
$d_{pr,eq}$	Equivalent sphere diameter [8]	0.085	0.073	m
ε_{pr}	Void fraction (porosity) [3]	0.4	0.4	--
$fresp$	Conversion factor (respiration heat) [12]	0.0059	0.0059	--

Continued …

m_{bin}	Weight of a bin {3}	40	40	kg
T_{ref}	Reference temperature [5]	283	283	K
$V_{m,O_2,ref}$	Max. O_2 consumption rate at T_{ref} [5]	80.69	87.1	nmol kg^{-1} s^{-1}
E_{a,O_2}	Activation energy [5]	52.7	64.6	kJ mol^{-1}
K_{m,O_2}	Michaelis constant: O_2 consumption [5]	5.9	6.2	kPa
K_{mn,CO_2}	Michaelis constant: CO_2 production [5]	15	70.7	kPa
E_{a,CO_2}	Fermentative activation energy [5]	87.9	58.5	kJ mol^{-1}
$K_{m,O_2,f}$	Fermentative Michaelis constant [5]	0.39	0.69	kPa
RQ	Respiration quotient [5]	0.85	0.76	--
$V_{m,CO_2,f,ref}$	Fermentative maximum rate of CO_2 production at T_{ref} [5]	37.82	43	nmol kg^{-1} s^{-1}

B.2.7. Room air

Symbol	Description	Value	Unit
ρ_a	Dry air density [2]	1.29	kg m^{-3}
c_p	Dry air specific heat [2]	1007	J kg^{-1}°C^{-1}
c_v	Water vapour specific heat [2]	1840	J kg^{-1}°C^{-1}
Pr_a	Prandtl number of air [2]	0.71	--

B.2.8. Ventilator[2]

Symbol	Description	Value		Unit
		Pilot	Industrial	
V_a	Air volume flow rate {1}	1.19	12.8	m^3 s^{-1}
q_{fan}	Ventilator rating {1}	100	550	W

[2] The ventilator fans are part of the coolers (Section B.2.5).

B.3. Refrigeration unit model parameters

B.3.1. Experimental refrigeration unit

Compressor: Maneurop MT 36 JG6, Danfoss Commercial Compressors, Reyrieux, France.

Symbol	Description	Value	Unit
V_{swept}	Compressor swept volume {1}	2.92×10^{-3}	$m^3\ s^{-1}$
$(Mc)_{cd}$	Condenser thermal mass (total) {3}	45268	$J\ °C^{-1}$
$\dot{m}_{w,cd}$	Cooling water flow rate to condenser {3}	0.18	$kg\ s^{-1}$
$T_{w,in}$	Cooling water inlet temperature {3}	12.5	°C
$(Mc)_e$	Evaporator thermal mass (total) {3}	70629	$J\ °C^{-1}$
$\dot{m}_{w,e}$	Flow rate of water to evaporator {3}	0.274	$kg\ s^{-1}$
$(Mc)_t$	Tank thermal mass (total) {3}	1.53×10^{6}	$J\ °C^{-1}$

B.3.2. Pilot plant refrigeration unit

Compressor: Maneurop MTZ 160HW 6T VE, Danfoss Commercial Compressors, Reyrieux, France.

Condenser: RLA 225 DV, CLIREF, France.

Evaporator: AC 130, Alfa-Laval N.V., Brussels, Belgium.

Holding tank: Schatten N.V., Brussels, Belgium.

Symbol	Description	Value	Unit
V_{swept}	Compressor swept volume {1}	1.31×10^{-2}	$m^3\ s^{-1}$
η_i	Compressor isentropic efficiency {2}	0.7	--
$(Mc)_{cd}$	Condenser thermal mass (total) {1}	222588	$J\ °C^{-1}$
A_{cd}	Condenser heat transfer area {1}	375	m^2
U_{cd}	Overall heat transfer coefficient (cond.) {2}	16.1	$W\ m^{-2}\ °C^{-1}$
$\dot{m}_{a,cd}$	Cooling air flow rate to condenser {1}	21500	$m^3\ h^{-1}$
$T_{a,in}$	Air inlet temperature [13]	16	°C

Continued …

$(Mc)_e$	Evaporator thermal mass (total) {1}	40559	J °C^{-1}
A_e	Evaporator heat transfer area {1}	9.9	m^2
U_e	Overall heat transfer coefficient (evap.) {2}	45.4	W m^{-2} °C^{-1}
V_t	Holding tank volume {1}	1	m^3
$(Mc)_t$	Holding tank thermal mass {1}	3.57×10^6	J °C^{-1}
m_{chill}	Flow rate from the chiller unit {1}	2.92	kg s^{-1}
m_{app}	Flow rate from applications {1}	2.66	kg s^{-1}

B.3.3. Industrial refrigeration unit

Compressor: SMC 116E, Sabroe B.V., Apeldoorn, The Netherlands.

Circulation Pumps: WITT Gp 52, Mod 5C, Wijbenga B.V., VC-Beesd, The Netherlands.

Evaporative condenser: VCL 285-OR, Baltimore Air Coil Int., Heidt-op-den Berg, Belgium.

Symbol	Description	Value	Unit
V_{swept}	Compressor swept volume {1}	0.38	m^3 s^{-1}
η_i	Compressor isentropic efficiency	0.7	--
$(Mc)_{cd}$	Condenser thermal mass (total) {1}	2.12×10^6	J °C^{-1}
A_{cd}	Condenser heat transfer area {1}	210	m^2
U_{cd}	Overall heat transfer coefficient (cond.) {2}	931	W m^{-2} °C^{-1}
$m_{a,cd}$	Cooling air flow rate {1}	331776	m^3 h^{-1}
$m_{w,cd}$	Cooling water flow rate {1}	24.2	s^{-1}
$T_{a,in}$	Air inlet temperature [13]	10	°C
$T_{w,in}$	Water inlet temperature {1}	12	°C

B.4. Gas handling unit model parameters

Pilot: Combi CO_2/O_2 Adsorber, Storex B.V., 's-Gravendeel, The Netherlands.

Industrial: US 600, BESSELING Agri-Technic B.V. A.G. Zwaag, The Netherlands.

Symbol	Description	Value		Unit
		Pilot	Industrial	
	N_2 generator			
L	Bed length {1}	1.3	--	m
R	Bed radius {1}	0.079	--	m
P	Adsorption pressure {3}	80	--	kPa
T	Adsorption temperature {3}	283	--	K
K_{O2}	Equilibrium constant for O_2 [7]	9.25	--	--
K_{N2}	Equilibrium constant for N_2 [7]	8.9	--	--
k_{O2}	Effective mass transfer coefficient of O_2 [7]	0.0027	--	s^{-1}
k_{N2}	Effective mass transfer coefficient of N_2 [7]	5.9×10^{-5}	--	s^{-1}
$q_{O2,s}$	Saturation solid phase concentration of O_2 [7]	2640	--	mol m^{-3}
$q_{N2,s}$	Saturation solid phase concentration of N_2 [7]	2640	--	mol m^{-3}
ε	Bed porosity [7]	0.4	--	--
	CO_2 scrubber			
L	Bed length {1}	1.3	2	m
R	Bed radius {1}	0.049	1	m
P	Adsorption pressure {3}	80	300	kPa
T	Adsorption temperature {3}	283	283	K
K_{CO2}	Equilibrium constant for CO_2 [7]	135.8	135.8	--
K_{N2}	Equilibrium constant for N_2 [7]	8.9	8.9	--
k_{CO2}	Effective mass transfer coefficient of CO_2 [7]	9×10^{-4}	9×10^{-4}	s^{-1}
k_{N2}	Effective mass transfer coefficient of N_2 [7]	5.9×10^{-5}	6×10^{-5}	s^{-1}
$q_{CO2,s}$	Saturation solid phase concentration of CO_2 [7]	2850	3970	mol m^{-3}
$q_{N2,s}$	Saturation solid phase concentration of N_2 [7]	2640	1055	mol m^{-3}
ε	Bed porosity [7]	0.4	0.4	--

Reference

[1] *Anonymous*. ASHRAE Fundamentals. (1993). American Society of Heating, Refrigerating and Air-Conditioning Engineers, Inc., Atlanta, USA.

[2] Hewitt, G.F., Shires, G.L., Bott, T.R. (1994). Process heat transfer. CRC Press, London.

[3] Hoang, M.L. (2003). Numerical computation of air, moisture and heat transfer in chicory root cold store. *Ph.D. Thesis* (554), Katholieke Universiteit Leuven, Leuven, Belguim.

[4] Incropera, F.P., De Witt, D.P. (1990). Fundamentals of Heat and Mass Transfer – 3rd Edition. John Willy & Sons, Inc., New York.

[5] Lammertyn, J., Franck, C., Verlinden, B., Nicolai, B.M. 2001. Comparative study of the O_2 and CO_2 and temperature effect on respiration between 'Conference' pear cell protoplasts in suspension and intact pears. *Journal of Experimental Botany*, 52(362), 1769-1777.

[6] Pirard, G., Vancayemberg, F., Deltour, J. (1993). Rapport d'activités de décembre 1993. [Research activities report of December 1993] Centre d'Etude de la Regulation Climatique de Serres (IRSIA), Gembloux.

[7] Ruthven, D.M., Farooq, S., Knaebel, K.S. (1994). Pressure swing adsorption. VCH Publishers Inc., New York.

[8] Schotsmans, W. (2003). Gas diffusion properties of pome fruit in relation to storage potential. *Ph.D. Thesis* (557), Katholieke Universiteit Leuven, Leuven, Belguim.

[9] Sprenger Institute (1980). Produktgegevens groente en fruit, Mededeling 30. Wageningen, The Netherlands.

[10] Valenzuela, D.P., Myers, A.L. (1989). Adsorption equilibrium data handbook. Prentice Hall, New Jersey.

[11] Veraverbeke, E. (2001). Changes in epicuticular wax structure and composition in relation to moisture loss of apple during posthrvest storage. *Ph.D. Thesis* (495), Katholieke Universiteit Leuven, Leuven, Belguim.

[12] www 1: http://postharvest.ucdavis.edu/Produce/Producefacts/index.shtml. Accessed on March 4, 2000.

[13] www 2: http://www.weather.com/weather/climatology/monthly/BEXX0005. Accessed on June 10, 2003.

Appendix C

Simulation results of the refrigeration and gas handling units

In this Appendix, some of the simulation results from the refrigeration and gas-handling units are presented.

C.1. Refrigeration unit

C.1.1. Holding tank

In Figure C.1 the measured and simulated glycol temperature (secondary refrigerant) in the buffer tank is depicted. The tank consists of two compartments, one for the refrigerant coming from the cells (represented by T_2) and the other for the refrigerant coming from the chiller unit (represented by T_2) (Figure 3.2). As can be seen from the RMSE (Root Mean Square Error), the model predicted the tank temperatures with accuracy level that is similar to the accuracy of the measurement instrument.

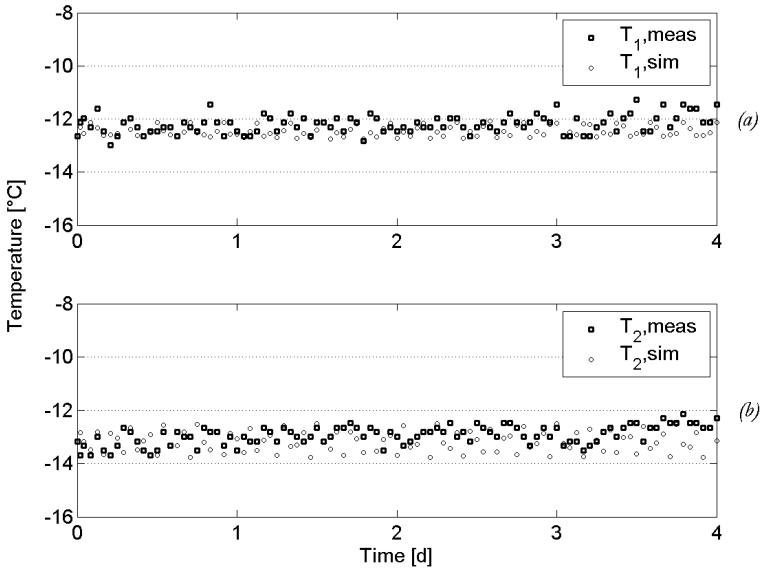

Figure C.1 Measured and simulated holding tank temperature of the pilot plant refrigeration unit, (a) glycol temperature from the chiller in the cold side of the buffer tank (T_1) (RMSE = 0.57°C), (b) glycol temperature from the cool cells in the warm side of the buffer tank (T_2) (RMSE = 0.47°C). (meas: measured, sim: simulated)

C.1.2. Condenser and evaporator

In Figure C.2, The simulated condenser and evaporator temperatures are shown. The simulation was carried out by considering a constant condenser out side temperature (16°C)[1]. The performance of the condenser is affected significantly by the ambient temperature, which in turn influences the performance of the unit as a whole. Obviously, higher performance is expected during the winter. Despite the transients observed in the condenser and evaporator temperatures, nearly constant secondary refrigerant temperature is attained, dumping the transients of the chiller unit, especially that of the evaporator.

[1] This is an average value for the month of September (30 years average). (Source: www 1)

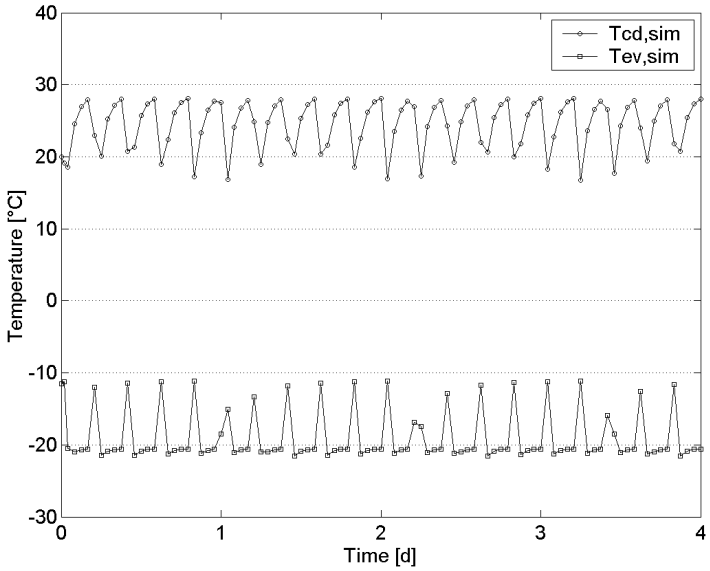

Figure C.2 Simulated condenser (Tcd,sim) *and evaporator* (Tev,sim) *temperature of the chiller unit of the pilot plant.*

C.2. Gas handling unit

C.2.1. N2 generator

Figure C.3 shows the mole fraction of O_2 in the product stream of the N_2 generator. The inflowing concentrations of the respiratory gases to the unit are as shown in Figures 4.31 and 4.32. The spikes in Figure C.3a show the adsorption operation of the unit at an interval of 2 hours. It can be observed that the spikes get shorter as the '*burning'* operation proceeds. As the O_2 load gets smaller due to both respiration and '*burning'*, the purity of N_2 out of the unit gets higher which explains the observed behaviour. In Figure C.3b the duration of the spikes is (the smaller width of the spikes) shorter. This is due to the shorter injection time calculated by the controller as the actual O_2 concentration in the room approaches the set point.

The details of one of the spikes in Figures C.3a and C.3b are shown in Figure C.4. At the beginning of the '*burning'* operation (day 7), where the O_2 concentration in the

feed is near normal air O_2 concentration, the product stream (the gas flowing out of the unit) concentration reaches a maximum of ±7% at the end of the adsorption process of 60 s. However, near the end of the '*burning'* operation (Figure C.4b), the maximum concentration of O_2 in the product stream was ±1.5%. Hence, the purity of N_2 obtained from the unit was more than 96% and 99% during the beginning and the end of the burring operation, respectively.

The corresponding N_2 concentration in the product stream of the unit and the details are also depicted in Figures C.5 and C.6, respectively.

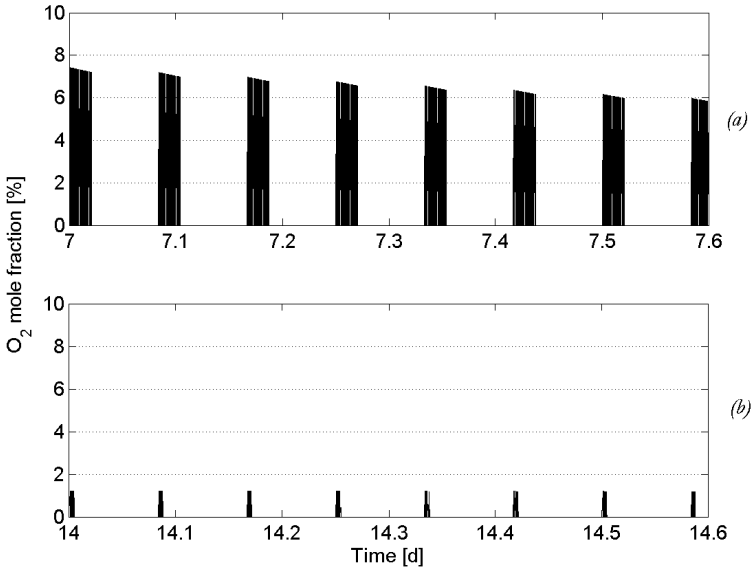

Figure C.3 O_2 mole fraction in the product stream of the N_2 generator (a) start of 'burning' operation: days 7 to 10 (b) near steady state respiratory gas concentrations

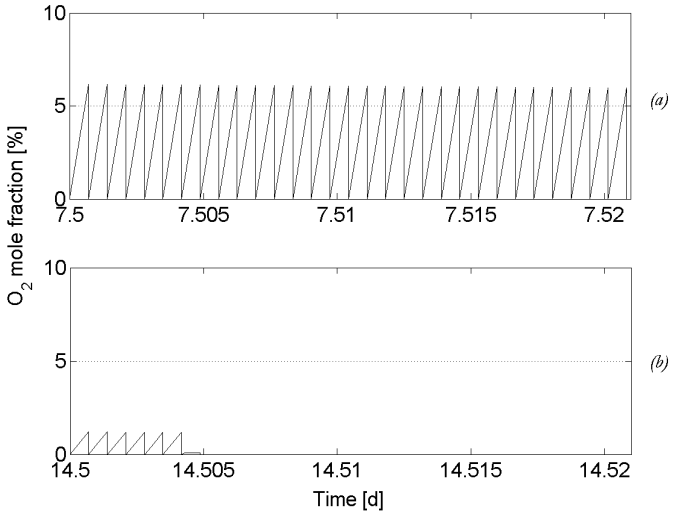

Figure C.4 O_2 mole fraction profiles in the product stream of the N_2 generator (details of Figure C.3) (a) during start of 'burning' operation (b) near steady state respiratory gas concentrations

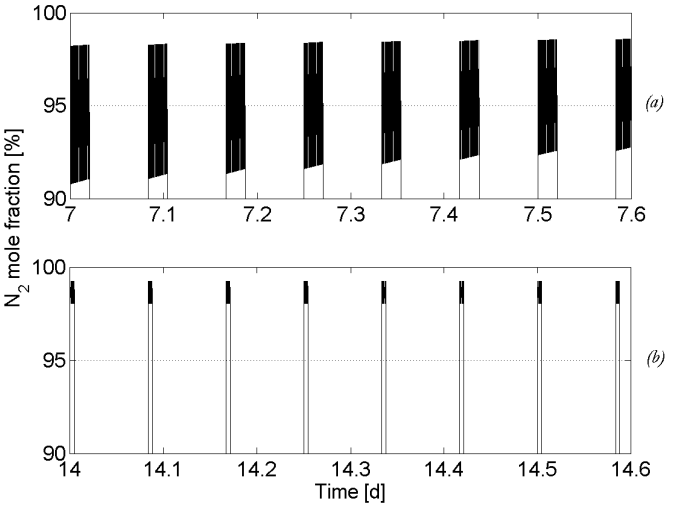

Figure C.5 N2 mole fraction in the air out flowing from the N_2 generator (a) start of 'burning' operation (b) near steady state respiratory gas concentrations

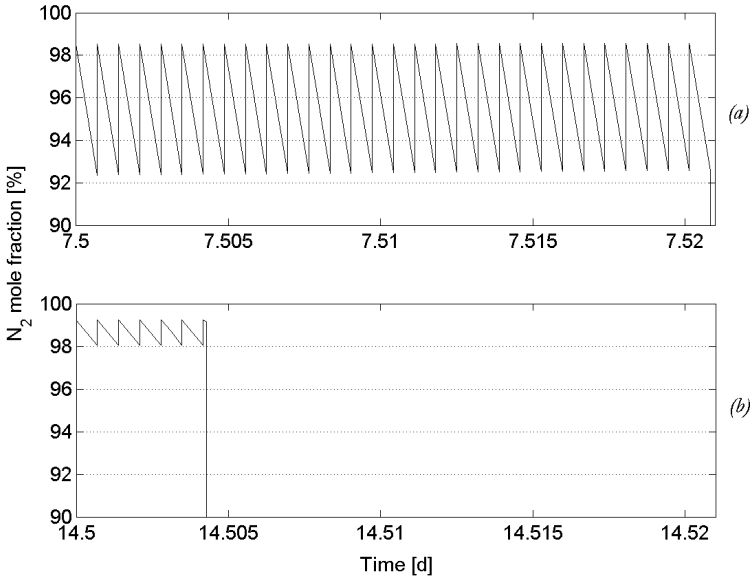

Figure C.6 N_2 mole fraction profiles in the product stream of the N_2 generator (details of Figure C.5) (a) start of 'burning' operation (b) near steady state respiratory gas concentrations

C.2.2. CO_2 scrubber

The CO_2 concentration in the product stream of the CO_2 scrubber is shown in Figure C.7. It can be observed that almost all the CO_2 in the feed stream was scrubbed and CO_2 free gas (0.001% CO_2) was injected back to the cool cell. When the ULO operation was set into action (day 7), higher concentration of CO_2 was fed to the scrubber (referring to the profile P_{CO2}, sim_1 in Figure 4.32). As the excess of CO_2 was removed lower CO_2 concentration gas is fed to the scrubber. As a result, higher purity gas (in terms of CO_2 concentration) is expected in the product stream, as can be observed in profile of Figure C.7. The corresponding N_2 concentration in the product stream of the CO_2 scrubber is shown in Figure C.8. Since negligible levels of CO_2 are present, the composition of the stream consists of N_2 and O_2 only.

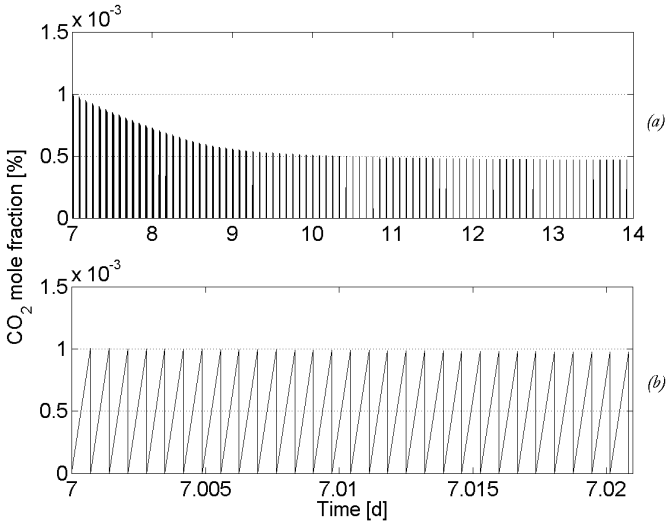

Figure C.7 CO_2 mole fraction in the product stream of the CO_2 scrubber (a) days 7 to14 (b) CO_2 mole fraction profile of the gas flowing out from the CO_2 scrubber (detail)

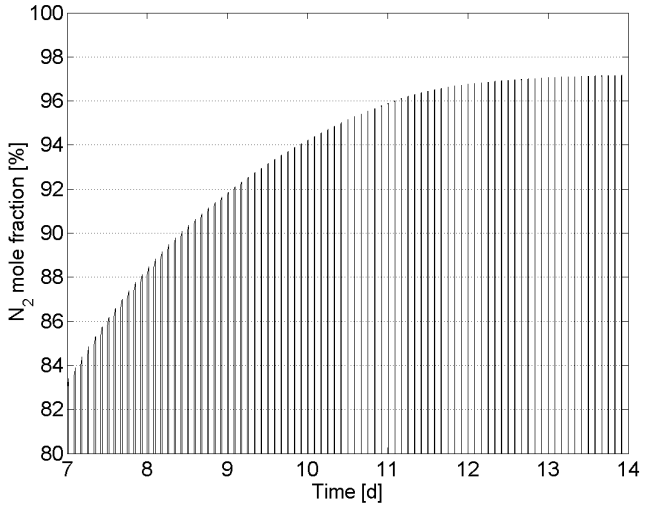

Figure C.8 N_2 mole fraction in the product stream of the CO_2 scrubber

Reference

www 1: http://www.weather.com/weather/climatology/monthly/BEXX0005. Accessed on June 10, 2003.

Symbols and abbreviations

Chapter 2

E_{a,CO_2}	activation energy of O_2 consumption rate [J mol^{-1}]
E_{a,O_2}	activation energy of CO_2 production rate [J mol^{-1}]
$k_{CO_2,leak}$	rate of CO_2 leakage [mol s^{-1}]
$k_{O_2,leak}$	rate of O_2 leakage [mol s^{-1}]
K_{m,O_2}	Michaelis-Menten constant for O_2 consumption rate [kPa]
K_{mc,CO_2}	Michaelis-Menten constant for competitive CO_2 inhibition rate [kPa]
K_{mn,CO_2}	Michaelis-Menten constant for non-competitive CO_2 inhibition rate [kPa]
K_{mu,CO_2}	Michaelis-Menten constant for uncompetitive CO_2 inhibition rate [kPa]
$K_{m,O_2,f}$	Michaelis-Menten constant for O_2 inhibition on fermentative CO_2 production rate [kPa]
M_{pr}	mass of produce [kg]

P_{CO_2}	partial pressure of CO_2 [kPa]
P_{O_2}	partial pressure of O_2 [kPa]
$P_{CO_2,amb}$	ambient partial pressure of CO_2 [kPa]
$P_{O_2,amb}$	ambient partial pressure of O_2 [kPa]
R	universal gas constant: 8.314 [J mol^{-1} K^{-1}]
RQ	respiration quotient
t	time [s]
T	temperature [K]
T_{ref}	reference temperature [K]
$U_m A$	Product of coefficient of mass transfer rate and area [m^3 s^{-1}]
V	volume of free space [m^3]
V_{CO_2}	CO_2 production rate [mol kg^{-1} s^{-1}]
V_{O_2}	O_2 consumption rate [mol kg^{-1} s^{-1}]
V_{m,O_2}	maximal O_2 consumption rate [mol kg^{-1} s^{-1}]
$V_{m,O_2,ref}$	maximal O_2 consumption rate at T_{ref} [mol kg^{-1} s^{-1}]
$V_{m,CO_2,f}$	maximal fermentative CO_2 production rate [mol kg^{-1} s^{-1}]
$V_{m,CO_2,f,ref}$	maximal CO_2 production rate at T_{ref} [mol kg^{-1} s^{-1}]

Chapter 3

a_w	water activity
A	area [m^2]
b	Langmuir constant
c_p	heat capacity [J kg^{-1} °C^{-1}]
c^g	gas phase concentration [mol m^{-3}]
C	moisture concentration [kg m^{-3}]
C^g	total gas phase concentration [mol m^{-3}]

$\mathbf{d}$	vector of disturbance variables
E_f	correction factor
f	conversion factor
$\mathbf{f}$	vector of functions
F	firmness [N]
F_c	correction term [N]
$F_{f,max}$	maximum firmness loss due to fermentation
$F_{o,max}$	maximum firmness loss due to respiration
h	heat transfer coefficient [W m^{-2} °C^{-1}], enthalpy [J kg^{-1}]
$\mathbf{h}$	vector of functions
h_m	mass transfer coefficient [m s^{-1}]
h_{fg}	latent heat of evaporation [J kg^{-1}]
Δh	Refrigerant enthalpy change during isentropic compression [J kg^{-1}]
J_m	moisture transfer rate [kg s^{-1}]
k	rate of gas flow [mol s^{-1}]
k_m	effective mass transfer coefficient [s^{-1}]
K_m	Michaelis constant [kPa]
$K_{mc,O_2,f}$	Michaelis constant for inhibition of fermentation by O_2 [kPa]
K_{mu,CO_2}	Michaelis constant for uncompetitive inhibition by CO_2 [kPa]
$\dot{m}$	mass flow rate [kg s^{-1}]
M	mass [kg]
n	total number of components
P	partial pressure [Pa]
q	heat transfer rate [W]
q^*	equilibrium value of $\bar{q}$ [mol m^{-3}]
$\bar{q}$	solid phase concentration [mol m^{-3}]
$\underset{\sim}{Q}$	power [W]
r	rate of accumulation [mol kg^{-1} s^{-1}]
R	thermal resistance [°C W^{-1}]
$R\underset{\sim}{Q}$	respiration quotient

t	time [s]
T	temperature [°C]
ΔT	log-mean temperature difference [°C]
u	vector of input variables
U	overall heat transfer coefficient [W m^{-2} $°C^{-1}$]
U_m	overall mass transfer coefficient [kg m^{-2} s^{-1}]
v	velocity [m s^{-1}]
V	volume [m^3]
V_{swept}	swept volume [m^3]
X	moisture content [kg kg^{-1}]
X_{db}	dry base moisture content [kg kg_{dm}^{-1}]
x	vector of state variables
y	vector of output variables
z	axial distance [m]
ε	porosity
ϕ	heat loss or gain to/from the environment [W]
η_{is}	isentropic efficiency
η_v	volumetric efficiency
ν	Specific weight at suction [m^3 kg^{-1}]
ρ	density [kg m^{-3}]

Subscripts

1,2	compartments of the holding tank
a	air
amb	ambient
app	from applications (end users)
b	packaging
c	room component
chil	from chiller
cd	condenser

CO_2	carbon dioxide
cp	compressor
d	door
da	dry air
dm	dry matter
e	evaporator
fl	floor
g	gas
he	heat exchanger
i	component
in	incoming
o	oxidative
out	out going
O_2	oxygen
p	pulse
pr	product
r	generation
refr	refrigerant
resp	respiration
s	surface
sat	Saturation
soil	soil
t	tank
v	vapour
w	water

Chapter 4

A	area [m^2]
A_c	cross sectional area [m^2]
d	thickness [m]
D	diameter [m]
c_p	heat capacity [J kg^{-1} $°C^{-1}$]

F_t	factor for pipe arrangement
h	heat transfer coefficient [W m^{-2} °C^{-1}]
h_m	Mass transfer coefficient [m s^{-1}]
H	height [m]
J	sensitivity
k	thermal conductivity [W m^{-1} °C^{-1}]
L	characteristic dimension [m]
Le	Lewis number
$\dot{m}$	mass flow rate [kg s^{-1}]
N_{str}	number of streams
Nu	Nusselt number
p	parameter
$\mathbf{p}$	vector of parameters
$\mathbf{p_o}$	vector of nominal parameters
Pr	Prandtl number
PR	pressure ratio
Re	Reynolds number
S_t	transverse pitch of pipes [m]
T	temperature [°C]
U	overall heat transfer coefficient [W m^{-2} °C^{-1}]
UA	product of overall heat transfer coefficient and area [W °C^{-1}]
v	overall heat transfer coefficient [W m^{2} °C^{-1}]
v_{max}	maximum overall heat transfer coefficient [W m^{2} °C^{-1}]
V	volume [m^3]
W	width [m]
$\mathbf{y}$	vector of model predictions
$\bar{\mathbf{y}}$	vector of model predictions at nominal parameters
y	model prediction
η_f	fin efficiency
μ	Kinematic viscosity [s m^{-2}]

ρ	density [kg m^{-3}]

Subscripts

a	air
amb	ambient
cd	condenser
e	volume element
ev	evaporator
f	fin
i	internal, index
j	index
o	external
p	pipe
refr	refrigerant
s	surface
t	tank
VA	volume average

Superscripts

a	absolute
r	relative

Chapter 5

q	heat transfer rate [W]
T	temperature [°C]

Subscripts

a	air
he	heat exchanger
refr	refrigerant

Chapter 6

C_{refr}	cost of refrigeration [€ ton^{-1}]
p	price of electricity [€ kWh^{-1}]
q	chilling and storage heat load [kJ ton^{-1}]
η_{cop}	coefficient of performance of whole cooling plant

Chapter 7

C	global capacitance matrix
C*	global capacitance matrix evaluated at the nominal volumetric heat capacity
E	applied energy [J]
f	global thermal load vector
F	fisher information matrix
F_{11}, F_{12}, F_{21}, F_{22}	elements of Fisher information matrix
g	auxiliary vector
h	surface heat transfer coefficient [W m^{-2} °C^{-1}]
$\mathbf{I}_n$	$n \times n$ identity matrix
k	thermal conductivity [W m^{-1} °C^{-1}]
k^*	nominal thermal conductivity [W m^{-1} °C^{-1}]
K	global conductance matrix
K*	global conductance matrix evaluated at nominal thermal conductivity
n	outward normal vector, number of data points, number of measurement positions
p	parameter vector
p*	nominal parameter vector
q	energy input per unit length [J m^{-1}]
Q	volumetric heat generation [W m^{-3}]
Q_l	heat input per unit length [W m^{-1}]
Q	square weighing function
r	radius [mm]
t	time [s]
t_f	final time [s]
t_o	initial time [s]

T	temperature [°C]
T_∞	ambient temperature [°C]
T_o	initial temperature [°C]
u	nodal temperature [°C]
$\mathbf{u}$	nodal temperature vector
$\mathbf{u}^*$	nodal temperature vector evaluated at the nominal parameter vector
$\mathbf{W}$	gaussian white noise vector
x,y,z	spatial co-ordinates [m]
$\mathbf{x}$	auxiliary vector
y	predicted value
$\mathbf{y}$	vector of model predictions
$\mathbf{y}^*$	vector of model predictions evaluated at the nominal parameters
y	measured value
$\mathbf{y}_m$	vector of measured value
Γ	boundary surface of the computational domain
$\delta_{t_1 t_2}$	the dirac delta
$\mathbf{\Phi}$	positive definite matrix
$\lambda_{max}, \lambda_{min}$	maximum and minimum eigenvalues
Λ	ratio of maximum to minimum eigenvalue
ρc	volumetric heat capacity [J m^{-3} °C^{-1}]
ρc^*	nominal volumetric heat capacity [J m^{-3} °C^{-1}]
σ	standard deviation
$\mathfrak{I}$	identification functional

Appendix

c_p	heat capacity [J kg^{-1} °C^{-1}]
C	control signal
G_p	proportional gain
f	flow fraction

P_{offset}	offset
s	normalised control signal
S	normalised control signal [%]
t	time [s]
T	temperature [°C]
V	volume [m^3]
ε	error
ρ	density [kg m^{-3}]
τ_D	derivative time [s]
τ_I	integral time [s]

List of publications

International journal publications

Nahor, **H.B.**; Scheerlinck, N.; Verniest; R.; De Baerdemaeker, J.; Nicolai, B.M. (2001). Optimal design of dynamic experiments for the parameter estimation of conduction heated foods. *Journal of Food Engineering,* 48 109-119.

Nahor, **H.B.**; Scheerlinck, N.; Van Impe, J.; Nicolaï, B.M. (2003). Optimisation of the temperature sensor position in a hot wire probe set up for estimation of the thermal properties of foods using optimal experimental design. *Journal of Food Engineering,* 57(1) 103-110.

Nahor, H.B.; Schotsmans, W.; Scheerlinck, N.; Nicolai, B.M. (2003). Assessment and validation of existing gas exchange models for bulk storage of respiring produce. *Postharvest Biology and Technology,* Submitted.

Nahor H.B.; Scheerlinck, N.; Verboven, P.; Van Impe, J.; Nicolai, B.M. (2004). Continuous/discrete simulation of controlled atmosphere (CA) cool storage systems: model development and validation using pilot plant CA cool storage. *International Journal of Refrigeration,* Submitted.

Scheerlinck N.; **Nahor H.B.**; Moles C.G.; Banga J.R.; Nicolaï B.M. (2004). Implementation and validation of optimal heat generation profiles for simultaneous estimation of thermal food properties using a hotwire probe. *Journal of Food Engineering,* Submitted.

National journal publications

Nahor, **H.B.**; Scheerlinck, N.; Van Impe, J.; Nicolaï, B.M. (2002). A simple model of a refrigeration plant for cool storage systems simulation. *Communications of the faculty of Agricultural and Applied Biological Sciences,* University of Ghent, 67(4) 293-296.

Nahor, **H.B.**; Scheerlinck, N.; Van Impe, J.; Nicolaï, B.M. (2003). Combined discrete and continuous simulation of Controlled Atmosphere (CA) Storage Systems. *Communications of the faculty of Agricultural and Applied Biological Sciences,* University of Ghent, 68(3) 17-21.

International Conference proceedings

Nahor H.B.; Scheerlinck N.; Moles C.G.; Banga J.R.; Nicolaï B.M. (2004). Implementation and validation of optimal heat generation profiles for simultaneous estimation of thermal food properties using a hotwire probe. Accepted to be presented in the *9th International Congress on Engineering and Food (ICEF9),* 7-11 March 2004, Montpellier, France.

Nahor H.B.; Scheerlinck, N.; Verboven, P.; Van Impe, J.; Nicolai, B.M. (2003). Dynamic Simulation Of Controlled Atmosphere (CA) Cool Storage Systems For Pip Fruits. *Proceedings of the 21st International Congress of Refrigeration,* Washington D.C., USA, (CD-ROM edition, ISBN 2-913149-32-4).

Nahor, H.B.; Teshome, E.J.; Scheerlinck, N.; Van Impe, J.F.; Nicolaï, B.M. (2002). Prediction of dynamic behaviour of ca cool rooms using lumped parameter approach. *Acta Horticulturae*, 599, 213-219.

Nahor, **H.B.**; Scheerlinck, N.; Van Impe, J.; Nicolaï, B.M. (2001). Optimisation of temperature sensor position in a hot wire probe set up for estimation of the thermal properties of foods. *An Engineering Odyssey – ASAE 94th Annual International Meeting*, Paper N° 016091, Sacramento Convention Centre, Sacramento, California, USA.

Nahor, H.B.; Scheerlinck, N.; Verniest, R.; De Baerdemaeker, J.; Nicolaï, B.M. (2000). Optimal design of dynamic experiments for the parameter estimation of conduction heated foods. *First International Conference on Simulation in Food and Bio-Industry, FOODSIM'2000*, Paper N° A-SFE-17, ENITIAA, Nantes, France, pp161-165.

Nahor, H.B.; Scheerlinck, N.; Verniest, R.; De Baerdemaeker, J.; Nicolaï, B.M. (1999). Optimal design of dynamic experiments for the parameter estimation of conduction heated foods. *Emerging Technologies for the 21st Century – ASAE/CSAE-SCGR Annual International Meeting*, Paper N° 99 3103, Sheraton Toronto Centre, Toronto, Ontario, Canada, 23 p.

Nicolaï, B.M.; Verboven, P.; Scheerlinck, N.; Hoang, M.L.; **Nahor, H.B**. (2001). Modelling of cooling and freezing operations. International Conference on Rapid

Cooling of Food. *Proceedings of the International Institute of Refrigeration,* Commission C2, on Rapid Cooling of Food, Bristol, UK, (CD-ROM version, ISBN 2-913149-23-5).

Nicolaï, B.M.; Verboven, P.; Scheerlinck, N.; Hoang, M.L.; **Nahor, H.B**. (2001). Modelling and simulation of cooling and freezing processes. *First International Workshop on Mathematical and Computing techniques for Agro-Food Technologies*, International Centre for Numerical Methods in Engineering, Barcelona, Spain. page 26.

Contribution to books

Nicolaï, B.M.; Hoang, M.L.; Jancsok, P.; Lammertyn, J.; **Nahor, H.B**.; Scheerlinck, N.; Verboven, P.; Verlinden, B. (2002). Modelling and simulation of cooling and freezing processes. Balsa-Canto E., Mora, J., Banga, J.R., Onate, E. (Eds.), Computational Techniques in Food Engineering. International Centre for Numerical Methods in Engineering (CIMNE), Barcelona, Spain, pp. 59-69.

Nederlandse samenvatting

Dit werk levert een bijgrage tot *(i)* de ontwikkeling van een methodologie om industriële bewaarsystemen onder gemodificeerde atmosfeer (CA) te modeleren en te simuleren door gebruik te maken van een continue/discrete simulatie methode met als finaliteit het systeem als geheel te schalen, een modelgebaseerde controlestrategie voor kwaliteit te ontwikkelen en operationele omstandigheden te optimaliseren voor een hogere productiviteit en rendabiliteit, en tot *(ii)* de ontwikkeling van een methodologie om de thermofysische eigenschappen van biologisch materiaal gelijktijdig en eenduidig te schatten via optimaal experimenteel ontwerp met een 'heet draad probe'.

Het model van het CA bewaarsysteem werd ontwikkeld door het systeem te verdelen in drie interagerende eenheden, namelijk: (i) de koelruimte, (ii) de koeleenheid en (iii) de gascontrole-eenheid. De dynamica van de warmte- en massaoverdracht van de componenten in de koelruimte en de koeleenheid werd beschreven door een algemene energie- en massabalans door de 'zoning' benadering te gebruiken, wat resulteerde in een beschrijving van de componenten door differentiaalvergelijkingen. De respiratie en de kwaliteitsafname van het biologisch product werden beschreven door Michaelis-Menten modellen. Een twee-fasen

isotherm plug-flow model werd gebruikt om de gascontrole-eenheid te benaderen waarbij de massaoverdracht van de vaste fase beschreven werd door een lineair drijvende krachtmodel. Het CA bewaarmodel werd geïmplementeerd met behulp van de algemene computersimulatie-omgeving EcosimPro (EA International, Madrid, Spain), die continue/discreet gecombineerde processen kan behandelen. Het model werd gevalideerd in een industriële CA koelinfrastructuur door enkele variabelen (temperatuur, relatieve vochtigheid, concentratie van de ademhalingsgassen, gewicht- en hardheidsafname van het product, generatie van ademhalingswarmte) te selecteren, die de koelruimte, het koelmiddel, de evaporator en de gascontrole-eenheid karakteriseren. Deze variabelen werden vergeleken met experimentele data in zowel een lege, een half gevulde als een volledig gevulde koelcel.

Het model kon de meest belangrijke discrete en continue processen benaderen met een nauwkeurigheid die kleiner was dan de variabiliteit van de verschillende gemeten variabelen (3°C voor de koelcel, 2.5°C voor de oppervlaktetemperatuur van de koeler, 4°C voor de producttemperatuur en 5% voor de relatieve vochtigheid) en in de beste gevallen zelfs een nauwkeurigheid die overeenkomt met deze van de meetinstrumenten (0.5°C voor temperatuur en 5% voor relatieve vochtigheid). Gevoeligheidsanalyses toonden aan dat de transiente koelingfase beïnvloed werd door de nauwkeurigheid van de geïmplementeerde waarden van de warmteoverdrachtscoefficiënten. Bovendien beïnvloedde de begintemperatuur van het product de koelingsnelheid en het vochtverlies ervan aanzienlijk met het gevolg dat een koelingstrategie moet toegepast worden waarbij een snelle koeling van het product steeds moet vergezeld worden met een heel hoge relatieve vochtigheid (nabij verzadiging) van het koelmedium.

In dit werk werd ook aangetoond dat met praktische industriële operationele procedures op een directe wijze de productkwaliteit en het ontwerp en performantie van een koelinfrastructuur geëvalueerd kan worden. De vernieuwing van het hier voorgestelde simulatiemodel is dat de praktische omstandigheden en planning, zoals het stapsgewijs vullen van de koelcel en de betrokken overgangsfases gesimuleerd worden en op deze wijze een juist beeld geeft van de realiteit. Bovendien werd ook de voorspelling van de kwaliteitsafname van het product in het model geïncorporeerd. Het globale model van het CA bewaarsysteem resulteerde in een pragmatisch werkmiddel voor de simulatie van CA bewaarinfrastructuren.

De toepassing van optimaal experimenteel ontwerp voor de schatting van thermische eigenschappen van biologisch materiaal leidde tot nauwkeurig geschatte parameters door optimale experimentele 'modi operandi' te vinden. Zowel een gewogen keuze van de praktisch 'implementeerbare' warmteontwikkeling, afkomstig van de theoretisch optimale profielen, als optimale meetposities zijn nodig om tot eenduidige en nauwkeurige schattingen te komen.